INVESTIGATING VITAMIN B6-DEPENDENT EPILEPTIC ENCEPHALOPATHIES IN HUMAN PATIENTS AND A MOUSE MODEL

by

Hilal Hamed Al Shekaili

BSc, Sultan Qaboos University, 2008
MSc, Sultan Qaboos University, 2011

A THESIS SUBMITTED IN PARTIAL FULFILLMENT OF
THE REQUIREMENTS FOR THE DEGREE OF

DOCTOR OF PHILOSOPHY

in

The Faculty of Graduate and Postdoctoral Studies

(Medical Genetics)

THE UNIVERSITY OF BRITISH COLUMBIA

(Vancouver)

August 2020

The following individuals certify that they have read, and recommend to the Faculty of Graduate and Postdoctoral Studies for acceptance, the dissertation entitled:

Investigating Vitamin B6-Dependent Epileptic Encephalopathies in Human Patients and a Mouse Model

submitted by Hilal Al Shekaili in partial fulfilment of the requirements for

the degree of Doctor of Philosophy

in Medical Genetics

Examining Committee:

Dr. Jan M. Friedman, Department of Medical Genetics

Supervisor

Dr. Blair R. Leavitt, Department of Medical Genetics

Co-supervisor

Dr. Lorne Clarke, Department of Medical Genetics

Supervisory Committee Member

Dr. Sylvia Stockler, Department of Pediatrics

University Examiner

Dr. Daniel Goldowitz, Department of Medical Genetics

University Examiner

Additional Supervisory Committee Members:

Dr. William T. Gibson, Department of Medical Genetics

Supervisory Committee Member

Dr. Clara van Karnebeek, Department of Pediatrics

Supervisory Committee Member

Abstract

PLPHP deficiency is a recently discovered form of vitamin B6-dependent epilepsies (B6Es) that is caused by recessive mutations in *PLPBP*. PLPHP is involved in pyridoxal 5'-phosphate (PLP) homeostatic regulation. However, the mechanism by which PLPHP dysfunction disrupts PLP homeostasis and leads to the observed encephalopathy in patients was still elusive. We characterized the clinical, genomic and biochemical abnormalities in a new series of 12 PLPHP deficiency patients. Our results identified previously undescribed clinical features of PLPHP deficiency, including non-epileptic movement disorder, fatal mitochondrial encephalopathy and folinic acid-responsive seizures. We characterized the pathogenicity of patients' *PLPBP* variants using *in silico* tools and 3D modelling of PLPHP and developed a system of clinical severity score. We generated and characterized *PLPBP* knockout models in HEK293 cells, yeast and zebrafish. Our *plpbp*-KO zebrafish model replicated the clinical phenotype of PLPHP-deficient patients by showing vitamin B6-dependent seizures and death in untreated KO larvae. Consistent with the biochemical picture in patients, Plphp-deficient fish displayed decreased systemic levels of PLP. In the future this model can be utilized as a tool for investigating the disease pathophysiology, drug screening and identifying diagnostic biomarkers. Pyridoxine-dependent epilepsy (PDE-ALDH7A1) is another form of B6Es that is caused by mutations in *ALDH7A1*, a gene which encodes an enzyme within the lysine catabolism pathway. We have successfully generated and characterized transgenic mouse strain with constitutive genetic ablation of *Aldh7a1*. Results showed that KO mice accumulated high concentrations of upstream lysine metabolites including Δ^1-piperideine-6-carboxylic acid (P6C), α-aminoadipic semialdehyde (α-AASA) and pipecolic acid (PIP), similar to the biochemical picture in ALDH7A1-defiecint patients. KO mice fed the regular diet (0.9% lysine) did not exhibit seizures based on EEG analysis. When KO mice are

switched to a diet containing higher amount of lysine (4.7%), they developed severe recurrent seizures which led to their quick death. In analogy to the patients' picture also, treating KO mice under high lysine diet with pyridoxine injections prevented seizures and prolonged their survival. This study provides a proof-of-concept for the utility of the model to study PDE-ALDH7A1 biochemistry and to test new therapeutics.

Lay Summary

Vitamin B6-dependent epilepsies (B6Es) are rare genetic diseases that cause frequent seizures that are resistant to conventional drugs but are well-controlled by administration of vitamin B6 (vitB6). We investigated two types of B6Es. The first one is known as PLPHP deficiency in which we studied 12 new patients and characterized their clinical, genetic and biochemical abnormalities. Our results showed vitB6 deficiency in patient cells. The zebrafish model that we developed for this disease replicated the patient symptoms and therefore can be used for future investigations and drug screening. The other form of B6Es that we studied is known as ALDH7A1 deficiency. We generated and characterized a mouse model for this disease. Results showed that the model reproduced the patients' clinical and biochemical features including accumulation of chemical compounds in the brain and seizures. This model can be used as a tool to study the disease biology and test new treatments.

Preface

All of the work performed by the candidate was conducted at the Center for Molecular Medicine and Therapeutics (CMMT) and the British Columbia Children's Hospital Research Institute at the University of British Columbia, Children's and Women's Hospital campus. Studies in human patients were approved by the Clinical Research Ethics Board of the British Columbia Children's and Women's Hospital, University of British Columbia (certificate # H12-00067). Ethical approval for studies in mice was obtained from the University of British Columbia's Animal Care Committee (Animal Protocols # A15-0200 and A15-0180).

Chapter 2: A version of this chapter has been published as Johnstone, D. L.*****, Al-Shekaili, H. H.*****, Maja Tarailo-Graovac, Nicole I. Wolf, Autumn S. Ivy, Scott Demarest, Yann Roussel, Jolita Ciapaite, Carlo W.T. van Roermund, Kristin D. Kernohan, Ceres Kosuta, Kevin Ban, Yoko Ito, Skye McBride, Khalid Al-Thihli, Rana A. Abdelrahim, Roshan Koul, Amna Al Futaisi, Charlotte A. Haaxma, Heather Olson, Laufey Yr. Sigurdardottir, Georgianne L. Arnold, Erica H. Gerkes, M. Boon, M. Rebecca Heiner-Fokkema, Sandra Noble, Marjolein Bosma, Judith Jans, David A. Koolen, Erik-Jan Kamsteeg, Britt Drögemöller, Colin J. Ross, Jacek Majewski, Megan T. Cho, Amber Begtrup, Wyeth W. Wasserman, Tuan Bui, Elise Brimble, Sara Violante, Sander M. Houten, Ron A. Wevers, Martijn van Faassen, Ido P. Kema, Nathalie Lepage, Care4Rare Canada Consortium, Matthew A. Lines, David A. Dyment, Ronald J.A. Wanders, Nanda Verhoeven-Duif, Marc Ekker, Kym M. Boycott, Jan M. Friedman, Izabella A. Pena, and Clara D.M. van Karnebeek. (2019). PLPHP deficiency: Clinical, genetic, biochemical, and mechanistic insights. *Brain*: *A Journal of Neurology*, 142(3), 542–559. (***** joint first authors).

I performed recruitment of index patients (Patients 1, 2, 8 and 9), SNP homozygosity mapping, analysis of exome candidate variant list and discovery of the causative gene (*PLPBP*, novel at the

time of discovery). Bioinformatics analysis of exome data and generation of the candidate variant lists for Patients 1 and 2 were performed by M. Tarailo-Graovac. Sanger validation of exome variants and SNP microarray experiment in Patients 1, 2, 8 and 9 was performed by C. Ross and B. Drögemöller. Patient 5 was recruited by M. Lines and D. Dyment. Remaining patients were recruited by C. van Karnebeek. Clinical patient descriptions were originally written by their referring clinicians (K. Al-Thihli and R. Abdelrahim for Patients 1, 2, 8 and 9; E. Gerkes and M. Boon for Patient 3; C. Haaxma and E. Kamsteeg for Patient 4; M. Lines and D. Dyment for Patient 5; H. Olson for Patient 6; A. Ivy for Patient 7; S. Demarest for Patients 10 and 11; L. Sigurdardottir and G. Arnold for Patient 12). I assembled the patient clinical reports, structured them for the manuscript and filled in missing patients' clinical and biochemical data by discussing them with the collaborative clinicians. I performed *PLPBP* variant annotations and *in silico* variant effect predictions (SIFT, Polyphen2, MutationTaster, MutationAssessor, FATHMM MKL, PROVEAN) for all patients. The genotype-phenotype correlation based on variant location relative to PLP binding pocket in PLPHP protein was first discovered by me. Clinical severity score assessment and related methods section and Table 4 were prepared by D. Johnstone. Analysis of patients' MRIs and related Figure 1 and Table 2 were prepared by N. Wolf. Table 1, Table 3 (with some contribution from D. Johnstone and I. Pena) and Figure 2A were prepared by me. Results sections 2.3.1 and 2.3.3 were jointly written by me and D. Johnstone. Results section 2.3.4 was written by me with contribution from D. Johnstone. Structural modelling of human PLPHP and related methods and figures in the manuscript (Figure 2B, C, D and Figure 4) were prepared by I. Pena. Protein analysis in Patient 5 fibroblasts and its related methods and immunoblot figure were prepared by D. Johnstone. Mitochondrial localization of PLPHP in HeLa cells and related methods section and figures were prepared by S. Houten. *PLPBP* studies in yeast and HEK293 cells and

related methods section and figures were prepared by C. van Roermund and R. Wanders. Seahorse assay in Patient's 5 fibroblasts was performed by D. Johnstone. Generation and characterization of *plpbp*-KO zebrafish and related sections and figures in the manuscript were prepared by I. Pena and D. Johnstone. Vitamin B6 vitamer analysis in patient samples, PLPHP-deficient HEK293 cells and *plpbp*-KO zebrafish and related methods section were prepared by J. Ciapaite, M. Bosma and N. Verhoeven-Duif. Introduction and Discussion sections were written by me, D. Johnstone and IAP.

Chapters 2 and 3: Versions of these two chapters has been combined in one manuscript and currently under publication as Al-Shekaili, H., T. Petkau, I. Pena, T. Lengyell, N. Verhoeven-Duif, J. Ciapaite, M. Bosma, M. van Faassen, I. Kema, G. Horvath, C. Ross, E. Simpson, J. Friedman, C. van Karnebeek and B. Leavitt. 2020. A Novel Mouse Model for Pyridoxine-Dependent Epilepsy Due to Antiquitin Deficiency. *Human Molecular Genetics* [provisionally accepted].

I contributed to experimental design and was responsible for all major areas of data collection and analysis, and all of the manuscript composition. Blastocyst microinjection, production of chimeric mice and breeding to germline transmission were conducted at the Mouse Animal Production Service core facility of the CMMT (experiments were performed by T. Lengyell and supervised by E. Simpson). Mass spectrometry experiments were performed by I. Pena, N. Verhoeven-Duif, J. Ciapaite, M. Bosma, M. van Faassen and I. Kema who also wrote the methods section for these experiments. Western blot experiment was performed by Mr. Ge Lu. T. Petkau performed NeuN and GFAP immunostaining and she wrote the related methods section and prepared the image in Figures 3-18 and 3-19. Mr. Ge Lu performed the initial steps of the EEG implantation surgery (induction of anesthesia, surgical incision and placement of electrodes). T. Petkau helped in monitoring of mice in follow up trials of special diets. T. Petkau and Mr. Ge Lu helped in

transcardial perfusion of mice and harvesting of mouse tissue specimens for mass spectrometry analysis.

Table of Contents

List of Tables

List of Figures

1 Introduction

1.1 Vitamin B6 and its biochemistry in the human body

Vitamin B6 (vitB6) is a generic term that refers to a group of six interconvertible chemical compounds that share a pyridine ring in their centre. These vitB6 compounds (also called vitamers) are pyridoxine (PN), pyridoxamine (PM), pyridoxal (PL) and their 5′-phosphorylated forms pyridoxine 5′-phosphate (PNP), pyridoxamine 5′-phosphate (PMP) and pyridoxal 5′-phosphate PLP) (di Salvo et al., 2011) (Fig. 1-1). VitB6 is required by all living organisms for their survival, but only microorganisms and plants can carry out *de novo* synthesis of this vitamin. Other organisms including humans acquire vitB6 from exogenous sources and interconvert its different forms according to their needs via a biochemical pathway known as the salvage pathway (di Salvo et al., 2011; Mooney et al., 2009).

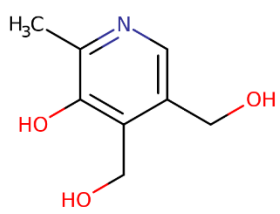

Pyridoxine (PN)

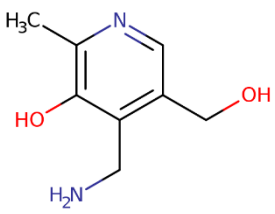

Pyridoxamine (PM)

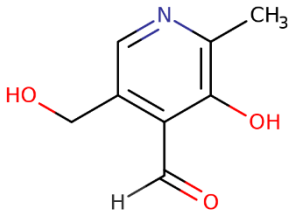

Pyridoxal (PL)

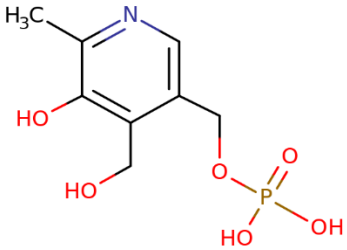

Pyridoxine 5′-phosphate (PNP)

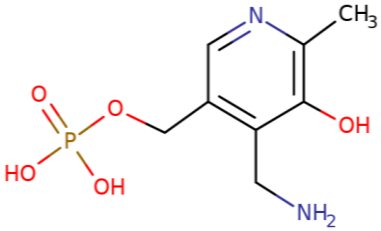

Pyridoxamine 5′-phosphate (PMP)

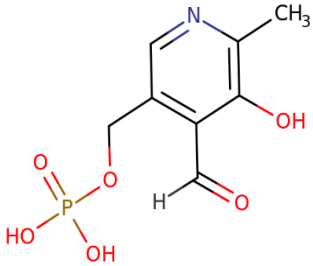

Pyridoxal 5′-phosphate (PLP)

Fig. 1-1: Chemical structures of the six vitamin B6 vitamers. Coloured atoms designate oxygen or hydroxyl group (red), nitrogen or amine group (blue) and phosphorus (brown). (retrieved from ChemIDplus database).

1.1.1 Metabolism of vitB6

Among the six vitB6 compounds, PLP is the biologically active and most important vitamer since it is required as a cofactor for a multitude of enzymes in the body. Humans and other mammals obtain PLP from vitB6 vitamers in the diet and recycle them in the salvage pathway (di Salvo et al., 2011) (Fig. 1-2). The central enzyme in this pathway is PNP oxidase (PNPO), a flavin mononucleotide (FMN)-dependent enzyme that is capable of converting PNP or PMP to the active cofactor PLP (di Salvo et al., 2011). Other important enzymes in the salvage pathway are PL kinase (PLK) and a number of different phosphatases (Ghatge et al., 2012).

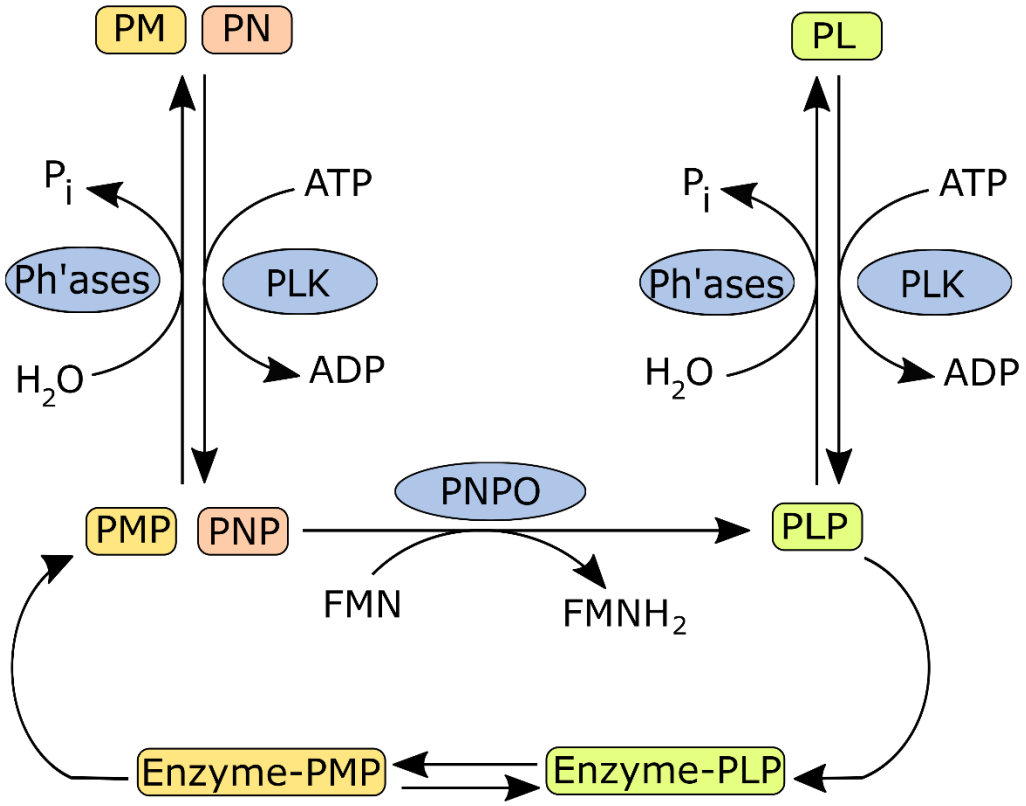

Fig. 1-2: The PLP salvage pathway. Phosphorylated vitamers are converted to PLP by the enzyme PNPO. PLP is also recycled from degraded holo-B6 enzymes through PMP as an intermediate step. ADP: adenosine diphosphate, ATP: adenosine triphosphate, $FMNH_2$: flavin mononucleotide reduced form, Ph'ases: phosphatases, Pi: inorganic phosphate. (based on Darin et al. (2016); Ghatge et al. (2012); Wilson et al. (2019)).

After being ingested, phosphorylated vitamers (PLP, PNP and PMP) undergo dephosphorylation by the ecto-enzyme tissue-specific intestinal phosphatase (IP) (Ghatge et al., 2012), whereas pyridoxine glucoside (PNG) vitamers from plants are hydrolyzed by a glucosidase before absorption (Clayton, 2006; di Salvo et al., 2011). Absorbed vitamers are carried by the portal circulation to the liver where they are phosphorylated by PLK (Ghatge et al., 2012). Inside liver cells, PNP and PMP are oxidized by PNPO to form PLP, which is then released to the circulation bound to lysine-190 residue of albumin (Fig. 1-3) (Bohney et al., 1992; Clayton, 2006; Footitt et al., 2013). Binding of PLP to albumin is thought to protect the cofactor from hydrolysis and other reactions (Footitt et al., 2013). About 60% of circulating vitB6 is in the form of albumin-bound PLP, while PN, PM and PL constitutes the remaining proportion (Ghatge et al., 2012).

Prior to delivering the circulating PLP to different tissues, it is dephosphorylated to PL by the ecto-enzyme tissue nonspecific alkaline phosphatase (TNSALP) to enable entry into the cells and through the blood-brain barrier. Inside the cell, PL is re-converted by PLK to PLP, which now can be used as a cofactor in many biochemical reactions (Fig. 1-3) (Clayton, 2006; di Salvo et al., 2011; Ghatge et al., 2012). Degradation of PLP-bound enzymes (holo-B6 enzymes) can generate PMP, which is then oxidized back to PLP by the action of PNPO (Wilson et al., 2019) (Fig. 1-2 & 3).

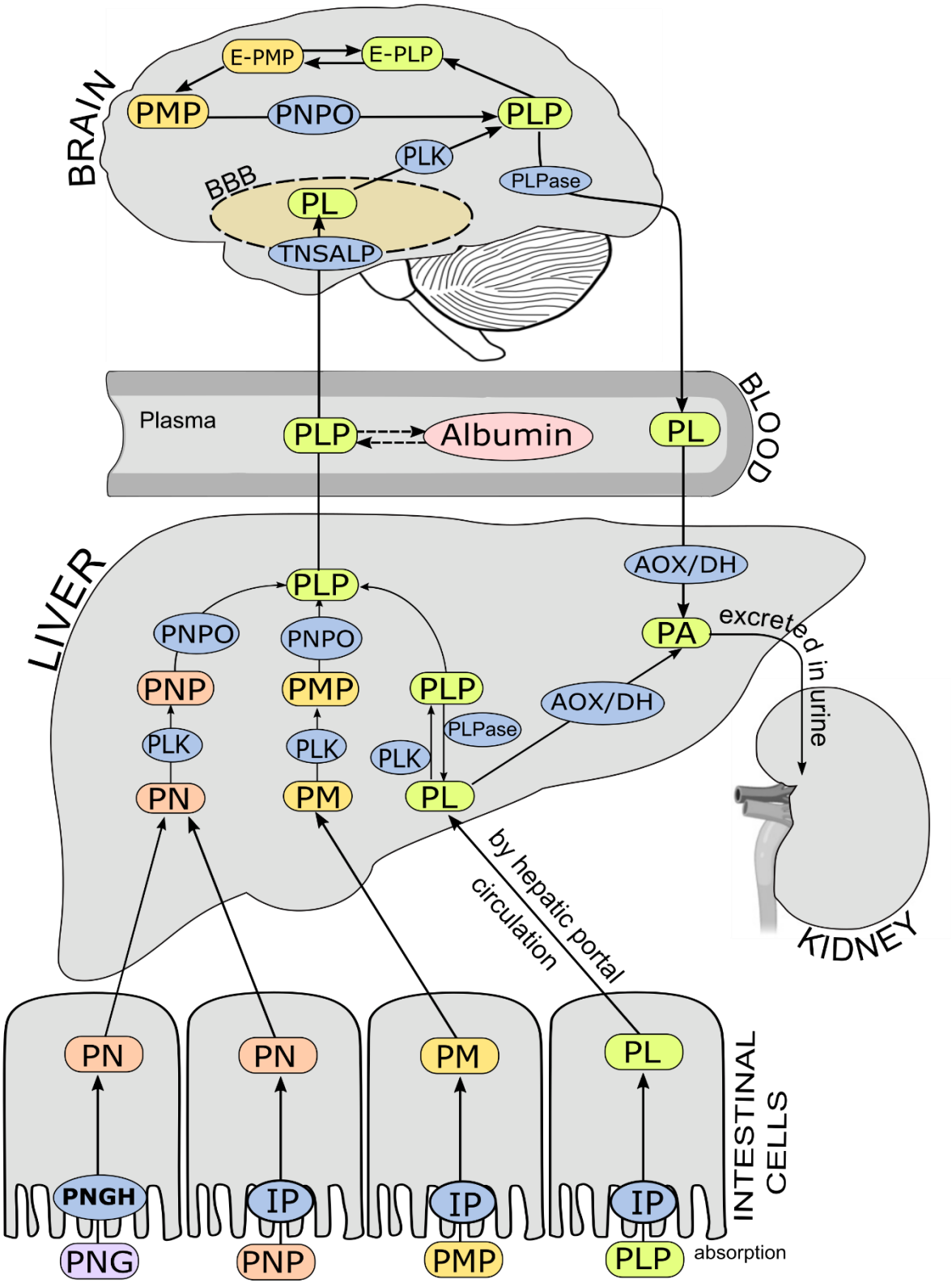
BRAIN
E-PMP
E-PLP
PMP
PNPO
PLP
PLK
PLPase
BBB
PL
TNSALP
BLOOD
Plasma
PLP
Albumin
PL
LIVER
PLP
AOX/DH
PNPO
PNPO
PA
excreted in urine
PNP
PMP
PLP
AOX/DH
PLK
PLK
PLPase
PLK
PN
PM
PL
by hepatic portal circulation
KIDNEY
PN
PN
PM
PL
INTESTINAL CELLS
PNGH
IP
IP
IP
absorption
PNG
PNP
PMP
PLP

Fig. 1-3: Metabolism of vitB6 vitamers in different tissues of the body. PNGH: PNG hydrolase; PLPase: PL phosphatase; AOX/DH: aldehyde oxidase/ dehydrogenase; BBB: blood-brain barrier; PA: pyridoxic acid; E-PLP: Enzyme-bound PLP; E-PMP: Enzyme-bound PMP. [vitamer routes from Wilson et al. (2019) and Darin et al. (2016)].

In addition to the liver, Albersen et al. (2013) suggested that the intestine is also an important organ for vitB6 metabolism. Using human intestinal epithelial Caco-2 cells as a model, Albersen et al. (2013) showed that incubation of enterocytes with different vitB6 vitamers resulted in PL being the only vitamer excreted at the basolateral side, which suggests that both PN and PM were converted to PL inside the intestinal cells. Basolateral PN and PM excretion was only observed when concentrations of these vitamers at the apical side were high. These results suggested that in normal dietary conditions PN and PM are converted to PL by intestinal cells, and then PL becomes the main vitamer that reaches the portal circulation. The liver and all other organs can then take up PL from the circulation and only require PLK to generate PLP. However, if amounts of PN or PM are ingested that exceed the capacity of the intestine to fully convert these vitamers to PL, then PN and PM will be released to the portal circulation and will be metabolized to PLP in the liver. The study also demonstrated full expression of the salvage enzymes in Caco-2 cells and in lysates of human intestine, further supporting a major role of the intestine in vitB6 metabolism (Albersen et al., 2013).

1.1.2 Catabolism of vitamin B6

At the other end of vitB6 metabolism, little is known about the catabolic pathways in humans or other mammals. In contrast, these mechanisms are well established in microorganisms (Footitt et al., 2013; Mooney et al., 2009; Mukherjee et al., 2011). In humans and other mammals, 4-pyridoxic acid (4-PA), which is excreted in urine, is the primary and principal product of the degradation of PLP (and all other B6 vitamers). This catabolite is formed in two steps. The first

step is hydrolysis of PLP to PL by an intracellular enzyme known as PL phosphatase (PLPase), followed by oxidation of PL by a non-specific aldehyde oxidase (AOX) or aldehyde dehydrogenase (Fig. 1-3) (Albersen et al., 2013; Gregory & Kirk, 1979; Mooney et al., 2009; Mukherjee et al., 2011; Wilson et al., 2019). In microorganisms, 4-PA is further degraded to other metabolites that can be utilized by the cell in various biochemical processes (Mukherjee et al., 2011). Some microbial vitB6 catabolic intermediates like 5-pyridoxic acid (5-PA), 5-pyridoxolactone (Mahuren et al., 1991) and 4-pyridoxolactone (Edwards et al., 1990; Mahuren et al., 1991) have been also detected in human subjects under high vitB6 intakes. Several other PN metabolites have been shown to exist in humans and/or other mammalian species, but the biochemical pathways associated with these secondary metabolites and their precise functions have not been clearly resolved.

For example, Coburn and Mahuren (1987) identified pyridoxine 3-sulfate, pyridoxal 3-sulfate and *N*-methylpyridoxine in domestic cats' urine, and, intriguingly, these compounds were excreted at amounts higher than 4-PA, even with moderate supplementation of PN. A number of PM derivatives were also detected in the urine of PM-treated diabetic and obese rats (Metz, Alderson, Chachich, et al., 2003; Metz, Alderson, Thorpe, et al., 2003). Moreover, at least nine unidentified vitB6 metabolites were detected in human urine after oral administration of radiolabeled PN (Coburn and Mahuren, 1987; Mahuren et al., 1991).

Oxidation of PN at the 5' position, followed by sequential dehydrogenation to form 5-PA, is known to exist only in the PN catabolic pathway of some bacterial species like *Pseudomonas* IA and *Arthrobacter* Cr-7, where the enzymes catalyzing these reactions have been characterized (Mukherjee et al., 2011). Similar reactions have been proposed to occur in mammals based on experimental clues. The first one was provided by the study of Coburn and colleagues (Coburn

and Mahuren, 1976) who showed that healthy men who ingested a structural analog of PN, 4'-deoxypyridoxine, excreted 4'-Deoxy-5-pyridoxic acid in their urine. A similar experiment was carried out in guinea pigs (Coburn et al., 1989), and the results indicated that these animals were also able to convert 4'-deoxypyridoxine to 4'-deoxy-5-pyridoxic acid. All together, these studies provided evidence for the possible existence of alternative but currently undiscovered catabolic routes of PN in humans and other mammals.

1.1.3 Vitamin B6 transportation across cellular membrane

Accumulating experimental evidence indicates that, as with most water-soluble vitamins (McCormick, 1994), the entry of vitB6 into mammalian cells is carrier-facilitated. Research in cultured human cells demonstrated the existence of an efficient and specific carrier-mediated mechanism of vitB6 uptake by human intestinal (Albersen et al., 2013; Said et al., 2003), colonic (Said et al., 2008), and renal cells (Said et al., 2002). Such a specific transporting membrane carrier was employed recently to produce a high affinity gene delivery system into cancer cells using a vitB6-coupled vector (Pandey et al., 2013). In animals, the work by Zhang and McCormick (1991) showed that importing of vitamin B6 by renal proximal tubular cells from rat is facilitated and Na^+-dependent. Despite the biochemical characterization of vitB6 uptake, its transporter proteins and their encoding genes have not yet been elucidated in any mammalian species (Albersen et al., 2013; Said, 2011). Among eukaryotes, the only vitB6 transporters identified so far are the yeast transporters, Tpn1p (Stolz & Vielreicher, 2003) and Bsu1 (Stolz et al., 2005), and, recently, PUP1 in plant species *Arabidopsis* (first to be identified in plants) (Szydlowski et al., 2013).

1.1.4 Physiological roles of vitamin B6

PLP, the coenzymatically active form of vitamin B6, plays an important role in maintaining the biochemical homeostasis of the body (Lee et al., 2008). In the human body, PLP is an essential cofactor for more than 140 distinct enzymatic activities, mainly associated with synthesis, degradation and interconversion of amino acids as well as with neurotransmitter metabolism (Dakshinamurti and Dakshinamurti, 2007; Nichols and Gaiteri, 2014; Barbara Plecko et al., 2014; Sorolla et al., 2010). PLP-dependent enzymes are also involved in a multitude of other cellular processes, including biologically active amine biosynthesis, lipid metabolism, heme synthesis, nucleic acid synthesis, protein and polyamine synthesis and several other metabolic pathways (Fig. 1-5) (Ghatge et al., 2012; Wilson et al., 2019). Furthermore, PLP is important in energy homeostasis through glycogen degradation and gluconeogenesis, since PLP is a cofactor for glycogen phosphorylase and gluconeogenic transaminases (Nichols & Gaiteri, 2014; Ulvik et al., 2014). In one-carbon metabolism that is mediated by folate, PLP serves as a cofactor for two isoenzymes, namely the cytoplasmic (SHMT1) and mitochondrial (SHMT2) forms of serine hydroxymethyltransferase. Folate-mediated one-carbon metabolism is an important pathway for a number of cellular processes, including biosynthesis of purines and thymidine, DNA methylation and redox homeostasis (Ducker & Rabinowitz, 2017; Nichols & Gaiteri, 2014).

As a coenzyme for the synthesis of several neurotransmitters including D-serine, D-aspartate, L-glutamate, glycine, γ-aminobutyric acid (GABA), serotonin, epinephrine, norepinephrine, histamine and dopamine, PLP is an important vitamer for normal brain function (Ghatge et al., 2012; Surtees et al., 2006). For example, PLP is an obligatory cofactor for the enzyme glutamate decarboxylase (GAD), that is required for the synthesis of GABA (a major inhibitory neurotransmitter in the central nervous system -CNS-) from L-glutamate. L-glutamate,

a major excitatory neurotransmitter, is synthesized from branched-chain amino acids like leucine and valine by the action of the PLP-dependent enzyme branched-chain amino acid aminotransferase (BCAT) (Ghatge et al., 2012). Another important PLP-dependent enzyme in the brain is aromatic L-amino acid decarboxylase (AADC), which catalyzes the final steps in the biosynthetic pathways of serotonin and dopamine (Fig. 1-4) (Ghatge et al., 2012; Nichols & Gaiteri, 2014). These neurotransmitters also serve as precursors for other important compounds in the brain, specifically melatonin, norepinephrine and epinephrine (Fig. 1-4) (Ghatge et al., 2012; Luboshitzky et al., 2002).

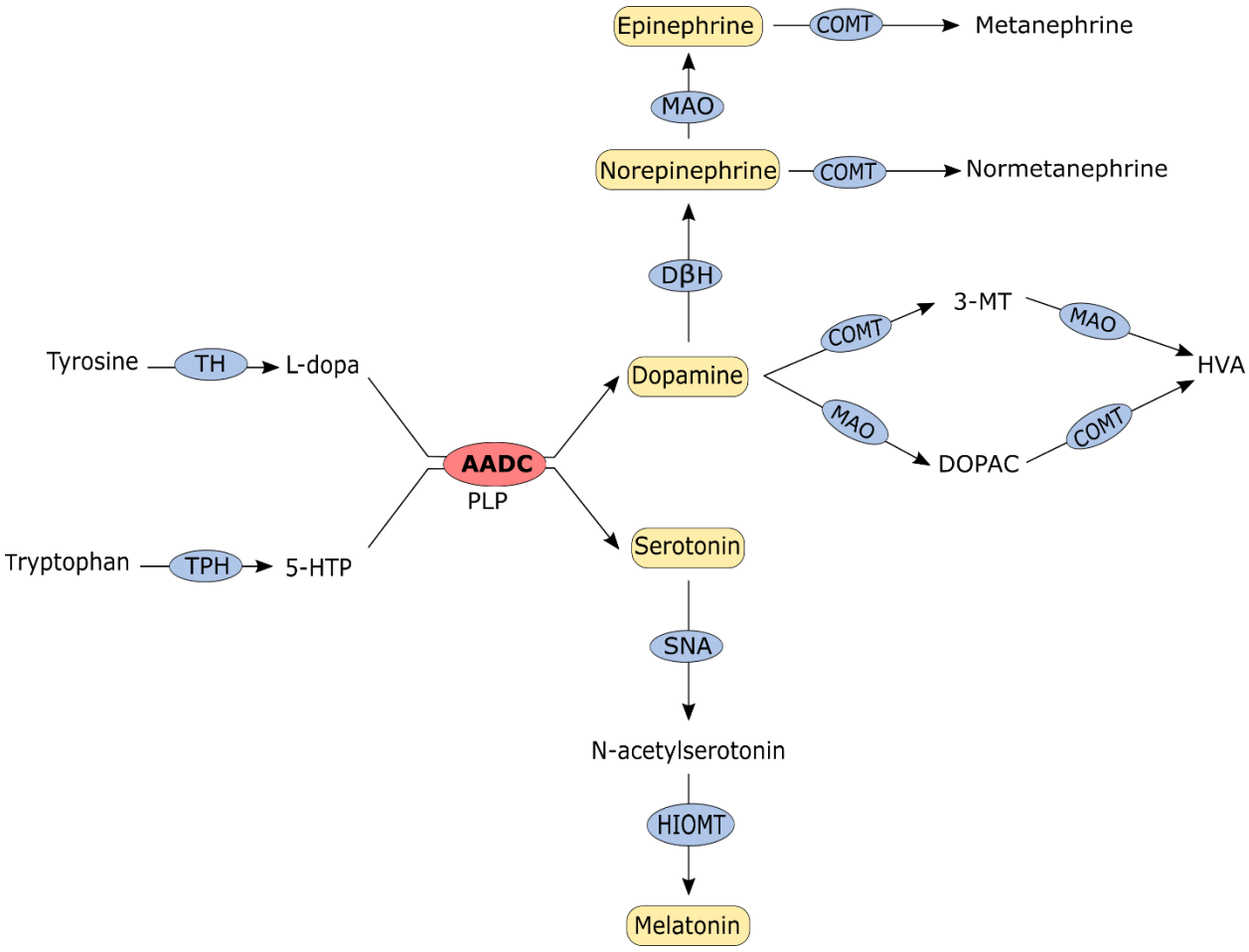

Fig. 1-4: Biosynthetic pathway for biogenic amine neurotransmitters and melatonin. The PLP-dependent enzyme, AADC, catalyzes a central step in this pathway. TH: tyrosine hydroxylase; TPH: tryptophan hydroxylase; L-dopa: levodopa; 5-HTP: 5-hydroxytryptophan; DβH: dopamine β-hydroxylase; MAO: monoamine oxidase; SNA: serotonin *N*-acetylase ; HIOMT: hydroxyindole *O*-methyltransferase; COMT: catechol-*O*-methyltransferase; 3-MT: 3-methoxytyramine; HVA: homovanillic acid; DOPAC: 3,4-dihydroxyphenylacetic acid. (Hyland, 1999; Korevaar & Grossman, 2011).

In addition to its role as an enzymatic cofactor, PLP has been shown to play a role in preventing DNA damage (Kanellis et al., 2007) and in modulating the activity and expression of steroid hormone receptors (Allgood & Cidlowski, 1992; Wilson et al., 2019). vitB6 has also been described as an efficient antioxidant in plants and fungi, with the ability of its different vitamers to quench reactive oxygen species (Bilski et al., 2000; di Salvo et al., 2011; Hellmann & Mooney, 2010).

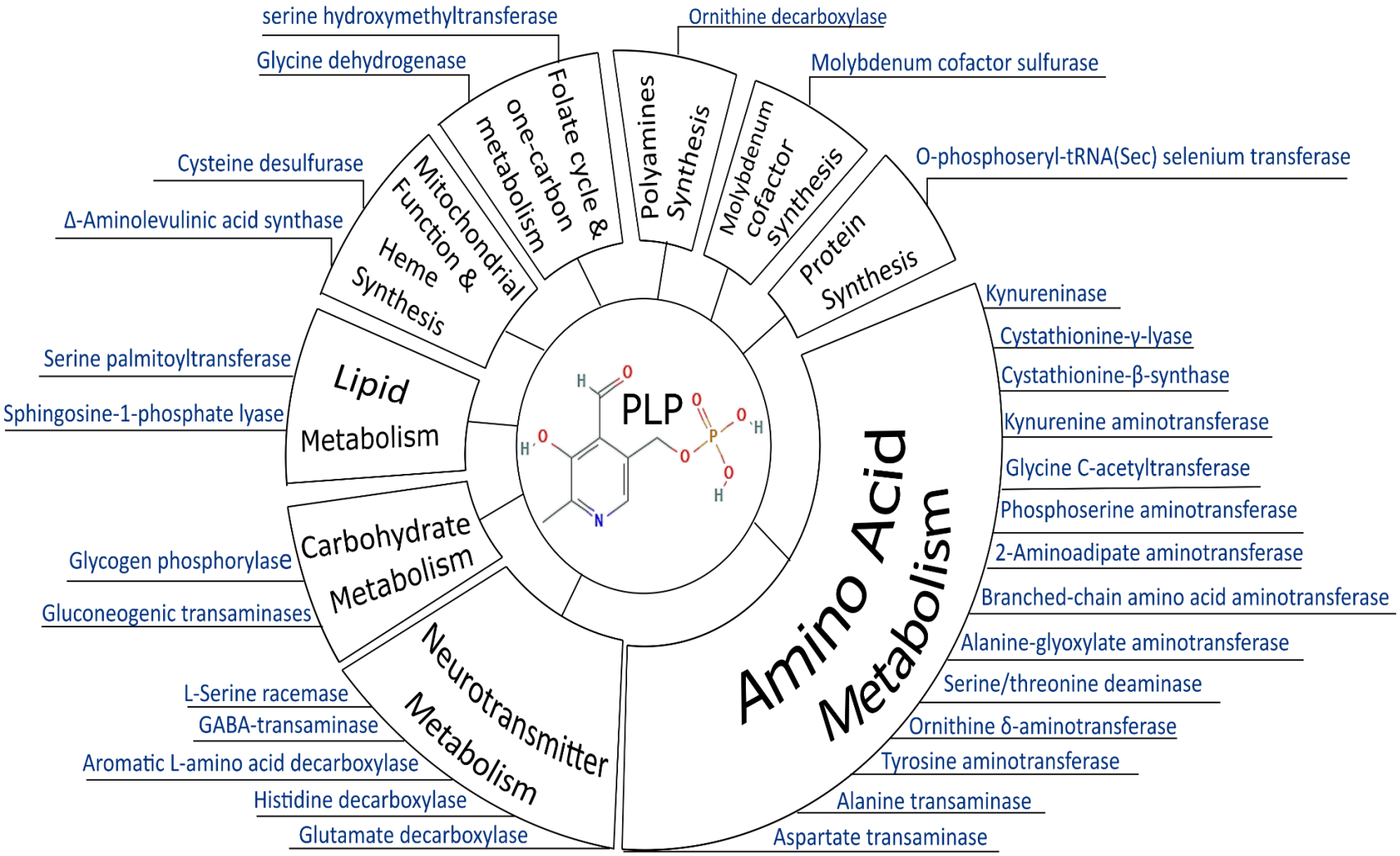

Fig. 1-5: The diverse cellular functions of PLP. Names in blue are the PLP-dependent enzymes involved in each metabolic process. Some enzymes can be implicated in mutiple processes. An example is branched-chain amino acid aminotransferase which can fall under amino acid and neurotransmitter metabolism. Glycine dehydrogenase can be classified under folate cycle and amino acid and neurotransmitter metabolism (Locasale, 2013; Wilson et al., 2019). PLP chemical structure was retrieved from PubChem database.

1.1.5 PLP homeostasis and its importance for human health

PLP is a very reactive compound because of its aldehyde group at the 4' position which can undergo spontaneous complexation with other molecules within the cell (Clayton, 2006; di Salvo et al., 2011). It may bind with amino groups in proteins and disrupt their structure (Wilson et al., 2019). For example, it has been shown that PLP can react with the lysine residue in the active site of human DNA topoisomerase I, causing its inhibition (Christmann-Franck et al., 2007; Vermeersch et al., 2004). Through a chemical reaction known as Knoevenagel condensation, PLP can also react with intermediate metabolites like Δ^1-pyrroline 5-carboxylate and Δ^1-piperideine 6-carboxylate, which form the molecular basis of PLP depletion in the neurometabolic diseases ALDH7A1 deficiency and hyperprolinaemia type II, respectively (Wilson et al., 2019). Because of its high reactivity and to prevent toxic accumulation of this cofactor, the intracellular pool of free PLP is maintained at very low concentration (about 1 µM in eukaryotic cells) (di Salvo et al., 2011; Ghatge et al., 2012; Wilson et al., 2019). It is therefore likely that PLP production in the cell is tightly regulated (Ghatge et al., 2012), and experimental work indicates the presence of an efficient mechanism that maintains intracellular PLP levels within optimum levels (Albersen et al., 2013). However, how the concentration of PLP is controlled in mammalian tissues is not entirely understood (Lee et al., 2008; Mooney et al., 2009).

A number of mechanisms have been proposed that help in PLP homeostasis. First, both enzymes that produce PLP, PLK and PNPO, are inhibited by their product PLP and its rate of synthesis can, therefore, be controlled by this feedback inhibition (di Salvo et al., 2011; Ghatge et al., 2012; Wilson et al., 2019). Enzymes that degrade PLP and PL, like PLPP and AOX, respectively, have also been proposed as a mechanism that keeps free PLP at low level within the cell (di Salvo et al., 2011; Ghatge et al., 2012; Wilson et al., 2019). Proteins that are known to

naturally bind PLP, like muscle glycogen phosphorylase, plasma albumin and hemoglobin in red blood cells, contribute to reducing the amount of free reactive PLP (Wilson et al., 2019).

Conditions that disrupt cellular PLP homeostasis can cause disease. For example, inactivation of PLPP in mice led to increase in PLP levels, anxiety and motor deficits (Jeanclos et al., 2019). In humans, intake of high doses of vitB6 is known to cause motor and sensory neuropathies (di Salvo et al., 2011; Ghatge et al., 2012). Deficiency of PLP in the cell is also implicated in several pathologies, most notably the so-called vitB6-dependent epileptic encephalopathies (Clayton, 2006; di Salvo et al., 2011; Ghatge et al., 2012; Plecko et al., 2014).

1.2 VitB6-dependent epileptic encephalopathies

VitB6-dependent epileptic encephalopathies (B6EEs) represent a clinically and genetically heterogeneous group of rare, autosomal recessive disorders (Basura et al., 2009; Baumgartner-Sigl et al., 2007). These debilitating conditions are characterized by recurrent seizures in the prenatal, neonatal, or postnatal period, which are typically resistant to conventional anticonvulsant treatment but well-controlled by the administration of PN or PLP (Baumgartner-Sigl et al., 2007; Mills et al., 2005; Striano et al., 2009; Walker et al., 2000). In addition to seizures, children affected with B6EEs may also suffer from developmental and/or intellectual disabilities, along with structural brain abnormalities (Stockler et al., 2011). The following types of B6EEs are known to date: PN-dependent epilepsy due to ALDH7A1 (antiquitin) deficiency (PDE-ALDH7A1) (MIM: 266100), hyperprolinemia type 2 (MIM: 239500), PLP-dependent epilepsy due to PNPO deficiency (MIM: 610090), hypophosphatasia (MIM: 241500), hyperphosphatasia with mental retardation syndrome (OMIM Phenotypic Series: PS239300), and PLPBP deficiency (MIM: 617290) (Clayton, 2006; Darin et al., 2016; Knaus et al., 2016; Stockler et al., 2011; Wilson et al., 2019) (Table 1-1). The pathological mechanisms underlying these subtypes of vitB6-dependent epilepsies can be

classified into 3 categories: 1) defects in amino acid metabolic pathways leading to accumulation of toxic metabolites that react with and inactivate PLP as in PDE-ALDH7A1 and hyperprolinemia type 2, 2) defects in the biochemical pathways that interconvert B6 vitamers as in PNPO deficiency, and 3) disorders affecting the mechanism of cellular uptake of PLP (hypo- and hyperphosphatasias) (Clayton, 2006; Wilson et al., 2019) (Table 1-1). In a recently discovered type, PLPBP deficiency, the exact mechanism that disrupts PLP homeostasis is not fully understood (Darin et al., 2016).

Hyperphosphatasia with mental retardation (HPMR) syndrome (also known as Mabry syndrome) refers to a group of congenital disorders caused by defects in the biosynthetic pathway of glycosyl phosphatidylinositol (GPI) anchor. GPI-anchor is a glycolipid that is required for tethering of TNSALP and several other proteins (more than 150 in total) to the cell surface and at the blood-brain barrier (BBB) (Knaus et al., 2016; Wilson et al., 2019). Six subtypes of HPMR syndrome have been identified to date with variable phenotypic spectrum that extends from mild nonsyndromic intellectual disability (ID) to more complex forms with severe ID, seizures, increased serum alkaline phosphates and dysmorphic features (Doğan et al., 2019; Horn et al., 2011). Table 1-1 lists the specific features of one example of HPMR syndrome, PIGV deficiency.

Table 1-1: Summary of the genetic, biochemical and clinical features of vitB6-dependent epileptic encephalopathies.

Disease name	**PN-dependent epilepsy (PDE-ALDH7A1)**	**PLP-dependent epilepsy**	**Hyperprolinemia type 2**	**Hypophosphatasia**	**HPMR syndrome due to PIGV deficiency**	**PLPBP deficiency**
Affected gene	*ALDH7A1*	*PNPO*	*ALDH4A1*	*ALPL*	*PIGV*	*PLPBP*
Affected enzyme or protein/ pathway(s)	α-AASA dehydrogenase/ lysine catabolism pathway	PNP oxidase/ vitB6 salvage pathway	P5C dehydrogenase/ Proline catabolism pathway	TNSALP/ Extracellular dephosphorylation of PLP, Bone mineralization	GPI-mannosyltransferase II/ GPI anchor biosynthesis pathway	PLPHP/ PLP homeostasis
Pathophysiological mechanism of PLP deficiency	Accumulating lysine metabolite, P6C, reacts with and inactivates PLP	PNPO is required for intracellular production of PLP from PNP/PMP	Accumulating proline metabolite, P5C, reacts with and inactivates PLP	TNSALP is required for extracellular conversion of PLP to PL to enable its cellular uptake	TNSALP ectoenzyme is anchored to cell surface by GPI anchor	PLPHP is required for maintaining cellular PLP homeostasis
Main clinical features	Neonatal seizures DD/ID	Neonatal seizures DD/ID	Infantile seizures DD/ID Ataxia	Rickets Osteomalacia Neonatal seizures	DD/ID Seizures dysmorphic features	Neonatal seizures DD/ID
Biomarkers (biofluid)	Elevated α-AASA (U/P), P6C (P), PIP (P)	Elevated PM/PA ratio (P)	Elevated Proline (P), P5C (U)	Low ALP (P), high PLP (P), high PE (U)	High ALP (P)	No specific biomarker
Commonly used vitB6 treatment	PN	PLP	PN	PN	PN	PN or PLP
References	(Clayton, 2006; Mills et al., 2006; Stockler et al., 2011)	(Mills et al., 2005; Wilson et al., 2019)	(Farrant et al., 2001; Geraghty et al., 1998; Stockler et al., 2011; Wilson et al., 2019)	(Clayton, 2006; Millán & Whyte, 2016; Rockman-Greenberg, 2013; Stockler et al., 2011)	(Knaus et al., 2016; Krawitz et al., 2010; Maeda et al., 2006; Stockler et al., 2011)	(Darin et al., 2016; Johnstone et al., 2019)

Abbreviations: α-AASA: α -aminoadipic semialdehyde; P6C: Δ^1-piperideine-6-carboxylic acid; DD: Developmental delay; ID: Intellectual disability; U: Urine; P: Plasma; PIP: Pipecolic acid; P5C: Pyrroline 5-carboxylic acid; ALP: Alkaline phosphatase; PE: Phosphatidylethanolamine GPI: Glycosyl phosphatidylinositol.

1.2.1 PN-dependent epilepsy

PN-dependent epilepsy (PDE-ALDH7A1) is the classical and most frequently encountered type of vitB6-dependent epileptic encephalopathy (Pena, MacKenzie, et al., 2017). The first case of this disease was described by Hunt and colleagues (1954), who reported a female infant with drug-resistant severe seizures that were effectively controlled by administration of PN. Convulsions recurred in this infant when PN treatment was discontinued. The authors used the term "PN dependency" to describe this novel condition. Since this first report, more than 200 cases of PDE-ALDH7A1 have been described; the estimated incidence rate of this rare disease based on clinical diagnosis ranges from 1: 783,000 to 1:20,000 (Baxter, 1999; Stockler et al., 2011). A recent study by Coughlin et al. (2018) assessed all known and predicted pathogenic variants in *ALDH7A1* reported in gnomAD database. Based on calculated allele frequencies, they estimated the incidence of PDE-ALDH7A1 to be 1:64,352 births. In search for the genetic cause, Cormier-Daire et al. (2000) studied 5 families with total of 10 PDE-affected individuals and was able to map the disease gene locus to chromosome 5q31. Six years later, the specific genetic cause of PDE-ALDH7A1 was identified by Mills et al. (2006) to be homozygous or compound heterozygous mutations in the *ALDH7A1* gene. The gene is also known as "antiquitin" (ATQ) because its sequence is highly conserved between different species all the way down the evolutionary ladder (Chan et al., 2011). *ALDH7A1* codes for α-aminoadipic semialdehyde dehydrogenase, an enzyme that functions within the lysine catabolism pathway in the brain and peripheral tissues (Mills et al., 2006).

1.2.1.1 Mechanism of PLP deficiency and diagnostic biomarkers in PDE-ALDH7A1

ATQ catalyzes the conversion of α-aminoadipic semialdehyde (α-AASA) to α-aminoadipic acid (α-AAA), an intermediate step in the lysine catabolism pathway (Brocker et al., 2011) (Fig.

1-6). In PDE-ALDH7A1, loss of the enzyme's function leads to the accumulation of three upstream lysine catabolites: Δ^1-piperideine-6-carboxylic acid (P6C), α-aminoadipic semialdehyde (α-AASA) and pipecolic acid (PIP) (Stockler et al., 2011) (Fig. 1-6). Through Knoevenagel condensation, accumulating P6C spontaneously conjugates with PLP, forming inactive complex products and causing cellular deficiency of this important cofactor (Mills et al., 2006). Measurement of these metabolites in PDE-ALDH7A1 patients revealed elevated concentrations of α-AASA in plasma (Plecko et al., 2007), cerebrospinal fluid (CSF) (Mills et al., 2006) and urine (Pérez et al., 2013; Plecko et al., 2007); PIP in plasma (Pérez et al., 2013; Plecko et al., 2000, 2007) and CSF (Pérez et al., 2013; Plecko et al., 2000); and P6C in plasma (Sadilkova et al., 2009) and urine (Struys et al., 2012). Therefore, α-AASA, PIP, and P6C have been established as diagnostic biomarkers for PDE-ALDH7A1 in patients.

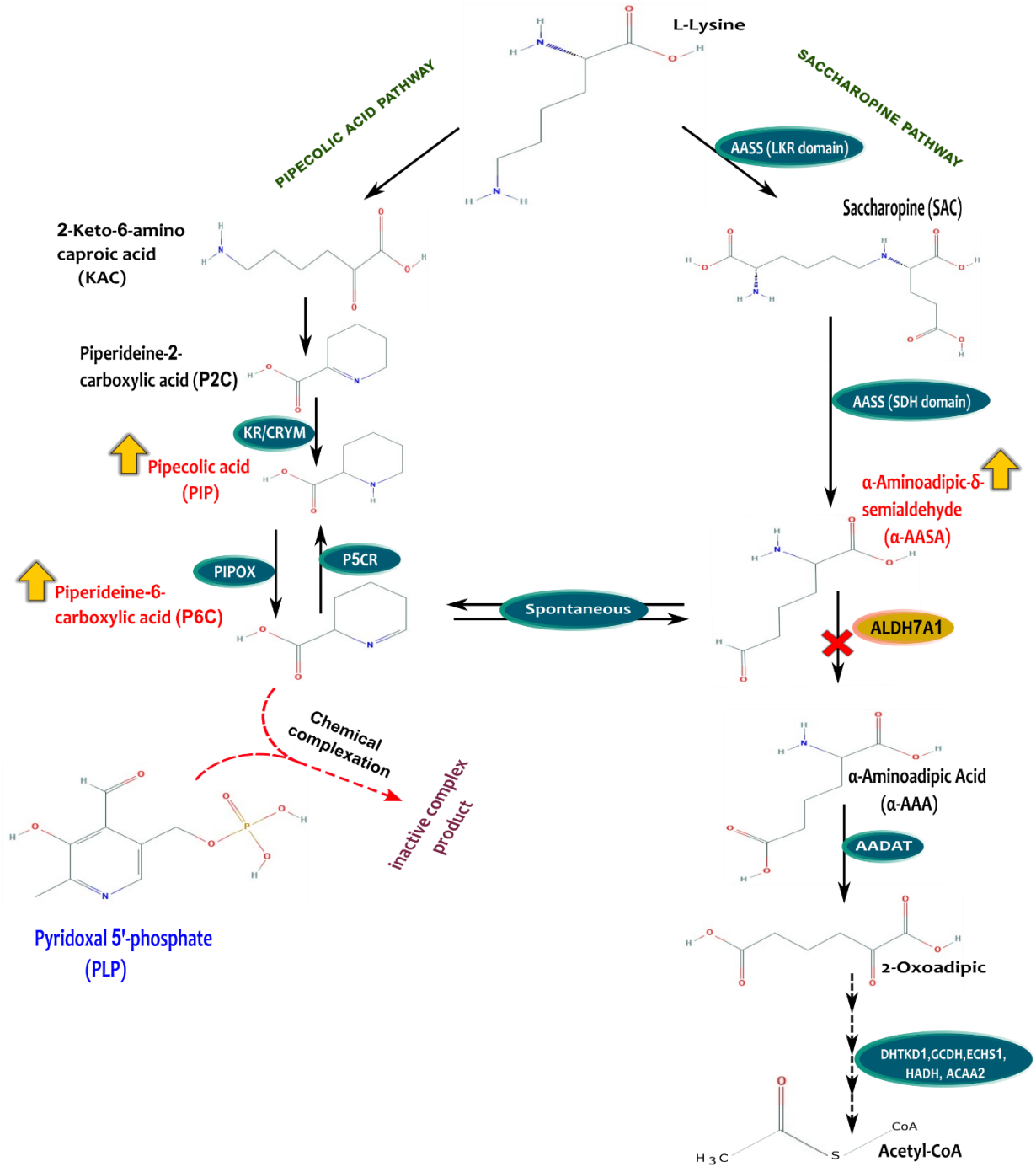

Fig. 1-6: Pipecolic acid (left) and saccharopine (right) pathways for L-lysine catabolism in mammals. The two pathways converge at the step of α-AASA/P6C synthesis. ALDH7A1 catalyzes the step indicated by the red "X". Inactivation of the enzyme in PDE-ALDH7A1 causes buildup of its two substrates, P6C and α-AASA, as well as of PIP (the 3 biomarkers in patients). Accumulating P6C condenses with PLP, forming an inactive product and leading to depletion of the cofactor. See Fig. 1-2 and 3 for PLP synthesis from vitB6 vitamers. AASS: Aminoadipic semialdehyde synthase; LKR: Lysine-ketoglutarate reductase;

Fig. 1-6 continued: SDH: Saccharopine dehydrogenase; AADAT: 2-aminoadipate aminotransferase; KR: Ketimine reductase; CRYM: Mu-crystallin homolog; PIPOX: Pipecolic acid oxidase; P5CR: Piperideine-5-carboxilic reductase; DHTKD1: Dehydrogenase E1 and transketolase domain containing 1; GCDH: Glutaryl-CoA dehydrogenase; ECHS1: Enoyl Coenzyme A hydratase short chain 1; HADH: Hydroxyacyl-Coenzyme A dehydrogenase; ACAA2: Acetyl-Coenzyme A acyltransferase 2 [based on Pena, Roussel, et al., (2017)].

1.2.1.2 Clinical features of PDE-ALDH7A1

Clinically, PDE-ALDH7A1 is characterized by recurrent perinatal-onset seizures that are resistant to conventional anticonvulsant treatment but show remarkable response to the administration of high doses of pyridoxine (PN) (Pena, MacKenzie, et al., 2017; Stockler et al., 2011). Seizures usually relapse when PN treatment is discontinued, either incidentally or for diagnostic purposes (Stockler et al., 2011). The interval from PN cessation to seizure recurrence can range from 1-51 days (Mills et al., 2010). Refractory seizures usually start within hours to days after birth (Pena, MacKenzie, et al., 2017). In a retrospective study of 63 PDE-ALDH7A1 patients, 44 (70%) had a neonatal onset of seizures (less than 4 weeks old) (Basura et al., 2009). In some cases, the mother of an affected child has described abnormal fetal movements during pregnancy, suggestive of pre-natal onset of seizures (Basura et al., 2009; Baxter, 2001; Bejsovec et al., 1967; Mills et al., 2010). In atypical cases, seizure onset can be delayed to up to 3 years of age (Stockler et al., 2011), and in one exceptional case, Srinivasaraghavan et al. (2018) reported an Indian female with genetically proven PDE-ALDH7A1 in whom seizures did not start until the age of 17 years (juvenile onset).

Various clinical seizure types have been described in PDE-ALDH7A1 patients, including clonic seizures (Goutières & Aicardi, 1985; Mills et al., 2010; Pérez et al., 2013), tonic seizures (Mills et al., 2010; Pérez et al., 2013), generalized tonic clonic seizures (Al Teneiji et al., 2017),

myoclonic seizures (Al Teneiji et al., 2017; Basura et al., 2009; Coker, 1992; Mills et al., 2010; Pérez et al., 2013), focal and multifocal seizures (Al Teneiji et al., 2017; Pérez et al., 2013), oculogyric seizures (Pérez et al., 2013), absence seizures (Al Teneiji et al., 2017; Coker, 1992), and infantile spasms (Basura et al., 2009; Pérez et al., 2013). Status epilepticus may occur in children with PDE-ALDH7A1 (Basura et al., 2009; Kluger et al., 2008; Mills et al., 2010; Pérez et al., 2013; van Karnebeek et al., 2016).

In addition to seizures, most PDE-ALDH7A1 patients also suffer from developmental delay and moderate to severe intellectual disability along with a variety of structural brain abnormalities (Pena, MacKenzie, et al., 2017; Stockler et al., 2011). van Karnebeek et al. (2016) reviewed the clinical features of 266 published PDE-ALDH7A1 cases with confirmed ATQ deficiency and found that about 70% of patients were affected with developmental delay and/or intellectual disability despite effective control of seizures with PN. In addition, as revealed by neuroimaging analysis, a spectrum of structural brain defects have been described in affected children with anomalies of corpus callosum (agenesis/hypoplasia/dysplasia) and white matter being common features (Friedman et al., 2014; Mills et al., 2010; van Karnebeek et al., 2016). Other reported congenital brain malformations include delayed myelination, cortical atrophy (Al Teneiji et al., 2017), ventriculomegaly (Mills et al., 2010; Pérez et al., 2013), white matter lesions, hydrocephalus, cerebral atrophy, cortical dysplasia (Mills et al., 2010) and mega cisterna magna (Pérez et al., 2013). Many of these structural abnormalities of the brain seem to be of prenatal origin as revealed by fetal neuroimaging performed in PDE-ALDH7A1 cases (Jain-Ghai et al., 2014; Marguet et al., 2016). Motor deficits (hypotonia/hypertonia/dystonia), irritability, autism spectrum disorder (ASD), attention-deficit hyperactivity disorder (ADHD) and anxiety have all

been described in patients with PDE-ALDH7A1 (Al Teneiji et al., 2017; Mills et al., 2010; van Karnebeek et al., 2016).

The phenotypic spectrum of PDE-ALDH7A1 may also include non-neuronal features, but these are less frequently observed in patients. Reported examples are ocular problems, hypoglycemia, hypothyroidism, lactic acidosis, profound electrolyte disturbances, diabetes insipidus, respiratory distress and hypotension (Mercimek-Mahmutoglu et al., 2012; Stockler et al., 2011; van Karnebeek et al., 2016; Yusuf et al., 2013).

1.2.1.3 Biochemical abnormalities in PDE-ALDH7A1

In PDE-ALDH7A1, blockade of the ATQ-catalyzed step in the lysine catabolism pathway leads to accumulation of 3 upstream metabolites, P6C, α-AASA and PIP, as discovered by screening of patients' body fluids. Presence of these metabolites in supraphysiological levels is considered the hallmark biochemical feature of ATQ deficiency (Pena, MacKenzie, et al., 2017). Recently, two additional lysine metabolites discovered to accumulate in patients have been suggested as novel biomarkers. The first one is 6-oxopipecolate (6-oxo-PIP), which was found to be present in large concentrations in blood, plasma, urine, and CSF of ATQ deficiency patients (Wempe et al., 2019). By means of an untargeted metabolomics approach, Coene et al. (2019) identified another novel metabolite, 6-(2-oxopropyl)piperidine-2-carboxylic acid, that accumulated in plasma of affected individuals. However, the exact route by which these metabolites are derived from lysine and their functional effects, if any, are still unclear.

Because P6C inactivates PLP and causes cellular depletion of this enzymatic cofactor, a number of biochemical abnormalities occur that are associated with secondary deficiencies of PLP-dependent enzymes, mainly affecting amino acid and neurotransmitter metabolism.

Table 1-2 summarizes amino acid changes reported in PDE-ALDH7A1 patients and possible links to PLP-dependent enzymes in their metabolic pathways. Neurotransmitter alterations have been also described in PDE-ALDH7A1 patients, most commonly affecting biogenic amine neurotransmitters.

The PLP-dependent enzyme, AADC, plays a central role in the biosynthetic pathways of these neurotransmitters (Fig. 1-4). Mills et al. (2010) reported elevated levels of 3-*O*-methyldopa (3-OMD) in pre-treatment CSF samples of three PDE-ALDH7A1 patients. 3-OMD is a metabolite of L-dopa, the direct precursor of dopamine (Hyland, 1999). 3-OMD was also found to be present in very high concentrations in CSF samples of three other PDE-ALDH7A1 patients reported by Pérez et al. (2013). The same study also found low CSF concentrations of homovanillic acid (HVA), a downstream metabolite of dopamine (Hyland, 1999), in two patients (Pérez et al., 2013).

1.2.1.4 Neuropathological abnormalities in PDE-ALDH7A1

There are only few studies on histopathological analysis of postmortem brain specimens from PDE-ALDH7A1 patients. The most comprehensive one was performed by Jansen et al. (2014), who performed neuropathological examination of surgically resected and postmortem brain specimens from a child affected with PDE-ALDH7A1 who died at the age of 9 years. Histologic analysis showed the presence of aberrant radial neuronal organization in the cortex, a feature that is typical of type Ia focal cortical dysplasia (FCD-Ia). Heterotopic neurons were noted in the subcortical white matter. The hippocampi were sclerotic and showed severe neuronal loss in CA1, CA3, and the dentate gyrus. Gliosis was observed in several regions including the cortex, ependyma of the lateral ventricles, basal ganglia and the cerebellar deep nuclei. Bergmann gliosis was also noted in the cerebellar cortex along with patchy loss of Purkinje cells. Neuronal ferrugination was evident in the basal ganglia and thalamus. The authors concluded that these

neuropathological findings indicate a defect in the neuronal migration process during early development of the brain and attributed this to glial cell dysfunction in PDE-ALDH7A1 (Jansen et al., 2014). In another study, Marguet et al. (2016) performed autopsy and immunohistochemical studies in postmortem brain from a child with PDE-ALDH7A1 who died at the age of 14 months. This analysis revealed a number of neuropathological abnormalities, including neuronal loss and diffuse vacuolization in the cortex and ischemic necrosis with gliosis in the white matter. The pyramidal tracts were dysmorphic and misplaced. Similar to the study of Jansen et al. (2014), there were cortical dyslamination (but without microcolumnar organization) and hippocampic sclerosis.

Table 1-2: Amino acid changes in PDE-ALDH7A1 and possible affected PLP-dependent enzymes in their metabolic pathways.

Amino acid *(tissue/fluid, change)******	**Implicated PLP-dependent enzyme(s)**** *(Enzyme Commission number)*	**Enzyme's function****
Glycine (CSF & plasma, ↑)	Glycine dehydrogenase (decarboxylating) (EC 1.4.4.2)	Important component of the glycine cleavage system
Threonine (CSF, ↑)	Glycine C-acetyltransferase (EC 2.3.1.29)	Catalyzes the second step in the pathway that converts threonine to glycine
	Threonine deaminase (EC 4.3.1.19)	Catalyzes the first step in the catabolic pathway of threonine (Yuzyuk et al., 2016)
Methionine (CSF, ↑)	None that is directly involved in methionine metabolism	Not applicable
Serine (plasma, ↑)	• Serine dehydratase (EC 4.3.1.17) • Serine hydroxymethyltransferase (EC 2.1.2.1) (Bender, 2012)	Involved in breakdown/conversion of serine to other metabolites
Proline (plasma, ↑)	None that is directly involved in proline catabolism	Not applicable

Table 1-2 continued:		
Amino acid *(tissue/fluid, change)****	**Implicated PLP-dependent enzyme(s)**** *(Enzyme Commission number)*	**Enzyme's function****
Alanine (CSF & plasma, ↑)	• Alanine-glyoxylate aminotransferase (EC 2.6.1.44) • Alanine transaminase (EC 2.6.1.2)	Involved in breakdown/conversion of alanine to other metabolites
Citrulline (plasma, ↓)	None that is directly involved in citrulline metabolism	Not applicable
Phenylalanine (CSF, ↑)	Aromatic L-amino acid decarboxylase (EC 4.1.1.28)	Converts phenylalanine to phenethylamine
Glutamine (CSF & plasma, ↑)	None that is directly involved in glutamine metabolism	Not applicable
Taurine (CSF & plasma, ↑)	None that is directly involved in taurine catabolism	Not applicable
Arginine (CSF, ↓)	Ornithine δ-aminotransferase (EC 2.6.1.13)	Catalyzes the formation of ornithine, an indirect precursor for arginine synthesis (Mills et al., 2005; Palanza et al., 2016)
Histidine (CSF, ↑)	Histidine decarboxylase (EC 4.1.1.22)	Converts histidine to histamine

* Amino acid changes were retrieved from the case series of Mills et al. (2010) and Yuzyuk et al. (2016). ↑: elevated, ↓: lowered

** Unless another source is specified, information on PLP-dependent enzymes and their catalytic activities were collectively retrieved from the review of Wilson et al. (2019) and KEGG Pathway database (Kanehisa & Goto, 2000).

1.2.1.5 Current treatment of PDE-ALDH7A1 and its outcome

In patients with PDE-ALDH7A1, seizures are effectively controlled by PN treatment in about 90% of cases (Wilson et al., 2019). Patients require lifelong intake of pharmacological doses of PN for seizure control as PN withdrawal leads to seizure recurrence (Stockler et al., 2011). To achieve seizure control in infants, the therapeutic dose of PN usually ranges from 15 – 30 mg/kg/day or as high as 200 mg/day in neonates and 500 mg/day in adults (Stockler et al., 2011).

In some cases, seizure suppression could be obtained with a much lower dose of PN (1 mg/kg/day), while other patients required a very high daily dose of 67.8 mg/kg (or 2,500 mg/day) (Basura et al., 2009). In comparison, the recommended daily allowance for pyridoxine is 40–300 µg in healthy children (Baxter, 2003) and 2.0–2.2 mg in healthy, nonpregnant adults (Levine & Saltzman, 2002). Some treated patients suffer breakthrough seizures during febrile illnesses, in which case a higher dose of PN is required for seizure control (Stockler et al., 2011). PLP, either alone or in combination with PN, has also been used to treat seizures in some cases (Basura et al., 2009).

In a subset of patients with ATQ deficiency, better seizure control is achieved when folinic acid is added to the PN regimen (known as folinic-acid responsive seizures or FARS) (Stockler et al., 2011). The subset of FARS patients can be distinguished by the appearance of a characteristic peak (Peak X) on CSF biogenic amine neurotransmitter analysis (Gallagher et al., 2009; Stockler et al., 2011). The exact mechanism behind seizure response to folinic acid and the identity of the "Peak X" metabolite are currently unknown.

Despite effective control of seizures with PN, treatment outcome is usually still poor, and a large proportion of children with PDE-ALDH7A1 have neurodevelopmental impairments (van Karnebeek et al., 2016). It has been suggested that PN monotherapy, even when started at early stage, is not sufficient to prevent the neurodevelopmental disabilities and brain structural malformations (Bok et al., 2012; Pena, MacKenzie, et al., 2017). In line with this, Friedman et al. (2014) analyzed brain magnetic resonance images (MRI) for 30 patients and found that all patients exhibited corpus callosum abnormalities. They also found that this common brain feature in PDE-ALDH7A1 did not correlate with treatment lag (i.e. time from seizure onset to initiation of PN treatment). Consistent with this finding, a long-term outcome study of a cohort of 14 Dutch patients

did not find a significant correlation between neurodevelopmental outcome and the age at which PN treatment was started (Bok et al., 2012).

In another study, Bok et al. (2010) compared the outcome of antenatal versus postnatal PN treatment in two families, each with two siblings affected with PDE-ALDH7A1. The study noted that antenatally treated children appeared to have higher IQ compared to their postnatally treated siblings. In contrast to this observation, Rankin et al. (2007) described 3 siblings with genetically proven PDE-ALDH7A1 who all had moderate to severe learning disabilities and brain abnormalities on MRI despite antenatal maternal PN treatment that was continued immediately after birth in two of them. Similar to their elder sibling who was not started on PN until the age of the 2 months, both of the prenatally treated children had poor cognitive outcome, although their seizures were well controlled and one of them had no documented seizures since birth (Rankin et al., 2007). Similarly, Marguet et al. (2016) reported unfavourable clinical outcome despite early postnatal PN treatment in 3 patients and antenatal PN supplementation in one of them.

A number of hypotheses have been put forward to explain the pervasive intellectual developmental disorder in PDE-ALDH7A1 patients even though their epilepsy is well-controlled. Jansen et al. (2014) suggested that PN treatment alone cannot prevent the accumulation of high levels of lysine intermediate metabolites (P6C, α-AASA and PIP) in the brain. These reactive compounds could be neurotoxic and thus contribute to the neuropathological phenotype in PDE-ALDH7A1 (Jansen et al., 2014). In line with this, Hassel et al. (2019) proposed that α-AASA, owing to its reactive aldehyde group, can non-enzymatically form adducts with cellular macromolecules like proteins, DNA and RNA that adversely affect their functions. In addition, these spontaneous reactions may also lead to the generation of a class of pathogenic compounds known as advanced glycation end products (AGEs), which are known to induce a pathological

type of inflammatory reaction by activation of RAGE receptors (Hassel et al., 2019). Accumulation of AGEs is thought to play a role in the neuropathology and cognitive dysfunction in Alzheimer's disease (Hassel et al., 2019; Srikanth et al., 2011).

Other authors suggested that ATQ might have another critical, yet unknown, function in brain development that is not compensated by PN treatment (Jansen et al., 2014; Marguet et al., 2016; Pena, Roussel, et al., 2017). In addition to its catalytic function in lysine degradation, ATQ has been described to play a role in cellular defence against osmotic (Brocker et al., 2010) and oxidative stress (Brocker et al., 2011) and in cell cycle progression (Chan et al., 2011).

1.2.1.6 Adjunct dietary treatments

In addition to PN, adjunct dietary therapies targeting reduction of lysine intake have been tested in PDE-ALDH7A1 patients. The approach is based on the observation that pathognomonic metabolites that accumulate in PDE-ALDH7A1 are derived from the lysine catabolism pathway. These metabolites, particularly P6C and α-AASA, are presumably cytotoxic and responsible for at least part of PDE-ALDH7A1 pathogenesis. Since lysine is the main substrate that fuels the production of these secondary metabolites, reducing lysine is expected to reduce the levels of its downstream catabolic by-products, including P6C and α-AASA, and thus improve the clinical outcome (Pena, MacKenzie, et al., 2017). The first trial of dietary lysine-restricted diet was carried out by van Karnebeek et al. (2012) and included 7 patients with evaluation of their biochemical and clinical outcomes before and after the dietary therapy. The study reported reduction in metabolite levels with the lysine-restricted diet that ranged from 20 – 67% for plasma PIP, 13 - 72% for urinary α-AASA, 45% for plasma α-AASA and 42% for plasma P6C. Four out of 5 patients showed improvement in neurodevelopmental skills after institution of the lysine-restricted diet (van Karnebeek et al., 2012). After this proof-of-concept study, more lysine-restriction trials

were carried out that also reported positive biochemical and neurodevelopmental outcomes in treated children (Mahajnah et al., 2016; Mercimek-Mahmutoglu, Corderio, et al., 2014; Yuzyuk et al., 2016). Two of these studies (Mahajnah et al., 2016; Mercimek-Mahmutoglu, Corderio, et al., 2014) described mild deficiency of serotonin in CSF as a side effect of lysine restriction.

Arginine supplementation was also tried as an alternative approach to lysine-restriction (Al Teneiji et al., 2017; Mercimek-Mahmutoglu, Cordeiro, et al., 2014). It is based on the fact that both amino acids, lysine and arginine, use the same transporter (known as the y + system) for their transportation across the BBB. Therefore, it was suggested that arginine could compete with lysine and limit its entry to the CNS (Mercimek-Mahmutoglu, Cordeiro, et al., 2014; Pena, MacKenzie, et al., 2017). Arginine fortification therapy was first proposed and tested in clinical trials by Mercimek-Mahmutoglu et al. (2014). In this study, a 12-year-old PDE-ALDH7A1 patient was started on arginine supplementation regimen of 400 mg/kg/day. His neuropsychological evaluation after 12 months of therapy showed improvements in both motor and cognitive abilities. Measurement of CSF α-AASA at 12 months post-therapy revealed 57% reduction in this metabolite compared to baseline level (Mercimek-Mahmutoglu, Cordeiro, et al., 2014).

In a more comprehensive approach, Coughlin et al. (2015) tested a combination therapy of lysine-restriction and arginine supplementation (in addition to PN treatment, therefore it was termed “triple therapy”) on 6 patients. The triple therapy led to decrease in lysine biomarkers in CSF, plasma, and urine. Introducing arginine supplementation to subjects already under lysine restriction and PN regimen led to further reduction in lysine metabolites and improved the neurodevelopmental outcome in some children (Coughlin et al., 2015).

1.3 Objectives

The main objectives of this thesis were 1) to improve our understanding of the clinical, biochemical and pathophysiological features of PLPHP deficiency using patients and model organisms, and 2) to generate and carry out phenotypic characterization of a mouse model of antiquitin (ALDH7A1) deficiency in order to evaluate its use as a model of PDE-ALDH7A1.

In the first part of this work, we described the clinical, genetic and biochemical features of PLPHP deficiency in 12 new patients and established a genotype-phenotype correlation based on the current and previously reported cases. We assessed mitochondrial function and quantified vitB6 vitamers in patient-derived fibroblasts. We then generated PLPHP deficiency models in zebrafish, yeast and HEK293 cells using targeted gene knockout approaches. We characterized the biochemical and pathophysiological consequences of PLPHP deficiency in these models.

In the second part of this work, we generated an *Aldh7a1*-knockout mouse model by blastocyst-microinjection of mouse embryonic stem cells carrying a conditionally-targeted allele for *Aldh7a1*. We produced three *Aldh7a1*-targeted strains of mice which are reporter-tagged, conditional floxed, and constitutive KO mice. We carried out subsequent phenotyping experiments on the constitutive KO mice.

We then performed phenotypic characterization of the biochemical, behavioral, neuropathological and electrophysiological abnormalities in *Aldh7a1*-KO mice under a regular diet containing low lysine level (0.9%). We started by biochemical analysis in which we quantified the concentrations of 5 lysine metabolites along with amino acids, vitB6 vitamers, neurotransmitters and oxidative stress marker in brain and liver tissues. We then conducted a

battery of neurobehavioral tests at two time points and qualitative neuropathology study. We finally assessed seizures in KO mice under the regular diet by *in vivo* electrophysiology.

Next, we carried out dietary manipulation experiments in which mice were switched to special diets containing variable amounts of lysine and PN. The first diet contained high lysine (4.7%) and minimal level of PN and was intended to test the susceptibility of KO mice to seizures by increasing the endogenous production of lysine metabolites. The second diet contained the same high level of lysine but was supplemented with more PN and was intended to test the effect of PN in controlling high lysine-induced seizures. Mice were divided into two cohorts, the first cohort received the first diet without further treatment, and the second cohort received the second diet in addition to PN injections. Survival and seizures were analyzed in these mice using EEG recording and visual inspection. Results are reported and discussed in the current thesis, and conclusions as well as future directions are expanded upon.

2 Clinical, genetic, biochemical, and mechanistic insights into PLPHP deficiency

2.1 Introduction

Pyridoxal 5'-phosphate (PLP), the bioactive form of vitamin B6 (vitB6), one of the most versatile organic cofactors in biology, is involved in a diverse array of cellular processes. Its widespread functions arise from its role as an essential co-enzyme for over 140 chemical reactions in the human body, accounting for 4% of all known catalytic activities classified by the Enzyme Commission (Amadasi et al., 2007; Mozzarelli & Bettati, 2006; Percudani & Peracchi, 2003). Although the main pathways of vitB6 metabolism have been characterized for long time (Lee et al., 2008), several aspects about its biology are still incompletely understood. For example, PLP is a highly reactive molecule and therefore cells maintain the pool of free PLP at very low concentration to avoid detrimental effects associated with its buildup (di Salvo et al., 2011; Ghatge et al., 2012). However, little is known about the mechanisms that effectively regulate PLP levels *in vivo* (Lee et al., 2008). Another long unresolved mechanism concerns how PLP is safely delivered to its dependent apoenzymes since its reactive aldehyde group readily forms aldimines with amino groups on non-vitB6 enzymes and amino acids (di Salvo et al., 2011; Ghatge et al., 2012).

The study of inborn errors affecting PLP homeostasis, like vitB6-dependent epileptic encephalopathies (B6EE), provides a unique tool to fill these knowledge gaps about vitB6 and about the role played by PLP-dependent enzymes in a variety of biological processes, and in pathological states. The disease described in this chapter is an example of how such studies provided a clue about a previously unknown function of a PLP-binding protein and how this could also answer a long-standing question about the secure cellular mechanisms that transfer PLP to apoenzymes. Biochemical and functional investigations of B6EE diseases are also important

clinically as identifying the pathobiochemical mechanism will help devise better treatments and biomarkers for early diagnosis. For example, identifying the blockade in lysine catabolism as the main biochemical defect in pyridoxine-dependent epilepsy (PDE-ALDH7A1) (Mills et al., 2006) has paved the road to develop adjunct treatments for PDE-ALDH7A1 patients like the use of lysine-restricted diet (Mahajnah et al., 2016; Mercimek-Mahmutoglu, Corderio, et al., 2014; van Karnebeek et al., 2012; Yuzyuk et al., 2016).

Recently, a novel form of B6EE was discoverd by Darin et al. (2016) that is caused by recessive mutations in a gene previously known as proline synthetase co-transcribed homolog (*PROSC*). The gene was later renamed PLP Binding Protein encoding PLP homeostasis protein (PLPHP). The product of this gene belongs to a highly conserved family of proteins known to bind PLP. The function of these PLP-binding proteins in humans as well as other species is poorly understood. Their structures have remarkable similarity with a bacterial enzyme known as alanine racemase (Ito et al., 2013) .

In bacteria (YggS) and yeast (YBL036C), the structures of PLPHP orthologous proteins show PLP covalently bound to a lysine residue, phosphate-binding motifs, and a typical triosephosphate isomerase (TIM)-barrel domain (Eswaramoorthy et al., 2003; Ito et al., 2013). Purified human PLPHP is also bound to PLP in the native state, but little is known about the molecular function of this protein (Tremino et al., 2018). Studies in YggS-deficient *Escherichia coli* (*E. coli*) revealed growth impairment and disrupted amino and keto acid homeostasis (Ito et al., 2013; Prunetti et al., 2016). In cyanobacteria, it has been suggested that the C-terminal helix may play a role in PLP exchange with apoenzymes (Tremino et al., 2017). VitB6 vitamer levels were significantly altered in human PLPHP loss-of-function (LOF) patient samples, and it has been hypothesized that this protein has a key role in B6 homeostasis (Darin et al., 2016;

Prunetti et al., 2016), possibly acting as a PLP-carrier that prevents PLP from reacting with other molecules, supplying it to dependent enzymes, and/or protecting PLP from phosphatases.

Similar to the general picture of other B6EE, PLPHP deficiency in humans is manifested by early-onset seizures that respond to treatment with pyridoxine (PN) and/or PLP. Affected infants also suffer from developmental delay and brain structural abnormalities, most notably simplified gyral pattern and cyst-like structures adjacent to the anterior horns (Darin et al., 2016). The genotypic and phenotypic spectra of this disease are not yet fully delineated, and the mechanisms through which seizures and other symptoms manifest are not known. We undertook a comprehensive genetic and biochemical study of PLPHP deficiency in a cohort of 12 previously undescribed patients, highlighting a unique movement disorder phenotype (without epilepsy) as well as a fatal mitochondrial encephalopathy phenotype, neither of which to our knowledge has previously been described. To better characterize the pathophysiology of this neurometabolic disease, we generated knockout models in zebrafish (*Danio rerio*), yeast (*Saccharomyces cerevisiae*) and HEK293 cells, providing insights into the biochemical consequences of PLPHP deficiency.

2.2 Materials and methods

2.2.1 Patients

This study was approved by the Clinical Research Ethics Board of BC Children's and Women's Hospital, University of British Columbia (H12-00067), the Children's Hospital of Eastern Ontario Research Ethics Board, and local institutional review boards at the University of Colorado. Patients 1, 2, 8 and 9 are the index cases who were investigated on a research basis as part of a project that aims to discover novel genetic causes of B6EE. These patients had an initial clinical diagnosis of PDE-ALDH7A1 which was subsequently ruled out by direct sequencing of

ALDH7A1 and/or biomarker analysis. *PLPBP* was first discovered as a novel gene in Patients 1 and 2 through massively parallel whole-exome sequencing (WES) and homozygosity mapping. Targeted Sanger sequencing was used to demonstrate the causal *PLPBP* variants in Patients 8 and 9. PLPHP deficiency was diagnosed in many of the remaining patients on clinical basis, and *PLPBP* mutations were identified through clinical WES by specialized diagnostic laboratories (detailed below). These patients were recruited through collaboration with their primary physicians. In some of these cases, B6EE was suspected initially and known causes were ruled out by direct gene sequencing or biomarker screening. In Patient 3, PNPO deficiency and PDE-ALDH7A1 were ruled out by Sanger sequencing of *PNPO* and measurement of urinary α-AASA, respectively. In Patient 10, PDE-ALDH7A1 was excluded based on direct sequencing of *ALDH7A1*. In Patient 11, a number of known genetic causes of epilepsy were excluded by GeneDx Infantile Epilepsy Panel testing which included *ALDH7A1* and *PNPO*. In Patient 12, PDE-ALDH7A1 was excluded by biomarker analysis (pipecolic acid). In the same patient, molybdenum cofactor deficiency and isolated sulfite oxidase deficiency were ruled out by analysis of urinary S-sulfocysteine. After obtaining signed informed parental consent, referring clinicians provided detailed reports of clinical, MRI and EEG features of study patients.

2.2.2 Whole-exome sequencing, Sanger sequencing and *in silico* analysis

All exomes were aligned to the human reference genome, February 2009 assembly (GRCh37/hg19).

Patients 1 and 2

Whole exome sequencing (WES) was performed on patients 1 and 2 using the SureSelectXT Library Prep Kit and Illumina HiSeq 4000 (Macrogen, Korea). The data were analyzed using a semi-automated bioinformatics pipeline (Tarailo-Graovac et al., 2016). Illumina sequencing reads were aligned to the human reference genome version hg19 using Bowtie2 aligner (Langmead & Salzberg, 2012), and local realignment was performed using Genome Analysis Toolkit (McKenna et al., 2010), achieving mean coverage of 24x for patients 1 and 2. Variants were called using SAMtools (Li et al., 2009) and annotated using SnpEff (Cingolani et al., 2012). Rare variants were identified using public databases, such as exome variant server (EVS), dbSNP v138 (Sherry et al., 2001) and the Exome Aggregation Consortium (ExAC) database (Lek et al., 2016), as well as our in-house database of more than 400 exomes and 40 genomes (UBC) and against an in-house database of 817 Saudi Arab exomes at Alfaisal University (Dr. Fowzan Alkuraya, personal communication) because these were Omani Arab patients. Manual inspection on variant quality was carried out with Integrative Genomics Viewer (IGV) (Robinson et al., 2011).

Patient 3

Clinical child-parents whole-exome sequencing (trio-WES) was performed at the Department of Human Genetics at the Radboudumc (Nijmegen, The Netherlands), with examination of all known genes according to previously described WES methods (de Ligt et al., 2012; Lelieveld et al., 2016).

Patient 4

Whole-exome sequencing of the proband and both parents was performed as described (Dyment et al., 2013).

Patient 5

Trio WES was performed using SureSelect Human All Exon Kit version 4 (Agilent) for target enrichment. The library was sequenced with 100 bp paired-end reads on a HiSeq 2000 platform (Illumina), and bioinformatics analysis was carried out as described previously (Dyment et al., 2013). Sanger sequencing showed that the affected individual was homozygous for this variant and that both parents were heterozygous.

Patients 6, 7, 10, 11 and 12

Using genomic DNA from the proband and parents if available, the exonic regions and flanking splice junctions of the genome were captured using the SureSelect Human All Exon V4 (50 Mb), the Clinical Research Exome kit (Agilent) or the IDT xGen Exome Research Panel v1.0. Massively parallel sequencing was done on an Illumina system with 100 bp or greater paired-end reads. Reads were aligned to human genome build GRCh37/UCSC hg19 and analyzed for sequence variants using a custom-developed analysis tool. Additional sequencing technology and variant interpretation protocol has been previously described (Tanaka et al., 2015). The general assertion criteria for variant classification are publicly available on the GeneDx ClinVar submission page (http://www.ncbi.nlm.nih.gov/clinvar/submitters/26957/). The variants in patient 11, a sibling of patient 10, were diagnosed through targeted Sanger sequencing.

Patients 8 and 9

The *PLPBP* variants in these first cousin patients were identified by targeted Sanger sequencing.

***In silico* assessment of variants**

In silico variant effect predictions and scores from 6 prediction algorithms (SIFT, Polyphen 2 HDIV, MutationTaster, MutationAssessor, FATHMM MKL and PROVEAN) for all *PLPBP* single-nucleotide variants (SNVs) were retrieved from GenomeBrowse 2.1.2 (Golden Helix, USA) using its data track "dbNSFP Functional Predictions and Scores 3.0". The track curates and visualizes functional predictions and scores that were originally obtained from the dbNSFP database (Liu et al., 2011, 2013). Only one tool (MutationTaster (Schwarz et al., 2014)) provided prediction for the 4 bp deletion mutation in patients 5 and 12 (obtained manually from http://www.mutationtaster.org). CADD scores (Kircher et al., 2014) were queried individually.

2.2.3 High-density single nucleotide polymorphism (SNP) genotyping

Whole-genome SNP genotyping was performed in patients 1 and 2 using Illumina MEGA array chips. The experiment was carried out according to the manufacturer's recommended protocol (Illumina). A manual protocol was used from the step of making the AMP5 plate to the BeadChip wash steps, and then an automated protocol (with Tecan robot) was used for the single-base extension and staining steps. Based on the obtained high-density SNP dataset, genome-wide runs of homozygosity (RoH) mapping was carried out using SNP & Variation Suite (SVS) software (Golden Helix, USA), with the following conditions:

1) minimum RoH length: 500 kb
2) minimum number of SNPs per RoH: 25
3) allowing inclusion of up to 10 missing genotypes

2.2.4 Structural model of human PLPHP

The 3D model of PLPHP protein (NP_009129.1) was obtained by homology modelling using MODELLER (Webb and Sali, 2014) and the yeast ortholog (YBL036C, PDB 1CT5, (Eswaramoorthy et al., 2003), 41% identical, 57% similar) as template. DOPE (discrete optimized protein energy) score was used to select the best model for subsequent refinement using Coot (v0.8.6.1, (Emsley et al., 2010)). Prosa-Web (Wiederstein & Sippl, 2007) and Coot's Ramachandran plot analysis module were used to validate model quality. PyMOL (Schrodinger, 2015) was used for structural superimposition of the human PLPHP model with yeast 1CT5, and the coordinates of the PLP co-crystalized with the yeast ortholog were transferred to the PLPHP model, with PLP covalently bound to p.Lys47. Images were prepared using PyMOL. Arpeggio was used to calculate contacts (Jubb et al., 2017). DUET (Pires et al., 2014) was used to calculate stability changes.

2.2.5 Clinical severity score

We assessed the clinical severity of patients within this study and previous studies (Darin et al., 2016; Plecko et al., 2017) based on published data. We adapted a scoring system of patients with B6EE due to pathogenic variants in *ALDH7A1* (Al Teneiji et al., 2017). The following criteria were used: A) global and/or intellectual delay: 0=normal; 1=mild; 2=moderate; 3=severe; B) age of onset of seizures and/or movement disorder: 0=absent; 1=>1month; 2=≥7 days; 3=<7 days; C) therapeutic response: 0=full cessation of seizures and normalization of EEG (if available) on <200mg B6 (PN and/or PLP) total daily; 1=no clinical seizures or abnormal movements on ≥200mg B6 total daily, with or without electrographic normalization OR clinical response to <200mg B6 total daily dose with persistently abnormal EEG; 2=no seizures with B6 (any dose)

AND other antiepileptic drug (AED) medication, with or without EEG normalization; 3=breakthrough seizures and/or persistent movement disorder, no responsiveness. We calculated the sum for each clinical feature (A, B and C, above), and classified each patient as mild (1-3), moderate (4-6) or severe (7-9) (Al Teneiji et al., 2017).

2.2.6 Primary skin fibroblast culture

For patient 5, a skin biopsy was taken from which a fibroblast cell line was established at the Centre for Applied Genomics (Toronto, Canada) and maintained in HyClone DMEM media (GE Healthcare Life Sciences) supplemented with 10% FBS, Penicillin-Streptomycin (SV30010, GE Healthcare Life Sciences) and 2mm L-glutamine (SH3003401, Thermo Scientific).

2.2.7 Patient fibroblast protein analysis

Total protein from the patient and three control lines was extracted in RIPA buffer containing protease inhibitors (Sigma) and was run on SDS-PAGE (20µg) following standard protocols. Antibodies used were rabbit anti-PROSC (Proteintech, 25154-1-AP, 1:5000); anti-β-tubulin (Abcam, ab6046, 1:20 000) and anti-GAPDH (ImmunoChemical, 200-901-BJ4, 1:10 000) were used as loading controls. HRP-linked anti-rabbit or anti-mouse IgG (1:2000) was used as secondary, and the Clarity ECL WB Substrate kit (BioRad) was used for protein detection using a ChemiDoc Touch Imaging System (BioRad).

2.2.8 Analysis of mitochondrial function in fibroblasts

A sample of the patient 5 fibroblast line was sent to the Mitochondrial Disease Laboratory (SickKids, Toronto). Measurements performed were pyruvate dehydrogenase (PDH) in its native

and dichloroacetate activated forms, pyruvate carboxylase (PC), cytochrome oxidase, succinate cytochrome c reductase, and the cellular lactate/pyruvate ratio.

Oxygen consumption rate (OCR) was measured in patient and control fibroblasts using a Seahorse XF-24 Extracellular Flux Analyzer and V7 PS cell culture microplates (Agilent). Cells were seeded 50 000/well 24 hours before the assay, which followed the standard protocols of the XF Cell Mito Stress Test (Agilent). Data were normalized to protein concentration

2.2.9 Isolation of pure mitochondrial fractions from HeLa cells and western blotting

Pure mitochondrial fractions were isolated from HeLa cells having HA-tagged mitochondria using an immunoprecipitation protocol as outlined previously (Chen et al., 2017). Whole cell and pure mitochondrial fractions were run on SDS-PAGE, and western blots were blocked in TBS-T 5% milk and probed with the following primary antibodies: rabbit anti-PROSC (Proteintech 25154-1-AP; 1:1000), rabbit anti-SHMT2 (SIGMA HPA020549; 1:1000), rabbit anti-VDAC (Cell Signaling 4661S; 1:1000), mouse anti-LAMP2 (Abcam ab25631; 1:1000), mouse anti-GAPDH (Santa Cruz sc-47724; 1:2000), and rabbit anti-GOLGIN-97 (Cell Signaling 13132; 1:1000). All antibodies were prepared fresh in TBS-T 5% BSA. HRP-conjugated goat anti-mouse (cat. no. sc-2055) and anti-rabbit (cat. no. sc-2054) secondary antibodies obtained from Santa Cruz Biotechnology were used at 1:3000.

2.2.10 Yeast strains and culture conditions

Saccharomyces cerevisiae BY4742 (MATα *his3Δ1 leu2Δ0 lys2Δ0 ura3Δ0*) was used as the Wild Type (WT) strain along with derivative strains: *fox1*::KAN, carrying a deletion of peroxisomal acyl-CoA oxidase and *ybl036C*::KAN mutant (Euroscaft). Yeast strains and

transformants containing the expression plasmids p*PROSC1a* and p*PROSC2a* (human *PLPBP*) were selected and grown in minimal medium containing 6.7 g/L yeast nitrogen base without amino acids (YNB-WO) supplemented with 5 g/L glucose and amino acids (20 mg/L), and growth was measured. For the induction of peroxisome and mitochondrial proliferation, cells were shifted to ethanol (YPE) 20g/L, glycerol (YPG) 20g/L, or oleate (YPO) medium containing 5g/L potassium phosphate buffer, pH 6.0, 3g/liter yeast extract, 5g/L peptone. YPO media were supplemented with 1.2 g/L oleate, and 2g/L Tween-80. Prior to shifting to these media, the cells were grown in minimal medium with 5 g/L glucose for at least 24h.

2.2.11 *PLPBP* targeting in HEK293 cells

Two guide RNAs were designed in exon 2 of *PLPBP* (NM_007198) targeting the region downstream of the start codon using the CRISPR design website (http://crispr.mit.edu/). The guide RNA sequences were TTGCTGACCGCCACTAGCCG (Guide 1 on reverse strand; primers 1F 5' CACCGTTGCTGACCGCCACTAGCCG 3' and 1R 5' AAACCGGCTAGTGGCGGTCAGCAAC 3') and CATCCAGCCCCGGCTAGTGG (Guide 2 on forward strand; primers 2F 5' CACCGCATCCAGCCCCGGCTAGTGG 3' and 2R 5' AAACCCACTAGCCGGGGCTGGATG C 3'). Oligonucleotide guide sequences were cloned into the pSpCas9(BB)-2A-GFP plasmid (Addgene Plasmid 48138). The resulting plasmids were transfected into HEK293 cells and GFP positive cells were sorted two days after transfection. These cells were used for obtaining clonal cell lines. We obtained two clonal cell lines with predicted biallelic disease-causing mutations; Guide 1_B, homozygous for c.124_127delCTAG (L42Wfs*12) and Guide 2_C, homozygous for c.128_129ins131bp (A44Gfs*55).

2.2.12 PLPHP overexpression in HEK293 cells and sample preparation for immunofluorescence

HEK293 cells were seeded in 12-well plates containing coverslips and transfected with a plasmid encoding Myc-DDK-tagged *PLPBP* (Origene, RC200853, C-terminal) using TurboFect (Thermo Fisher) following manufacturer specifications. Cells were fixed in pre-warmed 4% paraformaldehyde in PBS at room temperature for 10 minutes. After washing with PBS, coverslips were blocked for one hour with 1% BSA in PBS/0.3% Triton-X100. Primary antibodies (mouse anti-DDK monoclonal (Origene, TA50011, 1:100) and a rabbit polyclonal against human Tom20 (FL-145) (Santa Cruz sc-11415, 1:1000) were diluted in PBS containing 1% BSA and incubated for one hour. Secondary antibodies (Cy3-AffiniPure Goat anti-mouse IgG (H+L) (Jackson ImmunoResearch 115-165-003, 1:750) and Alexa Fluor 488 goat anti-rabbit IgG (H+L) (Life Sciences A11034, 1:750)) were diluted in PBS containing 1% BSA and incubated for one hour. Cover slips were stained for five minutes in DAPI. Microscopy was performed using AxioObserver Z1 LSM800 63x/1.4 (Zeiss).

2.2.13 Quantification of B6 vitamers in plasma, leucocytes and cultured cells

Plasma samples from patient 4 (prior to treatment with any form of vitamin B6) and patient 3 (during treatment with PLP) were collected, protected from light and stored at -80°C. B6 vitamers PLP, pyridoxal (PL), PN, pyridoxamine (PM) and the degradation product 4-pyridoxic acid (PA) were quantified by LC-MSMS as previously described (Mathis et al., 2016; van der Ham et al., 2012). Pyridoxine-5'-phosphate (PNP) was not quantified due to plasma-related technical limitations of the method (ion suppression) and pyridoxamine-5'-phosphate (PMP) was not quantified as it is known to be highly unstable in plasma.

Fibroblasts from patient 5 and four controls, and HEK293 cells were cultured in DMEM GlutaMAX-I (Gibco, cat # 31966) containing 10% fetal bovine serum and 1% penicillin-streptomycin. B6 vitamers were extracted with tricholracetic acid (50g/L) and quantified with UPLC-MS/MS in biological triplicates as described by van der Ham et al. (2012).

2.2.14 Generation of mutant zebrafish lines

Zebrafish were maintained following standard protocols (Westerfield, 1993), and experiments were in accordance with the animal care guidelines of the Canadian Council on Animal Care, the University of Ottawa animal care committee (protocol BL-2678), and the ARRIVE guidelines (Kilkenny et al., 2012). Handling, treatments, husbandry and nursery were performed as outlined previously (Pena, Roussel, et al., 2017). CRISPR/Cas9 was used to induce targeted indel mutations in the *plpbp* gene of zebrafish embryos as previously described (Hwang et al., 2013), using ZiFit targeter (Sander et al., 2010) to select CRISPR targets and design oligonucleotides (5' TAGGTGGAGCGGGTGAATCAAG 3' and 5' AAACCTTGATTCACCCGCTCCA 3') in the first exon. The target was chosen as having the fewest predicted off-targets (minimum three mismatches with any predicted off-target sequence). Generation of the sgRNA and CRISPR/Cas9 injection, as well as screening for mutants by PCR/HMA-PAGE, were performed as previously described (Pena, Roussel, et al., 2017; Zhu et al., 2014). Genotyping PCR was performed as described below. F0 larvae were raised to adulthood and backcrossed with WT to generate heterozygous F1 fish. These were again backcrossed with WT to minimize off-targets. Experimental compound heterozygous animals were obtained by crossing F2 heterozygotes.

Zebrafish genotyping

F1s were raised to adulthood and were fin-clipped for genotyping by HMA-PAGE. Fish with candidate variants causing frameshift mutations were backcrossed to WT fish to further reduce the chance of off-target effects, generating F2 heterozygotes. F3 larvae from the crossing of F2 heterozygotes were genotyped by extracting DNA from 3-4 days post-fertilization (dpf) larval fins and HMA-PAGE was used following previously described protocols (Kosuta et al., 2018; Pena, Roussel, et al., 2017). Primers used: *plpbp-F 5'* GCACTCTGGCTATGTGGAGA 3'; *plpbp*-R 5' AGCTGTCACTCATCCCTCGT 3'. Because differentiating homozygous mutants and homozygous WT genotypes requires two rounds of HMA-PAGE, and since no suitable primers could be identified for a reliable multiplex PCR strategy that would clearly identify homozygous mutants, two separate F2 mutant lines were crossed to generate compound heterozygous F3 offspring which facilitated genotyping by HMA-PAGE in a high-throughput manner. A pilot study was performed to show no difference in phenotype or survival between the compound heterozygous and homozygous mutant lines (Fig. 2-8).

Behavioral phenotyping

Sixteen 11 days post-fertilization (dpf) larvae per group were dispensed (one per well) in 48-well flat-bottomed culture dishes (Corning) containing 500µL of system water. Behaviour was monitored as previously described (Pena, Roussel, et al., 2017) using a ZebraBox system (ViewPoint Behavior Technology). Videos were also analyzed blindly by two observers to classify seizure scores using the S0-S3 system (Baraban et al., 2005).

Electrophysiology and c-fos expression

Electrophysiological local field potential recordings of activity in the optic tectum of five 11 dpf larvae per group selected randomly were obtained as previously described (Pena, Roussel, et al., 2017). Since *c-fos* expression can be used as a biomarker for increased neuronal activity and is known to increase with seizure activity (Baraban et al., 2005), we measured *c-fos* mRNA expression in pools of five 11 dpf larvae (mutants and WT) as well as in WT larvae treated with 15mM pentylenetetrazol (PTZ) as a positive control. RNA was extracted, reverse transcribed and quantified by qPCR as previously described (Pena, Roussel, et al., 2017). Primers used were: *cfos*-F 5' AACTGTCACGGCGATCTCTT 3' and *cfos*-R 5' TCTTCTGGAGAAAGCTGTTC 3' with β-*actin* as internal control: *actin*-F 5' CATCCATCGTTCACAGGAAGTG 3' and *actin*-R 5' TGGTCGTTCGTTTGAATCTCAT 3'.

Metabolite extraction and mass spectrometry

For analysis of B6 vitamers, three pools of six 10 dpf larvae (*plpbp*$^{-/-}$, WT) were analyzed as previously described (Pena, Roussel, et al., 2017). Measurement of amino acid panels was performed using three pools of five larvae per group (*plpbp*$^{-/-}$, WT, heterozygotes) following established protocols (Pena, Roussel, et al., 2017; van der Ham et al., 2012), with the modification that 10 dpf larvae were fasted for 24 hours prior to collection with metabolite extraction at 11 dpf. Neurotransmitter analytes (5 pools of *plpbp*$^{-/-}$ and 4 pools of WT; 6 larvae per pool) were measured following established methods (Vliet et al., 2015).

2.2.15 Statistical analysis

All statistical analyses and graphing were performed using GraphPad Prism. Where appropriate, one-way ANOVA with Tukey's test, or Krustal-Wallis with Dunn's *post hoc* test was performed. Student's t-test was used for pairwise comparisons.

2.3 Results

2.3.1 Phenotypic spectrum of patient cohort with biallelic pathogenic *PLPBP* variants

The 12 previously unreported patients described here presented with encephalopathic phenotypes comprising neonatal-onset of refractory epilepsy (or a movement disorder in one case), with or without additional clinical features (Table 2-1A and B, detailed clinical patient descriptions are provided in section 2.3.2 below). This cohort comprised six male and six female patients from seven different ethnic backgrounds. For patients 1 and 6, the pregnancy history was notable for excessive fetal movements, possibly indicating seizures *in utero*. Three patients experienced respiratory insufficiency after birth, including patient 3 who had progressive respiratory failure.

Epileptic seizures started within the first week of life in all affected infants except patient 7, who instead presented with a movement disorder (opisthotonos, oculogyric crises) at two months of age. Patients manifested multiple seizure types, and initial EEG showed various patterns of abnormal electrographic activity with burst suppression being common (6/11 reported). Seizures were refractory to AED treatment in all patients (Table 2-1A and B). All patients who received vitamin B6 (10/12) showed responsiveness and improvement of seizures or abnormal movements upon its institution. Vitamin B6 therapy was first tested as PN in eight patients, PLP in one patient and a combination of both vitamers in another patient (Table 2-1A and B). The

incomplete response to PN or PLP in patient 1 prompted the clinicians to add folinic acid to his treatment, which produced a marked reduction in seizure frequency (only two brief episodes in a three-month period). In patient 3, PLP was initially started but failed to exert sufficient seizure control, and adjuvant AED treatment was necessary. A similar picture was seen for patients 6, 11 and 12, who required treatment with PN and adjuvant AED.

Patients 1 (Fig. 2-1), 6, 7, 8 and 9 had normal brain MR imaging studies (with the exception of mild T2-hyperintense white matter signal in the neonatal period for patient 1) (Table 2-2A and B). The remainder (6/11 patients for whom brain imaging was done) had structural brain abnormalities (Fig. 2-1, Table 2-2A and B). Four patients (3, 4, 5 and 12) had simplified gyral pattern, suggesting prenatal onset of the disease and possible effect of PLPHP-deficiency on neuronal migration. In addition, these patients displayed large cysts adjacent to the anterior horns. In two patients, a lactate doublet was present in single voxel MR spectroscopy of the basal ganglia.

Clinical presentations deviating from previous descriptions of this disease were also reported. Patient 7 showed a prominent movement disorder and biochemical picture resembling aromatic l-amino acid decarboxylase (AADC) deficiency (MIM#608643). This patient had no pathogenic variant in *DDC* on exome sequencing. Patients 4 and 5 presented with signs and symptoms suggestive of severe mitochondrial disease with fatal epileptic encephalopathy, lactic acidosis and brain white matter lesions. Both patients deteriorated rapidly and died at two and eight weeks of age, respectively, due to uncontrolled seizures and respiratory failure. In neither case was the presentation deemed typical of pyridoxine-dependent epilepsy, nor was a trial of B6 vitamers administered.

Table 2-1A: Clinical features of PLPHP-deficient patients (Patients 1 – 6).

Patient's ID	Patient 1	Patient 2	Patient 3	Patient 4	Patient 5	Patient 6
Ancestry	Arab	Arab	African/Creole	Dutch	Cree First Nation	Arab
Consanguinity (degree)	+ (first cousin)	+ (first cousin)	+ (degree NA)	-	+ (second cousin)	+ (second cousin)
Amino acid change	p.Thr116Ile; p.His275Asp (VUS)	p.Arg41Gln	p.Glu67Lys	Splicing; p.Gly224Ala	p.Asp124Lysfs*2	p.Thr116Ile
Pregnancy / delivery complications	Abnormal fetal movements	-	C-section due to fetal distress	DCDA-gemelli pregnancy	C-section due to fetal distress	Abnormal fetal movements
Lactic acidosis	-	-	+	+	+	NA
Seizure onset	Day 5	Day 7	Day 2	Day 1	Day 1	Day 4
Seizure type	Myoclonic, generalized tonic-clonic	Staring and tonic-clonic	Tonic-clonic	Tonic spasms of the face, thorax and arms	Tonic posturing with occasional myoclonic jerks	Infantile spasms, clonic, generalized tonic-clonic
Initial EEG pattern	Burst suppression	NA	Discontinuous with tendency to burst suppression	Discontinuous	Burst suppression	Multifocal epileptiform activity
Response to initial AED treatment [3]	Partial response	No response	NA	Partial response	Partial response	Partial response
Initial B6 treatment (age/response [3])	PN (5 wks) PLP (2 yr, 6 mo / partial response)	PN (< 1 mo/ (seizure free)	PLP (5 days) PN (3 yr, 10 mo / good response)	Not tried	Not tried	PN (6 mo/ seizure free [4])

B6 withdrawal (vitamer/ response)	-	-	+ (PLP/ seizure relapsed)	Not applicable	Not applicable	+ (PN/ seizure relapsed)
B6 vitamer switch (type/ response)	+ (PN→PLP/ no improvement)	-	+ (PLP→PN/ no improvement)	Not applicable	Not applicable	-
Current treatment (dose)	PLP (58 mg/kg/day) Folinic acid (2mg/kg/day)	PN (5 mg/kg/day)	PN (9 mg/kg/day) Midazolam (used during seizures only)	Not applicable	Not applicable	PN (12.8 mg/kg/day) oxcarbazepine (53.8 mg/kg/day)
Breakthrough seizures with fever	+	+	+ (seizure relapse on viral infections)	Not applicable	Not applicable	+
Motor neurological exam	Unremarkable	Unremarkable	Hypertonia, stereotypies	NA	NA	Mild axial hypotonia, stereotypies
Developmental delay	+, with ASD	-	+	Not applicable	Not applicable	+, with ASD
Speech delay	+	-	+	Not applicable	Not applicable	+
School performance or IQ	NA	Average school performance	NA	Not applicable	Not applicable	DQ=70, 2nd percentile [6]
Brain MRI [7]	Initial: mild WM changes Follow up: Normal.	Not performed	WM changes, large paraventricular (pseudo)-cysts, thin posterior CC	WM changes, large paraventricular (pseudo)-cysts, thin posterior CC	cystic leukencephalopathy	Normal

Table 2-1B: Clinical features of PLPHP-deficient patients (Patients 7 – 12).

Patient's ID	**Patient 7**	**Patient 8**	**Patient 9**	**Patient 10**	**Patient 11**	**Patient 12**
Ancestry	Hispanic	Arab	Arab	Kurdish	Kurdish	African American
Consanguinity (degree)	-	+ (first cousin)	+ (first cousin)	+ (first cousins)	+ (first cousin)	1st degree relatives
Amino acid change	p.Ile94Phe	p.Arg41Gln	p.Arg41Gln	p.Glu67Lys	p.Glu67Lys	p.Asp124Lysfs *2
Pregnancy / delivery complications	-	-	-	C-section due to fetal decelerations	-	-
Lactic acidosis	+	- [1]	NA	- [2]	NA	+
Seizure onset	2 mo	1st wk	Day 5	Day 1	Day 1	Day 1
Seizure type	Infantile spasms [5]	Myoclonic	Generalized tonic-clonic	Flexor spasms, myoclonic jerks	Partial and generalized seizures	Focal seizures, myoclonic jerks
Initial EEG pattern	Continuously disorganized background	Burst suppression	Burst suppression	Discontinuous	Discontinuous with multifocal sharps	Burst suppression
Response to initial AED treatment [3]	Partial response	No response	Not tried	Partial response	No response	Partial response
Initial B6 treatment (age/response [3])	PN and PLP (2.5 mo/ seizure free)	PN (25 days/ seizure free)	PN (2nd week/ seizure free)	PN (2nd week/ seizure free[4])	PN (age NA/ good response)	PN (age NA/ no response) PLP (1 mo/seizure free)
B6 withdrawal (vitamer/ response)	-	-	-	+ (PN/ seizure relapsed)	+ (PN/ increased seizures)	-

B6 vitamer switch (type/ response)	-	-	-	-	-	+ (PN→PLP/ complete response)
Current treatment (dose)	PN (23 mg/kg/day) PLP (30 mg/kg/day)	PN (6 mg/kg/day)	PN (8.5 mg/kg/day)	PN (4.7 mg/kg/day) Lamotrigine (3.5 mg/kg/day) Clobazam (0.75 mg/kg/day)	PN (7.8 mg/kg/day) Lamotrigine (4.5 mg/kg/day) (1.25mg/kg/day)	PLP (40 mg/kg/day) Phenobarbital (9 mg/kg/day)
Breakthrough seizures with fever	-	+	-	+	+	-
Motor neurological exam	Unremarkable	Unremarkable	hyperreflexia of all limbs	Hypotonia, mild dysmetria, wide based gait	Hypotonia, mild dysmetria, wide based and ataxic gait.	mild hypotonia
Developmental delay	-	-	-	+	+	-
Speech delay	-	-	NA	+	+	Not applicable
School performance or IQ	NA	Excellent school performance	NA	NA	NA	Not applicable
Brain MRI [7]	Normal	Normal	Normal	underdeveloped frontal gyri. Subsequent, thin posterior CC.	Slight asymmetry in height of the hippocampi, WM changes.	WM changes, mild dilatation of the lateral and third ventricles

[1] elevated lactate but normal pH; [2] first measured after B6 treatment; [3] treatment response is graded as follows: no response, partial (= mild or only short-term reduction), good (= marked long-term reduction), seizure free;
[4] when combined with AEDs; [5] this patient has a movement disorder and lacks true epileptic seizures; [6] Bayley-III Cognitive Composite score; [7] showing only main findings here, detailed MRI features are described in Table 2-2A and B.

Abbreviations: **AEDs:** Anti-Epileptic Drugs, **ASD:** Autism spectrum disorder, **CC:** corpus callous, **C-section:** Caesarean section, **DCDA:** dichorionic diamniotic twin pregnancy, **DQ:** developmental quotient, **EEG:** Electroencephalography, **mo:** month(s), **MRI:** Magnetic Resonance Imaging, **NA:** Not Available, **PN:** Pyridoxine, **PLP:** Pyridoxal 5'-Phosphate, **VUS:** variant of uncertain significance, **wk(s):** week(s), **WM**: white matter, **yr:** year(s).

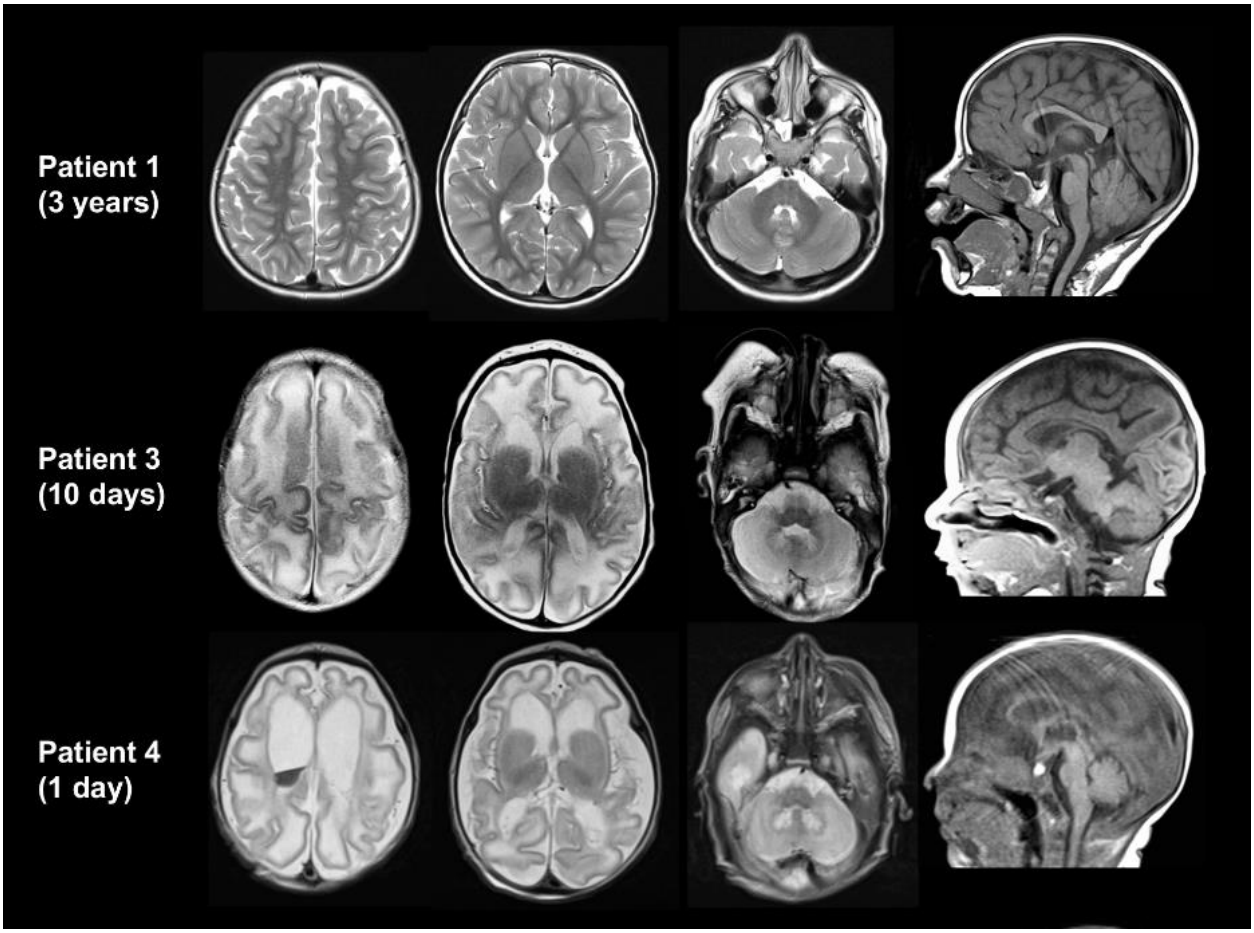

Fig. 2-1: Axial T2 (first 3 columns) and sagittal (last column) T1-weighted images of patients 1, 3 and 4. At age 3 years, the MRI of patient 1 is normal. Patients 3 and 4 show a simplified gyral pattern, cyst-like structures connected to the anterior horns and a T2-hyperintense signal of the hilus of the dentate nuclei. White matter signal is T2 hyperintense and the brain appears swollen. These abnormalities are more severe in patient 4 (who additionally has intraventricular blood) than in patient 3. The corpus callosum lacks the most posterior part.

Table 2-2A: Detailed MRI findings (Patients 1 – 6).

Patient ID	Patient 1	Patient 2	Patient 3	Patient 4	Patient 5	Patient 6
MRI age	6 wk, 8.5 mo, 3.5 yr	Not performed	10 days	1 day	6 days	8 mo
WM abnormalities	Very mild T2-hyperintense and T1-hypointense changes in periventricular WM at age 6 wk		Yes, T2 hyperintense and T1 hypointense, swollen aspect	Yes, T2 hyperintense and T1 hypointense, swollen aspect, subcortical cystic degeneration	Yes, T2 hyperintense and T1 hypointense, swollen aspect, subcortical cystic degeneration	No
Cortex abnormalities	no		Simplified gyral pattern	Simplified gyral pattern	Simplified gyral pattern	no
Basal ganglia abnormalities	no		no	no	no	no
Thalamus abnormalities	no		no	no	no	no
Cerebellar involvement	no		no	T2-hyperintense signal of the hilus of the dentate nucleus	no	no
Cysts anterior horn	no		++	++	+ (L>R)	no
CC abnormalities	no		Thin CC	Thin CC		no
Other abnormalities	Age 8 mo: mild communicating hydrocephalus with prominent external CSF spaces. Age 3.5 yr: normal MRI			Lactate doublet at MR spectroscopy (basal ganglia)	Cavum septi pellucidi; small lactate doublet at MR spectroscopy (basal ganglia)	MRI normal

Table 2-2B: Detailed MRI findings (Patients 7 – 12).

Patient ID	Patient 7	Patient 8	Patient 9	Patient 10	Patient 11	Patient 12
MRI age	12 wk, 3.5 mo	MRI not available for review	MRI not available for review	6 yr	2 yr	MRI not available for review
WM abnormalities	no			Mild T2-hyperintensity in the posterior periventricular white matter	Faint T2-hyperintensity in the posterior periventricular white matter	
Cortex abnormalities	no			no	no	
Basal ganglia abnormalities	no			no	no	
Thalamus abnormalities	no			no	no	
Cerebellar involvement	no			no	no	
Cysts anterior horn	no			no	no	
CC abnormalities	no			Pronounced isthmus	no	
Other abnormalities	MRI normal	MRI at age 4 wk reported as normal.	MRI at age 10 mo reported as normal.			MRI at ages of 2 days and 3 wk: Diffuse broadening of the gyri in both cerebral hemispheres, mild dilatation of the lateral and third ventricles. There are blood products in the left lateral ventricule.

Abbreviations: **CC:** corpus callous, **CSF:** Cerebrospinal fluid, **MRI:** Magnetic Resonance Imaging, **WM:** white matter, **mo:** month(s), **wk:** week(s), **yr:** year(s).

2.3.2 Clinical patient descriptions

Case vignettes with phenotypic features not previously described

Fatal mitochondrial encephalopathy

Patient 4

This girl of Dutch non-consanguineous origin, who died at 2 weeks of age, was the first of dichorionic diamniotic (DCDA) twins, born via spontaneous vaginal delivery at 36+6 weeks gestation. Her cotwin is healthy with normal development. Her birth weight was 2215 g (10^{th} percentile), head circumference 30.7 cm (-2.5 SD corrected for gestational age) and APGAR scores 6/7/8. The family history was negative for epilepsy or developmental problems. Immediately postpartum, spontaneous breathing was insufficient, requiring assisted ventilation for 5 minutes. One hour postpartum, she became hypoglycemic (glucose was <0.6 mmol/L). Initial lactate was 19 mmol/L, creatine kinase (CK) 3137 U/L (normalized to 232 U/L at day 9).

Neurologically, the girl showed strong motor unrest and progressive axial hyperextension upon light touch. Seizures probably started at day 1 postnatally (but could not be proven by EEG at that time) and escalated at day 3 (irritability, nystagmus, tonic spasms of the face, thorax and arms; later on also tachycardia, hypertension, apneas, and desaturations, followed by crying and grimacing). The first EEG (postnatal day 1) showed a diffusely abnormal and excessively discontinuous pattern. EEGs on day 4 and 7 displayed a similar background, progressively frequent brief ictal rhythmic discharges and progressive episodes of rhythmic sharp activity compatible with electrographic neonatal seizures, sometimes without clinical correlate. Over the course of two weeks, several AEDs were trialed, all leading to unsustained (minutes to one hour) and only partial seizure control. Seizures became intractable and on day 16, after elevating midazolam and adding morphine for comfort control, the girl died of respiratory depression and bradycardia. Permission

for restricted brain autopsy was granted by the parents. Histopathological examination showed focal abnormalities, mainly of the white matter consistent with hypoxic-ischemic injury.

Patient 5

This female neonate was the first child born to consanguineous parents (second cousins) of Cree First Nation ancestry. The pregnancy was unremarkable, but a Caesarean delivery was performed at term due to a non-reassuring fetal heart rate. Her birthweight was 3470 g (76^{th} percentile), head circumference was 35 cm (82^{nd} percentile) and length was 47cm (14^{th} percentile). The child briefly (10-15 seconds) received positive pressure ventilation for poor respiratory effort, being initially stable. Over the first hours of life, she developed progressive respiratory failure requiring intubation and transfer to a tertiary care neonatal intensive care unit.

Her neurological examination was notable for hypertonia, hyper-reflexia, and abnormal movements (persistent flexion and clenching of her upper extremities). Clinical seizures were noted on the first day of life; EEG was markedly abnormal with a burst-suppression pattern. Routine lab studies were notable for a persistently increased lactate level in blood (range 1.5 - 11.2 mmol/L) and cerebrospinal fluid (5.6 mmol/L).

The patient was successfully extubated post-transport, however her seizures proved to be refractory. Seizures were managed, to the extent possible, with an intravenous midazolam infusion (150 µg/kg/hour), followed by an escalating series of up to six simultaneous anticonvulsant agents, and high-dose prednisone. Empiric therapy with biotin and thiamine produced no obvious benefit (pyridoxine was not tried). Seizures and apneic episodes persisted, becoming increasingly frequent despite these treatments. At eight weeks of age, she acutely deteriorated with recurrent apnea,

acute renal failure, and hemodynamic compromise. Care was recognized to be futile and was withdrawn.

The patient's clinical presentation and imaging were considered most consistent with a mitochondrial disorder. Plasma amino acids were notable for hyperglycinemia (943-1010 µmol/L; reference interval 81-436) with corresponding high glycine in CSF (28 µmol/L; reference interval 3-23). Urine organic acids showed increased excretion of lactic, pyruvic, and 2-hydroxybutyric acids, consistent with lactic acidosis. cultured skin fibroblasts showed an elevated lactate-to-pyruvate ratio (41.7 +/- 7.13; reference interval 9.6-26.5), normal activities of several enzymes (pyruvate dehydrogenase (PDH) native: 0.94±0.06 nmoles/min/mg protein, reference 0.46-1.60; PDH: 1.32±0.06 nmoles/min/mg protein, reference 0.87-2.33; pyruvate carboxylase: 0.51, reference 0.35-5.18; and respiratory complexes II-IV), and normal mitochondrial morphology and inner membrane potential. Extracellular flux testing showed an apparent reduction of carbonyl cyanide-*4*-(trifluoromethoxy)phenylhydrazone (FCCP)-stimulated spare respiratory capacity.

Movement disorder without epilepsy

Patient 7

This boy, currently 23 months old, was born at term to non-consanguineous parents who originate from a small town in Guatemala. He was born with bilateral syndactyly of the third and fourth fingers. His birth weight was 3.317 kg (47.6th percentile), head circumference was 33 cm (12.5th percentile) and APGAR scores 9, 9. He initially presented at 2 months of age for abnormal movements: flexor posturing with arm abduction, tonic posturing of his upper extremities and lower extremities with internal rotation of his arms, jerking of the left arm and upward eye deviation with each event. He did not present with clear epilepsy. His initial routine EEG was read

as disorganized background and bursts of higher-amplitude activity. He was treated with high dose prednisolone because of clinical suspicion of infantile spasms with emerging hypsarrhythmia on EEG. CSF analysis of cell count, chemistry and culture were unremarkable.

His parents discontinued prednisolone on the 8th day of treatment due to side effects of irritability, diarrhea, persistence and worsening of his abnormal movements. An inpatient video EEG captured non-epileptic opisthotonic-like events (back arching, sometimes twisting at the trunk, occasional arm stiffening) and oculogyric crises. These movements did not correlate with electrographic changes on the EEG suggestive of seizures or spasms and were determined to be non-epileptic. He became extremely tachycardic with the events. His movements did not respond to lorazepam (0.1 mg/kg) but decreased in frequency during levetiracetam treatment (30 mg/kg twice daily) and parenteral hydration. Biochemical studies revealed a profile suggestive of aromatic L-amino acid decarboxylase (AADC) deficiency (see details below), and he was started on recommended treatment for this disorder: PN 50 mg BID, PLP 60 mg TID and Sinemet 0.4 mL TID at 2.5 months of age with complete resolution of symptoms on this regimen. Once his *PLPBP* mutation was identified, Sinemet was discontinued (at age of 8 months), and he is currently on a regimen of PN (23 mg/kg/day div BID) and PLP (30 mg/kg/day div TID). Following initiation of treatment, all subsequent EEGs have been normal.

Early developmental milestones were achieved within the normal age range; more recently, asymmetric delays were identified. At the age of 20 months, his vision and hearing were grossly intact and motor neurological exam was normal. At 23 months of age, significant delays were noted in expressive and receptive language skills with preservation of gross and fine motor development.

His serum lactate concentration remained normal when checked on hospital readmission

(1.7 mM, reference range: <2.0 mM). However, during a third admission, he was confirmed to have an elevated lactate concentration (8.46 mM) and metabolic acidosis on venous blood gas test with elevated anion gap (23) as well as hyperglycemia (325 mg/dL) in the setting of repeated opisthotonic events. His urine analysis showed 4+ glucose and 1+ ketones. His hyperglycemia and elevated lactate corrected quickly following a normal saline bolus. C-reactive protein and blood ammonia concentration were normal.

Urine organic acids analysis was positive for the presence of vanillactic acid, vanilpyruvic acid, and n-acetyl-vanilalanine; also, minor elevations of lactic, malic, 2-ketoglutaric, and n-acetylaspartic acids were seen. This profile is typical of aromatic AADC deficiency. Confirmatory testing with AADC enzyme assay revealed partial enzymatic activity (18.84 pmol/min/mL), suspicious for carrier status of the condition but not complete AADC enzyme deficiency. Biochemical analysis of CSF at age of 2 months (before vitB6 treatment) showed normal levels of glucose (71 mg/dL, reference range: >40 mg/dL) but elevated protein concentration (75 mg/dL, reference range: <45 mg/dL), which normalized after B6 treatment (25 mg/dL at age of 2.5 months).

Folinic acid responsive seizures

Patient 1

This Omani boy, now 3 years and 10 months old, was born to a G3P3 mother. His parents are first cousins, who are healthy with normal learning abilities. There is a family history of similar disease in a younger sibling in the newborn period. Antenatally, the mother experienced increased fetal movements. The patient was born at term, cried immediately, and APGAR scores were 9/10. His birth weight was 2.95 kg (10^{th} percentile); length, 49 cm (50^{th} percentile); and head circumference, 35 cm (50^{th} percentile).

Seizures were first observed on the 5th day of life, presenting with decreased consciousness, uprolling of the eyes and tonic-clonic movements of the body; each episode lasted 10-15 minutes and recurred after an interval of a few minutes. He was treated with phenytoin, phenobarbitone and midazolam infusion without clinical response; subsequently he was started on clonazepam and topiramate with initial reduction of seizures but subsequent relapse. His EEG showed burst suppression.

At 5 weeks of age, he was started on oral pyridoxine (25 mg BID) with immediate effect; he was sedated yet hemodynamically stable. All anti-epileptics were discontinued after the first dose of pyridoxine. EEG was repeated, and it showed marked improvement with no burst suppression. At the age of one year, seizures relapsed in the form of generalized tonic-clonic seizures but were brief and infrequent and mostly occurred during febrile illnesses.

At the age of 2 years and 4 months, the dose of pyridoxine was increased to 120 mg BID p.o. (= 24 mg/kg/d). This was increased to TID during febrile illness. His seizures were controlled for around 2 months but then he was admitted again with *status epilepticus*. PLP was substituted for pyridoxine, starting at a dose of 200 mg TID (= 42 mg/kg/d) which was then increased to PLP 300 mg TID (=58 mg/kg/day) with no notable improvement of his seizure control. Subsequently, folinic acid 15 mg BID (= 2mg/kg/day) was added to his PLP regimen. This combination resulted in the best seizure control during his entire course of treatment.

He had global developmental delay of a moderate to severe degree. When he was assessed at 2.5 years of age, his developmental age was around 12-18 months with speech and language development around 7-8 months of age. He was hyperactive and was diagnosed with autism spectrum disorder. After his seizures were controlled following folinic acid supplementation, his

development improved, and he started to gain some milestones. He had also become less hyperactive. Motor neurological examination showed no focal deficits.

Biochemical investigation at the age of 15 months showed high-normal urinary α-aminoadipic semialdehyde (α-AASA, 0.19 µmol/l, reference range: 0-0.2 µmol/l) but plasma pipecolic acid was within the reference range. Antiquitin deficiency was subsequently ruled out by Sanger sequencing of *ALDH7A1*. Plasma amino acids were measured twice and were normal, while blood lactate concentration was high-normal (1.7 mmol/l, reference range: 0.5-2.2 mmol/l at the age of 6 weeks).

Other cases according to phenotypic severity:

Severe phenotype

Patient 3

This girl from Curacao Island in the Dutch Antilles (African/Creole descent), now 5 years and 2 months old, was born at 37+5 weeks of gestation after an emergency Caesarian section because of fetal distress. She is the first and only living child of possibly consanguineous parents. APGAR scores were 8/9. There was meconium in the amniotic fluid. Birth weight was 2422 grams (5-10th centile), birth length was 47 cm (25th centile) and head circumference was 30 cm (-4,01 SD). Her fontanel was small. After birth, she needed Continuous positive airway pressure (CPAP) for breathing difficulties and she had trouble maintaining her temperature. Blood lactate concentration was between 4.2 and 8.8 mmol/L on days 1-5 (normal range =<2.2 mmol/L). Blood glucose was normal, CK was 6593 U/L (normal range: <600 U/L) at day 1 and went down to 460 U/L at day 5.

On day 1, she had clinically evident tonic seizures and an abnormal cerebral function monitoring. On the third day she manifested tonic-clonic seizures despite treatment with phenobarbitone (20+10 mg/kg), clonazepam and midazolam up to 0.2 mg/kg/hour. She had dysregulation of muscle tone. She was variably hypo- or hypertonic. EEG at day 5 was in keeping with encephalopathy showing a discontinuous pattern and a tendency to burst suppression.

At day 5, PLP was started orally at a dose of 40 mg TID (48mg/kg/d), after which the convulsions vanished, and blood lactate started to normalize after day 6 (between 1.6 and 2.9 mmol/L).

At 10 months of age, she had 15-20 minutes long tonic-clonic seizures shortly after stopping the PLP because *PNPO* Sanger analysis was normal as was urine concentration of α-AASA. The next days she had several epileptic seizures. PLP was restarted at 40 mg TID and her clinical condition improved significantly. Levetiracetam was started at 20 mg/kg/day.

At 14 months of age she had an epileptic seizure after sleep deprivation. She then had several epileptic seizures that were mostly induced by viral infections and fever or sleep deprivation. At the age of 3 years and 10 months, her vitB6 therapy was switched to pyridoxine at 100 mg QD (5.9 mg/kg/day), because PN has less severe side effects over the long term. VitB6 vitamer conversion went smoothly and at the age of 4 years and 2 months, levetiracetam was gradually discontinued. This did not seem to affect frequency of seizures. She had a seizure about once every two months at this time, more severe than on the PLP regimen. Seizures occurred mostly during intercurrent illnesses. At the same age (4 years and 2 months), her pyridoxine dose was increased to 150 mg BID (8.8 mg/kg/day), and her seizures became less frequent. The dose was adjusted to 100 mg BID (9.0 mg/kg/day) at the age of 5 years. Midazolam was used during seizure attacks.

Her development at 5 years of age is profoundly delayed; she could walk independently at 35 months of age, but she is autistic and does not speak.

Physical examination at 3.2 years of age showed no overt dysmorphisms except a slight upslant of the eyes and a slightly prominent forehead. Neurologically, at 3 years and 8 months she hardly made eye contact. She had some stereotypic hand movements, and her hand motor skills were slightly clumsy but not ataxic. She walked somewhat unstably with a wide-based gait. The leg tonus was slightly high, and reflexes were brisk with no Babinski reflex.

Metabolic screening of urine at day 3 before PLP therapy showed normal amino acid profile, a trace of sulfite, high lactate, and negative α-AASA. In blood, carnitines, acylcarnitines and methylmalonic acid levels were normal, and plasma amino acids showed elevated glycine (915 µmol/L, normal range 197-487 µmol/L) and ornithine (197 µmol/L, normal range 42-170 µmol/L).

Pre-treatment CSF screening at day 3 revealed normal total protein (670 mg/L, normal range: 450-1090 mg/L); high lactate (4.4 mmol/L, normal range: 1.1-2.4 mmol/L); high pyruvate (0.23 mmol/L, normal range: 0.03-0.15 mmol/L) and normal glucose (4.2 mmol/L, normal range: 2.2-4.4 mmol/L). Amino acids showed slightly high values of glycine (25 µmol/L; normal range: 3-17 µmol/L), threonine, glutamine, and ornithine. Neurotransmitters and pterins were normal.

Patient 6

This boy, now 4 years and 3 months old, was born to consanguineous parents (second cousins) from the United Arab Emirates after a pregnancy in which the mother noted rapid fetal movements in the late third trimester. There is a family history of similar epileptic encephalopathy with infantile spasms in a sibling who died from pneumonia.

Patient 6 was born at term with birth weight of 2.8 kg. He had irritability from the first day with possible seizures and clear diagnosis of seizures by day 4 of life. Initially he had infantile spasms and rapid clonic seizures. An EEG at 4 months showed multifocal epileptiform activity predominantly in the frontal and parietal regions. He had transient response to prednisolone and was seizure free, but the effect soon waned. He had no response to levetiracetam or vigabatrin. Around 6 months of age, pyridoxine 50 mg BID (approximately 6 mg/kg/day) was given, then cutting back to 25 mg BID. This resulted in complete control of spasms and clonic seizures, and his EEG normalized. Within 1-2 months, however, he developed generalized tonic-clonic seizures with illness or fever, lasting up to 30 minutes in duration, every 1-3 months. He had improvement in duration and frequency of seizures after treatment with oxcarbazepine and diazepam. His longest seizure-free interval was approximately 3 months. He had a brief withdrawal of PN for two days with recurrence of seizures, and treatment was resumed at a dose of 50 mg BID. After the PLPHP deficiency diagnosis was made, his PN dose was increased to 100 mg BID (12.8 mg/kg/day). He has been on this dose ongoing in addition to oxcarbazepine 420 mg BID (53.8 mg/kg/day).

Developmentally, he was severely delayed without achieving any milestones during the first 6 months prior to PN treatment; at that time he was markedly hypotonic and made no eye contact. After treatment, his development improved greatly, but he still had mild motor delays and a diagnosis of autism spectrum disorder (ASD) was made at 2 ½ years old. He sat independently by 12 months, walked by 2 years, and had a pincer gasp in one hand by 2 ½ years. He repeated words but did not talk independently or communicate with gestures, and his eye contact was limited. He had limited social reciprocity and joint attention. He has frequent stereotypies and self-stimulatory behaviors.

At 2 years and 7 months of age, he was assessed on the Bayley Scales of Infant and Toddler

Development, where his scores were: Cognitive Composite 70 (2nd percentile), Language Composite 62 (1st percentile), Motor Composite 85 (16th percentile).

Patient 10

This girl, currently 10 years and 6 months of age, was born from consanguineous (first cousins) parents of Kurdish descent. There is a family history of similar disease in the younger sister (patient 11). Patient 10 was born at 38 weeks gestation via Caesarian section due to fetal decelerations and meconium-stained amniotic fluid. Ultrasound examination performed at 20 weeks of gestation was remarkable for cysts in the head, but these were not seen on repeat ultrasound exam at 28 weeks. Her APGAR scores were 8 and 9. After birth, she was irritable with a high-pitched cry, disconjugate eye movements, and tonic posturing. Within the first day of life, she presented with seizures characterized by flexor spasms and eye deviations; oxygen desaturations were seen. She continued to exhibit irritability and seizure activity with segmental myoclonic jerks involving the upper trunk, eye deviation, crying, hiccupping and flexor spasms.

She was given a phenobarbital load during the first two days of life, with a mild response. On day four of life, an extended video EEG was obtained. At the beginning, a near burst suppression pattern was seen, characterized by spike and slow wave and polyspike and slow wave complexes lasting up to 10 seconds. There were also relative periods of quiescence lasting up to 20 seconds. During the burst of generalized paroxysmal discharges, she exhibited periodic episodes of high-pitched cry, flexor spasms with arm extension, with and without hiccupping and with and without eye bobbing, lip smacking or emesis.

A 50 mg dose of PN was given twice over a short period of time. After 5 minutes, the periodic episodes of high-pitched cry, flexor spasm, and hiccupping stopped, and there was a

significant improvement in the EEG background rhythm. Phenobarbital and phenytoin were discontinued, and the child remained without seizures. She was discharged home at 11 days of age, was breast feeding well and taking 75 mg PN per day.

At the age of 8 years and 2 months, the family took her off PN treatment for two weeks, which led to uncontrollable seizures. She was taken to the emergency department where her seizures could not be stopped until she was put back on PN.

She had speech delay. She began babbling at approximately 12 months of age and started to say "mama" and "dada" at 3 years of age.

A neurological exam found that she had hypotonia with joint laxity and mild dysmetria. She had a wide-based gait with poor coordination but was able to use an iPad.

For her seizures she now takes 100 mg PN BID (4.7 mg/kg/day). She also requires lamotrigine 50 mg BID (3.5 mg/kg/day) and clobazam 10 mg BID (0.75 mg/kg/day) for optimal seizure control. During illness, she may have breakthrough seizures.

Biochemical investigations included normal urine organic acids and purines; blood lactate, acylcarnitines, amino acids (both after PN therapy); and normal CSF amino acids (except for a slight increase in alanine (43 nmol/ml)), folate/5-methyltetrahydrofolate (5MTHF), lactate, protein, glucose, tetrahydrobiopterin (BH4), neopterin, PLP, and neurotransmitter metabolites (5-hydroxyindoleacetic acid (5HIAA), homovanillic acid (HVA), 3-*O*-methyldopa (3-OMD)).

Patient 11

This girl, who is now 6 years and 10 months old, is the sister of patient 10. She was delivered via Caesarian section after an unremarkable pregnancy. Her head circumference was in

the 2nd percentile. On the first day of life, she had ophisthotonus, irritability, and eye deviation (episodic, but up to 1 hour). This was not diagnosed as seizures until an EEG was performed at a few days of life. The EEG showed a discontinuous record with multifocal sharp waves (bilateral frontal/central/temporal). She was admitted to the neonatal intensive care unit for two weeks.

She was noted to have focal seizures (hemibody clonic activity with lateral eye deviation to either side) lasting 7 seconds to 5 minutes (average 2 minutes, 2-3 times a week), or generalized convulsions with whole body stiffening and neck extension, lasting more than 2 minutes, about twice a month. Her seizures typically occurred at night.

She had no initial response to anti-epileptic drugs (AEDs). Her seizures persist over several weeks after initial PN administration (dose unknown), and thus levetiracetam was added to her treatment. Subsequent additions of clobazam and lamotrigine were helpful, but she still had seizures with fever. At the age of 4 years and 10 months, her PN dose was reduced to 50 mg BID, and she suffered increase in frequency of seizures. She is currently on the following medications: 100 mg PN BID (7.8 mg/kg/day), lamotrigine 37.5 mg BID (4.5 mg/kg/day) and clobazam 10 mg BID (1.25mg/kg/day).

Her neurological examination revealed mild dysmetria and a wide-based and ataxic gait. She was very hypotonic in the trunk, making mobility much more difficult. She continued to progress in gross and fine motor skills, but still cannot climb up or down stairs. She has separation anxiety and severe stranger anxiety. She is interested in others, points at what she wants, but cries if approached by other children.

Biochemical investigations: A comprehensive metabolic panel (sodium, potassium, chloride, calcium, bicarbonates, glucose, blood urea nitrogen (BUN), creatinine, total protein,

albumin, A/G ratio, total bilirubin, alkaline phosphatase, aspartate aminotransferase, alanine aminotransferase) was normal.

Mild phenotype

Patient 2

This boy of Omani descent was born to consanguineous parents (first cousins). There is family history of 2 siblings' deaths; both were due to intractable seizures at the age of 2-4 months. He has 5 living siblings (3 males and 2 females) that are all healthy.

He was born at term without antenatal complications. His birth head circumference was at the 10th percentile.

At the age of 7 days, brief, frequent seizures were noted with behavioral arrest progressing to tonic-clonic movements. He was tried on different AEDs but no response until PN (dose unknown) was administered and subsequently seizures were controlled before the age of 1 month. Infrequent seizures occurred mainly during febrile illnesses, the most recent one at the age of 7-8 years. EEG reports are not available.

At 13 years 10 months old, physical examination revealed no dysmorphic features, anthropometric measurements on the 10th centile, no systemic abnormalities and no organomegaly. Development in all domains and cognition were normal for age; he had average school performance in grade 6. His neurological exam was reported as normal. He was being treated with pyridoxine 80 mg BID (5 mg/kg/day), increased during febrile illness to 80 mg TID. Biochemical screening revealed no detectable α-AASA in urine, and Sanger sequencing of *ALDH7A1* was negative. Given the striking response to pyridoxine, no other investigations were carried out.

Patient 8

This boy was born to consanguineous Arab parents with a family history of pyridoxine-dependent epilepsy. The patient is a 1st cousin with patient 9.

He was born at term via spontaneous vaginal delivery to a primigravida mother with insulin dependent diabetes mellitus. His APGAR scores were 7 and 9 at 1 and 5 minutes, respectively. At birth he weighed 2.98 kg (50th percentile), was 55 cm long (90th percentile) and his head circumference was 35 cm (50th percentile). He fed well and was active until the age of 1 week when he started to have daily clusters of myoclonic movements of the upper and lower limbs lasting for few seconds. He was irritable and crying with disturbed sleep. The seizures became very frequent and at the age of 3 weeks he was admitted to the hospital for the control of seizures. His initial EEG showed burst suppression. He was loaded with phenobarbitone, but there was no response. He was then started on midazolam infusion and IV levetiracetam, but he continued to have frequent seizures. At age of 25 days, 20 mg oral PN was tried, and the seizures immediately stopped. An EEG was repeated and it was normal.

He was gradually weaned off midazolam and levetiracetam and returned to his normal activity. Phenobarbitone was also tapered and discontinued. He continued to be on PN 40 mg BID with increasing the dose to TID during febrile illnesses. He has remained seizure free since then except at the age of 5 years when he had a febrile illness and was unable to obtain enough PN to increase the dose. After that he had no more seizures. He is currently on pyridoxine 80 mg BID (6 mg/kg/day), increased during febrile illness to 80 mg TID (8.8 mg/kg/day). Long-term EEG at age 4 years was normal.

At 8 years and 1 month old he had achieved all of his developmental milestones at an appropriate age. He was in grade 2 at school with excellent performance. A physical examination found no dysmorphic features and no organomegaly, and his neurological exam was normal.

Biochemical investigations found normal pipecolic acid levels, and metabolic workup revealed raised blood lactate but normal pH. Amino acids and acylcarnitines were unremarkable on tandem mass spectrometry in dried blood spots.

Patient 9

This boy was born to consanguineous Arab parents with a family history of pyridoxine-dependent epilepsy. The patient is a double first cousin of patient 8.

He was born at term by spontaneous vaginal delivery at 37 weeks gestation to a primigravida mother with no antenatal complications. His APGAR scores were 9 and 10 at 1 and 5 minutes, respectively. His birth weight was 2.56 kg (50^{th} percentile), his length was 49 cm (50^{th} percentile) and his head circumference was 33 cm (50^{th} percentile). He was admitted to the special care baby unit soon after delivery for transient tachypnea of the newborn and treated for presumed sepsis and jaundice. After discharge on day 5 of life, the parents started to notice frequent episodes of tonic seizures. The episodes were brief, lasting for seconds only. He continued to be active and was feeding well. His first EEG at the age of 10 days showed burst suppression. He was started on PN at home by his uncle (father of patient 8). At hospital, he received 40 mg PN and became very sleepy but had no more seizures. Within 24 hours he became active and was again feeding well. He was discharged on oral PN. He had no other symptoms. He was placed on 20 mg PN BID (8.5 mg/kg/day), increased during febrile illness to 80 mg TID (12.5 mg/kg/day). Repeat EEG at 10 months was normal.

Physical examination at 14 months of age revealed no dysmorphic features and his weight, height and head circumference were all in the 10^{th} - 50^{th} percentile. He had normal tone, power and cranial nerve examination but was noted to have hyper-reflexia in all limbs.

Biochemical investigations showed that urinary aminoadipic semialdehyde was mildly elevated at 0.35 mmol/mol creatinine (reference, 0 - 0.19). Urinary pipecolic acid and piperidine-6 carboxylic acid concentrations were normal. Amino acids and acylcarnitines were unremarkable on tandem mass spectrometry in dried blood spots.

Unclassified severity

Patient 12

This African American girl was born to consanguineous parents.

She was born by spontaneous vaginal delivery at 35 weeks of gestation to a 17-year-old G1 P0 mother after an uncomplicated pregnancy. Her APGAR scores were 7 at 1 minute and 9 at 5 minutes. Her birth head circumference was 31 cm (22^{nd} percentile). She started having repeated episodes of extremity jerking and irregular respirations within the first few hours of life; these evolved into refractory neonatal seizures. She was initially seizure free after phenobarbital loading but relapsed within the first week of life. Her seizures failed to respond to multiple antiepileptic medications, including phenobarbital, phenytoin, topiramate, levetiracetam, clonazepam, vigabatrin, midazolam, lorazepam, leucovorin, and dextrometorphan. She was given a single dose of PN (100 mg IV), but no improvement was noted on video EEG. She had focal seizures and myoclonic jerks followed by tonic posturing, and her initial EEG showed a burst suppression pattern. She was placed on a 3:1 ketogenic diet and serine supplementation for low CSF serine. PLP was started at one month of age, resulting in seizure freedom, significant improvement in EEG background activity and improvement in her neurologic exam. EEG background became

continuous, and no electrographic or clinical seizures occurred after PLP was started. Focal interictal epileptiform activity continued to be present, but overall there was much improvement.

On exam at age 2 months, she was microcephalic (z score -4.4), non-dysmorphic and was feeding well by mouth. She had conjugate eye movements and emerging visual fixation. She had normal axial tone and responded to localized pain to her extremities. Her deep tendon reflexes were 3+. No myoclonus was seen.

At 4.5 months of age, her EEG had 4-4.5 Hz background of normal voltage with no epileptiform activity. Her mother reported possible rare brief seizures but none was noted in 24 hour EEG. She was developing relatively well, had mild hypotonia but intact visual fixation, and was a good oral feeder. At 5 months of age, she was taking 40 mg/kg/day of PLP divided q12h and 9 mg/kg/day of phenobarbital. She had been weaned from the ketogenic diet.

Her laboratory work-up revealed initial elevated serum lactic acid which normalized within first 2 days, normal CSF lactic acid, normal CSF pyruvic acid, normal CSF glucose and normal CSF protein. Low CSF serine (30 nmol/mL, normal range: 44 - 136 nmol/mL) was noted, but other CSF amino acids were normal. Plasma amino acids at age of 6 days revealed elevated glycine (575 nmol/mL, reference range: 111 - 426 nmol/mL). Repeat plasma amino acids at 9 days of life showed normal glycine levels (370 nmol/mL). CSF glycine was normal at 3 weeks of age at 23 nmol/ml (reference range: 5 - 115 nmol/mL). Acylcarnitine, urine organic acids and uric acid were all within reference intervals. Pipecolic acid was 0.4 nmol/mL (normal range <6 nmol/mL). Urinary S-sulfocysteine was within limits. CSF neurotransmitters (5HIAA, HVA, 3-OMD) were all normal.

2.3.3 Genotypic spectrum, variant effect prediction and clinical severity

Eight variants in *PLPBP* were identified in our patient cohort, mostly novel missense variants (Fig. 2-2, Table 2-3A and B). The exceptions are a novel homozygous frameshift deletion (c.370_373del) leading to a premature stop codon in two unrelated patients (5, 12) and the splice site variant (c.320-2A>G) previously reported by Darin et al. (2016) (Table 2-3A and B) in another patient. To investigate potential genotype-phenotype correlations, we developed a clinical severity score to classify patients into three categories: mild, moderate and severe (Table 2-4). This score reflects the broad spectrum of clinical severity observed, ranging from B6-responsive epilepsy with normal developmental outcome, to perinatal lethality with lactic acidosis and structural brain malformations (e.g., patients 4 and 5). All truncating variants leading to complete LOF of PLPHP (c.207+1G>A, c.320-2A>G; p.Ser78Ter, p.Gln71Ter and p.Asp124Lysfs*2) are associated with the most severe forms of the disease (Table 2-4). In our cohort, this is evidenced in patients 5 (deceased) and 12, both affected by biallelic exon 5 frameshift variants (p.Asp124Lysfs*2) leading to absence of protein expression in patient fibroblasts (Fig. 2-3).

To study the pathogenic effect of the missense variants in our cohort on PLPHP function (here based on PLP-binding, folding or stability), we modeled the tridimensional structure of the human PLPHP protein (Fig. 2-2B-D). The model indicates that PLPHP folds in a typical (β/α)8-TIM barrel structure, with PLP covalently bound to Lys47 (Schiff base). As with several TIM barrel fold members, a structurally conserved "phosphate binding motif" exists; this is formed by the end of β-strands and loops, especially at the C-terminus (Nagano et al., 2002). Bound PLP interacts with R241, M225, S226, I242, G243, S244, V45, N68, I94 and M181 (Fig. 2-2C-D). Combining the novel and previously described variants (Darin et al., 2016; Plecko et al., 2017), 12 missense PLPHP variants have been reported in B6EE patients (Fig. 2-2A), seven in homozygotes

(Table 2-4). Patients 1, 3, 6, 10 and 11 from our cohort were classified as severe, with either p.Glu67Lys or p.Thr116Ile homozygous variants identified. Both substitutions were computationally predicted as damaging (Tables 2-3 and 2-4). Residues 67 and 116 are conserved (Fig. 2-4) and adjacently located to the predicted PLP-binding site (Fig. 2-2B-D); variants to Lys and Ile, respectively, likely lead to disruption of PLP-binding properties (Table 2-3A and B). Patients 4 and 2 were also classified as severe; patient 4 is compound heterozygous for the splice variant leading to LOF (c.320-2A>G) and the substitution of the highly conserved Gly224 (Fig. 2-4) to Ala (Table 2-3A and B). The p.Gly224Ala variant likely impacts loop 15 structure and orientation of key PLP-binding residues, especially due to alanine's reduced degree of freedom (φ and ψ angles). Patient 1 is uniquely homozygous for two missense variants; p.Thr116Ile (discussed above) and p.His275Asp (an American College of Medical Genetics and Genomics variant of uncertain significance). The importance of the C-terminal residues for ligand binding, stability and activity of proteins that fold as a TIM barrel is well known (Dias-Lopes et al., 2013; Wierenga, 2001); therefore, a drastic chemical change like replacing a positively-charged amino acid by a negatively-charged amino acid at the C-terminus in the p.His275Asp variant may negatively impact these functions.

Of the four mild cases reported here, three patients (2, 8 and 9) are homozygous for p.Arg41Gln. Normal intellectual development, average-excellent school performance, seizures that are well controlled with relatively low doses of pyridoxine, and normal brain structure on MRI were reported in each of these patients. Arg41 is not an invariant residue (Fig. 2-4) and is located in the distal face of the TIM-Barrel structure (Fig. 2-2), not directly involved in PLP-binding. The p.Pro40Leu variant (adjacent residue) seen in a previously reported mild case (Plecko et al., 2017)

still binds PLP but has reduced stability (Tremino et al., 2018); it is possible that p.Arg41Gln has similar impact.

Patient 7 was also classified as mild and is homozygous for a p.Ile94Phe variant. This substitution is predicted to be damaging, destabilizing and likely inducing misplacement of PLP due to the large size of Phe compared to Ile (Table 2-3 A and B and Table 2-4). Although Phe has not been observed at this position among known orthologues (Fig. 2-4), the milder phenotype in our patient with a p.Ile94Phe variant suggests that a hydrophobic/aromatic residue can be accommodated within the PLP-binding site.

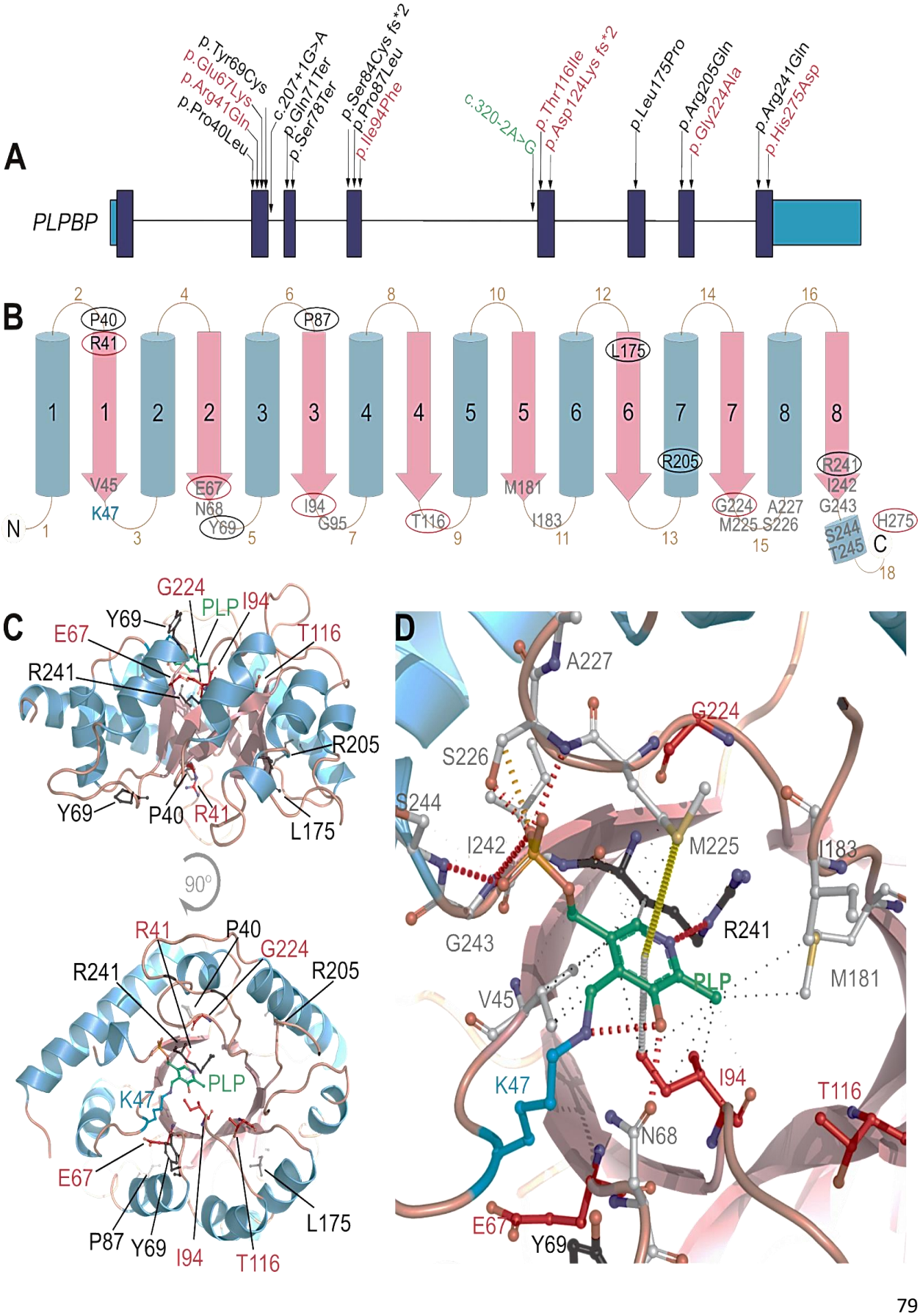
A
PLPBP
p.Tyr69Cys
p.Glu67Lys
p.Arg41Gln
p.Pro40Leu
c.207+1G>A
p.Gln71Ter
p.Ser78Ter
p.Ser84Cys fs*2
p.Pro87Leu
p.Ile94Phe
c.320-2A>G
p.Thr116Ile
p.Asp124Lys fs*2
p.Leu175Pro
p.Arg205Gln
p.Gly224Ala
p.Arg241Gln
p.His275Asp
B
N
C
P40
R41
P87
L175
R205
R241
V45
K47
E67
N68
Y69
I94
G95
T116
M181
I183
I242
G224
M225
A227
S226
G243
S244
T245
H275
C
G224
PLP
I94
Y69
E67
T116
R241
R205
P40
L175
90°
D
A227
G224
S226
S244
I242
M225
I183
G243
R241
PLP
M181
V45
K47
I94
T116
N68
E67
Y69

Fig. 2-2: Pathogenic variants in *PLPBP* and their genetic location, predicted secondary structure and tridimensional structure in the PLPHP protein in the context of PLP-binding. (A) Human *PLPBP* gene structure, protein coding exons shown in dark blue and 5' and 3' UTR shown in light blue. Position of the variants reported previously by Darin et al. (2016) and Plecko et al. (2017) are shown in black, seven novel variants identified by this study are shown in red and a splicing variant reported previously but also observed in our cohort is shown in green. (B) 2D graphical representation of the PLPHP protein based on secondary structure prediction and the tridimensional model (shown in D). Blue cylinders represent the outer α-helices and pink arrows represent the inner β-strands that comprise the (β/α)8-TIM barrel structure. Residues observed mutated in PLPHP-deficiency are shown in circles, black for variants reported previously or red for novel variants reported here. Residues located within 6Å of the modeled PLP position are shown in blue, from which the residues that establish contacts with PLP shown in cyan. (C) Predicted PLP-binding pocket showing the key Lysine 47 predicted to form the PLP-Lys adduct, black dashed lines indicate hydrogen bonds and salt bridges, green solid line show hydrophobic interactions. (D) tridimensional structure of the human PLPHP model showing the PLP molecule in green and the positions of the residues found mutated in PLPHP-deficiency in black or red according to A. Note that the variant p.His275Asp was co-inherited homozygously with p.Thr116Ile in patient 1; we report this as a variant of unknown significance, but we also modelled it in panels B-D. Images in C and D were prepared using PyMOL (Schrodinger, 2015).

Table 2-3A: List of *PLPBP* variants found in our cohort of 12 patients. All variants are expressed as found in PLPHP (NP_009129.1). Part A of the table is showing CADD and DUET scores and predictions. DUET uses as input the structural model developed for the human PLPHP to predict if a given amino acid change is stabilizing or destabilizing (ΔΔG). * Not modelled due to lack of this residue in yeast model used as template. NA: not available; NR: not reported.

Variant annotation			**DUET Predicted Stability Change (ΔΔG) (predicted effect)**	**CADD score**
Genomic (GRCh37)	**cDNA and protein**	**Variant frequency (gnomAD)**		
chr8: g.37630300 C>T	NM_007198: c.347C>T; p.Thr116Ile	NR	0.123 Kcal/mol (Stabilizing)	29.20
chr8: g.37635617 C>G	NM_007198: c.823C>G; p.His275Asp	NR	Not modeled*	23.3
chr8: g.37623066 G>A	NM_007198: c.122G>A; p.Arg41Gln	$4.06*10^{-6}$	-0.265 Kcal/mol (Destabilizing)	28.7
Chr8: g.37623143 G>A	NM_007198.3: c.199G>A; p.Glu67Lys	$4.06*10^{-6}$	-2.127 Kcal/mol (Destabilizing)	35
Chr8: g.37630271 A>G	NM_007198.3: c.320-2A>G splicing	$1.08*10^{-5}$	-	24.7
Chr8: g.37633509 G>C	NM_007198.3: c.671G>C; p.Gly224Ala	NR	-0.966 Kcal/mol (Destabilizing)	27.7
Chr8: g.37630323_37630326del	NM_007198: c.370_373del; (p.Asp124Lysfs*2)	NR	-	NA
chr8: g.37623834 A>T	NM_007198: c.280A>T; p.Ile94Phe	NR	-1.398 Kcal/mol (Destabilizing)	29.6

Table 2-3B: List of *PLPBP* variants found in our cohort of 12 patients. All variants are expressed as found in PLPHP (NP_009129.1). Part B of the table is showing variant effect predictions from 6 *in silico* prediction tools (SIFT, Polyphen2 HDIV, MutationTaster, MutationAssessor, FATHMM MKL, PROVEAN).

Variant (cDNA and protein)	**Detailed *in silico* predictions [predicted effect (score)]**					
	SIFT	**Polyphen2 HDIV**	**MutationTaster**	**MutationAssessor**	**FATHMM MKL**	**PROVEAN**
NM_007198: c.347C>T; p.Thr116Ile	Damaging (0.003)	Probably damaging (1)	Damaging (1)	Functional (high) (3.855)	Damaging (0.98019)	Damaging (-5.56)
NM_007198: c.823C>G; p.His275Asp	Damaging (0.017)	Benign (0.361)	Damaging (0.918861)	Non-functional (low) (1.1)	Damaging (0.96396)	Neutral (-0.71)
NM_007198: c.122G>A; p.Arg41Gln	Damaging (0.04)	Probably damaging (0.978)	Damaging (1)	Non-functional (low) (1.795)	Damaging (0.99714)	Damaging (-2.73)
NM_007198.3: c.199G>A; p.Glu67Lys	Damaging (0)	Probably damaging (1)	Damaging (1)	Functional (high) (4.1)	Damaging (0.99824)	Damaging (-3.96)
NM_007198.3: c.320-2A>G splicing	NA	NA	Damaging (1)	NA	Damaging (0.99207)	NA
NM_007198.3: c.671G>C; p.Gly224Ala	Damaging (0)	Probably damaging (0.999)	Damaging (1)	Functional (high) (4.07)	Damaging (0.99191)	Damaging (-5.69)
NM_007198: c.370_373del; (p.Asp124Lysfs*2)	NA	NA	Damaging (1)	NA	NA	NA
NM_007198: c.280A>T; p.Ile94Phe	Damaging (0.001)	Probably damaging (1)	Damaging (1)	Functional (high) (4.43)	Damaging (0.99692)	Damaging (-3.96)

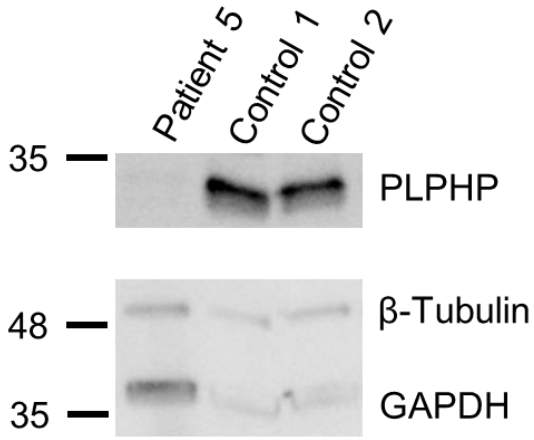

Fig. 2-3: Western blot of fibroblast lysates (20µg protein) from patient 5 showing that the patient is deficient for PLPHP. β-Tubulin and GAPDH were used as loading controls.

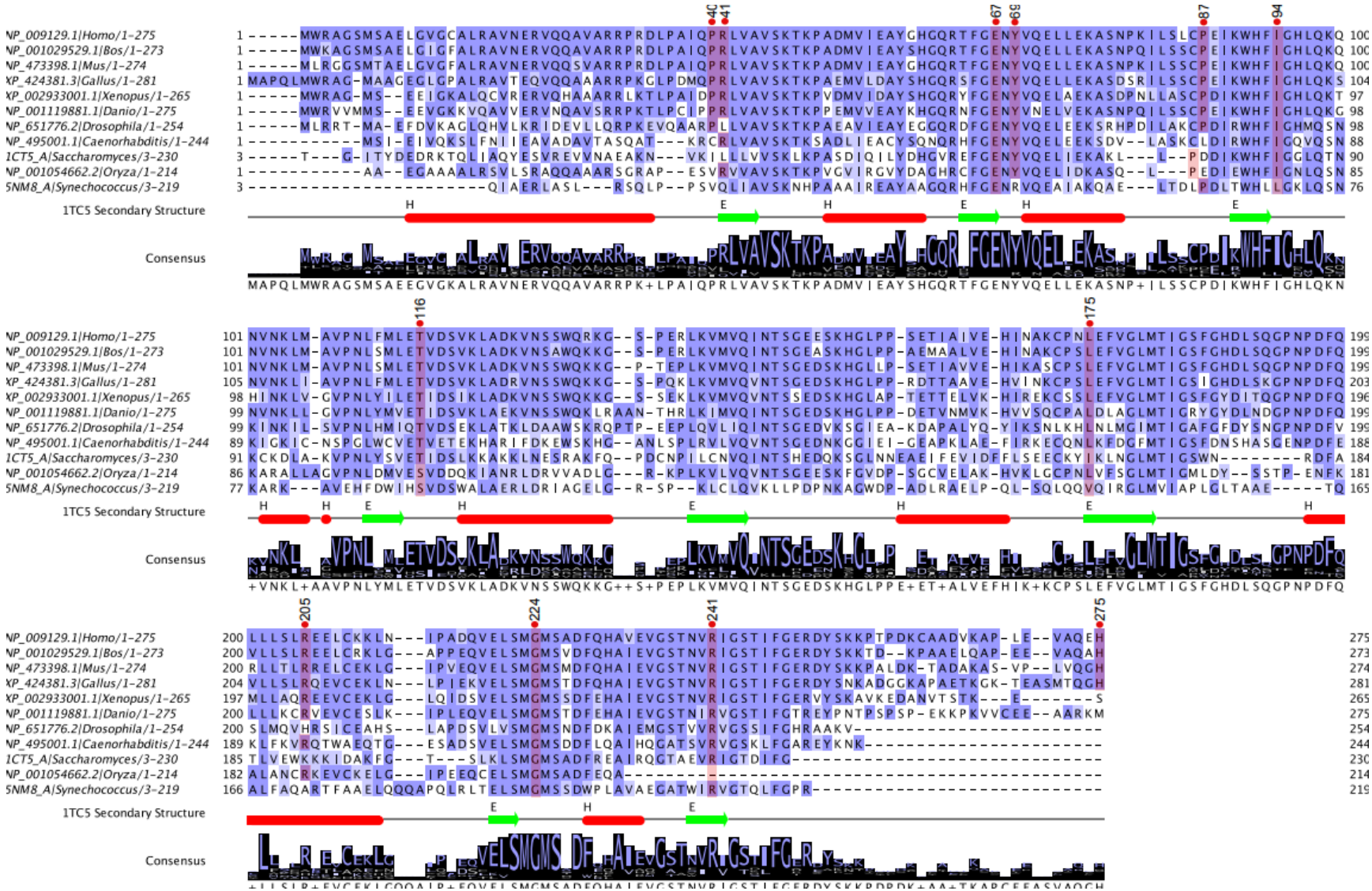

Fig. 2-4: Protein sequence alignment of PLPHP orthologues from several species (RefSeq identifiers shown in the sequence labels). Residues found mutated in patients are highlighted in red (missense mutations). Secondary structure as in the yeast orthologue (PDB 1CT5) is shown under the alignment. Consensus sequence is also shown. Image produced using Jalview (Waterhouse et al., 2009).

Table 2-4: Clinical severity scores based on system adapted from Al Teneiji et al. (2017). Variants are organized by whether seen in homozygotes or compound heterozygotes, then based on variant type (missense, truncating, splicing). Note that truncating variants are associated with the most severe phenotypes. NA[a], NA[b], NA[c], full clinical scores could not be calculated due to early death of these patients but assumed severe based on lethality. NA* full clinical score could not yet be calculated due to early age of patient, so GDD/ID cannot yet be assessed. [1]Variant reported by Darin et al. (2016). [2] Variant reported by Plecko et al. (2017). [3]Variant experimentally studied by Tremino et al. (2018).

Patient ID	Variant type	Amino acid change	First seizure/ movement episode score	GDD/ ID score	B6 response score	Severity score sum	Protein effect
Patients reported in this study							
1	Homozygous missense	p.Thr116Ile;	3	2	2	Severe (7)	Predicted LOF - variant likely impacts PLP binding
	Homozygous missense	p.His275Asp					Variant of unknown significance: variant likely impacts PLP binding
2	Homozygous missense	p.Arg41Gln	2	0	0	Mild (2)	Predicted to still bind PLP, but stability is reduced
3	Homozygous missense	p.Glu67Lys	3	3	2	Severe (8)	Predicted LOF - variant likely impacts PLP binding
4	Compound heterozygous nonsense & missense	c.320-2A>G;	3	NA[a]	NA[a]	Deceased: Severe (9)	LOF - Truncated protein[1]
		p.Gly224Ala					Predicted LOF - Variant likely disrupts loop 15 structure and orientation of several PLP binding residues
5	Homozygous nonsense	p.Asp124Lys fs*2	3	NA[b]	NA[b]	Deceased: Severe (9)	LOF - Truncated protein (band absent as in Supp. Fig 1)
6	Homozygous missense	p.Thr116Ile	3	2	3	Severe (8)	Predicted LOF - variant likely impacts PLP binding

7	Homozygous missense	p.Ile94Phe	1	1	1	Mild (3)	Predicted LOF? Variant likely impacts PLP binding, but it is possible Phe could still establish aromatic/hydrophobic contacts with PLP;
8	Homozygous missense	p.Arg41Gln	3	0	0	Mild (3)	Predicted to still bind PLP, but stability is reduced
9	Homozygous missense	p.Arg41Gln	3	0	0	Mild (3)	Predicted to still bind PLP, but stability is reduced
10	Homozygous missense	p.Glu67Lys	3	2	2	Severe (7)	Predicted LOF - variant likely impacts PLP binding
11	Homozygous missense	p.Glu67Lys	3	2	2	Severe (7)	Predicted LOF - variant likely impacts PLP binding
12	Homozygous deletion	p.Asp124Lysfs*2	3	NA*	2	NA*	LOF - Truncated protein (band absent as in Supp. Fig 1)
Patients reported by Darin et al. (2016)							
1	Homozygous nonsense	p.Ser78Ter	3	NA[c]	NA[c]	Deceased Severe (9)	LOF - Truncated protein[1]
2	Homozygous nonsense	p.Ser78Ter	3	2	3	Severe (8)	LOF - Truncated protein[1]
3	Homozygous nonsense	p.Ser78Ter	3	3	3	Severe (9)	LOF - Truncated protein[1]
4	Homozygous missense	p.Leu175Pro	3	3	2	Severe (8)	LOF - Misfolded protein[1,3]
5	Compound heterozygous missense & missense	c.207+1G>A; c.320-2A>G;	3	3	2	Severe (8)	LOF - Truncated protein[1]; absent band in Western blot1
6	Homozygous nonsense	p.Gln71Ter	3	2	3	Severe (8)	LOF - Truncated protein[1]

7	Compound heterozygous missense	p.Pro87Leu;	1	1	1	Mild (3)	Lower solubility and some precipitated; Folded forms still binds to PLP [3]
		p.Arg241Gln					LOF - variant abolishes PLP binding3, drastic reduction in stability (Tm shift - 14^{o}C)[3]
Patients reported by Plecko et al. (2017)							
1	Compound heterozygous missense & missense	p.Pro40Leu;	2	0	1	Mild (3)	Reduced stability (Tm shift - 6^{o}C); Still binds to PLP [3]
		p.Arg241Gln					LOF - variant abolishes PLP binding, drastic reduction in stability (Tm shift - 14^{o}C)[3]
2	Compound heterozygous truncating & missense	p.Ser84Cysfs*21;	2	1	1	Moderate (4)	LOF - Truncated protein [2]
		p.Arg205Gln					Reduced stability (Tm shift - 7^{o}C); Still binds to PLP 3
3	Homozygous missense	p.Pro87Leu	3	3	1	Severe (7)	Lower solubility and some precipitated; Folded forms still binds to PLP [3];
4	Homozygous missense	p.Tyr69Cys	2	0	2	Moderate (4)	Cys forms disulfide bridges that creates an artificial dimer that hides PLP. Decreased PLP binding in 30%[3]

2.3.4 Biochemical and vitamer profiles of PLPHP deficiency patients

Biochemical investigations performed in patients prior to B6 treatment uncovered several abnormal profiles. The most consistently observed alterations were hyperlactatemia (6 patients) and hyperglycinemia (3 patients). Investigation of urine organic acids in patient 7 revealed the presence of vanillactic acid, vanillpyruvic acid, and n-acetyl-vanilalanine, similar to what is commonly seen in AADC deficiency. Minor elevations of urine lactic, malic, 2-ketoglutaric, and n-acetylaspartic acids were also observed. Pre-treatment CSF metabolomics analysis showed elevated 3-methoxytyrosine (Z-score = 4.2) with normal 3-methoxytyramine levels, and mild elevations of: palmitoyl-GPA 16:0 (Z-score= 3.7), α-ketoglutarate (Z-score= 3.2), adenosine (Z-score= 2.6), 2-aminooctanoate (Z-score= 2.6) and tryptophan (Z-score= 2.5).

VitB6 vitamer analysis in plasma from patient 4 (on no vitB6 treatment) revealed low levels of PLP (1.1nM, reference >20.5nM) and elevation of 4-pyridoxic acid (PA) (130 nM, reference <84 nM). Analysis of vitB6 vitamers from patient 5 primary skin fibroblast lysates revealed significant decreases in PLP ($p<0.0001$), pyridoxamine 5'-phosphate (PMP) ($p=0.007$) and PN ($p=0.0018$), along with accumulation of pyridoxine 5'-phosphate (PNP) ($p<0.0001$, ANOVA) in the patient cells compared to the controls, whereas PL, pyridoxamine (PM) and PA showed no difference (Fig. 2-5). Similarly, in PLPHP-deficient HEK293 cells, PLP was markedly decreased ($p<0.0001$) and PNP was greatly increased ($p<0.0001$) (Fig. 2-7).

Table 2-5: concentrations of B6 vitamers in plasma from 2 patients affected with PLPHP deficiency. Concentrations are expressed in nM.

	PL	PM	PN	PA	PLP
Patient 4	39	<2.7	0.1	130	1.1
Patient 3, treated	276	<2.7	0.1	365	685
Reference interval, untreated (Mathis et al., 2016)	6.6-54	<2.7	<1	6.7-84	16-269

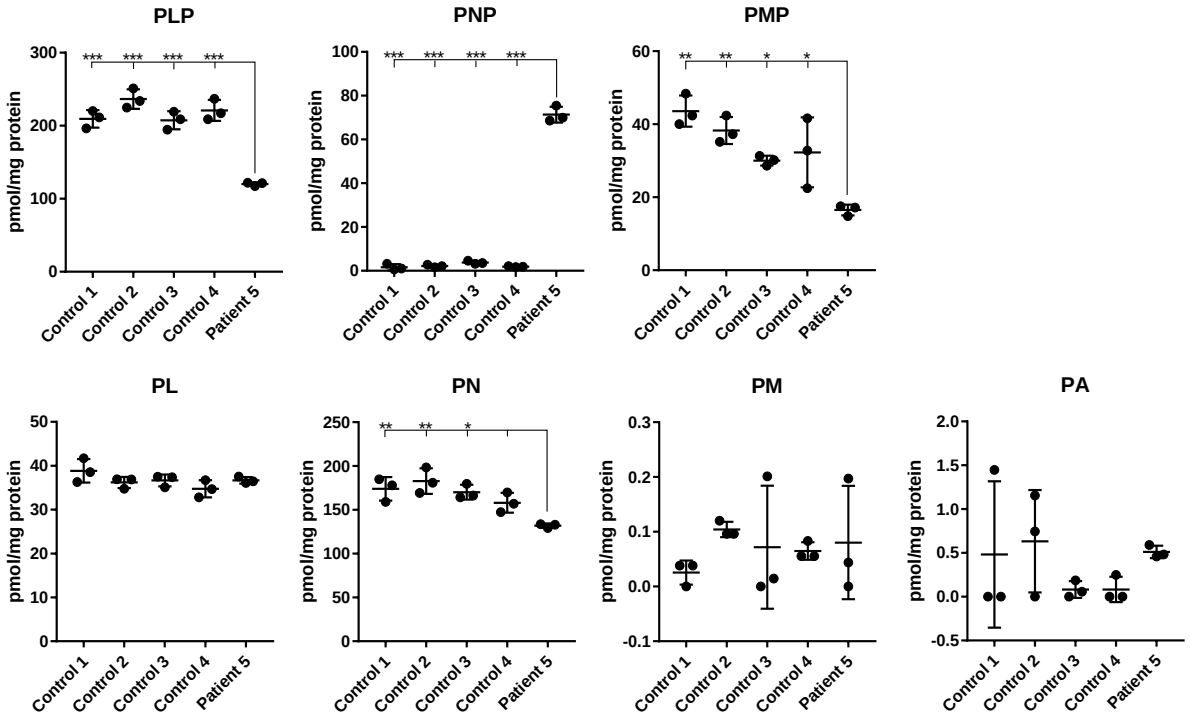

Fig. 2-5: B6 vitamer profiles in cultured fibroblasts from four control subjects and patient 5. Data are n=3 biological replicates per group. PA, pyridoxic acid; PL, pyridoxal; PLP, pyridoxal 5'-phosphate; PM, pyridoxamine; PMP, pyridoxamine 5'-phosphate; PN, pyridoxine; PNP, pyridoxine 5'-phosphate. ANOVA ***p<0.001, **p<0.01, *p<0.05.

2.3.4 PLPHP mitochondrial localization and effects on energy metabolism

2.3.4.1 Studies in human cells

To provide further insights on PLPHP function, we investigated its subcellular localization in human cells. Some evidence suggests that PLPHP resides primarily in the cytoplasm (Ikegawa et al., 1999; Uhlen et al., 2015) (Human Protein Atlas available from www.proteinatlas.org). The MitoCarta 2.0 database, however, suggests a mitochondrial localization for human and mouse PLPHP (Calvo et al., 2016; Pagliarini et al., 2008). Furthermore, MitoMiner 4.0 rates the protein as "known mitochondrial" (Integrated Mitochondrial Protein Index score 0.991), based on mass-spectrometry evidence (Smith and Robinson, 2016). To test if PLPHP does indeed localize to the mitochondria, we purified mitochondrial fractions using a recently developed method for immunoprecipitation of HA-tagged mitochondria in HeLa cells (Chen et al., 2017). The pure mitochondrial fractions were enriched for PLPHP, further evidencing the mitochondrial localization of this protein (Fig. 2-6A). Cytosolic and mitochondrial localization were also evidenced by immunofluorescence assays (Fig. 2-7B-C).

Furthermore, we observed that the skin fibroblast cell line obtained from Patient 5 displays reduced growth in the presence of galactose as carbon source in the culture medium, while normal growth was observed in the presence of glucose (Fig 7C-D). Patient 5 fibroblasts also showed an elevated lactate-to-pyruvate ratio (41.65±7.13 SD; reference 9.57-26.49), which is consistent with NADH accumulation. Activities of mitochondrial pyruvate dehydrogenase and respiratory complexes II-IV were normal, as were mitochondrial morphology and inner membrane potential (data not shown). Extracellular flux testing showed an apparent reduction of carbonyl cyanide-*4*-(trifluoromethoxy)phenylhydrazone (FCCP)-stimulated spare respiratory capacity. These data may indicate that a direct role in electron transport is unlikely. However, considering that primary

skin fibroblasts do not always replicate the disease phenotype in mitochondrial disorders (Soiferma and Saada, 2015), we decided to test other cell models.

2.3.4.2 Studies in yeast

Yeast is a well-established model to study mitochondrial function and disease (Lasserre et al., 2015). In yeast cells, ATP is produced through two mechanisms. In the presence of glucose, ATP is primarily generated via glycolysis, while gluconeogenesis and mitochondrial respiration are repressed. In the absence of fermentable carbon sources, the cell resorts to oxidative phosphorylation (OXPHOS) for the production of ATP. As a result, mutations affecting OXPHOS components are not lethal and the levels of expression of these components can be manipulated simply by changes in culture conditions (Barrientos, 2003).

To determine if PLPHP could play a role in energy metabolism, we studied the function of the PLPHP ortholog of *S. cerevisiae*: YBL036C. Growth of *ybl036Δ* yeast cells was completely normal on glucose medium but markedly reduced under conditions in which either glycerol, oleate, or ethanol was used as a carbon source (Fig. 2-6B-D). Since oxidation of the latter three substrates (but not glucose) is fully dependent on the proper functioning of the mitochondrial citric acid cycle and oxidative phosphorylation system, these findings suggest that YBL036C affects mitochondrial metabolism. Introduction of human PLPHP in *ybl036cΔ* yeast partially rescued the growth phenotype, which is consistent with a conserved function (Fig. 2-6D). Because PLP is a cofactor for key mitochondrial metabolism enzymes (Percudani and Peracchi, 2003) including aspartate aminotransferase (AST) in the malate-aspartate shuttle and serine hydroxymethyltransferase (SHMT2) involved in one-carbon metabolism, the metabolic pleiotropy of PLPHP deficiency is expected, although the mechanisms through which *PLPBP* variants produce mitochondrial dysfunction remain to be elucidated.

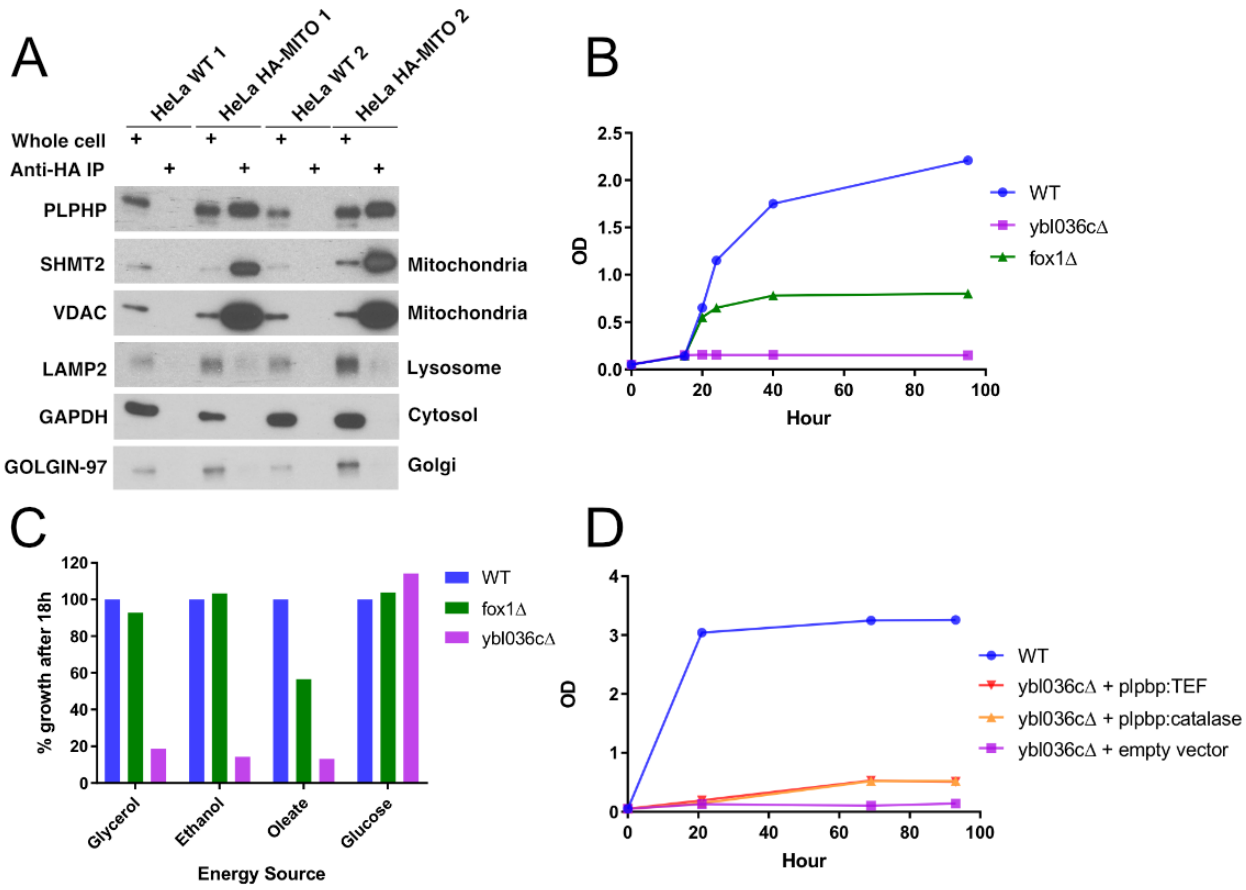

Fig. 2-6: Evidence of mitochondrial enrichment of PLPHP in HeLa cells and growth defects in yeast null for the PLPHP ortholog in several energy sources requiring active mitochondrial metabolism. (A) Western blot of WT HeLa cells and HeLa cells with HA-tagged mitochondria (HeLa HA-MITO) that were immunoprecipitated for mitochondrial purification, showing PLPHP enrichment in the mitochondrial fraction, other antibodies show minimal contamination from the cytosol or other organelles; (B) Growth curves of wild-type yeast cells and mutant strains on rich oleate medium. The strains shown are: WT (BY4742) (blue), *fox1Δ* (green) and *ybl036cΔ* (purple). (C) Growth of wild-type and mutant cells after 18 hours on 20g/L glucose and non-fermentable carbon sources: rich oleate, 2% ethanol and 2% glycerol medium. Values are expressed as % growth relative to WT. The strains shown are: WT (BY4742) (blue), *fox1Δ* (green) and *ybl036cΔ* (purple). (D) Growth of wild-type cells and mutant cells on 2% ethanol medium. The strains shown are: WT (BY4742) (blue), *ybl036cΔ* + pPROSC1a (human PLPHP under catalase promoter (orange) or pPROSC2a (human PLPHP under Tef promoter) (red) and *ybl036cΔ* + empty vector (purple).

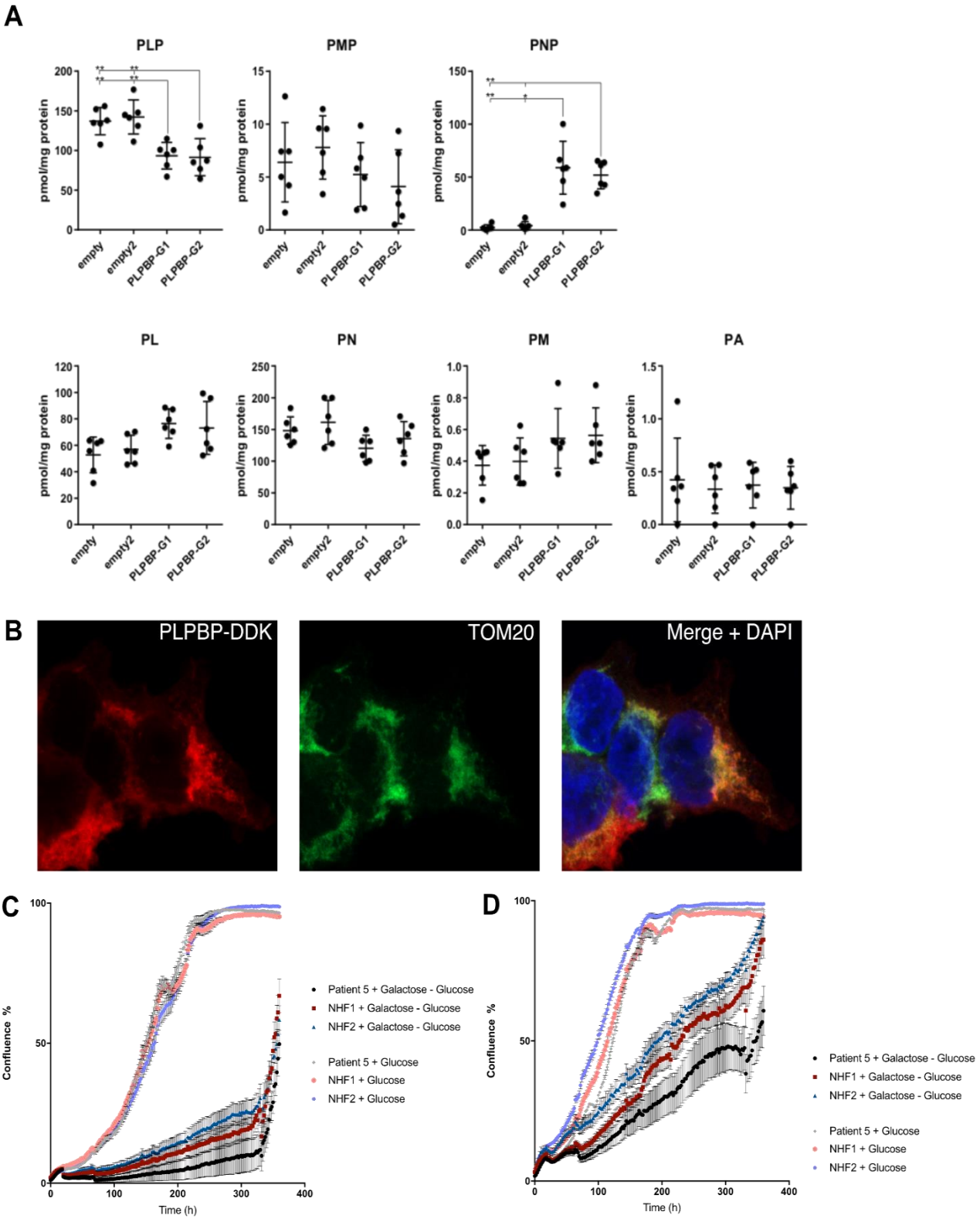
A
PLP
PMP
PNP
PL
PN
PM
PA
pmol/mg protein
empty
empty2
PLPBP-G1
PLPBP-G2
B
PLPBP-DDK
TOM20
Merge + DAPI
C
D
Confluence %
Time (h)
Patient 5 + Galactose - Glucose
NHF1 + Galactose - Glucose
NHF2 + Galactose - Glucose
Patient 5 + Glucose
NHF1 + Glucose
NHF2 + Glucose

Fig. 2-7: (A) B6 vitamer profiles in control (WT+empty vector) and PLPHP-deficient HEK293 cells (PLPHP-KO: PLPBP-G1 and PLPBP-G2). Data are from n=6 independent experiments (each consisting of 3 biological replicates per group), ±SD. **(B)** HEK293 cells overexpressing PLPHP with a C-terminal Myc-DDK tag shows co-localization of PLPHP with Tom20, a mitochondrial marker. Incucyte analysis of cell growth in 5mM galactose or 25mM glucose as carbon source seeded at 500 cells per well (C) or 1000 cells per well (D) in 96 well plates. DMEM no glucose + 1mM sodium pyruvate was used as base media for C and D. Abbreviations: PN, pyridoxine; PL, pyridoxal; PM, pyridoxamine; PNP, pyridoxine 5'-phosphate; PLP, pyridoxal 5'-phosphate; PMP, pyridoxamine 5'-phosphate; PA, pyridoxic acid. **$p<0.01$, *$p<0.05$.

2.3.4 Loss of Plphp in zebrafish leads to spontaneous seizures and early death

We developed zebrafish lines carrying two different *plpbp* mutant alleles: a 4bp deletion (chr23:34037190-chr23:34037193) (NM_001126409; p.Asp23Lysfs*138) (*plpbp*^{ot101}) and the mutation CGG**GTGAATCA**A>CGG**TGG--TGG**A (chr23:34037185-34037192) (*plpbp*^{ot102}), the latter resulting in a 2bp frameshift, in the transcript (NM_001126409; p.Asp23Trpfs*56) (Fig. 2-9A). We crossed the F2s from each heterozygous line (*plpbp*$^{+/ot101}$ x *plpbp*$^{+/ot102}$) to generate compound heterozygous *plpbp*$^{ot101/ot102}$ (henceforth referred to as *plpbp*$^{-/-}$). F3 homozygous mutants and/or compound-heterozygous *plpbp*$^{-/-}$ displayed loss of function of Plphp as evidenced by Western blot analysis (Fig. 2-9B). There were no phenotypic differences between homozygous mutants and compound heterozygous mutants (Fig. 2-8), and the latter were used for experiments due to the relative ease of genotyping. In the F3 generation, there were no obvious morphological or behavioral differences between genotypes up until ~9 dpf. As early as 10 dpf, *plpbp*$^{-/-}$ larvae showed spontaneous seizure-like behavior, and all mutants died by 16 dpf (Fig. 2-9C).

Epilepsy in zebrafish can be characterized by episodes of excessive locomotion, sustained rhythmic jerking (clonus), stiffening (tonus) and/or tonic-clonic seizures (Baraban et al., 2005, 2013; Hortopan et al., 2010; Teng et al., 2010). We measured the amount of high-speed movements as a correlate of hyperactivity and found that untreated *plpbp*$^{-/-}$ larvae spent significantly more time ($p<0.01$) and moved a greater distance in high-speed movements ($p<0.01$) than WT or heterozygous siblings (Fig. 2-9D-E). 11 dpf *plpbp*$^{-/-}$ larvae displayed increased *c-fos* mRNA expression (a biomarker of neuronal activity (Baraban et al., 2005)) compared to WT larvae, but less than WT treated with 15mM PTZ (Fig. 2-9F). Finally, tectal field recordings of agar-immobilized 11 dpf larvae showed that mutant larvae (n=5) displayed spontaneous electrical discharges with high amplitude and duration, similar to ictal-like events previously reported in

other zebrafish models, whereas WT siblings (n=5) showed only normal activity (Fig. 2-9G and 2-10G). We conclude that *plpbp*$^{-/-}$ larvae recapitulate a seizure phenotype.

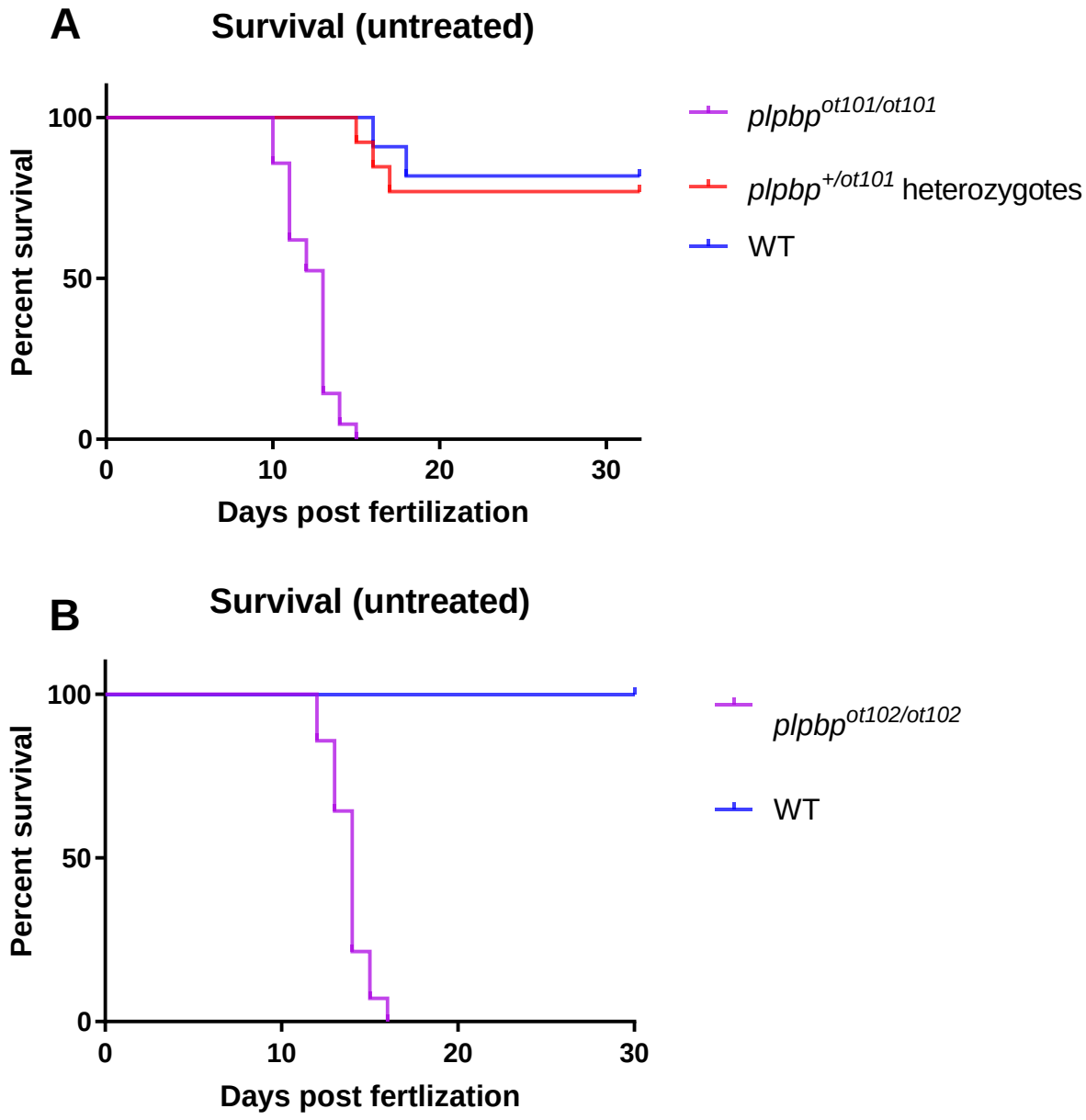

Fig. 2-8: Mutant zebrafish larvae homozygous for either the 4bp (A) or 2bp (B) frameshift mutations show a similar survival pattern as the compound heterozygous larvae *plpbp*$^{ot101p/ot102}$ (Fig. 2-9C). Additionally, these larvae start seizing by 10dpf/11dpf. We thus did subsequent experiments with compound heterozygotes due to ease of genotyping.

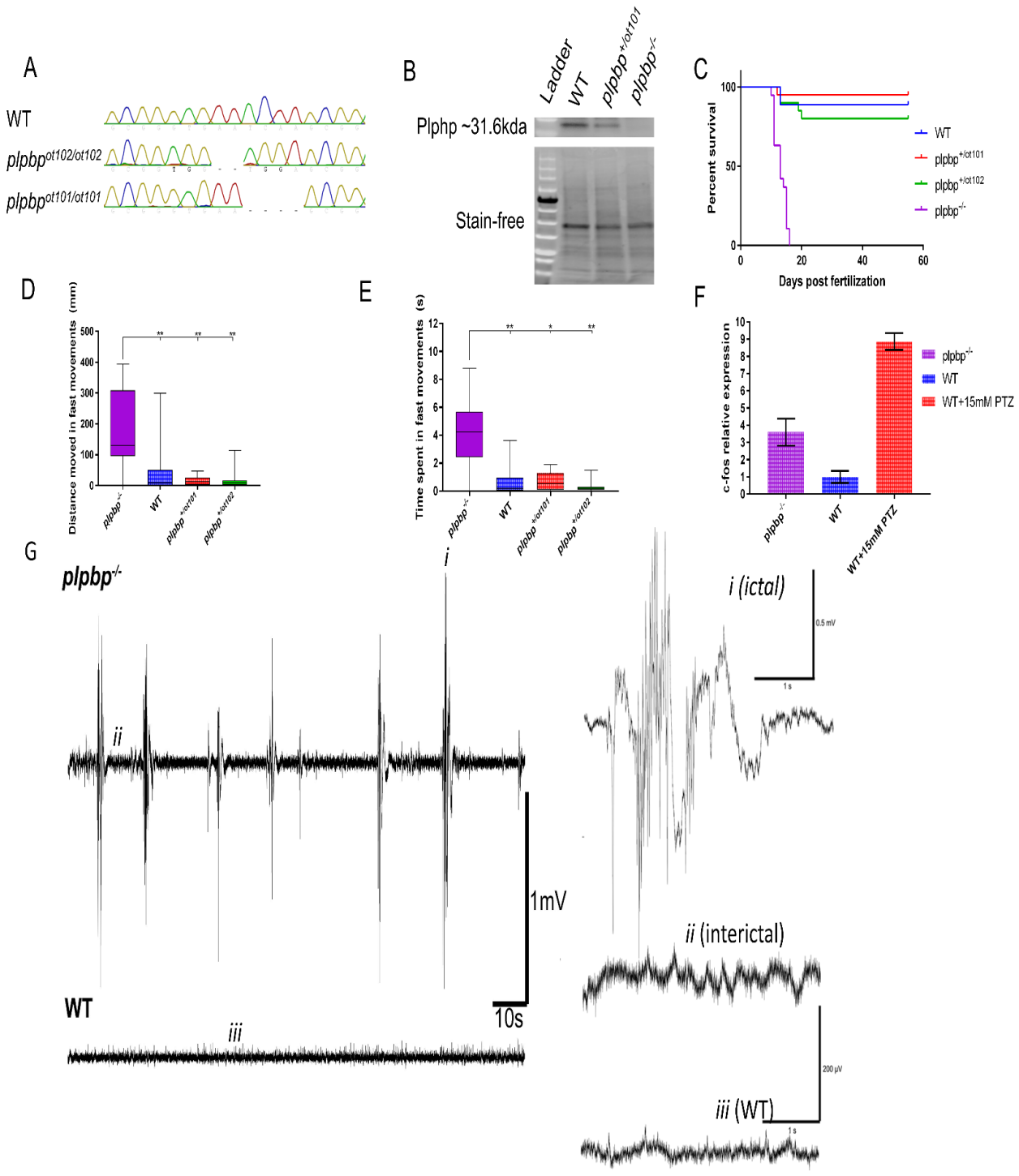
A
WT
plpbp ot102/ot102
plpbp ot101/ot101
B
Ladder
WT
plpbp +/ot101
plpbp -/-
Plphp ~31.6kda
Stain-free
C
Percent survival
Days post fertilization
WT
plpbp +/ot101
plpbp +/ot102
plpbp -/-
D
Distance moved in fast movements (mm)
E
Time spent in fast movements (s)
F
c-fos relative expression
plpbp -/-
WT
WT+15mM PTZ
G
plpbp -/-
i
i (ictal)
0.5 mV
1 s
ii
1mV
10s
ii (interictal)
WT
iii
200 µV
iii (WT)
1 s

Fig. 2-9: Development of *plpbp*$^{-/-}$ zebrafish model by CRISPR/Cas9 and epileptic phenotypic analysis. A) Chromatograms of zebrafish larvae showing WT and the genotypes for homozygous mutants *plpbp*$^{ot101/ot101}$ *and plpbp*$^{ot102/ot102}$. Compound heterozygous mutant larvae (*plpbp*$^{ot101/ot102}$) (not shown) were used for most experiments with the same phenotype as the homozygotes. (B) Cropped Western blot (for clarity) showing that no Plphp protein was detected in mutant larvae. Total protein (Stain free blot) is shown underneath for standardization. (C) Survival curves showing reduced survival of mutant larvae compared to WT and the two heterozygous parental types (n=20 larvae per group). (D and E) Mutant larvae moved a greater total distance during fast speed (>20mm/s) movements and spent more time in fast movements, respectively (n=16 larvae per group). (F) Relative mRNA expression showing increased expression of *c-fos* in mutant larvae compared to WT larvae, PTZ treatment was used as a positive control. (G) Example electrophysiology recordings of mutant (top) and WT (bottom) larvae showing increased number of ictal-like events. Inset are zoomed-in examples (4 seconds) of ictal-like, interictal and WT recordings. Significance: ** ($p<0.01$), * ($p<0.05$).

2.3.5 Vitamin B6 responsiveness and dependency in *plpbp*$^{-/-}$ larvae

We tested if seizures in *plpbp*-null zebrafish larvae show beneficial response to PLP and PN. Although we observed a PLP dose-dependent increase in the lifespan, all larvae died by 26 dpf, even at the highest dose (500 µM PLP) (Fig. 2-10A). Treatment with PN showed a more remarkable effect, with dose-dependent rescue of survival to nearly 100% until juvenile stages using 5 or 10 mM PN (Fig. 2-10B). Removal of PN daily treatments induced seizures and death within days, indicating B6-dependence, as previously reported for *aldh7a1*$^{-/-}$ larvae (Pena, Roussel, et al., 2017).

In agreement with the B6-dependency and rescue, PN treatment significantly reduced the number of hyperactive movements as measured by the time spent ($p=0.0028$) and distance travelled in high-speed movements ($p<0.0001$) (Fig. 2-10D-E). Additionally, by classifying larval movements as little movement (S0), increased spontaneous swim bursts (S1), whirlpool-like swimming (S2) or whole-body convulsions with loss of posture (S3) (Baraban et al., 2005) through blinded analysis, we observed that only untreated *plpbp*$^{-/-}$ larvae displayed S2 or S3 swimming behavior (Fig. 2-10F). Similarly, treatment with 5mM PN resulted in a 5-fold reduction of the

number of high-amplitude spikes of electrographic activity in tectal field recordings (p=0.0458) (Fig. 2-10G). We conclude that *plpbp*$^{-/-}$ larvae have B6-responsive and dependent epilepsy.

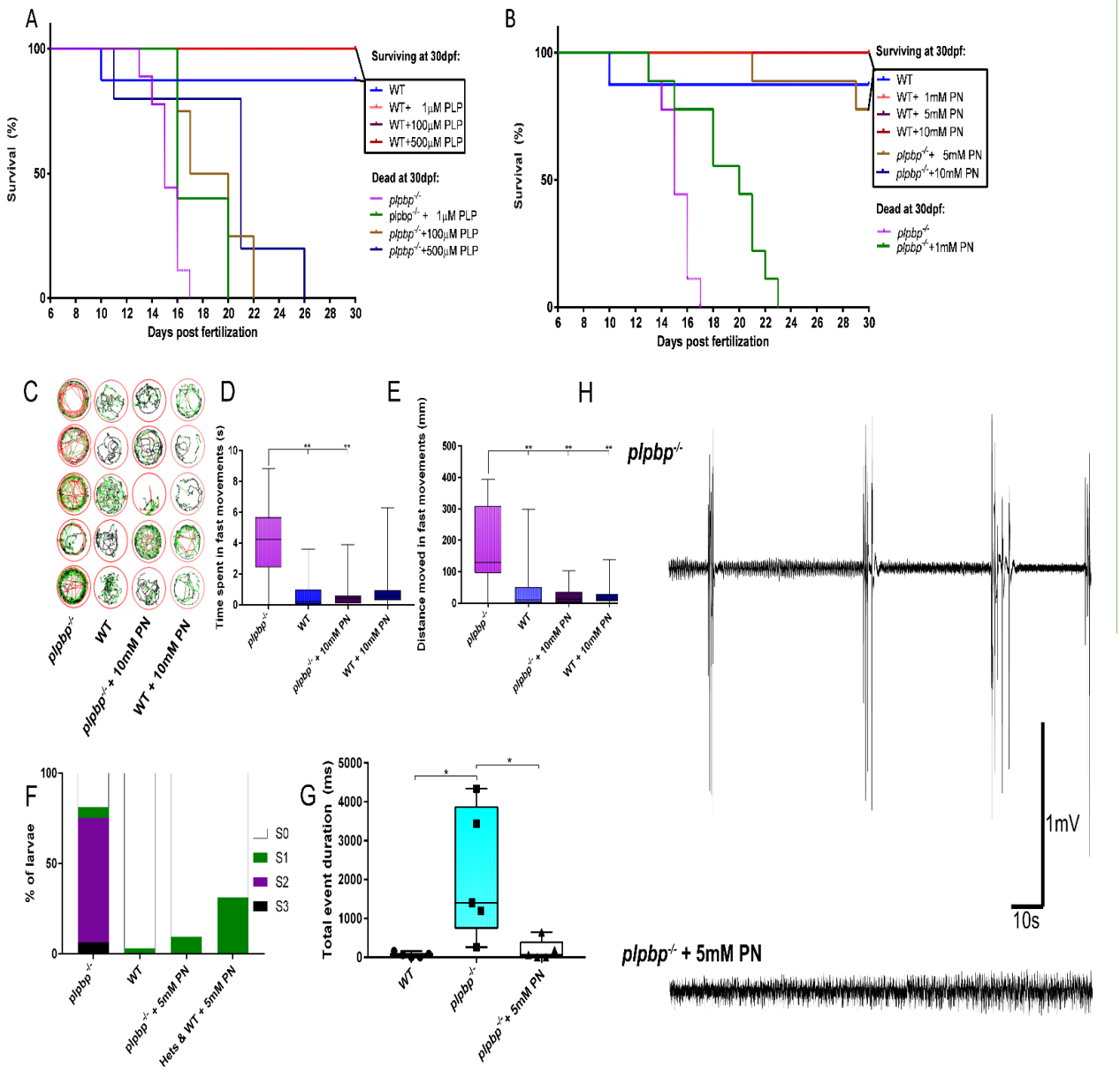

Fig. 2-10: Vitamin B6-responsive epilepsy in *plpbp*$^{-/-}$ zebrafish larvae. Survival in mutants was moderately improved using PLP (A) but showed a better response that was clearly dose-dependent with pyridoxine (B). (C) 5-minute trace recordings of 11 dpf zebrafish larvae showing increased hyperactivity in the mutants which was alleviated with 10mM pyridoxine treatment, as measured by (D) time spent in fast movements and (E) distance moved in fast movements. (F) Highest seizure-like behavior category identified by blinded observers. Only untreated mutant larvae showed evidence of S2 or S3 seizure-like activity. (G) Electrographic activity in mutant larvae was normalized by treatment with 5mM pyridoxine. (H) Example electrophysiology recordings of untreated and treated mutant larvae. Significance: ** ($p<0.01$), * ($p<0.05$).

2.3.6 Biochemical abnormalities in *plpbp*$^{-/-}$ zebrafish

B6 vitamer levels were quantified in untreated 10 dpf larval lysates. The *plpbp*$^{-/-}$ larvae displayed significant reductions in systemic concentrations of PLP and PL (1.4 and 5.5-fold reductions, p=0.0026 and p=0.0003, respectively) compared to WT siblings, together with non-significant reductions in PMP and PN levels (Fig. 2-11A). PNP was not detectable in either group. As PLP was markedly low in *plpbp*$^{-/-}$ larvae, we hypothesized that neurotransmitter and amino acid metabolism would be greatly affected since most transamination/decarboxylation reactions require PLP. Neurotransmitters were also analyzed in fasted 11 dpf larval lysates (Fig. 2-11B). We noted a significant decrease in levels of adrenaline ($p<0.001$) as well as significant accumulations of 3-methoxytyramine (3-MT), normetanephrine and 5-hydroxyindoleacetic acid (5-HIAA) ($p<0.001$).

Analysis of amino acid levels by liquid chromatography-mass spectrometry in fasted larvae revealed 17 analytes significantly different between homozygous mutants and the heterozygous/WT siblings (Fig. 2-11C). Nine analytes were found reduced in *plpbp*$^{-/-}$ larval extracts: threonine, asparagine, glutamate, glutamine, proline, alanine, α-aminobutyric acid, γ-aminobutyric acid (GABA), and lysine (Tukey's post-hoc comparison: p= 0.0315, <0.0001, 0.0015, <0.0001, 0.0020, <0.0001, 0.0006, <0.0001, and 0.0068, respectively). Eight compounds were significantly elevated in *plpbp*$^{-/-}$ larvae compared to WT: methionine, cystathionine, isoleucine, tyrosine, ß-alanine, phenylalanine, aminoisobutyric acid and tryptophan (p=0.0147, <0.0001, <0.0001, 0.0005, <0.0001, <0.0001, <0.0001, and 0.0013, respectively). Low GABA levels were also observed in *aldh7a1*$^{-/-}$ zebrafish and could constitute part of the pathophysiologic mechanism for seizure occurrence. We conclude that Plphp deficiency leads to significant

disruptions in amino acid and neurotransmitter metabolism and likely other metabolic pathways that are dependent on PLP in zebrafish.

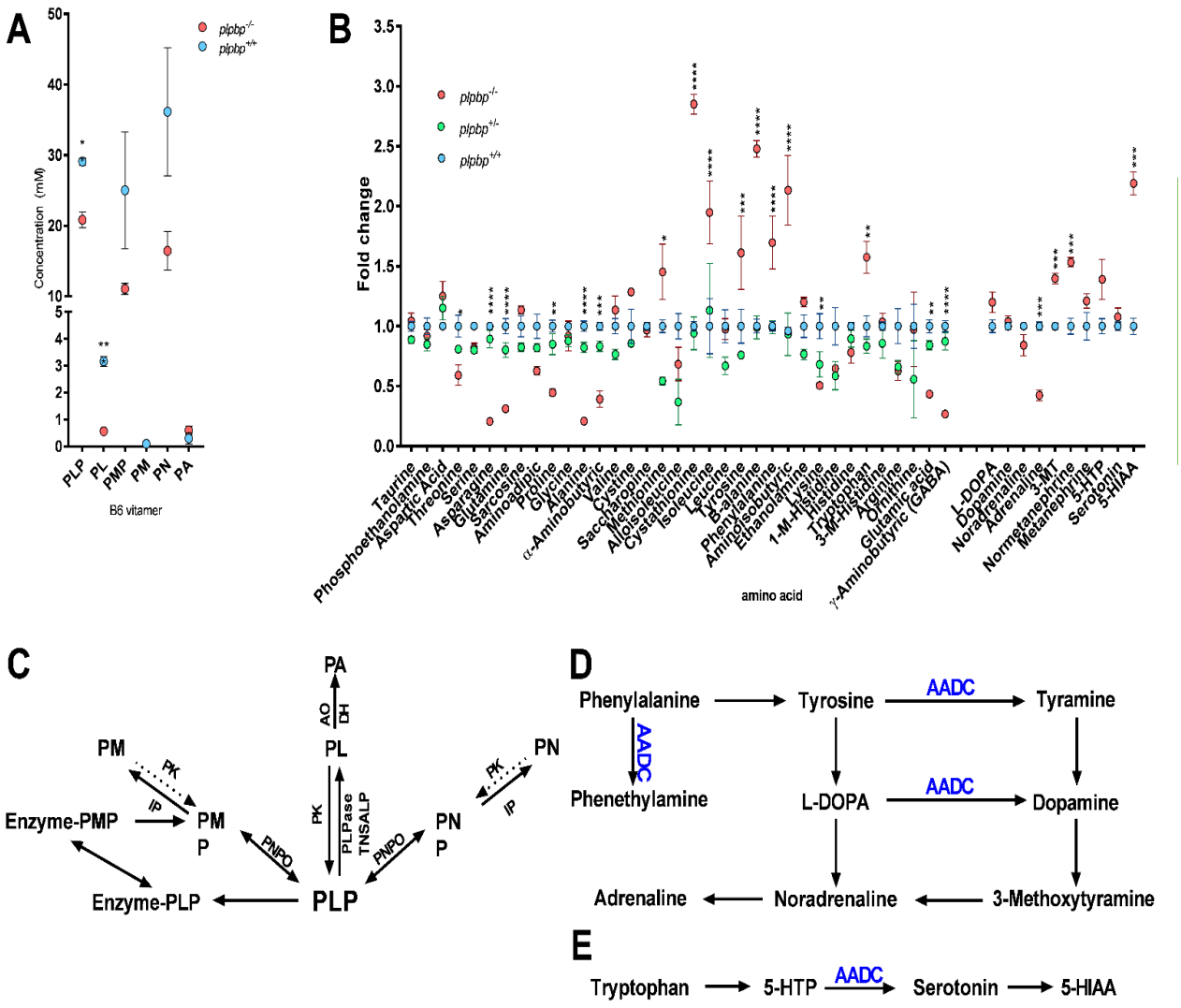

Fig. 2-11: Targeted mass spectrometry studies of *plpbp*$^{-/-}$ zebrafish larvae indicates changes in B6 vitamer, amino acid, and neurotransmitter profiles. (A) B6 vitamer profile of Mutant and WT 10 dpf larvae. (B) Amino acid and neurotransmitter profile of whole larval mutant, heterozygous and WT 11 dpf larvae after 24 hours fasting. (C) Metabolic pathways for the synthesis and degradation of PLP. (D). Biosynthetic pathways of catecholamines and trace amines, highlighting (in blue) the role of AADC. (E) The serotonin biosynthesis pathway, highlighting the role of AADC. Abbreviations: 3-MT: 3-methoxytyramine, 5-HIAA: 5-hydroxyindoleacetic acid, 5-HTTP: 5-hydroxytrytpophan, AADC: aromatic-L-amino acid decarboxylase, AO: *aldehyde oxidase I*, DH: β-NAD dehydrogenase, PA: 4-pyridoxic acid, PK: pyridoxal kinase, PL: pyridoxal, PLP: Pyridoxal 5'-Phosphate, PM: pyridoxamine, PMP: pyridoxamine 5'-phosphate, PN: pyridoxine, PNP: pyridoxine 5'-phosphate, PNPO: PNP oxidase Significance: ****($p<0.0001$), ***($p<0.001$), ** ($p<0.01$), * ($p<0.05$).

2.4 Discussion

Here we report a cohort of 12 patients, six novel disease-causing variants in *PLPBP*, and experimental models to further elucidate the pathophysiology of this B6EE. Many of the clinical features of PLPHP deficiency in this new cohort of patients concur with those described by Darin et al. (2016) and Plecko et al. (2017), thus confirming the previously described phenotypic spectrum. Additionally, our patients presented with novel features: one patient required folinic acid in addition to vitB6 for adequate seizure control, two patients suffered a lethal mitochondrial encephalopathy phenotype, and another patient presented with an AADC deficiency-phenocopy without clear epilepsy. Folinic acid-responsive seizure have been also described in some patients with *ALDH7A1* deficiency (Stockler et al., 2011), suggesting a common mechanism between these two forms of B6EE that underlie the favorable response to folinic acid. Ramos et al. (2017) reported decreased concentrations of 5-methyltetrahydrofolate (5MTHF) in vitB6-deprived Neuro-2a cells. Since folinic acid is a precursor for 5MTHF, the study suggested that the low 5MTHF levels might justify the response of some B6EE patients to folinic acid supplementation (Ramos et al., 2017). In our cohort of patients, 5MTHF was measured in CSF of patient 10 and found to be within normal range. Darin et al. (2016) described increased levels of AADC substrates in another PLPHP-deficient patient, and our zebrafish *plpbp*$^{-/-}$ model accumulated phenylalanine, tryptophan and tyrosine, in keeping with reduced AADC function. It is possible that reduction of AADC function may contribute to the clinical picture in PLPHP-deficient patients, given it is a PLP-dependent enzyme important in the biosynthesis of serotonin, dopamine, epinephrine and norepinephrine (Brun et al., 2010). Paroxysmal involuntary movements that are non-epileptic in origin were also reported in other B6EEs like PDE-ALDH7A1 and PNPO deficiency and were attributed to impaired AADC activity and dopaminergic neurotransmission (Gospe, 2010; Schmitt et al., 2010; Wilson et al., 2019).

The severe clinical presentation of patients 4 and 5 with respiratory failure, chronic lactic acidosis, NADH accumulation, and periventricular cerebral cysts prompted us to investigate whether PLPHP could have a role in mitochondrial energy metabolism. We observed enrichment of PLPHP in pure mitochondrial fractions extracted from HA-tagged mitochondria in HeLa cells (Fig. 2-6). The mitochondrial enrichment was also evidenced by immunofluorescence studies (Fig 7). *In silico* prediction tools and previous high-throughput mass spectrometry experiments suggested intracellular localization of PLPHP for both the cytoplasm and mitochondria (Calvo et al., 2016; Smith and Robinson, 2016). Although we could not identify clear electron transport chain defects in in the primary skin fibroblast cell line obtained from patient 5 by Seahorse assay, its reduced growth in galactose and our identified mitochondrial enrichment of PLPHP encouraged us to investigate other models.

S. cerevisiae is a well-established model to study mitochondrial defects (Lasserre et al., 2015), and we observed that energy metabolism is affected in yeast cells deficient for the PLPHP ortholog, YBL036C (*ybl036cΔ* cells) (Fig. 2-6B-D). It is not yet clear if this is due to a direct effect or to indirect changes in key energy metabolism substrates. Several PLP-dependent enzymes, such as SHMT2 (Giardina et al., 2015), AST and the glycine cleavage system (Kikuchi et al., 2008) have mitochondrial localization. It has also recently been shown that loss-of-function variants in *KYNU,* encoding a PLP-dependent enzyme, lead to deficiencies in the synthesis of NAD (Shi et al., 2017). The kynurenine pathway uses tryptophan as a precursor for NAD biosynthesis, and several PLP-dependent enzymes are involved (Rios-Avila et al., 2013). The multitude of enzymatic functions of PLP may explain the complex array of biochemical phenotypes associated with B6EEs, suggestive of a key role of PLPHP in PLP homeostasis.

By adapting a clinical severity score used for another B6EE (Al Teneiji et al., 2017), we observed that the patients with severe phenotypes (scores 7-9) and/or early mortality were usually associated with proven or predicted LOF variants (Table 2-4). These included splicing defects, truncating variants, and missense variants predicted or experimentally shown (Tremino et al., 2018) to affect PLP binding negatively. A missense variant associated with a severe disease presentation (Darin et al., 2016), p.Leu175Pro, was experimentally proven to induce PLPHP loss of function due to protein misfolding (Tremino et al., 2018). In contrast, it seems that missense variants in residues not associated with the PLP-binding site are seen in patients with milder disease presentations (Table 2-4). Darin et al. (2016) exploited an *E. coli* complementation assay to test the functional effect of a number of *PLPBP* mutations. The p.Pro87Leu variant that is located distant from the PLP-binding pocket (Fig. 2-2C) had the least adverse effect on *E. coli* growth (almost no notable growth inhibition) among all verified variants. In contrast, the p.Arg241Gln variant located within the PLP pocket (Fig. 2-2C-D) exerted the strongest growth inhibition effect on *E. coli.* Using a different approach (protein thermodynamics), Tremino et al. (2017) investigated the same two variants and found that the p.Arg241Gln variant negatively affected protein yield and thermal stability and amount of PLP binding, while none of these parameters were affected in the p.Pro87Leu mutant protein. When stability and folding are not drastically affected, it is possible that PLPHP is still able to bind PLP, as evidenced experimentally for another two variants; p.Pro40Leu and p.Arg205Gln (Tremino et al., 2018). Residual PLP binding and PLPHP function may be associated with milder presentations of the disease. *In silico* molecular dynamics simulations or *in vitro* assessment of PLP binding, PLPHP folding and stability should be performed to further access these scenarios in the missense variants reported here.

A number of biochemical abnormalities were observed in this cohort of PLPHP-deficient patients, mostly affecting amino acids and lactate as well as vitB6 vitamers. Among amino acids, elevated glycine in plasma and/or CSF was most frequent alteration. Increased CSF glycine was also described in the case series of Darin et al. (2016). The enzyme that breaks down glycine, glycine cleavage system, requires PLP as a cofactor (Wilson et al., 2019). In both lysates derived from patient fibroblasts and PLPHP-deficient HEK293 cells, decreases in intracellular PLP were observed. Intracellular PLP was found to accumulate as reported by Darin et al. (2016); further work may be necessary to resolve this discrepancy. A significant accumulation of PNP levels was found in PLPHP-deficient patient 5 and HEK293 cells, but our methods were not sensitive enough for the detection of PNP in plasma, CSF or whole zebrafish larvae. PNP accumulation, therefore, may be of limited use as a biomarker of the disease, but it may help to unravel the functional role of PLPHP.

To enable analysis of the untreated biochemical status, improve our understanding of the pathophysiology of this disease, and establish a platform for potential drug discovery, we successfully developed a *plpbp*-null zebrafish model. The *plpbp*$^{-/-}$ larvae recapitulated the disease, and seizure activity was detected as early as 10 dpf, with 100% mortality by 16 dpf. Treatment with PN fully reversed these phenotypes, and treated *plpbp*$^{-/-}$ larvae often survived to adulthood, but PLP was not very effective, similar to *aldh7a1*$^{-/-}$ larvae (Pena, Roussel, et al., 2017). It is possible that low water solubility, instability, or light sensitivity of PLP plays an important role in the ineffectiveness of PLP. Larvae showed significant changes in the levels of B6 vitamers, particularly PLP and PL, which lend further support to the hypothesis that PLPHP is important for PLP homeostasis (Darin *et al.*, 2016; Prunetti *et al.*, 2016). By quantifying systemic amino acid levels, our results indicate disruption of many key PLP-dependent enzymes. Furthermore, the

reduction of GABA may provide a possible explanation for the increased neuronal activity of mutants, as has been previously reported in *aldh7a1*$^{-/-}$ zebrafish (Pena, Roussel, et al., 2017). Another mechanism to consider as part of disease pathophysiology is altered biosynthesis of catecholamines (especially adrenaline), likely due to reduced availability of PLP for AADC activity (Fig. 2-11D). This is further evidenced in the mutant animals by the accumulation of phenylalanine, tryptophan and tyrosine (precursors to monoamine neurotransmitter synthesis). PLPHP-deficiency patients with AADC deficiency-like symptoms may provide support to this observation. Given that systemic dopamine levels were unchanged, a reduction of metabolic flux towards AADC is likely taking place, rather than a complete inactivation of this enzyme; alternatively, small amounts of dopamine may be formed via tyramine hydroxylation by renal CYP2D6, as suggested by (Wassenberg et al., 2010). Our results illustrate the dynamic and complex nature of PLP binding to dependent enzymes and its turnover in the context of PLPHP deficiency.

3 Development and characterization of a novel conditional mouse model of pyridoxine-dependent epilepsy caused by antiquitin mutations

3.1 Introduction

Knockout mouse models are powerful research tools for understanding pathophysiological mechanisms underlying human genetic diseases. They also offer a front-line testing system for studying the efficacy of novel therapeutic approaches before conducting clinical trials on human subjects (Clarke, 1994; Strachan & Read, 1999). The use of mouse models to study human genetic diseases has a number of advantages over other model organisms and systems including fully sequenced and well-annotated genome, comprehensive resources and databases on gene and protein expression and biochemical pathways, and well-established methods for gene targeting and phenotypic characterization.

Of particular relevance to this project, antiquitin (Aldh7a1) protein expression in mouse brain was characterized previously and shown to have similar expression pattern to human antiquitin (Jansen et al., 2014). Moreover, several studies exist on characterization of the mouse lysine catabolism pathway and its enzymes and metabolites, providing valuable resources when studying disorders of lysine catabolism using a mouse model (Biagosch et al., 2017; Garweg et al., 1980; Gutierrez & Giacobini, 1985; Han et al., 2010; Higashino et al., 1971; Huck et al., 1984; Kim & Giacobini, 1985; Murthy & Janardanasarma, 1999; Papes et al., 1999, 2001; Pena, Marques, et al., 2017; Posset et al., 2015; Sauer et al., 2011).

Pyridoxine-dependent epilepsy (PDE-ALDH7A1) is an inborn error of lysine metabolism that causes a severe form of refractory seizures, intellectual developmental disorder and brain structural defects (Stockler et al., 2011). It is caused by bi-allelic mutations in *ALDH7A1* that encodes an intermediate enzyme in the lysine catabolism pathway known as antiquitin (ATQ).

Enzyme dysfunction leads to accumulation of its two substrate metabolites, Δ^1-piperideine-6-carboxylic acid (P6C) and α-aminoadipic semialdehyde (α-AASA), in addition to pipecolic acid (PIP) (Fig. 3-1). Deficiency of ATQ is thought to cause seizures because accumulating P6C reacts with pyridoxal 5'-phosphate (PLP) and inactivates this cofactor that is essential for neurotransmitter metabolism, explaining the seizure response to pyridoxine (PN) supplementation (Mills et al., 2006) (Fig. 3-1).

Despite discovery of the genetic and main biochemical defects in PDE-ALDH7A1, many questions about disease biology have remained unresolved. Although high-dose pyridoxine (PN) treatment usually leads to seizure control in PDE-ALDH7A1 patients, a large proportion of them (about 70%) still suffer persistent neurodevelopmental deficits and brain malformations, of which the underlying pathophysiological mechanism is not recognized. Progress in this field has been hampered by two factors: difficulty in studying biochemical and neuropathological changes directly in patients' tissues and the lack of an appropriate animal model for PDE-ALDH7A1. As a consequence, devising effective treatments to prevent the neurodevelopmental disorder in PDE-ALDH7A1 patients has been challenging.

ATQ deficiency causes two known concomitant abnormalities; accumulation of upstream metabolites and depletion of intracellular PLP (Mills et al., 2010). It has been proposed that cellular injury might be caused by buildup of lysine catabolites in the brain (Jansen et al., 2014) which do not normalize on conventional PN therapy. Available data on brain concentrations of these presumably neurotoxic compounds, mainly P6C and α-AASA, are limited to a single post-mortem study in a PDE-ALDH7A1 patient (Jansen et al., 2014). It is currently unknown if ATQ deficiency causes similar biochemical abnormalities in peripheral organs because no quantification data are available from these tissues.

The exact etiology of seizures in ATQ-deficient patients is not fully understood. It has been hypothesized that diminished levels of PLP in PDE-ALDH7A1 may impair the function of the PLP-dependent enzyme glutamic acid decarboxylase (GAD). GAD catalyzes the conversion of glutamate to gamma-aminobutyric acid (GABA), the main inhibitory neurotransmitter within the CNS. Compromised activity of GAD leads to decrease in GABA levels compared to the excitatory neurotransmitter, glutamate, which subsequently causes seizures (Murty et al., 2013; Pena, Roussel, et al., 2017). However, data obtained from patients were inconsistent with this hypothesis. For example, GABA was found to be normal to moderately elevated in CSF of a PDE-ALDH7A1 patient (Goto et al., 2001), while glutamate was normal or reduced in pre-treatment CSF of other patients (Mills et al., 2010).

With an aim towards filling these knowledge gaps in disease biology and to produce a platform for therapeutic trials, we developed a novel mouse model for PDE-ALDH7A1 by targeted ablation of *Aldh7a1* in embryonic stem cells. The current report includes the results of biochemical, behavioral and electrophysiological characterization of *Aldh7a1*-null mice. We tested the mice for the presence of the two main biomarkers in PDE-ALDH7A1 patients, P6C and α-AASA. We additionally explored various other metabolic compounds for abnormal profiles that might be indirectly caused by the enzymatic defect. The data provides the first proof-of-concept for the disease model, including a metabolic signature consistent with blockade of the lysine catabolism pathway in *Aldh7a1*-deficient mice.

3.2 Materials and Methods

3.2.1 Generation of constitutive *Aldh7a1* knock-out mice

An embryonic stem cell (ESC) line with conditionally-targeted allele for *Aldh7a1* (MGI allele name: *Aldh7a1*$^{tm1a(EUCOMM)Hmgu}$) was obtained from the International Knockout Mouse Consortium (IKMC). These genetically-modified ESCs harbor a targeting construct that is incorporated between exons 5 and 6 of the *Aldh7a1* gene. The mutant allele with a full version of the targeting construct is known as **tm1a**. As shown in Fig. 3-2A, the tm1a allele contains multiple built-in features that, using different breeding strategies, allows the generation of three strains of mice; LacZ-tagged (**tm1b**), conditionally-targeted or "floxed" (**tm1c**), and constitutive null or "knock-out" (**tm1d**) mice.

Three clones of the ESCs were microinjected into C57BL/6J blastocysts and implanted in pseudopregnant female mice. Resulting chimeric male mice were backcrossed with wild-type (WT) C57BL/6J female mice (JAX Stock# 000664) to establish germline transmission. Genotype-confirmed germline mice carrying the tm1a allele were crossed with global Cre recombinase-expressing mice (JAX Stock# 003376) to generate mice that carry the lacZ-tagged tm1b allele. In parallel, tm1a heterozygous mice were also bred with mice ubiquitously expressing FLPo recombinase (Mutant Mouse Resource & Research Centers -MMRRC- Stock# 032247-UCD). Following excision with FLPo, we generated mice in which *Aldh7a1* is expressed normally but exon 6 of the mouse *Aldh7a1* gene is now flanked by loxP sites (floxed mice). These mice, which harbor the conditional tm1c allele, were crossed with Cre recombinase-expressing mice to yield mice that carry the tm1d allele. The tm1d allele is the constitutive null or "knock-out" (KO) allele in which the floxed exon is removed. Removal of this critical exon generates a frameshift in exon 7 that introduces a premature stop codon and results in the loss of *Aldh7a1* expression. Mice from

each of these four different strains (tm1a, tm1c, tm1b, and tm1d) were identified using allele-specific PCR-based genotyping assays.

Mice of mixed sexes and from mixed litters were used for all experiments. Analysis of lysine metabolites, amino acids, vitamin B6 (vitB6) vitamers and neurotransmitters was done in tissues and biofluids derived from individual mice (for adult mice: N=8 WT, 8 HET, and 8 KO mice, for P0 mice: N=5 WT, 5 HET, and 5 KO except for vitB6 vitamers where N=3 WT, 3 HET, and 3 KO). Samples from P0 mice were collected at postnatal day 1 and adult samples were collected from mice at ages that ranged from 10.6 to 22 weeks.

The mouse model described in this report was generated in accordance with guidelines of the Canadian Council on Animal Care and approved protocol by the University of British Columbia Animal Care Committee (Animal Protocols # A15-0200 and A15-0180). Mice were housed on ventilated racks in specific pathogen-free barrier facility with a 12hr light/dark cycle. Mice were group-housed with their littermates to a maximum of five mice per cage and given free access to food and water. Mice were fed a regular chow used at our animal facility (Envigo 2018 Teklad Global 18% protein Rodent Diet) containing (w/w) 18% total protein, 0.9% lysine and 18 ppm PN.

3.2.2 Western immunoblots

For Western immunoblotting, brain and kidney tissue samples harvested from P0 mice killed by decapitation were snap frozen in isopentane in dry ice. Frozen samples were homogenized in radioimmunoprecipitation assay (RIPA) buffer containing protease inhibitors. Fifty µg of protein from each sample were separated by 12% Bis-Tris gel electrophoresis (Nupage, Invitrogen) and transferred overnight at 30 V to a polyvinylidene difluoride membrane. On the next day the membrane was blocked for 20 minutes with 5% bovine serum albumin (BSA) mixed

with phosphate-buffered saline containing 0.05% tween-20 (PBS-T). Then the membrane was incubated with primary antibodies against antiquitin and GAPDH overnight at 4^{o} C. Primary antibodies used were monoclonal anti-ALDH7A1 antibody (ab53278, Abcam) diluted 1:1000 in 5% BSA and PBS-T, and monoclonal anti-GAPDH antibody diluted 1:3000 in a similar buffer. The anti-ALDH7A1 antibody is directed against the C-terminal end of the protein. On the following day, the membrane was washed 2X for 15 minutes with PBS-T. The blot was then incubated with secondary antibodies (goat antirabbit -Alexa Fluor 680; Molecular Probes, Eugene, OR- or goat antimouse -IRDye 800, LI-COR) for 2 hours at room temperature. Subsequently, the blot was washed 2X for 15 minutes with PBS-T. Finally, the blot was imaged and protein levels were quantified using a LI-COR Odyssey Infrared Imaging System.

3.2.3 Collection of samples for mass spectrometry analysis

For mass spectrometry analysis, mice were sacrificed by decapitation. Brain and liver tissue samples were promptly harvested and snap-frozen with isopentane in dry ice. Blood was immediately collected from neck vessels in EDTA dipotassium tubes. The blood tubes were spun in a microcentrifuge at 3500-3600 rpm for 10 minutes to separate the plasma. The plasma was transferred to another tube and quickly frozen with isopentane in dry ice. Tissue and plasma samples were stored in a -80^{o} C freezer until time of shipment to analyzing laboratories.

3.2.4 Quantification of lysine metabolites

α-AASA and P6C in adult brain and liver were analyzed according to a published method (Mills et al., 2006) in methanol extracts prepared for amino acid analysis. Lysine, P6C, PIP, saccharopine and α-aminoadipic acid in brain and liver of P0 mice were quantified using liquid chromatography-tandem mass spectrometry according to previously published methods (Pena, Marques, et al., 2017; Pena, Roussel, et al., 2017).

3.2.5 Quantification of B6 vitamers

Pieces of snap-frozen liver and brain tissue were powdered in liquid nitrogen. Tissue powder was quickly weighed and 100 µl of ice cold trichloracetic acid (TCA; 50g/l) were added per 10 mg tissue powder. The solutions were homogenized with zirconium oxide beads (0.5 mm) using a bullet blender tissue homogenizer (Next Advance Inc., Averill Park, NY, USA) at a speed of 8 for 5 min at 4 °C following the manufacturer's recommendations. The homogenates were centrifuged at 16200 g for 5 min at 4 °C. The supernatants were diluted 10 times with TCA (50g/l) and 80 µl of the diluted sample was mixed with 80 µl of solution containing isotopically labeled internal standards, vortexed, incubated 15 min in the dark and centrifuged at 16200 g for 5 min at 4 °C. The supernatants were used for vitamer B6 analysis with ultra-performance liquid chromatography tandem mass spectrometry (UPLC-MS/MS) as described in detail in van der Ham et al. (2012). The content of B6 vitamers was expressed in nmol per gram tissue wet weight. During all steps, samples were protected from light as much as possible.

3.2.6 Quantification of amino acids and methionine sulfoxide

Tissue powder was homogenized in methanol (100 %; 100 µl per 10 mg tissue) using a bullet blender tissue homogenizer (Next Advance Inc., Averill Park, NY, USA) for 5 min at 4 °C. The homogenates were centrifuged at 16200 g for 5 min at 4 °C. Amino acids and methionine sulfoxide were analyzed in undiluted supernatants using the UPLC-MS/MS as described previously (Prinsen et al., 2016). The content of amino acids was expressed in µmol per gram tissue wet weight.

3.2.7 Quantification of neurotransmitters

Gamma-aminobutyric acid (GABA) and glutamic acid were quantified in whole brain hemisphere and liver homogenates of P0 mice using liquid chromatography-tandem mass spectrometry according to previously published methods (Pena, Roussel, et al., 2017).

Biogenic amine neurotransmitters and their metabolites were analyzed in whole brain hemisphere homogenates (2% w/v homogenates in 0.08 M acetic acid) and plasma with liquid chromatography in combination with isotope dilution tandem mass spectrometry as previously described (Vliet et al., 2015).

3.2.8 Behavioral tests

Two cohorts of mice were tested for behavioral abnormalities using a pipeline of neurobehavioral tests that consisted of open field, forced swim, novel object recognition, elevated plus maze, Morris water maze and accelerating rotarod tests. Cohort 1 was tested at age of 6 months and included 16 WT and 13 KO mice of mixed sexes. Cohort 2 was tested at age of 2.5 months and consisted of 11 WT and 10 KO mice of mixed sexes, except for accelerating rotarod test in which there were 9 WT and 8 KO mice. Video analysis was carried out using EthoVision XT software versions 7.0 or 13.0 (Noldus, VA).

For open field (OF) test, each mouse was placed in 50 cm x 50 cm x 20 cm arena and allowed to explore the environment for or 10 minutes while being recorded from a camera placed directly above the arena and analyzed by image tracking system (Ethovision). Measurements that were obtained from each trial included time spent in the centre of the open field versus the periphery of the open field, distance traveled, and speed. For the novel object recognition (NOR) test, the mouse was put in an arena similar to OF arena and allowed to explore two identical objects placed in opposite corners of the arena for 5 min. Approximately 5 hours later, mice were returned

to the arena in which one of the objects had been replaced with a novel object, and again allowed to explore the objects for 5 minutes. Total time spent exploring each object was defined as the amount of time that the nose point of the animal was detected in the zone around each object, a square approximately 5 cm x 5 cm.

For the Morris water maze (MWM), a round pool of approximately 100 cm diameter was filled with water (20-21^{o}C) to a depth of approximately 50 cm and painted with non-toxic white tempera paint. Visible cues of geometric shapes were placed around the pool at a level visible to the mice. On Day 1, a habituation trial was performed by placing the mouse in a random but pre-determined release point in the pool and allowing it to explore for 60 sec. On days 2-5, training trials were performed in blocks of 4 trials per day performed at approximately the same time each day. For the training trials, each mouse was assigned a random platform location in one of four possible positions in the pool (NW, NE, SE, or SW), which was kept consistent throughout training. The platform (10 cm diameter) was submerged approximately 1 cm under the water. On each training day, the mouse was released from each of four possible release locations (N, S, E, W) in a random order and allowed to search for the hidden platform for a maximum of 60 sec. The latency to reach the platform was recorded for each trial. If a mouse failed to find the platform within the allowed period, a time of 60 seconds was recorded and the mouse gently guided to the platform by the experimenter. After each trial, the mouse remained on the platform for about 10 sec before being returned to its home cage. On Day 8, a probe trial was performed where the hidden platform was removed from the pool. Each mouse was released from a semi-randomized released point. The mouse was allowed to search for the platform for 60 sec, after which it was returned to its home cage. For the analysis, the pool was divided into four quadrants and the time spent in each quadrant was recorded as well as the number of times a mouse crossed the platform location. The

protocol was slightly modified in Cohort 2, in which there were 3 training days followed by the probe trial on Day 7.

For the forced swim test (FST), each mouse was placed in a transparent cylindrical tank (about 25 cm in diameter) filled with water to a depth of approximately 20 cm and was allowed to swim for 8 min. Recorded video was scored using automated software (EthoVision XT), and the cumulative time spent immobile during the period 2-6 min was recorded and used for analysis.

For the elevated plus maze (EPM) test, the mouse was placed in the centre of an elevated, plus-shaped (+) apparatus with two open and two enclosed arms and allowed to explore the maze for 5 min. Total time spent in open versus closed arms was recorded for each mouse.

An accelerating rotarod test was used to assess motor learning and coordination. For training, mice were placed on a fixed speed (18 RPM) rotarod (Ugo Basile, Italy) for three consecutive days with three trials per day spaced one hour apart (each trial lasted for 120 sec). For the test trial, the rotarod was accelerated from 5 to 40 RPM over 300 sec and the latency to fall was recorded. Three test trials spaced one hour apart were done for each mouse and the average time to fall was used for analysis.

At the end of behavioral tests, all mice from both cohorts were transcardially perfused and their brains were harvested using the procedure described in section 3.2.9 below, except that tissues were stored in PBS post fixation. Collected brains were used for brain weight measurements.

3.2.9 Neuropathology analysis

Mice were examined for neuropathological abnormalities by immunohistochemical techniques using two biomarkers; NeuN (marker for neurons) and GFAP (marker for astrocytes). Analysis was done on brain tissue sections obtained from 3 KO and 3 WT mice at age of 4 months.

3.2.9.1 Tissue preparation for neuropathology

Mice were anaesthetized by intraperitoneal injection of 0.5 mg/g avertin (2,2,2 tribromoethanol) and terminally perfused through the ascending aorta with ice-cold 1X PBS followed by ice-cold 4% paraformaldehyde. The brains were then removed and post-fixed in 4% paraformaldehyde overnight. Post fixation, the tissue was equilibrated in 10%, then 30% sucrose in PBS overnight at 4^{o}C, after which it was embedded in Optimal Cutting Temperature compound (Sakura), frozen in liquid nitrogen, and stored at -80^{o}C. Serial 25 µm sections of embedded tissue were cut on a cryostat and placed in multi-well plate containing PBS.

3.2.9.2 Immunohistochemistry

Floating sections were placed in netwell inserts and washed for 10 min in PBS. Endogenous peroxidase activity was quenched with 1% H_2O_2 for 45 min. After a 15 min wash in PBS with 0.1% Triton X (PBS-T), sections were blocked in 5% normal serum and 5% bovine serum albumin diluted in PBS-T, followed by overnight incubation shaking at room temperature in primary antibody diluted in 5% normal serum and PBS-T. After two 15 min washes in PBS-T, secondary antibody diluted in 1% normal serum and PBS-T was applied for 2 hrs shaking at room temperature. Sections were washed for 30 min in PBS before an amplification step was performed using an avidin–biotin–HRP complex kit (Vector Laboratories). Colorimetric detection was achieved with the peroxidase substrate kit Vector DAB (Vector Laboratories) according to the manufacturer's instructions. Sections were mounted by hand on onto glass slides (Fisherbrand

Superfrost Plus) and dried overnight. Next, sections were conterstained with cresyl violet (only for GFAP) before being dehydrated through a series of alcohols and xylene and cover-slipped with DEPEX (Electron Microscopy Sciences). Antibodies used were as follows: the neuronal marker NeuN (Chemicon, Millipore, 1:2000, mouse monoclonal) and the astrocyte marker GFAP (Sigma; 1:2000, mouse monoclonal), and appropriate biotinylated secondary antibodies (Vector, 1:2000).

3.2.10 *In vivo* electrophysiology

In vivo EEG recording was performed in WT and KO mice from two background strains: the original inbred B6 strain and an N5 incipient congenic 129 S1/SvImJ (B6;129) strain (established by backcrossing HET B6 mice to WT mice from inbred 129 S1/SvImJ strain for 5 generations). Experiments included 3 KO and 3 WT mice (age: 10 months) from the B6 strain and 2 KO and 2 WT mice (age: 2 months) from the B6;129 strain. The procedure consisted of three main steps: surgical implantation of electrodes, connection of the recording device, and data downloading and processing (Fig. 3-22). All animal surgeries were carried out using aseptic techniques and in accordance with guidelines of the Canadian Council on Animal Care and approved protocol by the University of British Columbia Animal Care Committee.

3.2.10.1 Electrode implantation surgery

Fig. 3-22 summarizes the workflow for EEG surgery. For electrode placement, animals were anesthetized with 3% isoflurane and placed in a stereotaxic frame. After exposing the cranium, four burr holes were drilled bilaterally over the frontal and parietal cortices (approximate bregma coordinates, frontal: AP = +1.5 mm, ML = -/+1.8 mm, parietal: AP = -2.4 mm, ML = +/-2.2 mm) and one over the occipital segment (approximate bregma coordinates AP = -5.03, ML = +0.6). Miniature stainless-steel screws (Part No. 0-80 X 1/16, Invivo1, USA) pre-soldered to insulated copper wire leads were screwed onto the skull holes with above coordinates to serve as

EEG electrodes. Four electrodes (the two frontal and two parietal) were used to record EEG signals. A bipolar occipital screw was exploited as ground and reference electrodes. Wire terminals from these electrodes were connected to a 7-pin header that is mounted over the animal head. Screws and pin connector were further fixed in place and insulated by acrylic dental cement (Stoelting, USA). After surgery, mice were singly housed and allowed to recover for at least three weeks before proceeding with EEG recording.

3.2.10.2 EEG recording

EEG recording was performed in freely-moving animals using Neurologger 2A (Evolocus, USA, http://www.evolocus.com/neurologger-2A.htm) (Fig. 3-21A). This wireless non-telemetric system allows EEG data to be stored directly into a memory chip that is integrated within the head mount unit, therefore avoiding any background noise interference associated with radiotelemetric transmission. It is also equipped with a 3-dimensional (3-D) accelerometer that provides a simultaneous tracking of animal movement during EEG recording (Fig. 3-21B). To begin recording, Neurologger was connected to the implanted pin header with pre-set sampling rate of 400 Hz. EEG was continuously recorded in each animal for 24 - 48 hours.

3.2.10.3 Data acquisition and analysis

At the end of each recording session, Neurologger was disconnected from the animal's head and connected to a computer using Neurologger USB Adapter (Evolocus, USA). EEG and accelerometer data were downloaded offline from the logger memory to computer. Retrieved data were then converted from binary to text or Float32IE formats. Data downloading and conversion were carried out using Downloader software tool version 1.27 (Evolocus, USA). Electrophysiological and accelerometer data were visualized and processed using EEGLAB

versions 14.1.1 and 14.1.2 (Delorme and Makeig, 2004) running under Matlab version R2017b or R2019a (The MathWorks Inc., USA). Traces obtained from the four active EEG channels were plotted and analyzed in parallel with the synchronised animal acceleration data along the three orthogonal axes (x, y and z). EEG data were visually screened to identify potential convulsive seizure events. A convulsive seizure is defined by the presence of large-amplitude (> 2x baseline), high-frequency (> 5 Hz) discharges associated with sudden and vigorous changes in the animal movement along the three accelerometer axes.

3.2.11 Statistical analysis

One-way ANOVA followed by post-hoc Dunnett's multiple comparisons test was used to compare mean concentrations in lysine metabolites, vitamin B6 (vitB6) vitamers amino acids, and methionine sulfoxide. Unpaired Student's t-test was used to compare mean concentrations in neurotransmitters and for analysis of behavioral tests and brain weight. For analysis of correlation, Pearson correlation coefficient (Pearson's r) was used. Pearson's χ^2 test was applied to test the Mendelian segregation of mice from heterozygous parents. All statistical analyses and graphical plotting of data were carried out using GraphPad Prism software. *p* values below 0.05 were considered significant.

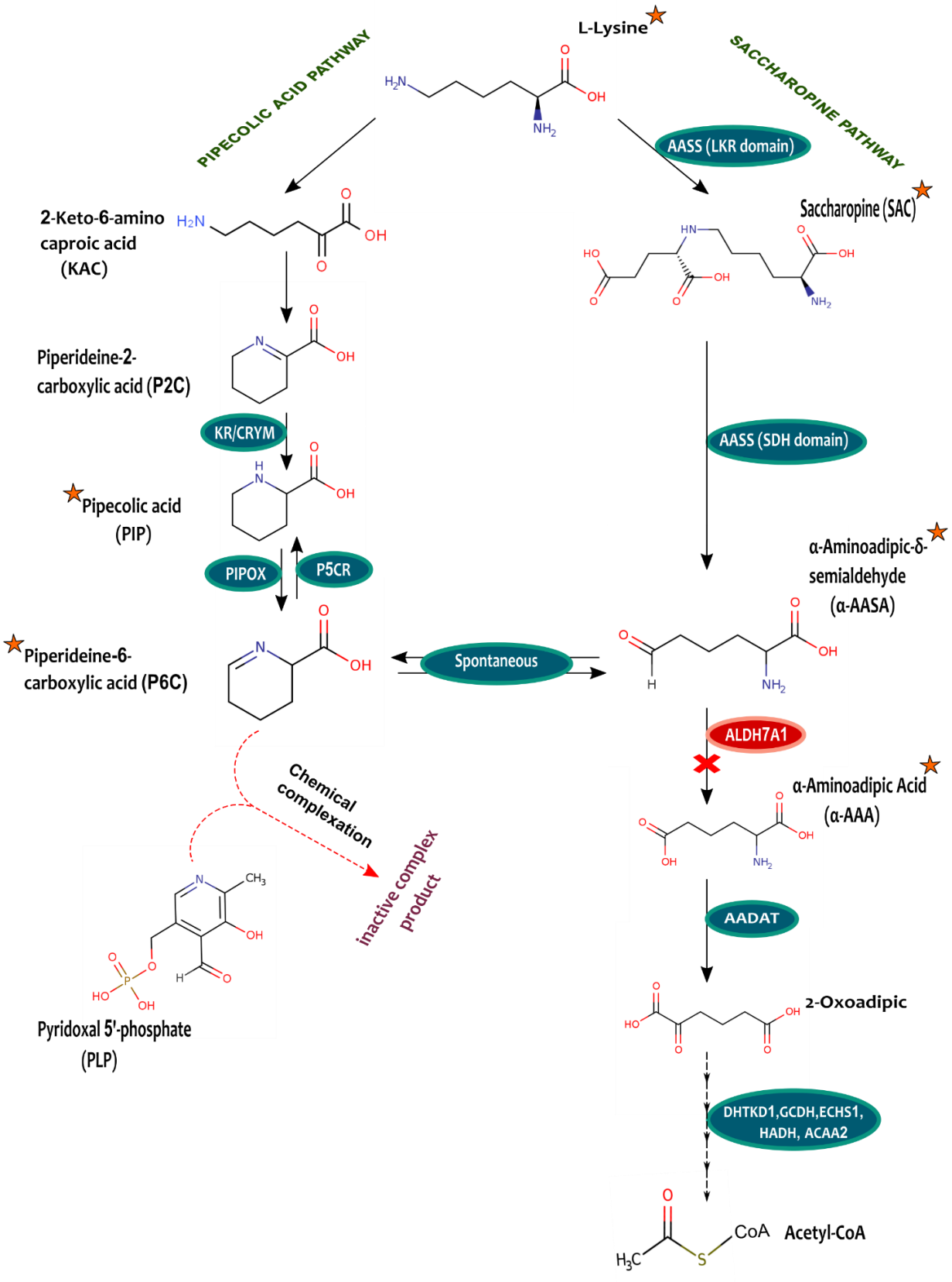
L-Lysine
PIPECOLIC ACID PATHWAY
SACCHAROPINE PATHWAY
AASS (LKR domain)
2-Keto-6-amino caproic acid (KAC)
Saccharopine (SAC)
Piperideine-2-carboxylic acid (P2C)
KR/CRYM
AASS (SDH domain)
Pipecolic acid (PIP)
PIPOX
P5CR
α-Aminoadipic-δ-semialdehyde (α-AASA)
Piperideine-6-carboxylic acid (P6C)
Spontaneous
ALDH7A1
Chemical complexation
inactive complex product
α-Aminoadipic Acid (α-AAA)
AADAT
Pyridoxal 5'-phosphate (PLP)
2-Oxoadipic
DHTKD1,GCDH,ECHS1, HADH, ACAA2
CoA
Acetyl-CoA

Fig. 3-1: Pipecolic acid (left) and saccharopine (right) pathways for L-lysine catabolism in mammals. ALDH7A1 catalyzes the step indicated by the red "X". Inactivation of the enzyme in PDE-ALDH7A1 causes buildup of its two substrates: P6C and α-AASA. Through Knoevenagel condensation, accumulating P6C complexes with PLP forming an inactive adduct and leading to depletion of the cofactor. Star symbols denote the compounds that were analyzed in *Aldh7a1*-KO mice. AASS: aminoadipic semialdehyde synthase, LKR: lysine-ketoglutarate reductase, SDH: saccharopine dehydrogenase, AADAT: 2-aminoadipate aminotransferase, KR: ketimine reductase, PIPOX: pipecolic acid oxidase, P5CR: piperideine-5-carboxilic reductase (based on Pena et al. (2017)).

3.3 Results

3.3.1 Establishing *Aldh7a1*-targeted strains

We generated three *Aldh7a1*-targeted strains of mice by blastocyst injection of ESC's carrying the *Aldh7a1*$^{tm1a(EUCOMM)Hmgu}$ allele followed by sequential crossings with mice ubiquitously expressing Cre recombinase or FLPo recombinase, respectively: reporter-tagged (tm1b allele), conditional floxed (tm1c allele), and constitutive KO (tm1d allele) mice. Intercrossing of heterozygous KO (HET) mice resulted in live homozygous KO (KO) offspring that were able to reach adulthood. However, based on genotyping done at weaning, KO mice occurred with significantly lower than expected frequency (Table 3-1), consistent with increased prenatal or early postnatal mortality among KO mice.

KO mice that survived weaning were indistinguishable from their WT littermates as adults in size, appearance, and apparent home cage behavior. No spontaneous seizure activity was noted on short-term visual inspection of KO mice. Western blot analysis of brain and kidney homogenates confirmed complete loss of Aldh7a1 expression in KO mice (Fig. 3-2B).

Table 3-1: Comparisons and Chi-square for goodness-of-fit of observed versus expected Mendelian frequencies of each genotype from offspring resulting from intercrossing of heterozygotes. Numbers are based on pups living to and genotyped at weaning (WT=Wild-type, HET=Heterozygous knockout, KO=Homozygous knockout).

Genotyped at Weaning

	WT	**HET**	**KO**	**Total**
Observed	123 (28.4%)	224 (51.9%)	85 (19.7%)	432
Expected	25%	50%	25%	

$$X_2^2 = 7.28$$

$$p = 0.026$$

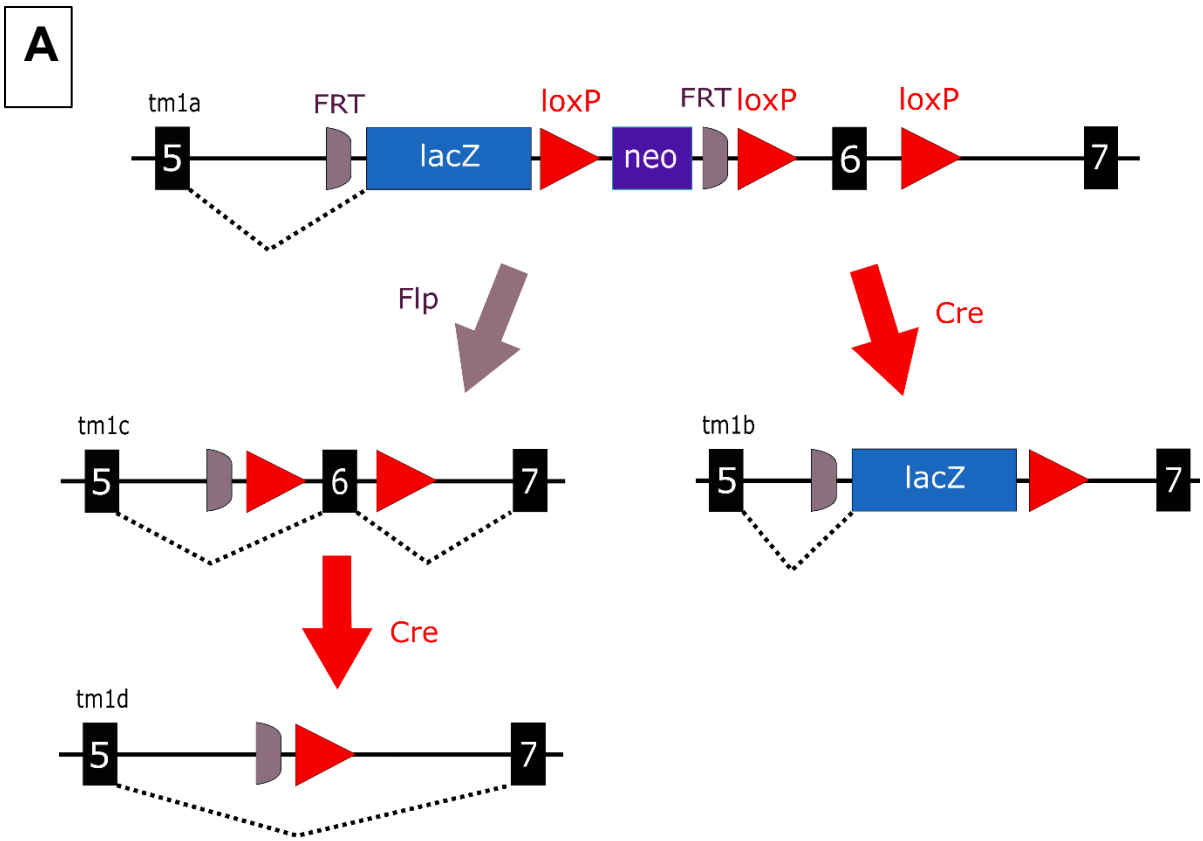
A
tm1a
FRT
loxP
FRT
loxP
loxP
5
lacZ
neo
6
7
Flp
Cre
tm1c
tm1b
5
6
7
5
lacZ
7
Cre
tm1d
5
7

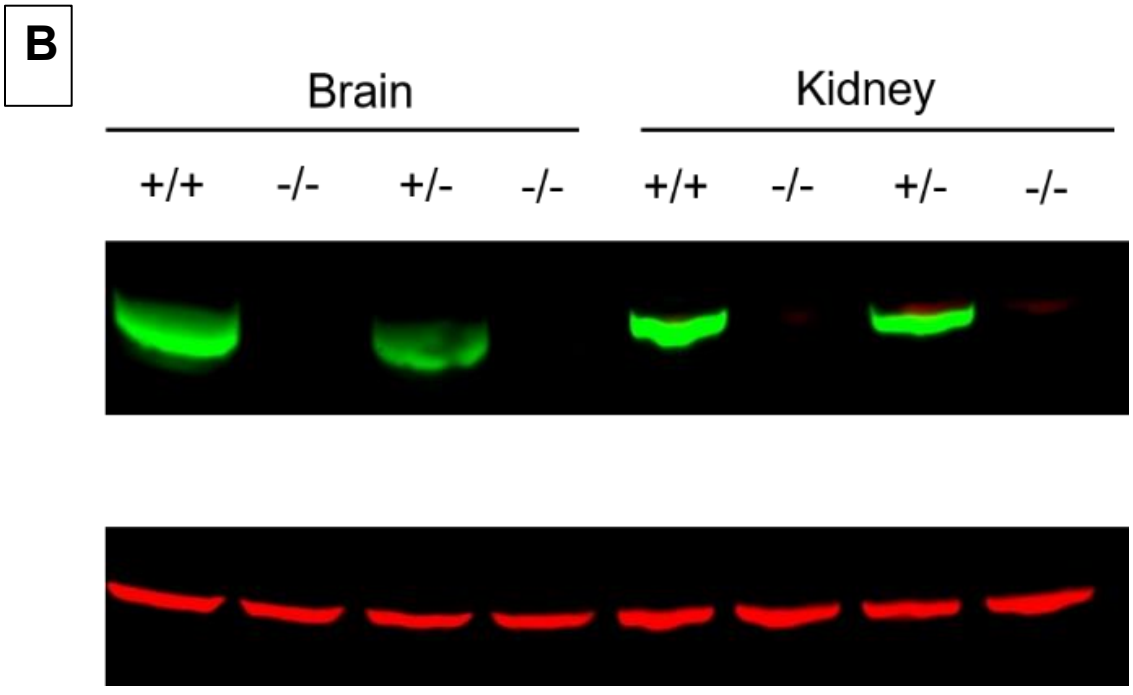
B
Brain
Kidney
+/+
-/-
+/-
-/-
+/+
-/-
+/-
-/-

Fig. 3-2: Generation of Aldh7a1-targeted mice. A) Flowchart showing targeting strategy, breeding scheme used to generate each strain and structure of different mutant alleles: tm1a (full inserted construct), tm1b (lacZ-tagged), tm1c (conditional) and tm1d (deletion). Numbered boxes represent Aldh71 exons. B) Western immunoblot from brain & kidney homogenates showing complete absence of Aldh7a1 expression in the homozygous KO (-/-) as compared to WT (+/+) and heterozygous KO (+/-) mice. Gapdh (red) was used as a loading control.

3.3.2 Analysis of lysine metabolites

To gain insight into the metabolic consequences of *ALDH7A1* deficiency, we quantified multiple metabolic intermediates surrounding the ALDH7A1-catalyzed step in the lysine catabolism pathway in brain and liver tissues of heterozygous and homozygous KO mice in comparison to their WT counterparts in neonatal (P0) and/or adult mice. The intermediates included 5 upstream compounds: lysine (Lys), P6C, α-AASA, saccharopine (SAC), and pipecolic acid (PIP), and a downstream compound: α-aminoadipic acid (α-AAA). In adult mice, all assayed lysine catabolic products (P6C, α-AASA and PIP) accumulated in significantly higher concentrations in brain and liver tissues of KO mice compared to low or undetectable levels in HET and WT mice (Fig. 3-3). Lysine, on the other hand, had significantly lower concentration in the brain of adult KO mice (Fig. 3-5). In P0 mice, all assayed lysine catabolites (P6C, PIP, SAC and α-AAA) were present in significantly higher concentrations in brain tissue of KO mice (Fig. 3-4 and 3-5). In liver tissue of P0 mice, PIP was significantly elevated in KO mice (Fig. 3-4).

P6C and PIP were screened at two time points; P0 and adulthood. On average, P6C accumulated to higher levels in brain tissue of adult KO mice compared to that of neonatal mice (156.1 ± 12.48 versus 66.05 ± 9.856 nmol/g, mean ± SEM, p=0.0004), while a converse trend was observed for PIP (395.8 ± 32.96 nmol/g in P0 versus 205.4 ± 21.74 nmol/g in adults, mean ± SEM, p=0.0004) (Fig. 3-6). Tissue-specific differences were also observed. For example, P6C was present at nominally higher average concentration in liver tissue compared to brain of adult KO

mice (210.6 ± 25.64 versus 156.1 ± 12.48 nmol/g, mean ± SEM, p=0.0763). PIP, on the other hand, accumulated to significantly higher levels in brain versus liver tissue of neonatal KO mice (395.8 ± 32.96 versus 109.2 ± 39.88 nmol/g, mean ± SEM, p=0.0005) (Fig. 3-7A). As noted previously, the levels of P6C and its open-chain isomer, α-AASA, correlated significantly in all tested tissues in patients (Struys et al., 2012) (R^2= 0.9301, p<0.0001) (Fig. 3-7B).

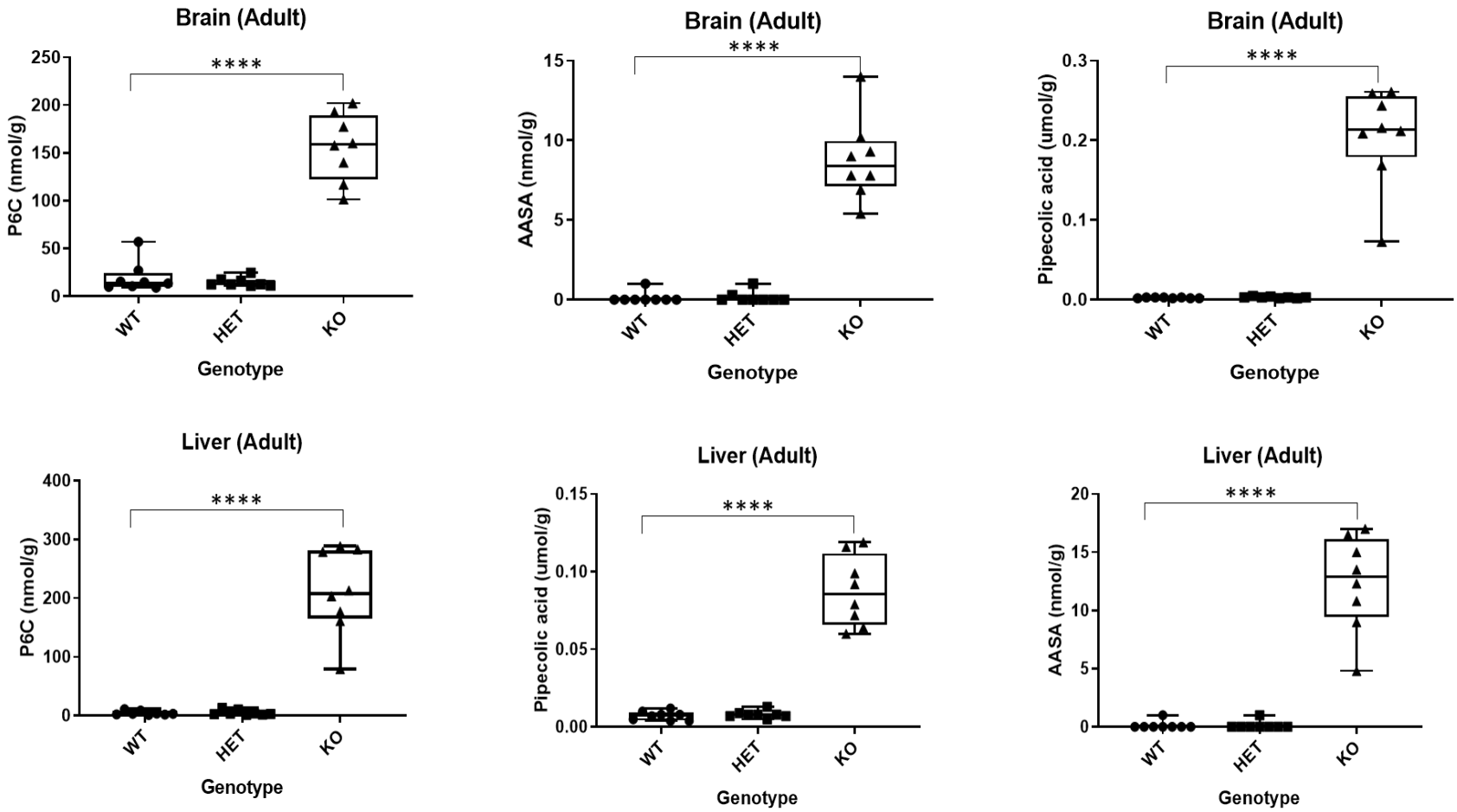

Fig. 3-3: Aldh7a1-null mice reproduce the human biochemical phenotype. Mass spectrometry data from brain (upper) and liver (lower) of adult mice showing elevated levels of the 3 key biomarkers in PDE-ALDH7A1 in homozygous KO (KO) mice compared to low or no detectable levels in wildtype (WT) and heterozygous KO (HET) mice. (Boxes extend from 25^{th}-75^{th} percentiles, horizontal lines inside boxes represent median values, whiskers extend from min-max values). (**** $p<0.0001$**).**

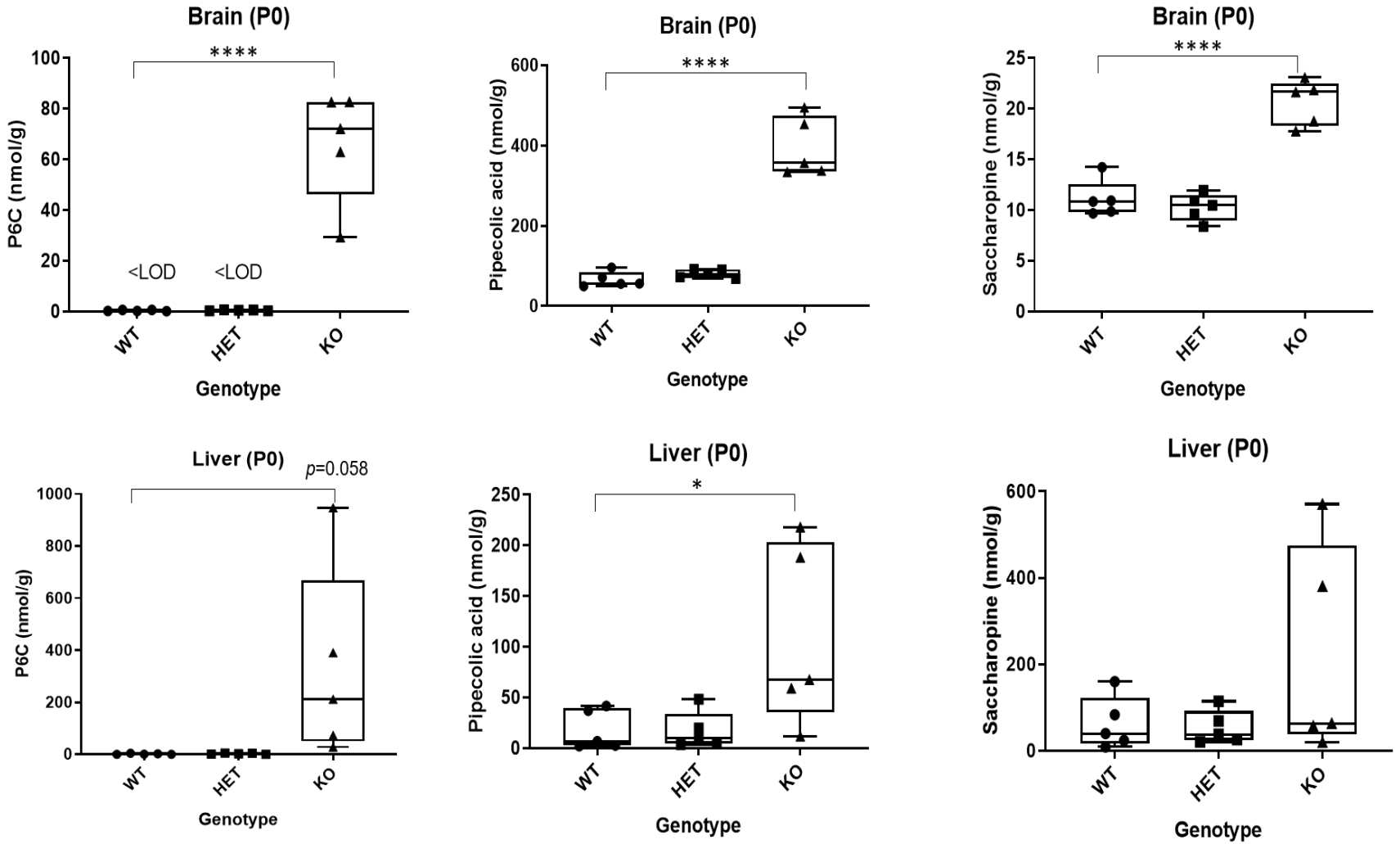

Fig. 3-4: Mass spectrometry data from brain (upper) and liver (lower) of P0 mice showing accumulation of lysine metabolites, P6C, pipecolic acid and saccharopine in homozygous KO mice (KO). (LOD: limit of detection). (* $p<0.05$, **** $p<0.0001$).

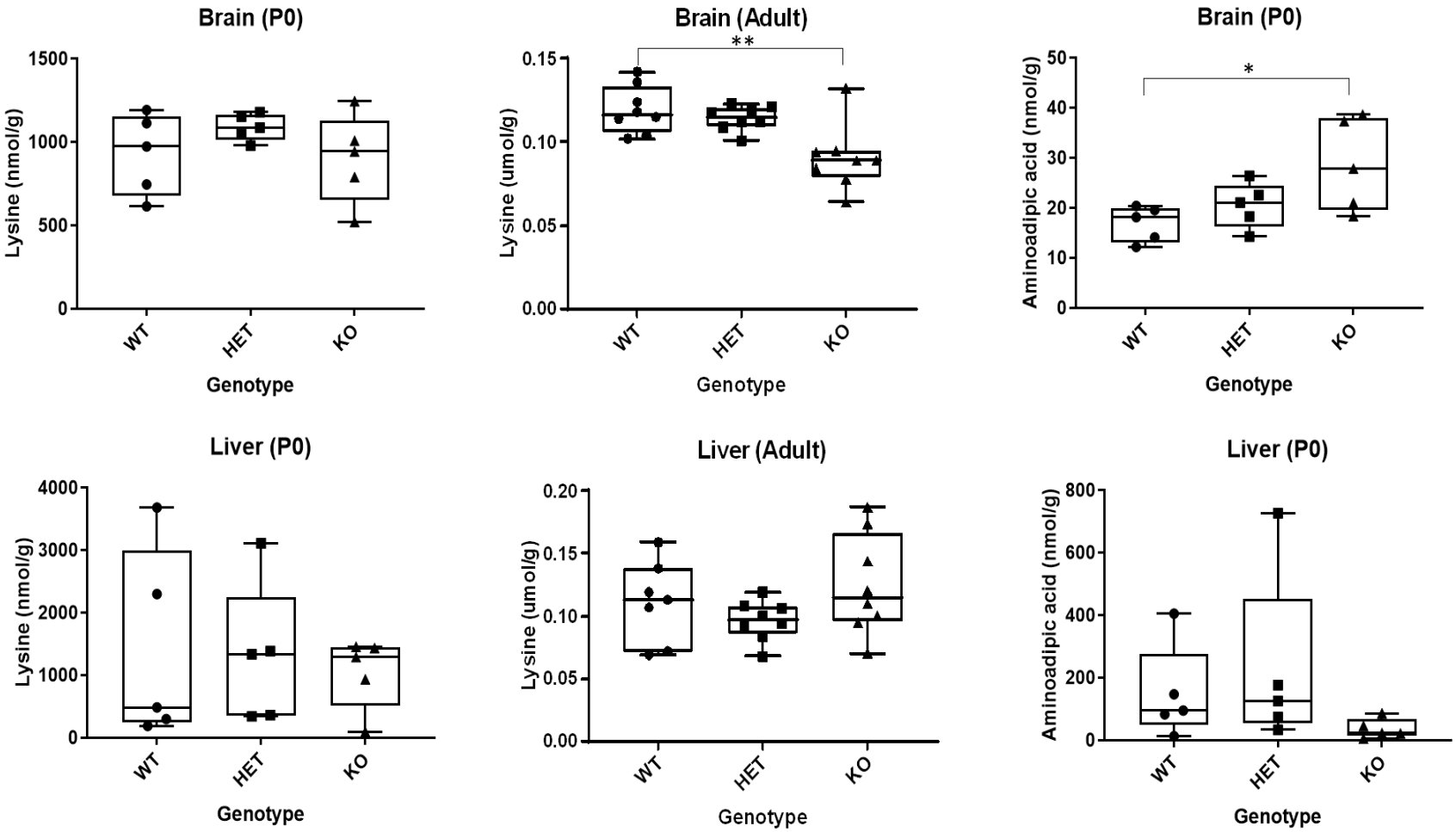

Fig. 3-5: Extended profiling of the lysine pathway shows the trends of lysine (upstream substrate) and α-aminoadipic acid (downstream metabolite) in brain of adult and P0 KO mice, respectively. (* $p<0.05$, ** $p<0.01$).

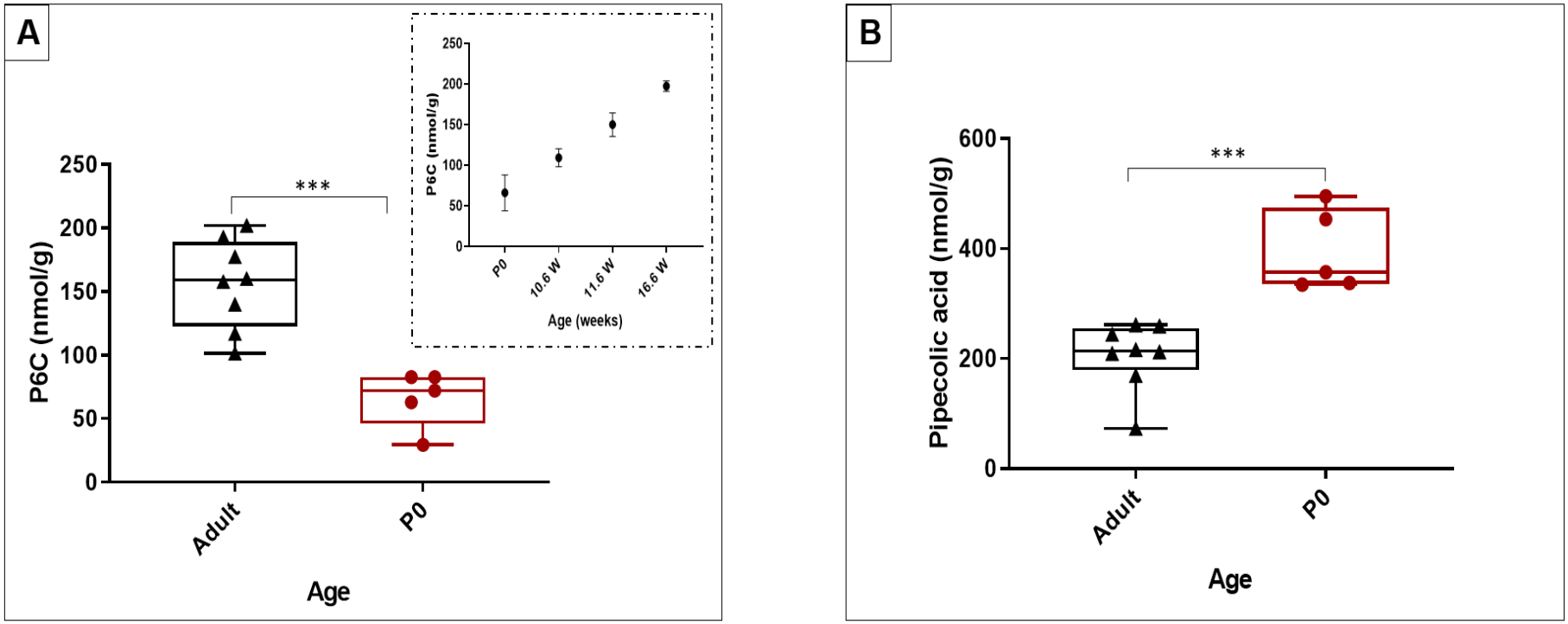

Fig. 3-6: Graphs comparing levels of lysine metabolites P6C (A) and pipecolic acid (B) between adult and neonatal KO mice. Inset in (A): dividing adult P6C data into individual timepoints shows a trend of increasing concentration with age (points represent mean ± SD, N=5 in P0 and 2 per timepoint in adult data, timepoints with only a single measurement were excluded from the graph). (*** p<0.001).

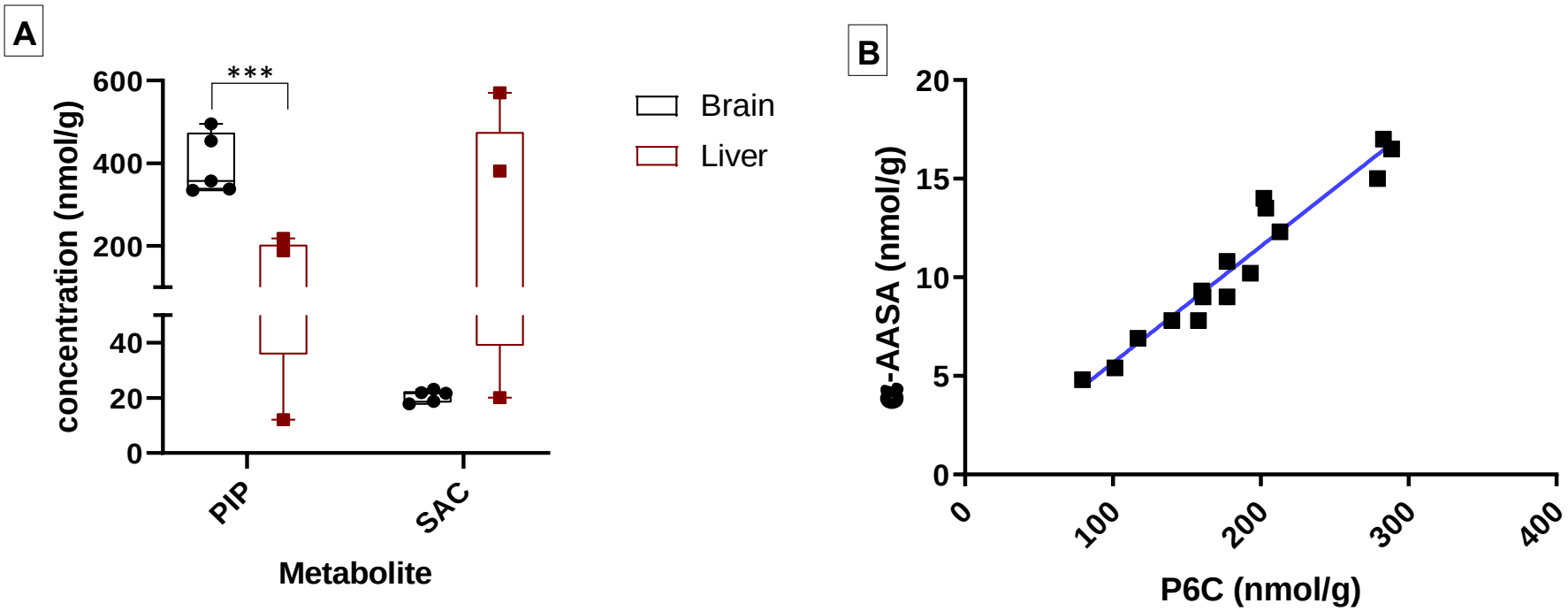

Fig. 3-7: A) Box and whisker plots comparing levels of lysine metabolites pipecolic acid (PIP) and saccharopine (SAC) between brain and liver tissues of neonatal KO mice. (*** $p<0.001$). **B)** Relationship between concentrations of α-AASA and its heterocyclic form, P6C, in brain and liver tissues of adult KO mice (Pearson correlation $R^2=0.9301$, $p<0.0001$).

3.3.3 Analysis of B6 vitamers

A comprehensive battery of vitB6 vitamers (pyridoxine [PN], pyridoxal [PL], pyridoxamine [PM] and their phosphorylated forms: PNP, PLP and PMP, respectively), along with their major catabolite, pyridoxic acid, were analyzed in plasma, brain and liver of adult mice. Results demonstrated no significant difference in the concentration of vitB6 vitamers between KO and WT animals fed a regular (Fig. 3-8 and 3-9).

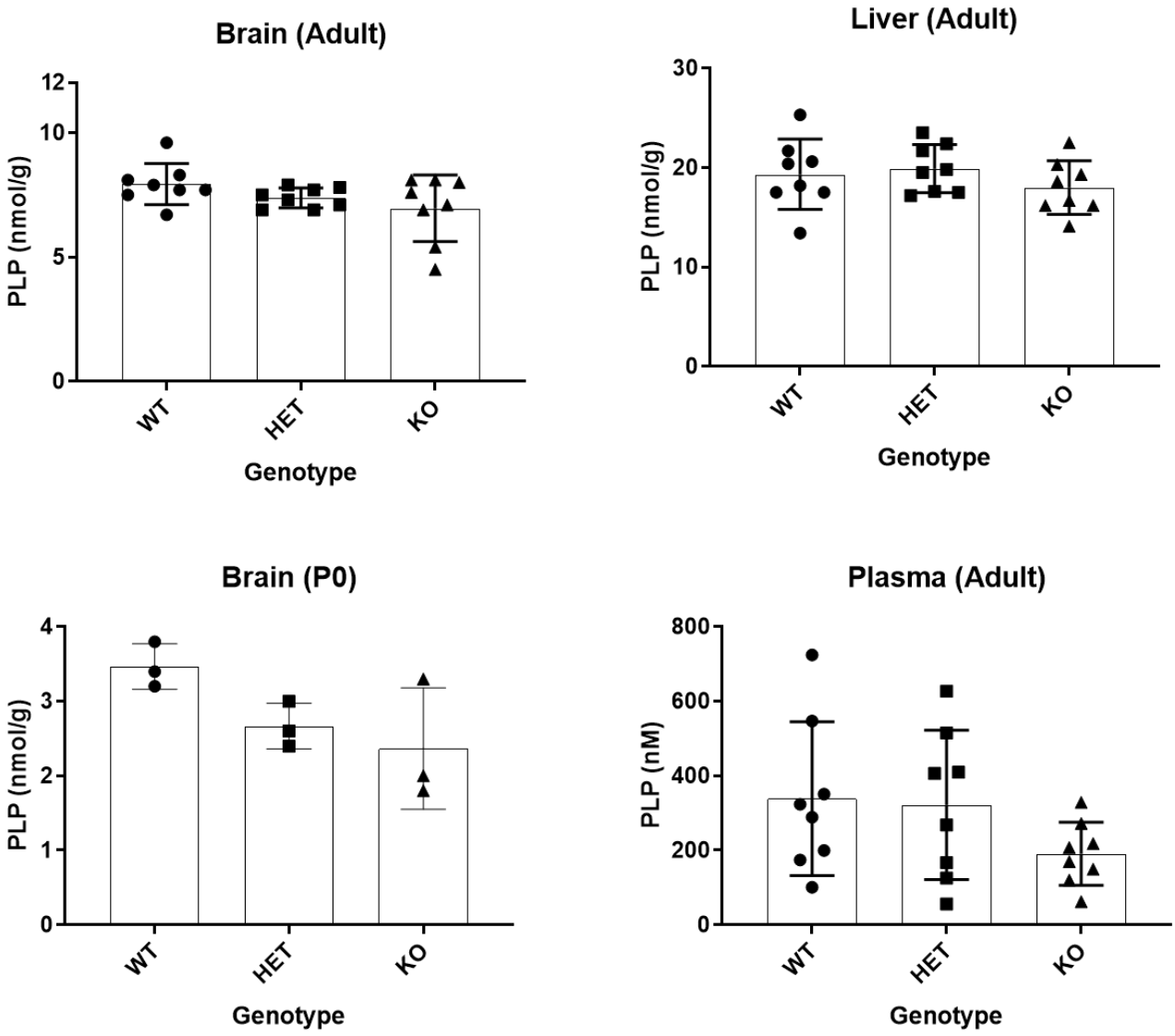

Fig. 3-8: Bar and dot plots comparing levels of pyridoxal 5'-phosophate (PLP) levels between the three genotypes in adults (upper graphs) and P0 mice (lower graph). (Bars represent mean ± SD, N=8 mice per genotype in adults and 3 mice per genotype in P0 mice).

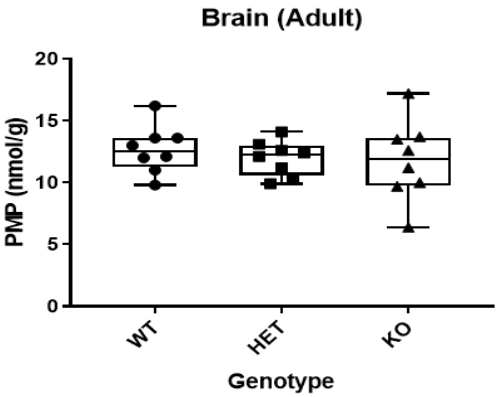
Brain (Adult)
PMP (nmol/g)
20
15
10
5
0
WT
HET
KO
Genotype

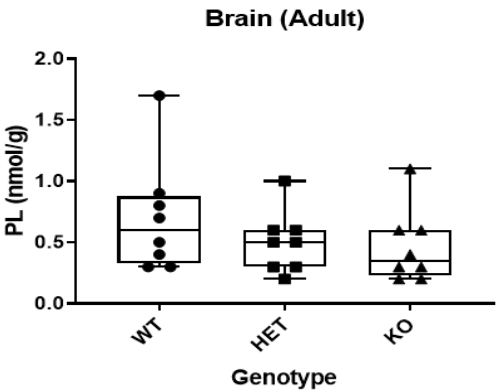
Brain (Adult)
PL (nmol/g)
2.0
1.5
1.0
0.5
0.0
WT
HET
KO
Genotype

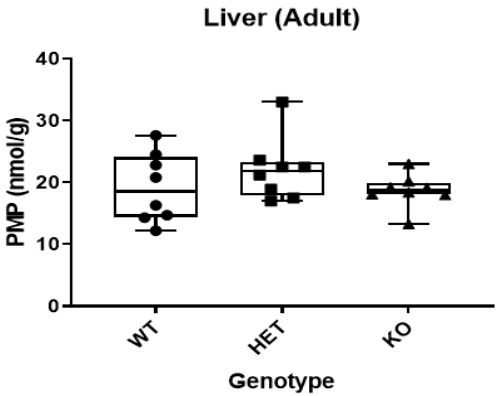
Liver (Adult)
PMP (nmol/g)
40
30
20
10
0
WT
HET
KO
Genotype

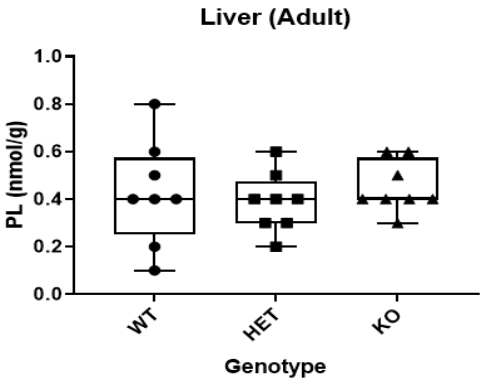
Liver (Adult)
PL (nmol/g)
1.0
0.8
0.6
0.4
0.2
0.0
WT
HET
KO
Genotype

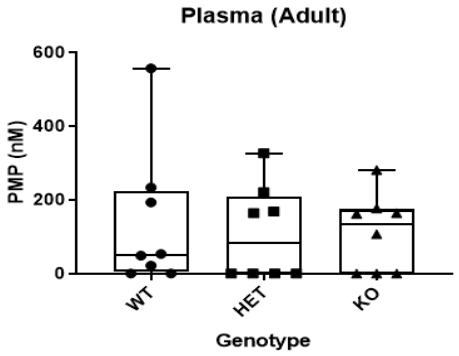
Plasma (Adult)
PMP (nM)
600
400
200
0
WT
HET
KO
Genotype

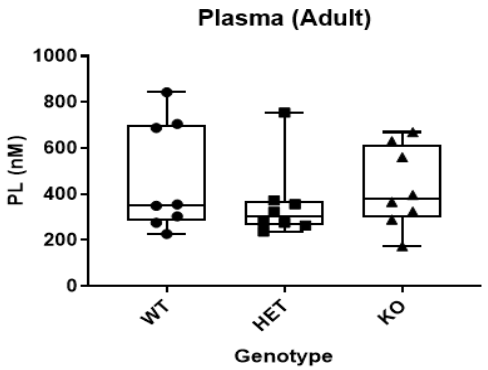
Plasma (Adult)
PL (nM)
1000
800
600
400
200
0
WT
HET
KO
Genotype

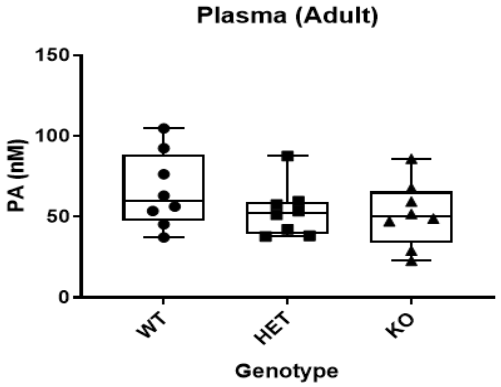
Plasma (Adult)
PA (nM)
150
100
50
0
WT
HET
KO
Genotype

Fig. 3-9: Graphical representation of vitamin B6 vitamer concentrations in brain (upper panel), liver (middle panel) and plasma (bottom panel) of adult mice from the 3 genotypes. No statistically significant differences were noted. PL: pyridoxal, PMP: pyridoxamine 5'-phosphate, PA: pyridoxic acid.

3.3.4 Analysis of amino acids and methionine sulfoxide

A panel of 22 amino acids was analyzed in brain and liver tissues of adult mice using targeted UPLC-MS/MS methods. Measurements showed a number of abnormal amino acid profiles in brain and liver of KO mice. In brain, glycine was present at significantly lower levels compared to WT mice, while ornithine had elevated concentrations (Fig. 3-10). In liver, the effect was more pronounced: 11 amino acids had abnormally elevated levels in KO mice (Fig. 3-11). One WT sample was deemed an extreme outlier across multiple amino acids and was excluded from the final amino acid analyses due to suspicion of technical error.

Furthermore, we quantified the levels of methionine sulfoxide, an oxidative stress biomarker, in brain and liver tissues. Methionine sulfoxide showed elevated concentrations in brain tissue of HETs (($p<0.05$) and KOs ($p=0.05$ after correction for multiple comparisons) relative to WT mice (Fig. 3-12).

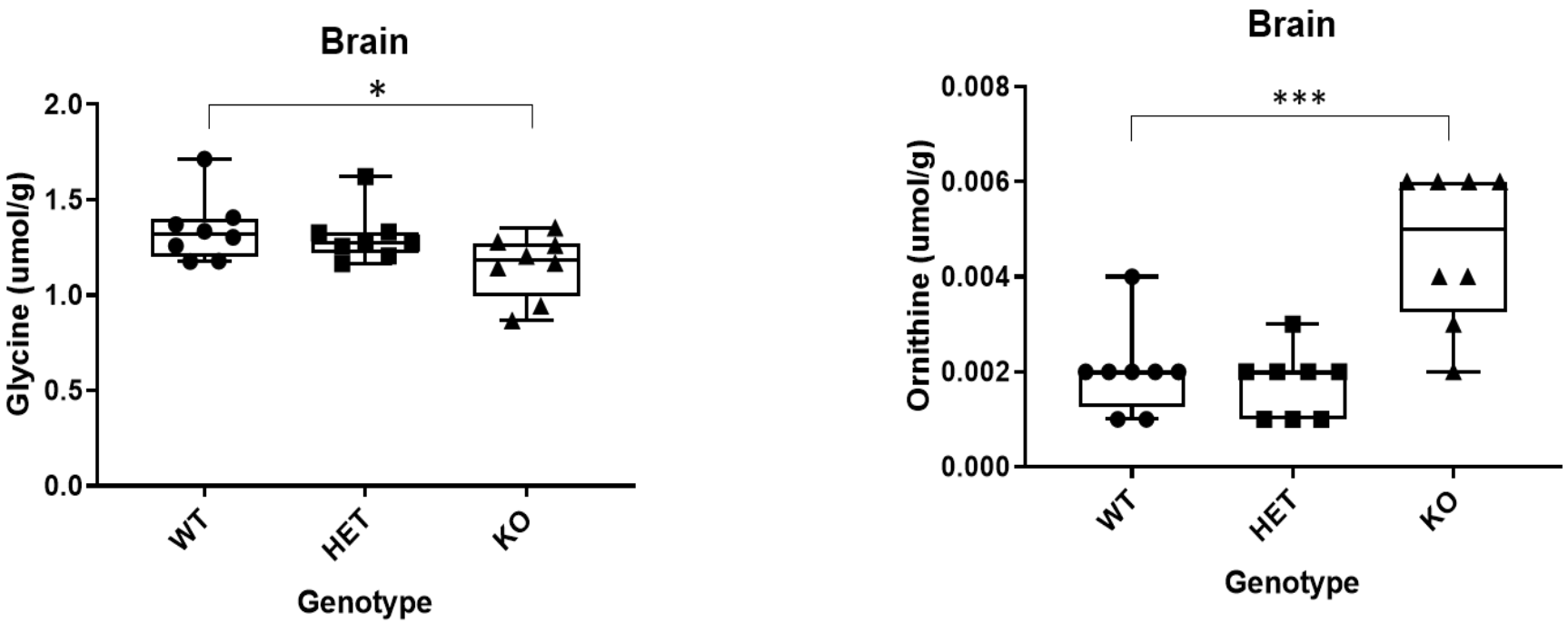

Fig. 3-10: Amino acid quantification in adult brain shows significant changes in glycine and ornithine. (* $p<0.05$, *** $p<0.001$).

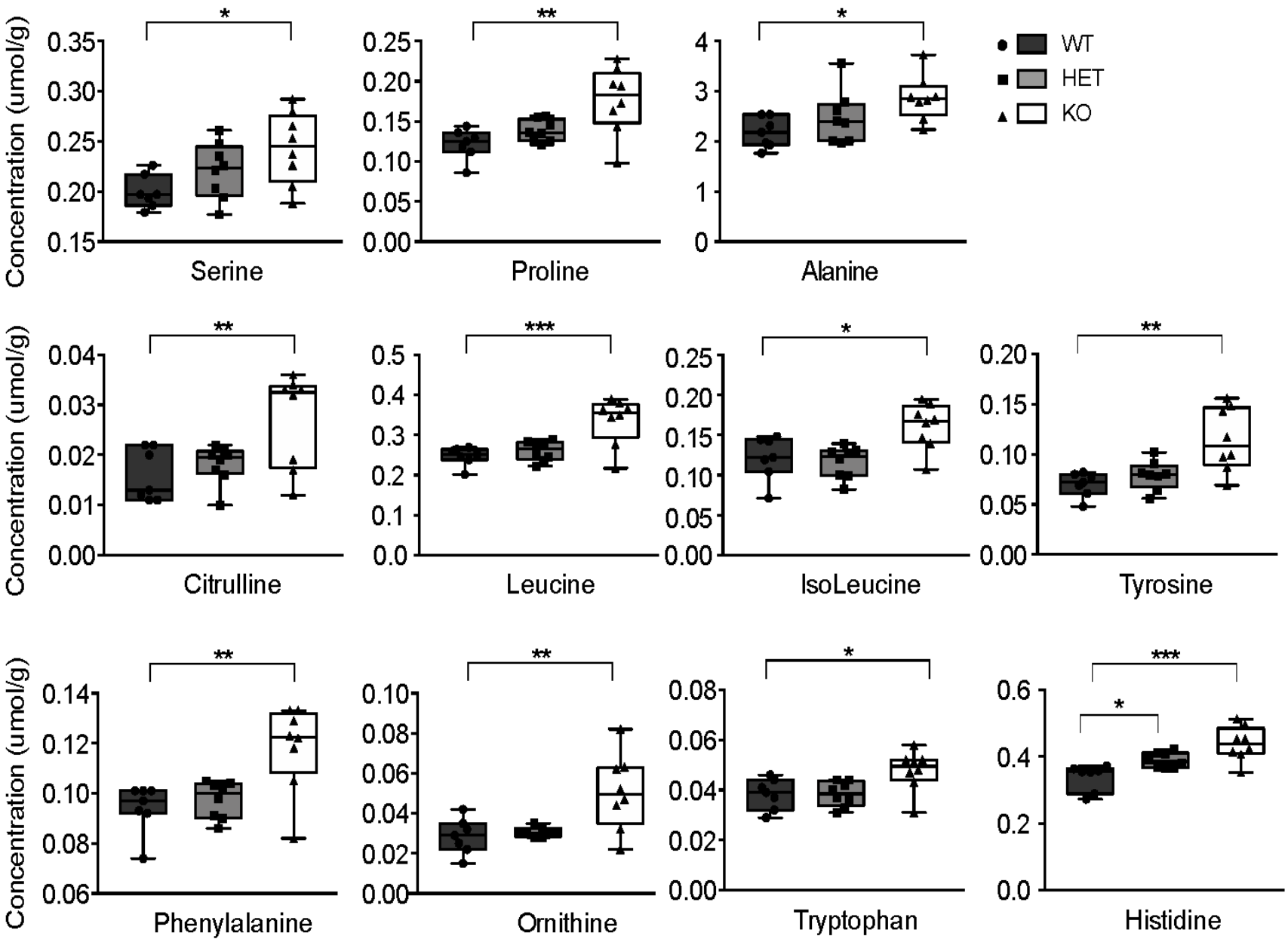
Concentration (umol/g)
Serine
Proline
Alanine
WT
HET
KO
Citrulline
Leucine
IsoLeucine
Tyrosine
Phenylalanine
Ornithine
Tryptophan
Histidine

Fig. 3-11: Amino acid quantification in adult liver reveals aberrant profile across 11 amino acids. (* $p<0.05$, ** $p<0.01$, *** $p<0.001$).

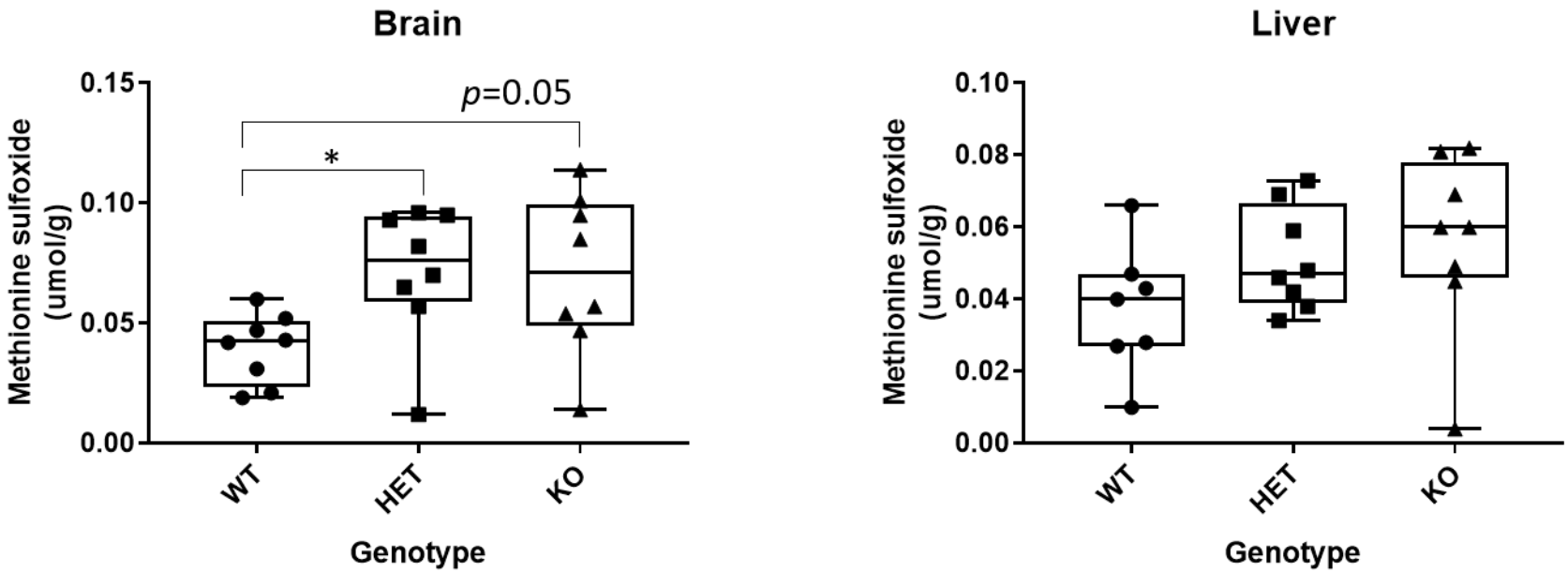

Fig. 3-12: Measurement of oxidative stress biomarker, methionine sulfoxide, in brain (left) and liver (right) of adult mice uncovers high levels in brain of KO (borderline significant) and HET mice (* $p<0.05$).

3.3.5 Analysis of neurotransmitters

Gamma-aminobutyric acid (GABA) and glutamic acid were assayed in neonatal and adult brain and liver tissue. Results showed no significant differences in the levels of these neurotransmitters between the 3 genotypes (Fig. 3-13).

Further analysis included a more comprehensive panel of 10 monoamine neurotransmitters and/or their metabolites (L-DOPA, dopamine, epinephrine, norepinephrine, 3-methoxytyramine, normetanephrine, metanephrine, 5-hydroxytryptophan [5-HTP], serotonin and 5-hydroxyindoleacetic acid [5-HIAA]) in brain and plasma of adult mice. Two compounds, norepinephrine and its metabolite, normetanephrine, were present at significantly higher concentrations in plasma of KO mice compared to WTs (Fig. 3-14 and Fig. 3-15 for remaining neurotransmitters).

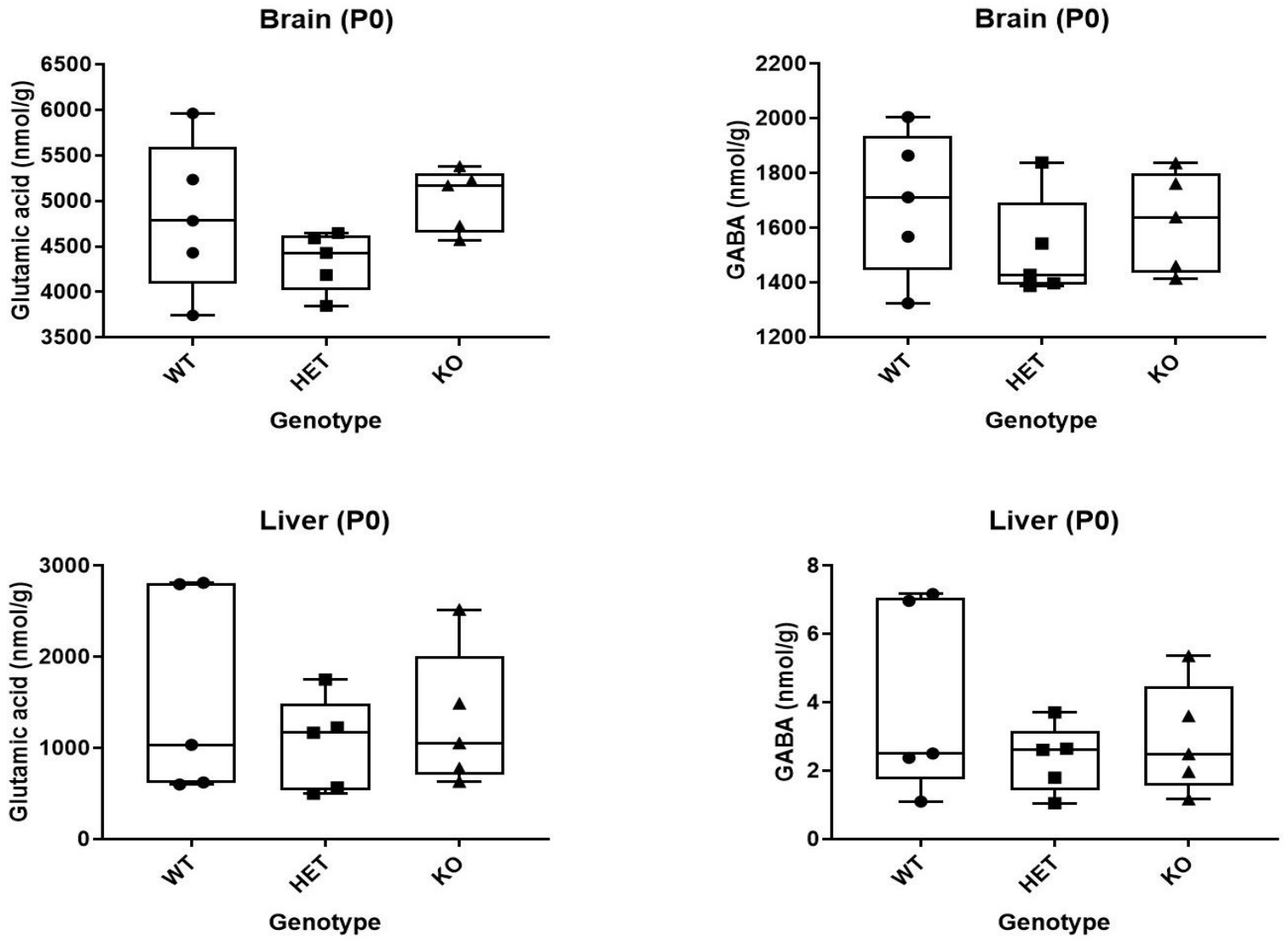

Fig. 3-13: Analysis of two neurotransmitters, glutamic acid and gamma-Aminobutyric acid (GABA), in brain and liver tissues of neonatal mice show no remarkable differences between the 3 genotypes.

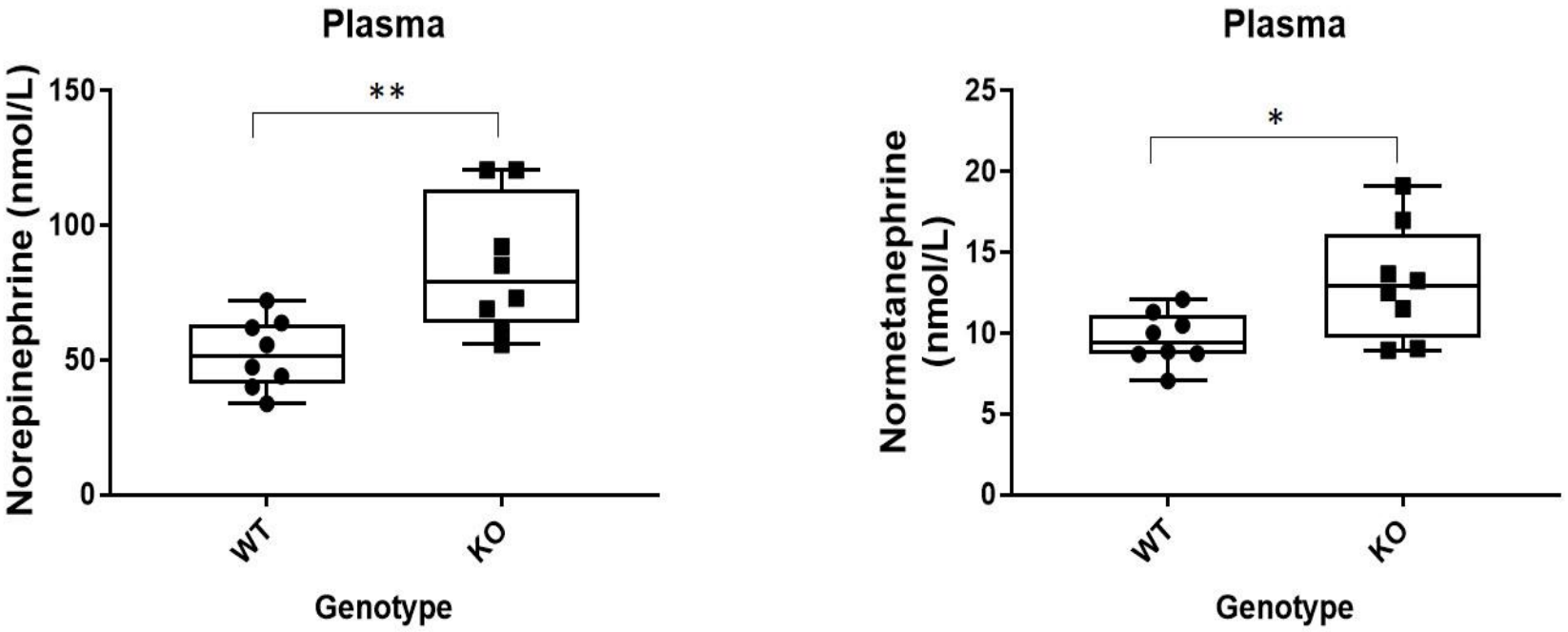

Fig. 3-14: Graphical representation of LC-MS/MS analysis of noradrenaline (left) and its metabolite, normetanephrine (right), in plasma of KO and WT mice. (* $p<0.05$, ** $p<0.01$).

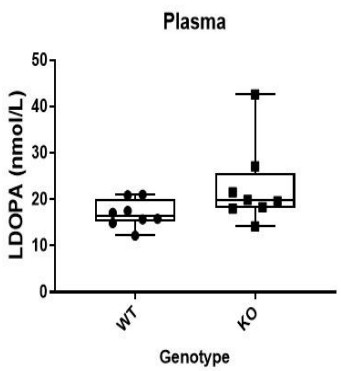
Plasma
LDOPA (nmol/L)
50
40
30
20
10
0
WT
KO
Genotype

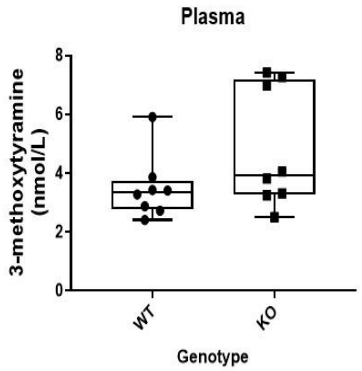
Plasma
3-methoxytyramine (nmol/L)
8
6
4
2
0
WT
KO
Genotype

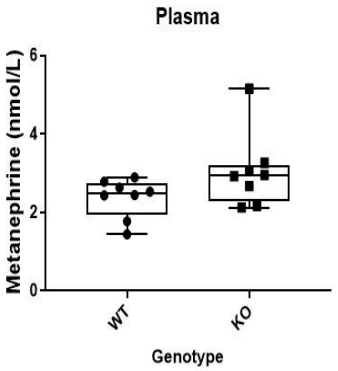
Plasma
Metanephrine (nmol/L)
6
4
2
0
WT
KO
Genotype

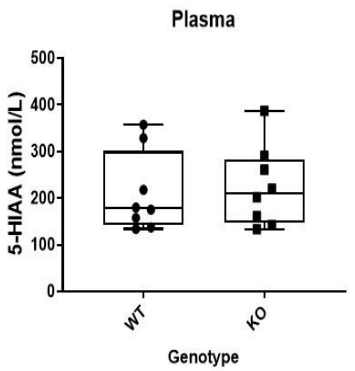
Plasma
5-HIAA (nmol/L)
500
400
300
200
100
0
WT
KO
Genotype

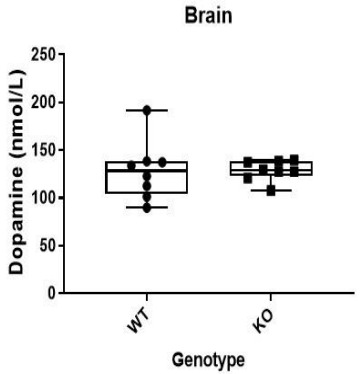
Brain
Dopamine (nmol/L)
250
200
150
100
50
0
WT
KO
Genotype

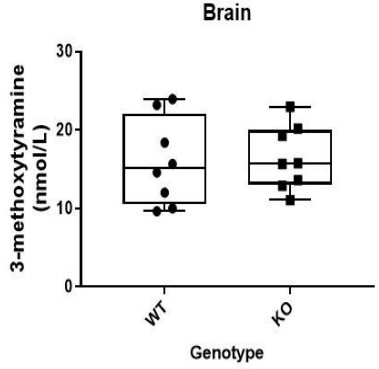
Brain
3-methoxytyramine (nmol/L)
30
20
10
0
WT
KO
Genotype

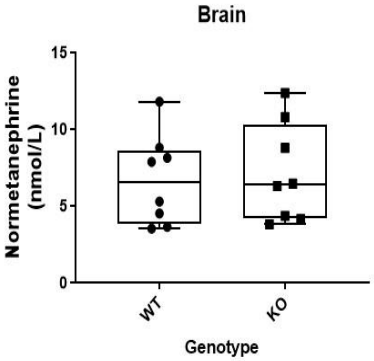
Brain
Normetanephrine (nmol/L)
15
10
5
0
WT
KO
Genotype

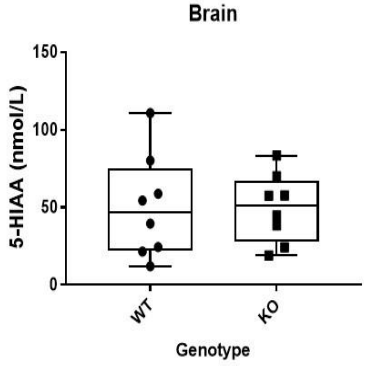
Brain
5-HIAA (nmol/L)
150
100
50
0
WT
KO
Genotype

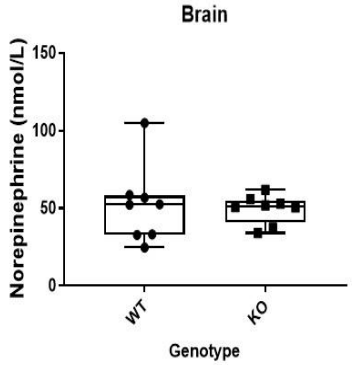
Brain
Norepinephrine (nmol/L)
150
100
50
0
WT
KO
Genotype

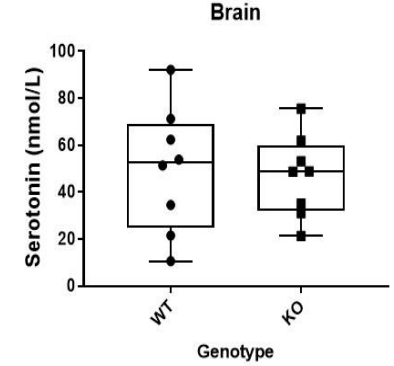
Brain
Serotonin (nmol/L)
100
80
60
40
20
0
WT
KO
Genotype

Fig. 3-15: Box and dot plots comparing levels of monoamine neurotransmitters and their metabolites in plasma and brain tissue of adult WT and KO mice. 5-HIAA: 5-hydroxyindoleacetic acid.

3.3.6 Behavioral phenotyping

A battery of behavioral tests was conducted on *Aldh7a1*-KO mice at two time points: 2.5 and 6 months. These tests were used to assess locomotor activity (open field), anxiety-like behavior (open field, elevated plus maze and novel object recognition), depressive-like behavior (forced swim test), spatial memory and learning (Morris water maze), and motor coordination and motor learning (accelerating rotarod). Analysis of the results using standard pipelines revealed no differences in performance between WT and KO mice at either age analyzed (Fig. 3-16 and 3-17).

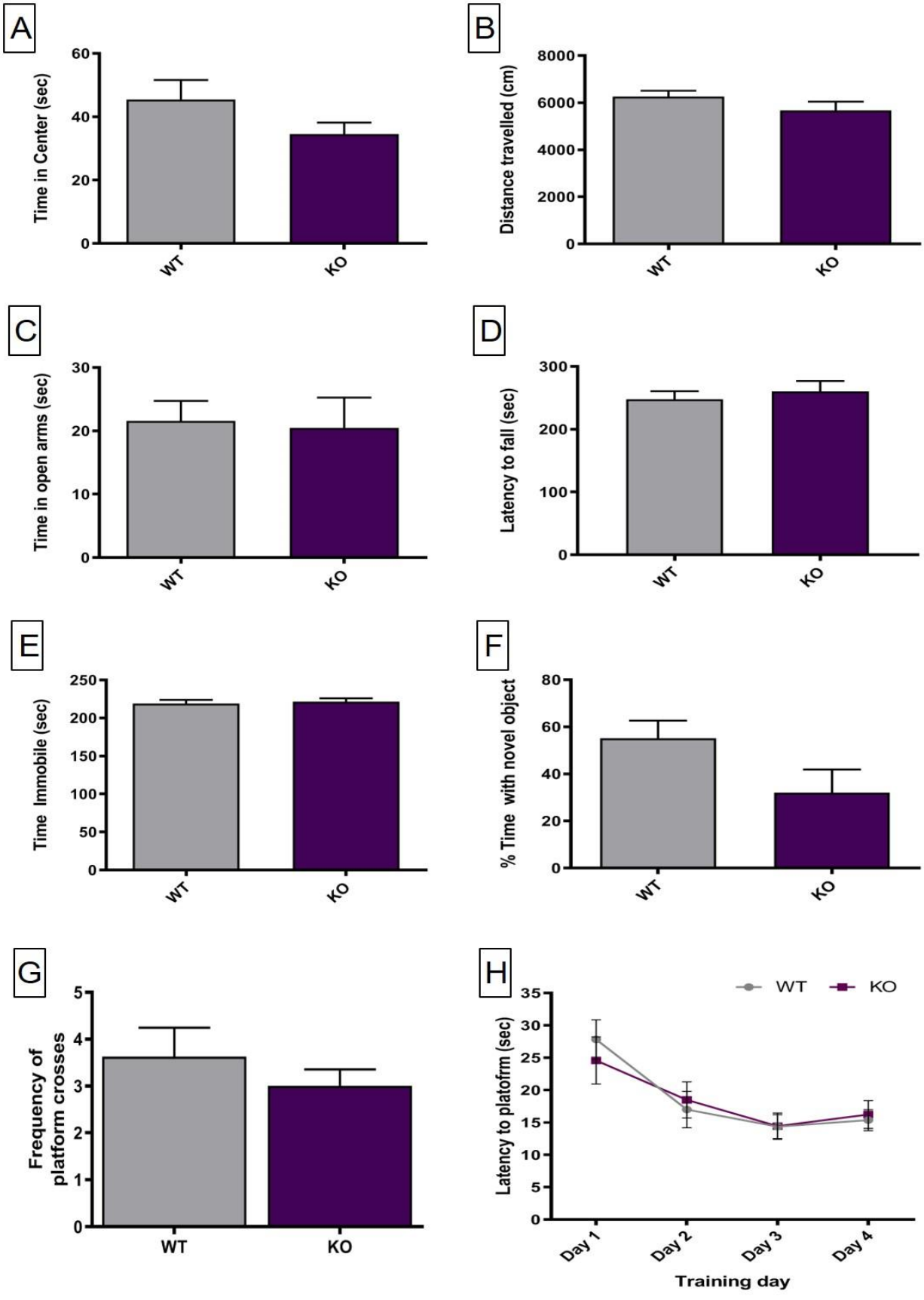
A
Time in Center (sec)
60
40
20
0
WT
KO
B
Distance travelled (cm)
8000
6000
4000
2000
0
WT
KO
C
Time in open arms (sec)
30
20
10
0
WT
KO
D
Latency to fall (sec)
300
200
100
0
WT
KO
E
Time Immobile (sec)
250
200
150
100
50
0
WT
KO
F
% Time with novel object
80
60
40
20
0
WT
KO
G
Frequency of platform crosses
5
4
3
2
1
0
WT
KO
H
WT
KO
Latency to platofrm (sec)
35
30
25
20
15
10
5
0
Day 1
Day 2
Day 3
Day 4
Training day

Fig. 3-16: Aldh7a1-deficient mice show no behavioral abnormality at 6 months of age. (A) Frequency of center crosses in an open field arena over a 10-minute trial. (B) Distance traveled in an open field arena over a 10-minute trial. (C) Time spent in open arms in elevated plus maze test. (D) Latency to fall from an accelerating rotarod in WT and KO mice. (E) Total immobility time during the middle 4 minutes of forced swim test. (F) Preference for a novel object expressed as [time spent with novel object / (time with novel object + time with familiar object) X 100]. (G) Number of platform crosses in the probe trial of the Morris water maze. (H) Latency to find the hidden platform during 4-day training trials in the Morris water maze. Data shown are the averages of four trials per day ± SEM. (N=16 WT and 13 KO mice).

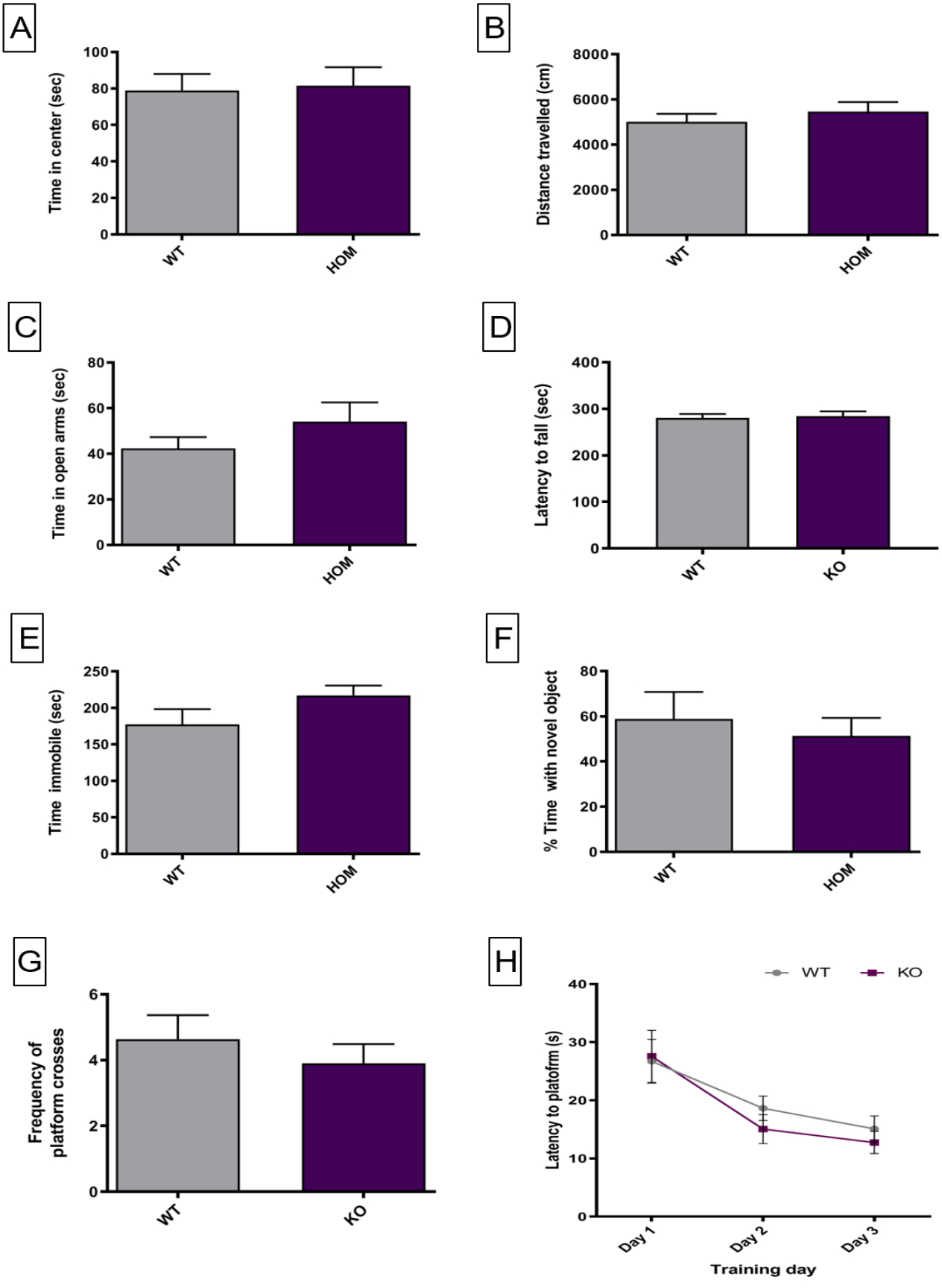
A
Time in center (sec)
100
80
60
40
20
0
WT
HOM
B
Distance travelled (cm)
8000
6000
4000
2000
0
WT
HOM
C
Time in open arms (sec)
80
60
40
20
0
WT
HOM
D
Latency to fall (sec)
400
300
200
100
0
WT
KO
E
Time immobile (sec)
250
200
150
100
50
0
WT
HOM
F
% Time with novel object
80
60
40
20
0
WT
HOM
G
Frequency of platform crosses
6
4
2
0
WT
KO
H
WT
KO
Latency to platofrm (s)
40
30
20
10
0
Day 1
Day 2
Day 3
Training day

Fig. 3-17: Behavioral analyses of Aldh7a1-deficient mice at 2.5 months of age. (A) Frequency of center crosses in an open field arena over a 10-minute trial. (B) Distance traveled in an open field arena over a 10-minute trial. (C) Time spent in open arms in elevated plus maze test. (D) Latency to fall from an accelerating rotarod in WT and KO mice. (E) Total immobility time during the middle 4 minutes of forced swim test. (F) Preference for a novel object expressed as [time spent with novel object / (time with novel object + time with familiar object) X 100]. (G) Number of platform crosses in the probe trial of the Morris water maze. (H) Latency to find the hidden platform during 3-day training trials in the Morris water maze. Data shown are the average of four trials per day ± SEM. (N= 11 WT and 10 KO mice, except for accelerating rotarod test in which N= 9 WT and 8 KO mice).

3.3.7 Neuropathology

We performed qualitative assessment of neuropathological changes in Aldh7a1-KO mice at 4 months of age using immunohistochemical staining with NeuN and GFAP. Coronal serial brain sections from WT and KO mice were examined for gross structural differences, neuronal distribution, neuronal density, and the presence of astrogliosis in multiple brain regions. No differences were apparent between WT and KO mice in the assessed neuropathological features (Fig. 3-18 and 3-19). There were also no differences between the two genotypes in whole and forebrain weight measured at 2.5 and 6 months of age (Fig. 3-20).

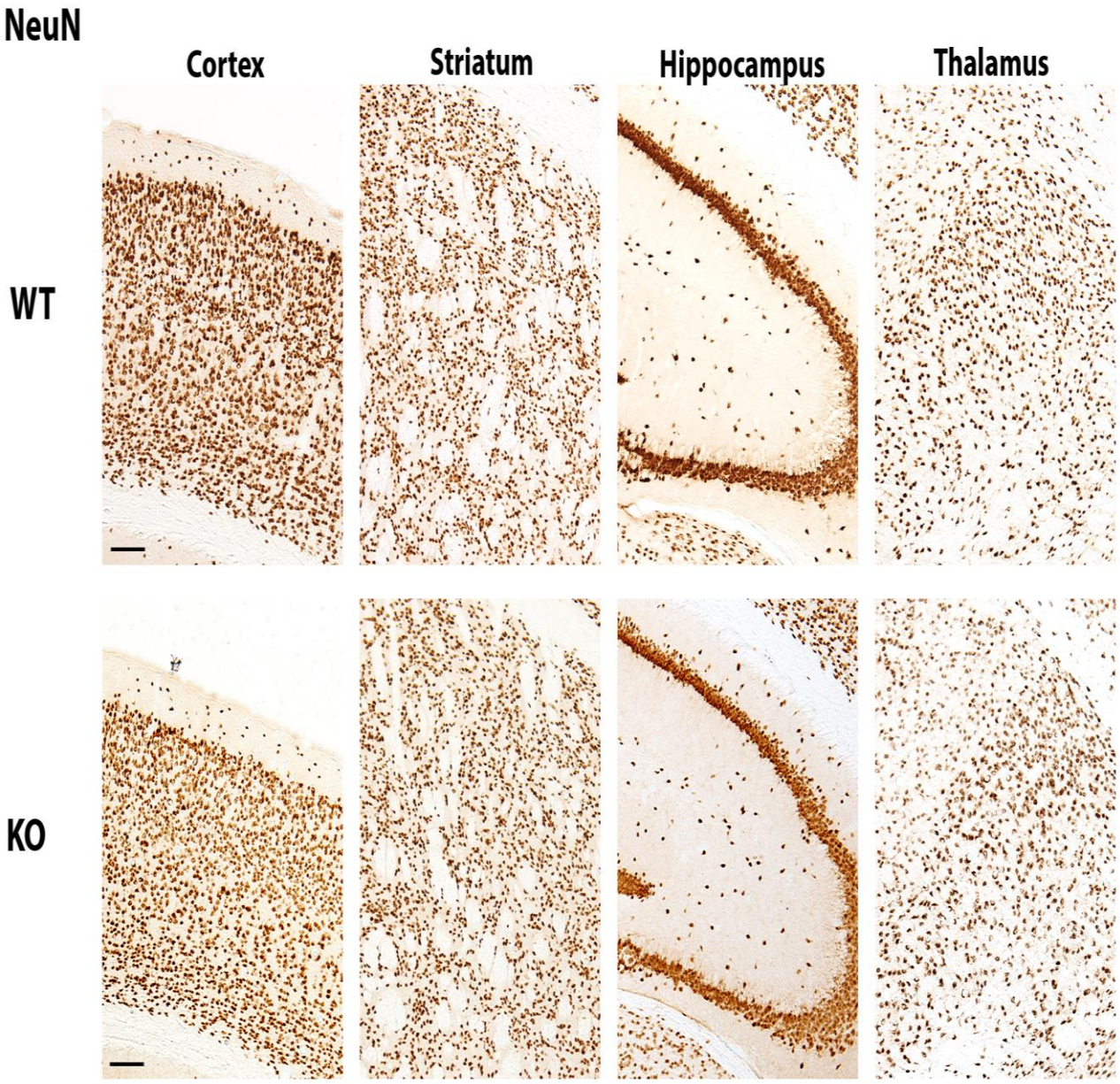

Fig. 3-18: Qualitative neuropathology in Aldh7a1-deficient mice using neuronal marker NeuN. Light micrographs from WT and KO mice showing NeuN immunostaining in different brain regions. Scale bar = 100 μm.

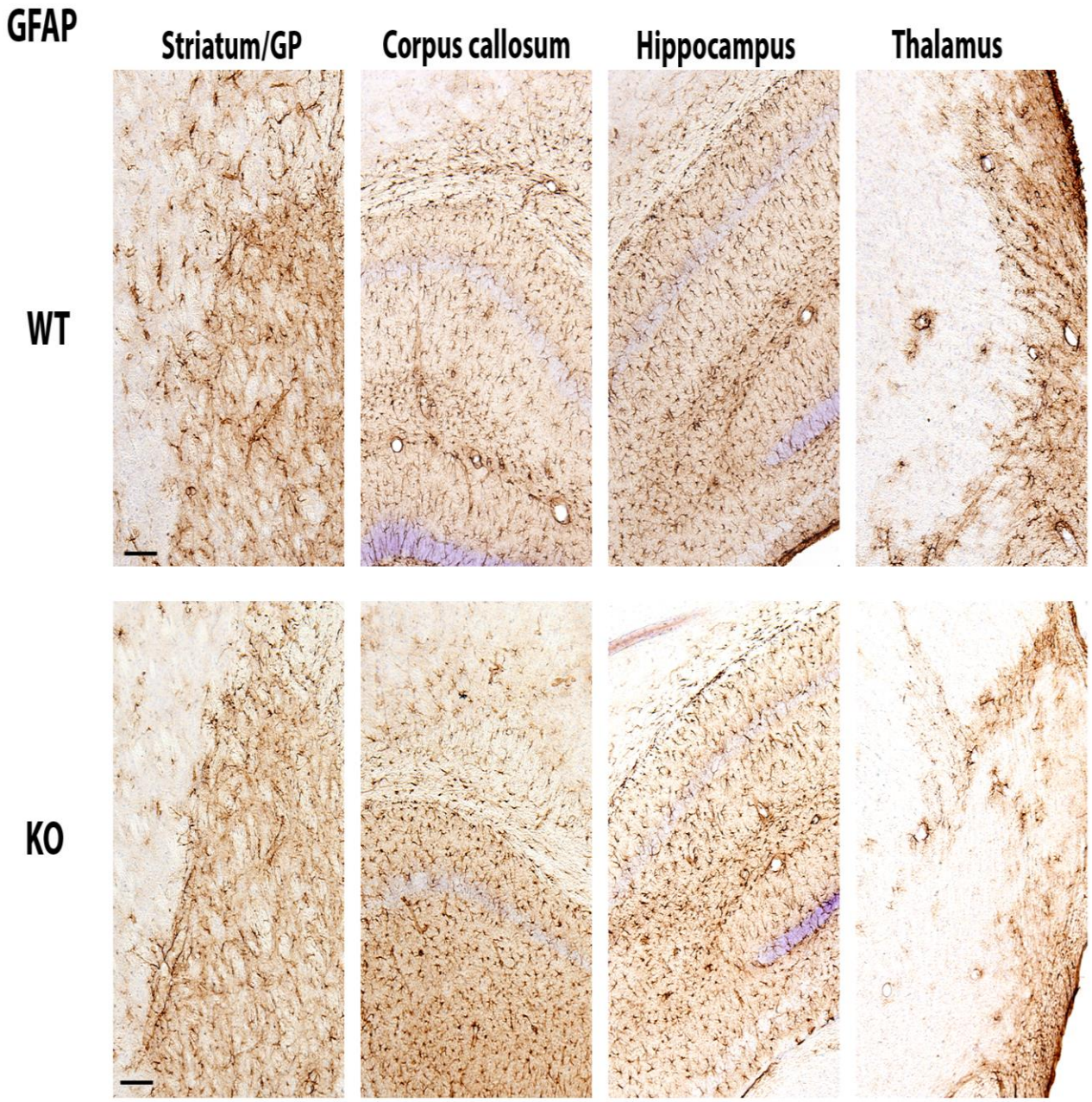

Fig. 3-19: Qualitative neuropathology in Aldh7a1-deficient mice using astrocyte marker GFAP. Light micrographs from WT and KO mice showing GFAP immunostaining in different brain regions. Sections were counterstained with cresyl violet (purple color). Abbreviations, GP: Globus pallidus. Scale bar = 100μm.

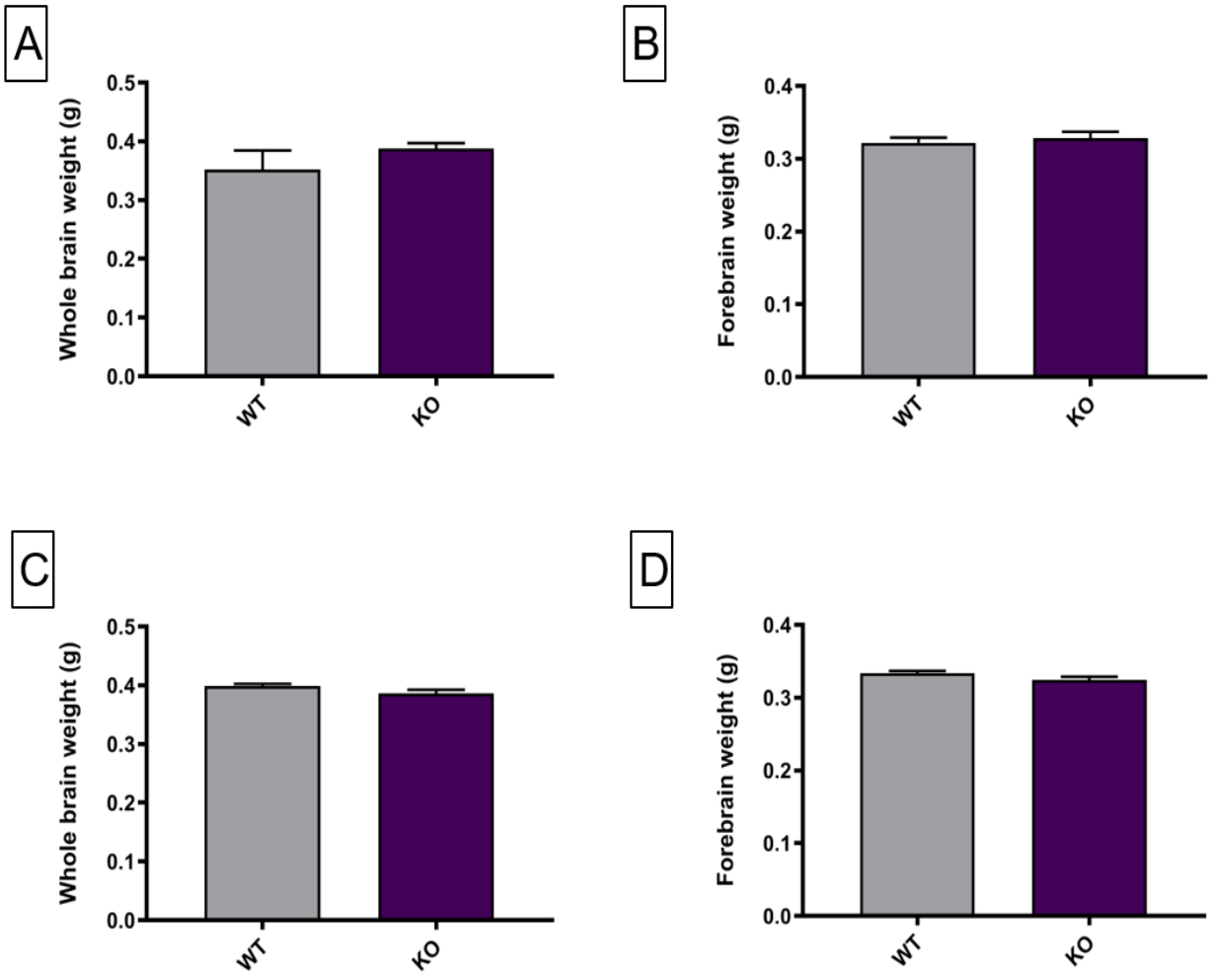

Fig. 3-20: Whole and forebrain weight analysis at 2.5 (A and B) and 6 months (C and D) show no differences between WT and KO mice (2.5 month measurements were taken from 11 WT and 10 KO animals; 6 month measurements were taken from another group that included 13 WT versus 12 KO animals).

3.3.8 *In vivo* electrophysiology

Mice had good post-operative recovery. A total of 48-96 hours of multi-channel EEG recordings and concurrent acceleration data were obtained from each mouse using the Neurologger 2A wireless system (Fig. 3-21 and 3-22). There was no evidence of convulsive seizure in KO mice under regular diet from both background strains by analysis of their EEG data (Fig. 3-23).

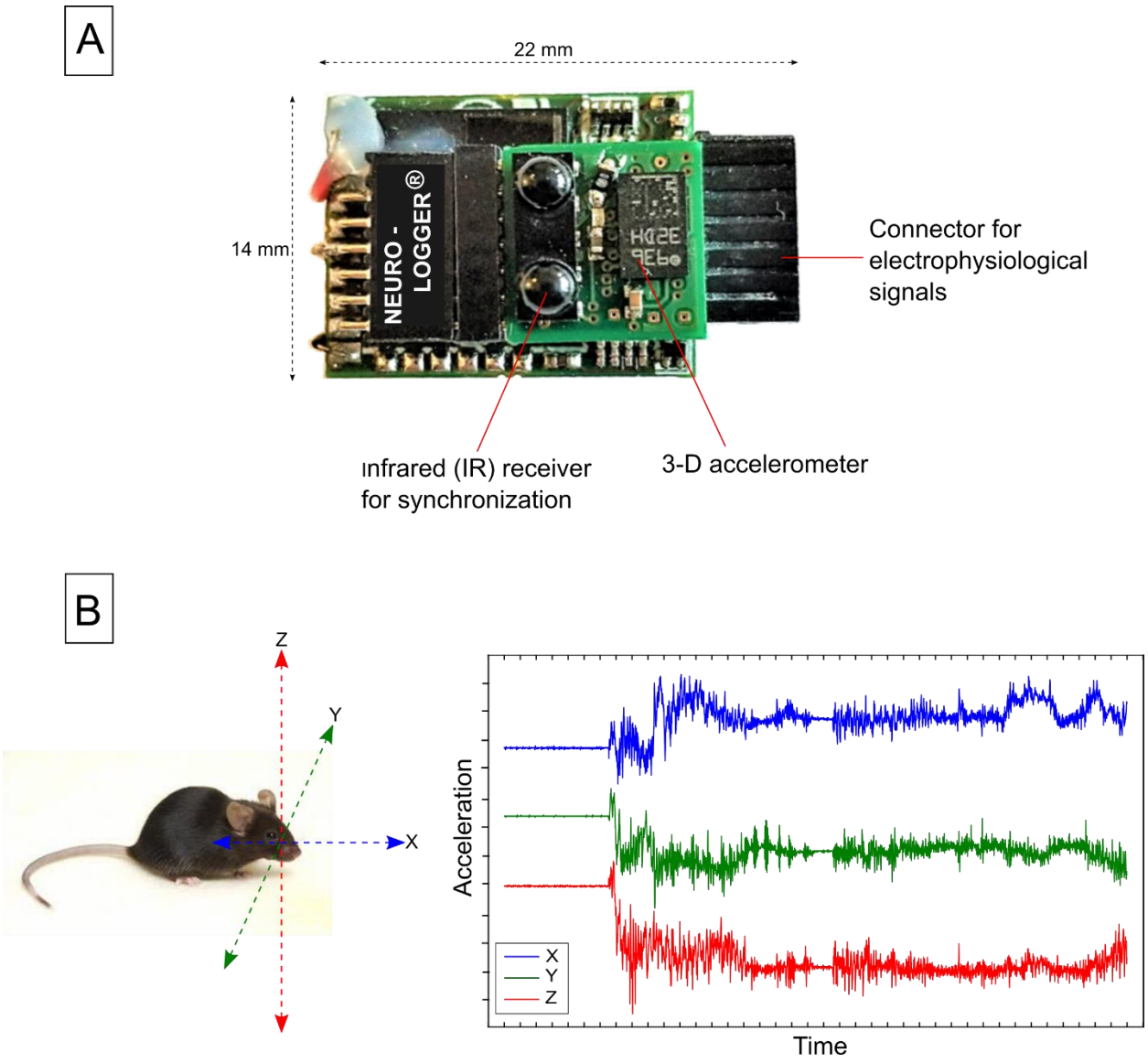

Fig. 3-21: EEG recording system in Aldh7a1-KO mice. A) Enlarged picture of Neurologger 2A. This miniature device contains 1 GB built-in memory for storing electrophysiological signals, 3-D accelerometer and infrared receiver for synchronizing with other devices like video camera. B) The accelerometer records animal acceleration in the 3-D space in milli-G (mG, where G is acceleration of Earth's gravity (~9.8 m/s^2)). The chromatogram shows an example of the accelerometer readout along the three orthogonal axes (X, Y and Z).

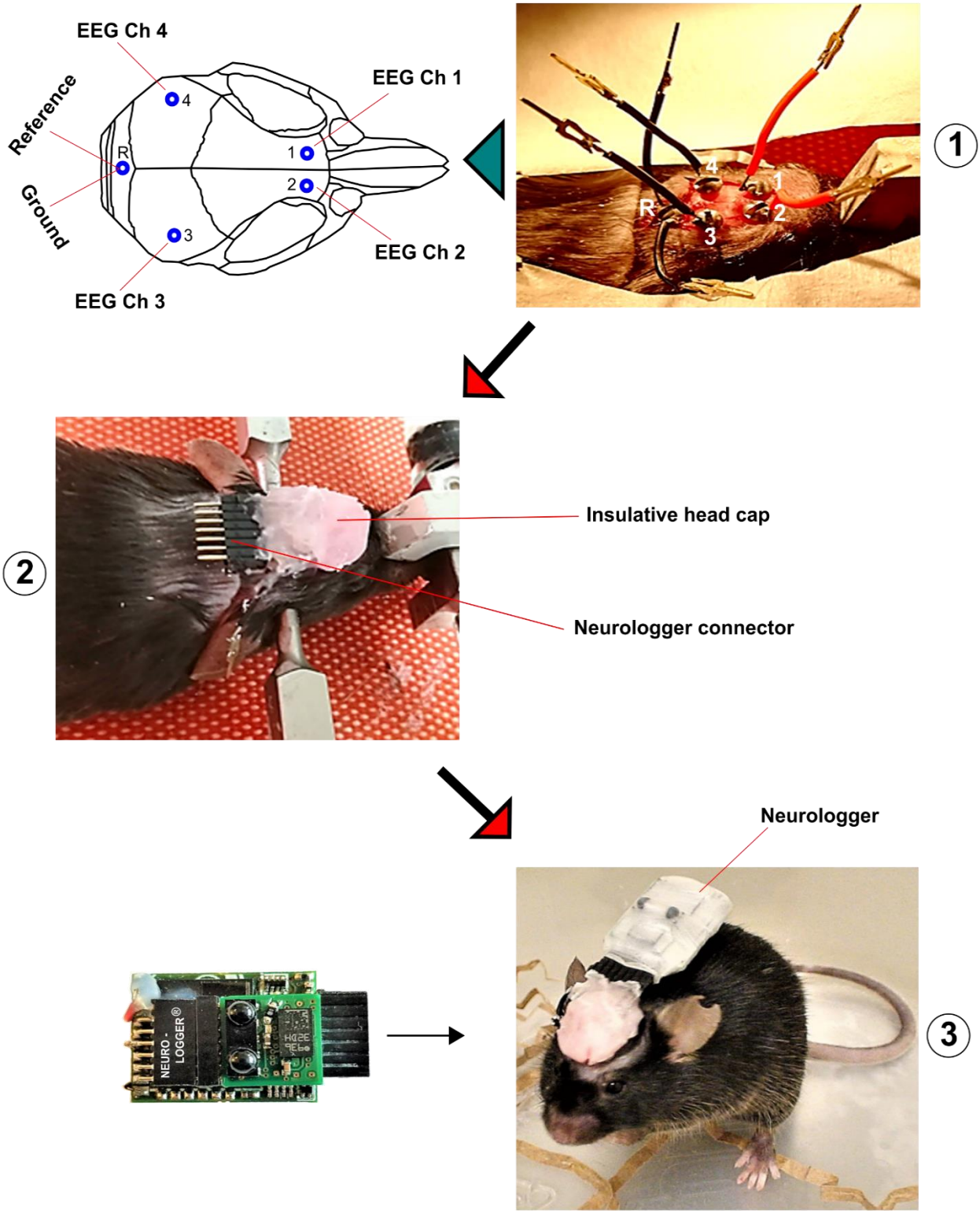
EEG Ch 4
Reference
EEG Ch 1
R
4
1
2
Ground
3
EEG Ch 2
EEG Ch 3
1
2
Insulative head cap
Neurologger connector
Neurologger
NEURO - LOGGER®
3

Fig. 3-22: EEG implantation and recording procedure. (1) Surgical placement of trans-cranial EEG electrodes. Skull drawing shows layout of implanted electrodes. (2) Electrodes are inserted into a pin connector that acts as a relay to Neurologger, fixed and insulated with acrylic material. (3) After mouse recovery, Neurologger is plugged into the head-mounted connector to start EEG recording.

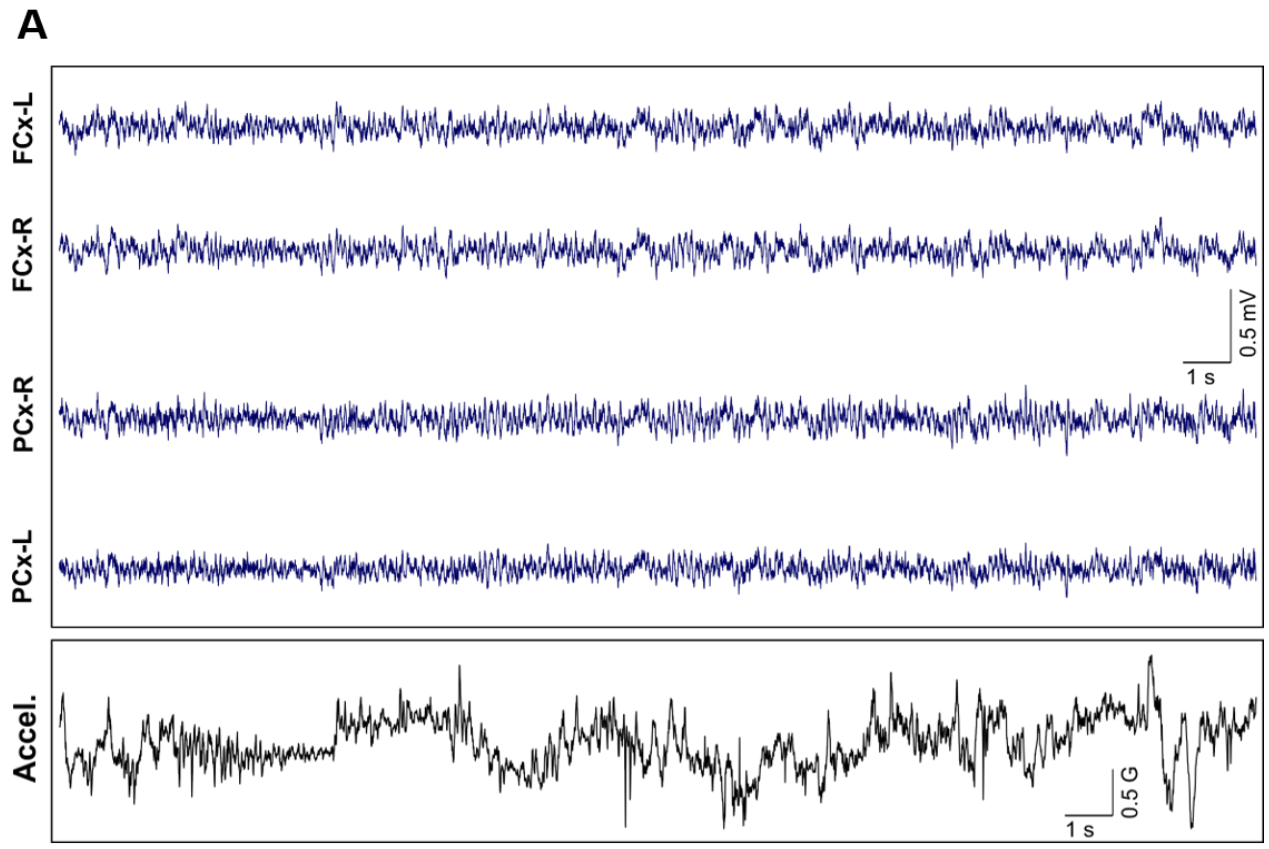
A
FCx-L
FCx-R
PCx-R
PCx-L
0.5 mV
1 s
Accel.
0.5 G
1 s

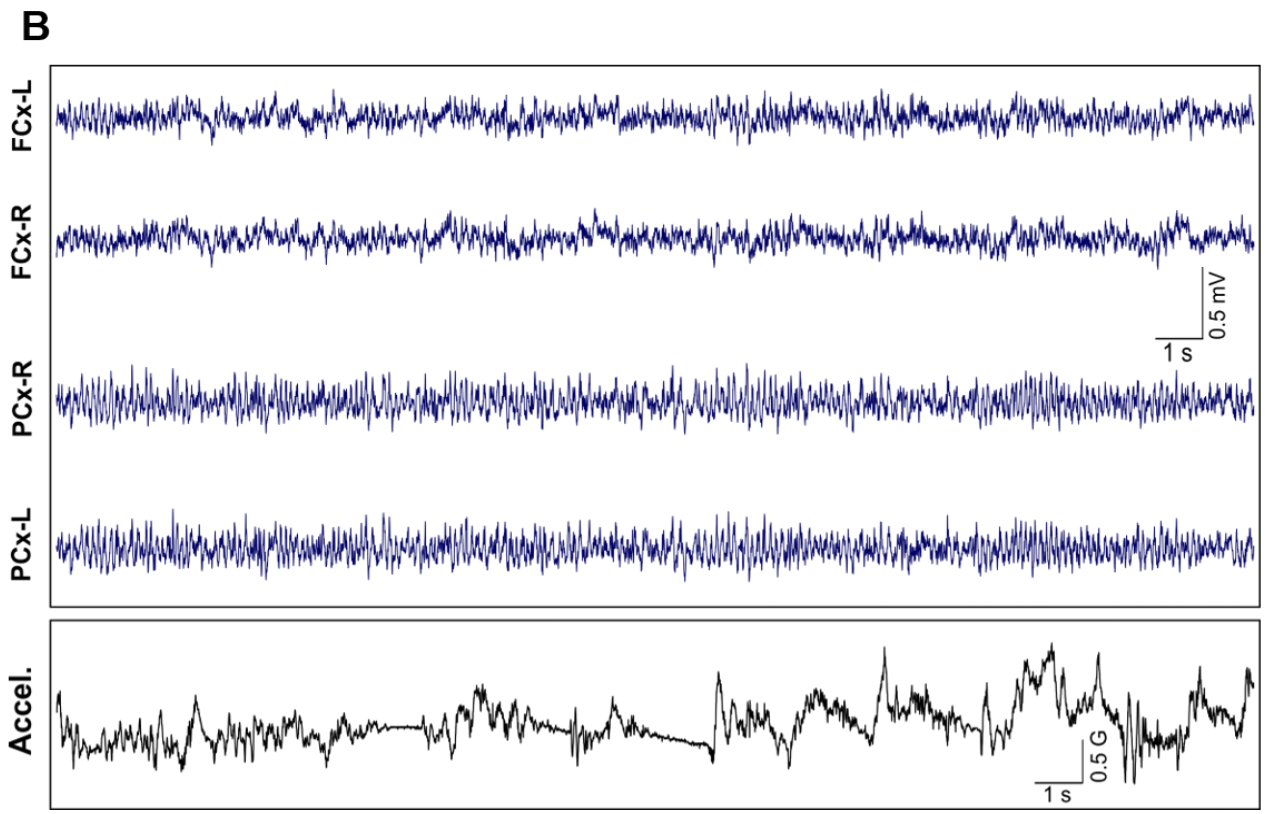
B
FCx-L
FCx-R
PCx-R
PCx-L
0.5 mV
1 s
Accel.
0.5 G
1 s

Fig. 3-23: *In vivo* electrophysiology in Aldh7a1-KO mice. 4-channel EEG recording with simultaneous accelerometer readout showing normal EEG in Aldh7a1-KO mice from the B6 (A) and B6;129 background strains (B). Abbreviations, FCx-L: left frontal cortex, FCx-R: right frontal cortex, PCx-L: left parietal cortex, PCx-R: right parietal cortex, Accel.: accelerometer, s: seconds, G: acceleration of Earth's gravity (~9.8 m/s^2).

3.4 Discussion

The current work describes the generation and phenotypic characterization of a novel mouse model for pyridoxine-dependent epilepsy caused by inactivating mutations in the *ALDH7A1* (antiquitin) gene. We found that *Aldh7a1*-KO mice recapitulated many biochemical abnormalities characteristic of PDE-ALDH7A1 patients, suggesting that these mice represent an accurate mouse model of the human disease and will be useful for future therapeutic testing. The discovery of novel biochemical changes in the KO mice suggests that this mouse model may also be useful for uncovering unidentified pathophysiological mechanisms contributing to the spectrum of phenotypic abnormalities that occur in PDE-ALDH7A1 patients.

Crossing of HET mice yielded fewer homozygous KO offspring at weaning than expected for Mendelian proportions (19.68% observed, 25% expected). This low rate of homozygous KO mice is suggestive of a partially lethal phenotype expressed in the prenatal or early neonatal period. In line with this, a recent study by Coughlin et al. (2018) calculated the carrier frequencies for all known and predicted pathogenic variants in *ALDH7A1* among humans reported in the gnomAD database. Based on this and using the Hardy‑Weinberg model, they estimated that the incidence of PDE-ALDH7A1 should be 1:64,352 births, which is higher than most of the previously reported PDE-ALDH7A1 incidences based on clinical diagnosis and that ranged from 1:783,000 to 1:20,000 (Coughlin et al., 2018). The authors attributed this discrepancy to a number of reasons

including the possibility of underestimated *in utero* and neonatal mortality (Coughlin et al., 2018). Increased mortality also occurs in untreated human infants with PDE-ALDH7A1 (Jansen et al., 2014). In an *aldh7a1*-KO zebrafish model (Pena, Roussel, et al., 2017), untreated KO fish died within 14 days post fertilization (larvae stage).

Aldh7a1-deficient mice had a biochemical profile that recapitulated the human PDE-ALDH7A1 biochemical phenotype with accumulation of supraphysiological levels of the lysine catabolites P6C, α-AASA and PIP, the hallmark biochemical features of PDE-ALDH7A1 (Stockler et al., 2011). The majority of human patient data on lysine biomarkers (namely P6C, α-AASA and PIP) comes from analysis of plasma, urine and, less commonly, CSF. The actual magnitude of the increase of these compounds in brain tissue of affected children is limited to one post-mortem study (Jansen et al., 2014). In brain tissue of adult KO mice, P6C accumulated in the range of 101.4 – 202.0 nmol/g, which is 12-24-fold higher than the patient's P6C concentration reported by Jansen et al. (2014), but the patient's brain specimen was analyzed 12 hours post mortem. Information on stability of these analytes in actual brain tissue is lacking. In serum, both P6C and α-AASA are very unstable at 23 and 4°C (Sadilkova et al., 2009).

In addition to the three known biomarker molecules (P6C, α-AASA and PIP), we found that another upstream lysine catabolite, saccharopine (SAC), was also highly elevated in KO mice. A similar observation was reported in the *aldh7a1*-KO zebrafish model by Pena, Roussel, et al. (2017). The finding of high SAC levels in the brains of Aldh7a1-deficient mice lends further support to previous studies suggesting that the saccharopine pathway is an active lysine catabolism pathway in the brain (Crowther et al., 2019; Pena, Marques, et al., 2017).

Our study also reports the level of lysine metabolites in a peripheral tissue (liver) for the first time in an *in-vivo* model of Aldh7a1 deficiency. Quantification revealed that these metabolites

accumulate in *Aldh7a1*-null liver at concentrations comparable to or even higher than in brain tissue (Fig. 3-3 and 3-4). The presence of high accumulation of PIP in liver speaks in favor of an active pipecolic acid pathway in liver, as has been suggested by recent studies (Pena, Marques, et al., 2017; Posset et al., 2015). Another possible source of accumulated PIP is through retrograde conversion of saccharopine-derived P6C, as proposed by the study of Struys and Jakobs (2010). Using isotopic tracking in ALDH7A1-deficient fibroblasts, this study demonstrated that PIP was derived from the saccharopine pathway and postulated that P6C is the direct precursor for the retrograde formation of PIP. In a subsequent study (Struys et al., 2014), it was shown that pyrroline-5-carboxylate reductase is the enzyme responsible for the conversion of P6C to PIP. PIP resulting from the pipecolic acid pathway can be reversibly converted to P6C by the enzyme pipecolic acid oxidase, establishing a point of convergence between the two catabolic pathways (Fig. 3-1). However, few recent studies (Crowther et al., 2019; Pena, Marques, et al., 2017; Posset et al., 2015) have challenged this presumed convergence step by showing that, using labelled lysine that discriminates the two pathways, only minor or no α-AAA could be formed form the pipecolic acid pathway, leaving questions about the possible metabolic fate of accumulated PIP. The accumulation of this metabolite in *Aldh7a1*-null mice suggests that this mouse model may be useful in answering important questions about lysine catabolism.

We assayed two further compounds in the lysine pathway, both of which showed unexpected trends in brain tissue. First, lysine, the principal upstream substrate, was present in lower concentrations in brain tissue of KO mice (Fig. 3-5). Low plasma lysine was previously described in a PDE-ALDH7A1 patient (Mercimek-Mahmutoglu, Cordeiro, et al., 2014). A possible explanation can be inferred from the study of Crowther et al. (2019), who noted increased activity of the α-aminoadipic semialdehyde synthase (AASS) enzyme in patient-derived

ALDH7A1-deficient fibroblasts. AASS is a bifunctional enzyme that catalyzes the first two steps in the saccharopine pathway of lysine catabolism (Fig. 3-1). Overactivity of AASS is expected to increase lysine degradation and thus lower lysine levels. The notion of AASS upregulation in ALDH7A1 deficiency (Crowther et al., 2019), along with an earlier study showing that the saccharopine pathway is the main stream that fuels the production of cerebral P6C and α-AASA (Pena, Marques, et al., 2017), highlights the AASS enzyme as a plausible therapeutic target for PDE-ALDH7A1.

Unexpectedly, α-AAA, a downstream lysine metabolite, was also elevated in the brains of KO mice (Fig. 3-5). In contrast, hepatic α-AAA displayed a tendency to lower levels in KOs compared to WT and HET mice (Fig. 3-5). No published quantification data for this compound are available for brain or CSF from human PDE-ALDH7A1 patients. In patients' fibroblasts, α-AAA was either undetectable (Struys and Jakobs, 2010) or had lower levels compared to control fibroblasts (Crowther et al., 2019). In view of the controversy surrounding a number of steps in the lysine catabolism pathway (Biagosch et al., 2017; Crowther et al., 2019; Hallen et al., 2013; Murthy and Janardanasarma, 1999a; Pena, Marques, et al., 2017; Posset et al., 2015; Sauer et al., 2011; Struys and Jakobs, 2010; Wempe et al., 2019), our finding may point to the presence in brain of an alternate route of α-AAA production. Given the uncertainty about the fate of accumulated PIP, we speculate that a novel pathway may exist linking PIP to α-AAA that bypasses the ALDH7A1-catalyzed step.

A similar hypothesis that re-routes PIP to a further downstream metabolite was put forward by Biagosch et al. (2017) in an attempt to explain their unexpected lysine metabolite profile in *Dhtkd1*-/*Gcdh*- double knockout mice. The products of both of these genes, *Dhtkd1* and *Gcdh*, function in the lysine catabolism pathway downstream of the metabolic block in ALDH7A1

deficiency. Of note here, the enzyme that converts α-AAA to its downstream catabolite, 2-aminoadipate aminotransferase, is PLP-dependent (Wilson et al., 2019). Further investigation using isotopic tracing studies in Aldh7a1-KO mice may help decipher the origin of accumulating α-AAA in brain.

Comparison of the pattern of lysine metabolites in adult versus P0 KO mice and in brain versus liver revealed a few noteworthy trends. First, P6C was present in higher concentration in adult compared to neonatal brain (Fig. 3-6). This may be attributable to less flux through the lysine catabolism pathway during the early neonatal period when active brain development requires the synthesis of more lysine and less is subject to catabolism (Coughlin et al., 2015). Interestingly, analyzing the adult data with ages broken down by specific timepoints reveals a trend of escalating concentrations of cerebral P6C with age (Fig. 3-6). This could indicate that the level of this pathogenic molecule builds up with age, although this cannot be confirmed based on the current data only.

A contrary trend to P6C was observed for PIP, which was markedly higher in neonatal than in adult brain (Fig. 3-6). PIP reaches its peak concentration during the perinatal period in the developing mouse brain and then subsides gradually after birth, reaching its lowest levels in adulthood (Kim and Giacobini, 1985). This correlates with the observation that synthesis of PIP from the lysine catabolism pathway in mouse brain occurs at a faster rate around the time of birth (Hallen et al., 2013).

PIP accumulated in higher concentrations in brain compared to liver in P0 mice, while SAC exhibited an opposite trend (Fig. 3-7). These trends could be a reflection of the differential activity across the two lysine catabolic pathways between the two organs during the perinatal period. For

example, it was shown that in developing rat brain activity of the pipecolic acid pathway is 2-fold higher than in liver (Rao et al., 1993).

In ALDH7A1 deficiency, accumulating P6C is thought to undergo a spontaneous Knoevenagel complexation with intracellular PLP, forming an inactive adduct and thus leading to reduced PLP availability (Mills et al., 2006) (Fig. 3-1). Data on PLP levels in individuals affected with PDE-ALDH7A1 are sparse. Some patients showed reduced concentrations of PLP in CSF (Footitt et al., 2011; Mills et al., 2010; Pérez et al., 2013), plasma (Footitt et al., 2013; Pérez et al., 2013) or frontal cortex of post-mortem brain (Lott et al., 1978), while a normal B6 vitamer profile has been reported in other patients (Coughlin et al., 2015; Footitt et al., 2013; Goto et al., 2001; Mathis et al., 2016; Pérez et al., 2013). Similar inconsistency in PLP profiles has been noted in other vitB6-dependent epilepsies like PNPO deficiency (Levtova et al., 2015; Ormazabal et al., 2008) and PLPHP deficiency (Darin et al., 2016; Johnstone et al., 2019). *aldh7a1*-null zebrafish (Pena, Roussel, et al., 2017) had only marginally lower PLP despite an overt clinical and biochemical phenotype.

In the current investigation, we measured PLP in homogenized whole brain, liver tissue and plasma of 11 KO mice (3 neonatal and 8 adult) and matched cohorts of WT mice. In brain, only 4 out of the 11 KO mice had PLP concentrations that were clearly below the concentration range of their WT counterparts (Fig. 3-6). The mean PLP concentration in both age groups did not significantly differ between KOs and WTs.

Analysis of Aldh7a1-deficient mice uncovered several amino acid perturbations (Fig. 3-10 and 11). Table 3-2 provides a literature review of the previously reported similar amino acid abnormalities in related human diseases and in animal and cellular models. As shown in the table, the majority of amino acid changes we observed have been also described in patients with PDE-

ALDH7A1 and/or other vitB6-dependent epilepsies. A discrepancy is noted in the glycine profile, which was decreased in the brain of Aldh7a1-deficient mice compared to raised levels in CSF of PDE-ALDH7A1 (Mills et al., 2010) as well as PNPO deficiency patients (Hoffmann et al., 2007). In concordance with the Aldh7a1-deficient mice, low glycine was reported in vitB6-deprived Neuro-2a cells (Ramos et al., 2017). The table also provides a list of the PLP-dependent enzyme(s) with catalytic functions in the metabolic pathways for each altered amino acid. Pena, Roussel, et al. (2017) reported significant changes in *aldh7a1*-KO zebrafish that encompassed 8 amino acids; four of them (serine, alanine, citrulline and tyrosine) overlap with the profile of our Aldh7a1-deficient mouse model.

Neurotransmitter analysis in Aldh7a1-deficient mice was remarkable for elevated norepinephrine and its metabolite, normetanephrine, in plasma (Fig. 3-14). To our knowledge, neither compound has previously been evaluated in PDE-ALDH7A1 patients. In animal models, high plasma norepinephrine was observed in pyridoxine-deficient rats (Paulose et al., 1988). The possible pathophysiological mechanism underlying the high concentration of this catecholamine in the current model remains unclear.

Analysis of remaining neurotransmitters and metabolites of biogenic amines in homogenized whole brain did not reveal any notable trends (Fig. 3-13 and 3-15). It is possible that these neurotransmitters are affected by local changes that can only be detected by comparing regional levels as opposed to whole brain analysis.

Table 3-2: Summary of amino acid changes in *Aldh7a1*-KO mice, relevant PLP-dependent enzymes and previous reports of amino acid changes in related human diseases and animal/cellular models.

Amino acid abnormalities in Aldh7a1-KO mice		**PLP-dependent enzymes in amino acid metabolic pathways***	**Enzyme's function***	**Previously reported abnormalities for the same amino acid in related diseases and models** (tissue/fluid, change)
Amino acid	**Affected tissue** (change)			
Glycine	Brain (↓)	• Serine hydroxymethyltransferase (EC 2.1.2.1)	Catalyzes the first step in the glycine biosynthetic pathway from serine	• ALDH7A1 deficiency patients (CSF, ↑) *(Mills et al. 2010)* • PNPO deficiency patients (CSF, ↑) *(Hoffmann et al. 2007)* • vitB6-deprived Neuro-2a cells (Neuro-2a cell line, ↓) *(Ramos et al. 2017)* • vitB6-restricted HepG2 cells (HepG2 cell line, ↑) *(da Silva et al., 2014)*
		• Glycine C-acetyltransferase (EC 2.3.1.29)	Catalyzes the second step in the glycine biosynthetic pathway from threonine	
Ornithine	Brain & liver (↑)	• Ornithine δ-aminotransferase (EC 2.6.1.13) • Ornithine decarboxylase (EC 4.1.1.17)	Involved in breakdown/ conversion of ornithine to other metabolites	• PNPO deficiency patients (CSF & plasma, ↑) *(Mills et al., 2005; Ruiz et al., 2008)*
Serine	Liver (↑)	• Serine dehydratase (EC 4.3.1.17) • Serine hydroxymethyltransferase (EC 2.1.2.1) *(Bender, 2012)*	Involved in breakdown/ conversion of serine to other metabolites	• ALDH7A1 deficiency patient (plasma, ↑) *(Mills et al. 2010)* • PNPO deficiency patients (CSF, ↑) *(Hoffmann et al. 2007)* • *aldh71a*-KO zebrafish (whole body, ↑) *(Pena, Roussel, et al., 2017)* • vitB6-deprived Neuro-2a cells (Neuro-2a cell line, ↓) *(Ramos et al. 2017)* • nutritionally pyridoxine-deficient rats (brain, ↓) *(Plecko et al., 2005; Tews, 1969)*
Proline	Liver (↑)	None that is directly involved in proline catabolism	Not applicable	• ALDH7A1 deficiency patients (plasma, ↑) *(Mills et al. 2010)* • PLPHP deficiency patient (CSF & plasma, ↑) *(Darin et al., 2016; Plecko et al., 2017)*

Alanine	Liver (↑)	• Alanine-glyoxylate aminotransferase (EC 2.6.1.44) • Alanine transaminase (EC 2.6.1.2)	Involved in breakdown/ conversion of alanine to other metabolites	• ALDH7A1 deficiency patients (CSF & plasma, ↑) *(Mills et al. 2010)* • PLPHP deficiency patients (CSF & plasma, ↑) *(Plecko et al. 2017; Johnstone et al. 2019)* • nutritionally pyridoxine-deficient rats (brain, ↓) *(Plecko et al. 2005; Tews, 1969)*
Citrulline	Liver (↑)	None that is directly involved in citrulline catabolism	Not applicable	• ALDH7A1 deficiency patient (plasma, ↓) *(Mills et al. 2010)* • *aldh71a*-KO zebrafish (whole body, ↑) *(Pena, Roussel, et al., 2017)*
Leucine	Liver (↑)	• Branched-chain amino acid aminotransferase (EC 2.6.1.42)	catalyzes the first step in leucine degradation	• PLPHP deficiency patient (CSF, ↑) (*Plecko et al. 2017)*
Isoleucine	Liver (↑)	• Branched-chain amino acid aminotransferase (EC 2.6.1.42)	catalyzes the first step in isoleucine degradation	• PLPHP deficiency patient (CSF, ↑) *(Plecko et al. 2017)*
Tyrosine	Liver (↑)	• Tyrosine aminotransferase (EC 2.6.1.5)	Catalyzes the first and rate-limiting step in tyrosine degradation[4]	• PNPO deficiency patients (plasma, ↑) *(Ruiz et al. 2008)* • PLPHP deficiency patient (CSF, ↑) *(Plecko et al. 2017)* • *aldh71a*-KO zebrafish (whole body, ↑) *(Pena, Roussel, et al., 2017)*
		• Aromatic L-amino acid decarboxylase (EC 4.1.1.28)	Catalyzes the conversion of tyrosine to tyramine	
Phenylalanine	Liver (↑)	• Aromatic L-amino acid decarboxylase (EC 4.1.1.28)	Converts phenylalanine to phenethylamine	• ALDH7A1 deficiency patients (CSF, ↑) *(Mills et al. 2010)*
Histidine	Liver (↑)	• Histidine decarboxylase (EC 4.1.1.22)	Converts histidine to histamine	• ALDH7A1 deficiency patient (CSF, ↑) *(Mills et al. 2010)* • PNPO deficiency patients (CSF, ↑) *(Hoffmann et al. 2007; Mills et al. 2005)*
Tryptophan	Liver (↑)	• Kynureninase (EC 3.7.1.3) • Kynurenine aminotransferase (EC 2.6.1.7)	Catalyze intermediate steps in the degradative pathway of tryptophan	• PLPHP deficiency patient (CSF, ↑) *(Johnstone et al. 2019)*

*****Unless another source is specified, information on PLP-dependent enzymes and their catalytic activities were collectively retrieved from the review of Wilson et al. (2018), KEGG Pathway database and Bender (2012).

Neurotransmitter analysis in human patients with PDE-ALDH7A1 has shown inconsistent results. GABA was found to be reduced in post-mortem frontal and occipital cortices in one patient (Lott et al., 1978) but normal to moderately elevated in CSF in another case (Goto et al., 2001). Similar variable profiles were documented for glutamic acid (Goto et al., 2001; Mills et al., 2010) and metabolites of biogenic amine neurotransmitters like homovanillic acid (Pérez et al., 2013) and O-methyldopa (Mills et al., 2010; Pérez et al., 2013; Scharer et al., 2010). Data from other animal models were also discordant. For example, low GABA levels were noted in *aldh7a1*-KO zebrafish (Pena, Roussel, et al., 2017) while the concentration of this inhibitory neurotransmitter in the brain of pyridoxine-deficient rats did not significantly differ from control animals despite the presence of seizures (Plecko et al., 2005).

In addition to its role in the lysine degradation pathway, ALDH7A1 might be also involved in as yet unknown functions within the CNS. For example, a newly discovered cellular function of ALDH7A1 is protection from toxic aldehydes derived from oxidative stress and lipid peroxidation processes (Brocker et al., 2011). These reactive species have not been quantified in body tissues of human patients with ALDH7A deficiency, but we quantified the levels of methionine sulfoxide, a known and potential biomarker of oxidative stress *in vivo* (Mashima et al., 2003; Suzuki et al., 2016), in our mouse model. Methionine sulfoxide is formed when reactive oxygen species (ROS) oxidize the amino acid methionine, a molecule that exhibits high susceptibility to spontaneous oxidation by oxidants like ROS (Suzuki et al., 2016). Therefore, methionine sulfoxide, the oxidation product of methionine, can serve as a marker of cellular oxidative stress. Quantification data revealed that *Aldh7a1* KO mice accumulated excessive levels of methionine sulfoxide in their brain tissue (Fig. 3-9), indicative of increased intracellular ROS content. Interestingly, HET mice had also high cerebral levels of this biomarker, which may

indicate an indispensable role of ALDH7A1 in cellular detoxification such that even loss of one copy of the gene can reduce cellular detoxification of ROS.

The data presented here shed light on possible new pathobiochemical mechanisms in ALDH7A1 deficiency. First, in addition to the previously known metabolites (P6C, α-AASA and PIP), we found accumulation of two other lysine catabolites, SAC and α-AAA. Both of these compounds have been reported to cause detrimental cellular effects at high concentrations. In a recent *Aass*-KO mouse model (Zhou et al., 2019), accumulation of SAC was found to induce fatal mitochondrial damage in hepatocytes and consequent growth retardation and death in KO mice. In the current study, this mitochondrial toxin (Leandro & Houten, 2019) was detected in concentrations up to 570 nmol/g in liver tissue of neonatal *Aldh7a1*-KO mice. The levels of SAC in adult KO mice were not measured but concentrations would be expected to be even higher because the saccharopine pathway becomes several times more active in adult liver compared to the neonatal period (Rao et al., 1992).

α-AAA, a structural analogue of glutamate, has been shown to cause glial cell toxicity at high concentrations (Brown & Kretzschma, 1998; Huck et al., 1984; Khurgel et al., 1996). ALDH7A1 has been found to be predominantly expressed in glial cells in human brain and, based on a post-mortem study of PDE-affected brain, glial dysfunction appears to underlie some of the neuropathological abnormalities that occur in PDE-ALDH7A1 (Jansen et al., 2014). In light of these findings, we suggest that the mechanism of neurotoxicity in PDE-ALDH7A1 may involve accumulation of these cytotoxic compounds and reactive aldehyde and oxygen species.

In fact, even metabolic derangements seen in PDE-ALDH7A1 seem be more complex than can be explained by PLP insufficiency alone (Hallen et al., 2013). For example, in the current model, there was widely deranged amino acid metabolism despite the lack of a consistently low

PLP profile in KO mice. Given the subcellular localization of ALDH7A1 to mitochondria (Wong et al., 2010), it has been hypothesized that mitochondrial dysfunction due to increased oxidative stress may play a role in PDE-ALDH7A1 pathogenesis (Pérez et al., 2013).

Despite the remarkable biochemical phenotype, Aldh7a1-deficient mice fed a standard laboratory diet did not show any epileptic, behavioural or neuropathological phenotype detectable by the methods and analyses performed in this study. To exclude strain-specific effects, and given that the B6 strain on which our model was based is known to be relatively seizure-resistant (Engstrom and Woodbury, 1988; Ferraro et al., 1995, 2002; Kosobud and Crabbe, 1990), we crossed the *Aldh7a1*-null allele onto a 129 S1/SvImJ background which has an intermediate susceptibility to seizures (Ferraro et al., 2002; Frankel et al., 2001). However, *in vivo* EEG performed in KO mice from this strain fed a standard laboratory diet also showed no evidence of epileptic seizures.

In as much as the clinical symptoms of PDE-ALDH7A1 are believed to be mainly caused by accumulation of lysine catabolites, we suggest that the amount of lysine in regular mouse chow (0.9%), and hence the levels of its catabolic byproducts that occur in Aldh7a1-deficient mice, are insufficient to drive an overt clinical phenotype. Human and mice may also differ in their tolerance of these metabolites. We therefore hypothesized that increasing the amount of dietary lysine would induce a clinical phenotype in Aldh7a1-deficient mice, and experiments to test this hypothesis are described in Chapter 4.

In summary, the present report describes the first biochemical data on mice with constitutive genetic ablation of *Aldh7a1*. The data showed a metabolite signature consistent with blockade of the lysine catabolism pathway along with widely deranged amino acid metabolism that is similar to the biochemical picture seen in ALDH7A1-deficient patients. This study provides

the first insight regarding the metabolite profile of an extra-cerebral tissue in Aldh7a1-deficient mammals and broadens our knowledge about the spectrum of biochemical abnormalities that may be associated with ALDH7A1 deficiency. These data also provide a proof-of-concept for the utility of the model to study PDE-ALDH7A1 biochemistry and to test new therapeutics that aim to abolish the accumulation of lysine metabolites.

4 A diet-induced model for pyridoxine-dependent epilepsy

4.1 Introduction

Lysine is an essential amino acid which is degraded in mammalian brain by two distinct pathways, the saccharopine pathway and the pipecolic acid pathway. The two pathways subsequently converge at the step of non-enzymatic interconversion between Δ^1-piperideine-6-carboxylic acid (P6C) and α-aminoadipic semialdehyde (α-AASA) and later form a common catabolic pathway (Hallen et al., 2013) (Fig. 4-1).

In addition to pyridoxine-dependent epilepsy due to ALDH7A1 deficiency (PDE-ALDH7A1), there are another 6 known inborn errors of metabolism that result from defects within the lysine catabolism pathways (Fig. 4-1). These diseases have variable degrees of severity and clinical presentations but, like PDE-ALDH7A1, they are mostly associated with neurological symptoms thought to be caused by pathological accumulation of lysine intermediate metabolites surrounding the metabolic block (Hoffmann & Kölker, 2012). One of the most well-characterized disorders of lysine catabolism is glutaric aciduria type 1 (GA-1). GA-1 is caused by inherited deficiency of the lysine catabolic enzyme glutaryl-CoA dehydrogenase (GCDH). It is clinically manifested by neuromotor deficits like dystonia and brain defects. Biochemically, GCDH deficiency leads to accumulation of secondary metabolites like glutaric acid (GA), 3-hydroxyglutaric acid (3-OH-GA), and glutarylcarnitine (C5DC) (Fig. 4-1) (Barić et al., 1998; Kölker et al., 2011).

Gcdh-knockout (KO) mice fed regular chow showed elevation of these metabolites in a manner consistent with the biochemical picture of GA-1 patients. However, the mice exhibited only a mild clinical phenotype and failed to recapitulate many of the clinical aspects of GA-1 in

humans (Koeller et al., 2002). In a subsequent study (Zinnanti et al., 2006), *Gcdh*-KO mice were fed a high (4.7%) lysine diet, which led to severe clinical phenotype, including a specific striatal injury similar to GA-1 patients, followed by death. This study provided a proof-of-concept that high lysine intake can aggravate the symptoms of lysine catabolic defects in which the main pathology is driven by accumulation of intermediate catabolites.

We have generated mice with constitutive deletion of *Aldh7a1* to create a model for PDE-ALDH7A1. Phenotypic characterization of *Aldh7a1*-KO mice fed a regular 0.9% lysine diet revealed a remarkable biochemical phenotype that closely resembled the patients' picture. This included accumulation of upstream lysine metabolites, P6C, α-AASA and pipecolic acid (PIP), in brain and liver tissues and extensive amino acid perturbations. The mice, however, had no apparent epileptic, behavioural or neuropathological abnormalities.

Learning from the successful story of dietary manipulation in the GA-1 mouse model, we undertook a study in which *Aldh7a1*-KO mice were placed on special diets with modified lysine and/or pyridoxine (PN) contents. We here report the results of seizure and survival analysis of *Aldh7a1*-KO mice fed these modified diets.

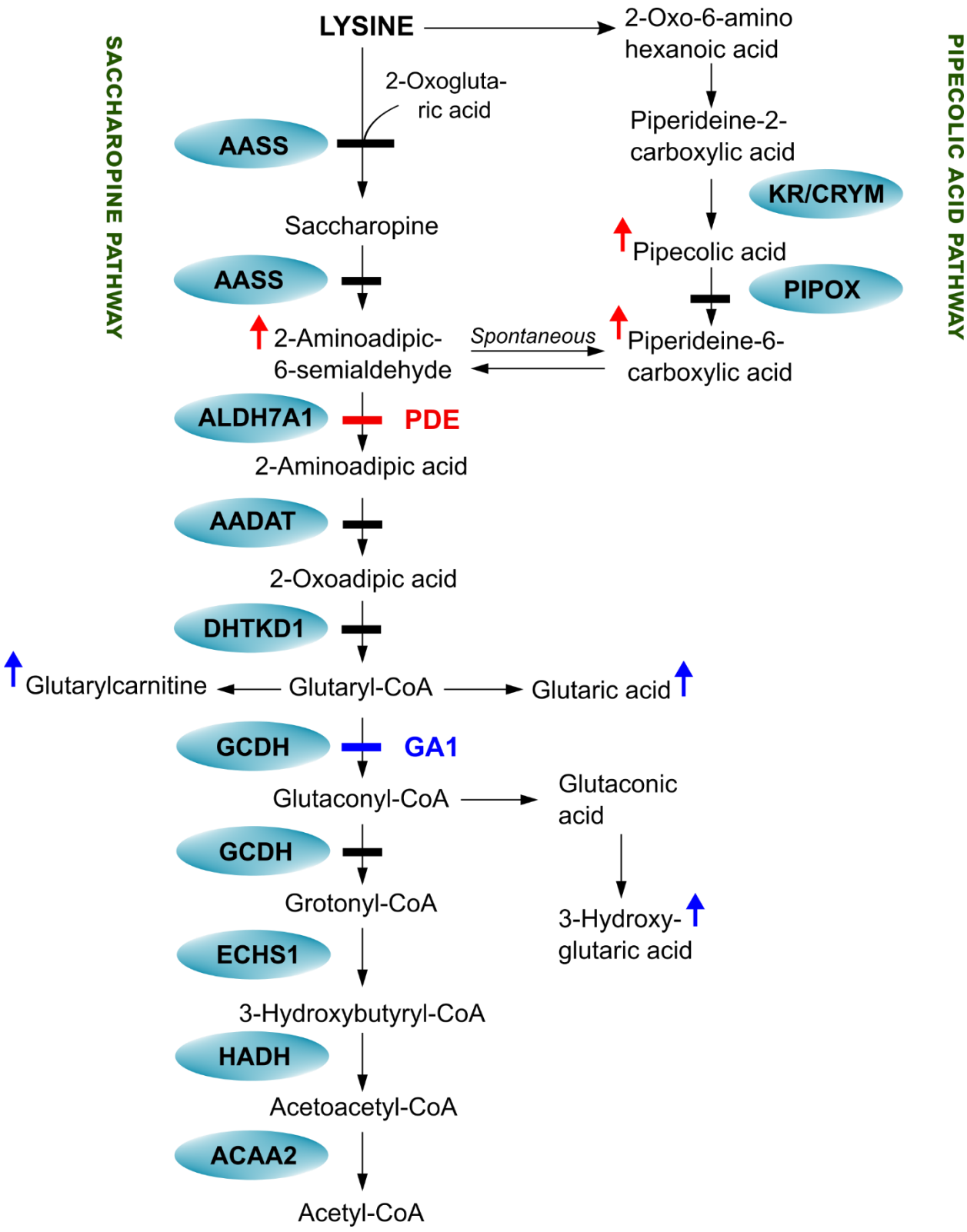
SACCHAROPINE PATHWAY
PIPECOLIC ACID PATHWAY
LYSINE
2-Oxo-6-amino hexanoic acid
2-Oxogluta-ric acid
AASS
Piperideine-2-carboxylic acid
KR/CRYM
Saccharopine
Pipecolic acid
AASS
PIPOX
2-Aminoadipic-6-semialdehyde
Spontaneous
Piperideine-6-carboxylic acid
ALDH7A1
PDE
2-Aminoadipic acid
AADAT
2-Oxoadipic acid
DHTKD1
Glutarylcarnitine
Glutaryl-CoA
Glutaric acid
GCDH
GA1
Glutaconyl-CoA
Glutaconic acid
GCDH
Grotonyl-CoA
3-Hydroxy-glutaric acid
ECHS1
3-Hydroxybutyryl-CoA
HADH
Acetoacetyl-CoA
ACAA2
Acetyl-CoA

Fig. 4-1: Lysine catabolism pathways in brain and associated neurometabolic diseases. Saccharopine (left) and pipecolic acid (right) catabolic pathways proceed as two distinct routes but later converge at the P6C/α-AASA synthesis step into a common pathway. Solid bars along the arrows indicate enzyme deficiencies known to cause inborn errors of metabolism in humans. Upward colored arrows denote lysine metabolites elevated in PDE-ALDH7A1 or GA-1. *Abbreviations:* AASS: Aminoadipic semialdehyde synthase; ALDH7A1: Aldehyde dehydrogenase 7 family, member A1 (antiquitin); AADAT: 2-aminoadipate aminotransferase; KR: Ketimine reductase; CRYM: Mu-crystallin homolog; PIPOX: Pipecolic acid oxidase; DHTKD1: Dehydrogenase E1 and transketolase domain containing 1; GCDH: Glutaryl-CoA dehydrogenase; ECHS1: Enoyl Coenzyme A hydratase short chain 1; HADH: Hydroxyacyl-Coenzyme A dehydrogenase; ACAA2: Acetyl-Coenzyme A acyltransferase 2. (based on Hoffmann & Kölker (2012); (Houten et al. (2013); Pena et al. (2017)).

4.2 Materials and methods

4.2.1 Mice

Constitutive *Aldh7a1*-KO mice on the C57BL/6J inbred strain and incipient congenic 129 S1/SvImJ (B6;129) strain were generated as described in Chapter 3. All mice were fed a regular diet (Envigo 2018 Teklad Global 18% protein Rodent Diet) since weaning before being placed on the special diets used in this study. Experiments described here were performed in accordance with guidelines of the Canadian Council on Animal Care and approved protocol by the University of British Columbia Animal Care Committee (Animal Protocol # A15-0200).

4.2.2 Dietary modifications

To validate the effect of dietary lysine and pyridoxine (PN) in inducing a clinical phenotype in KO mice, we designed two types of special diets that vary in their lysine and/or PN contents (Table 4-1). Special Diet 1 (SD1) contained high lysine and minimal PN levels (in adult mice, PN at 1 ppm in diet is adequate for growth and maintenance [National Research Council, 1995]). SD1 was intended to induce an epileptic phenotype in KO mice. Special Diet 2 (SD2) contained high lysine and higher PN levels and was used along with PN injections to test the effect of PN in suppressing seizures induced by high lysine. All special diets were manufactured by Envigo (USA).

Table 4-1: Lysine and PN composition of modified diets in comparison to regular diet.

Diet ID	**Lysine level** (%)	**PN level** (ppm)	**Catalogue No.**
Special Diet 1 (SD1)	4.7	1.6	TD.180908
Special Diet 2 (SD2)	4.7	11.5	TD.180907
Regular Diet	0.9	18	2018

4.2.2.1 Pilot dietary induction trial

Special diets were tested on mice in two stages; a pilot trial with small number of animals and then a follow-up trial with larger cohort of mice. All mice used in the pilot trial were originally maintained on the regular diet, underwent surgical EEG implantation and baseline EEG recording, and were then switched to special diets followed by post-diet EEG recording. The EEG implantation and recording procedure as well as the results of baseline EEG analysis in KO mice were detailed in Chapter 3.

In the pilot trial, mice were divided into two groups. The first group received SD1 without any other treatment. The second group were fed SD2 and the KOs further received daily PN-HCl injections i.p. at a dose of 200 µg/g of body weight starting from day 2 and cutting down to 100 µg/g on day 6 of the trial. Similar dose of PN-HCl (200 µg/g i.p.) was previously shown to cause no adverse effects in wildtype (WT) mice (Eifel et al., 1983). Each group comprised 2 KO and 2 WT mice, one from each background strain. Age of animals was 12 months for the B6 mice and 3 months for the B6;129 mice. Mice were monitored and their diet consumption was recorded regularly. Table 4-2 shows number of hours of continuous EEG recording that were collected from each mouse throughout the trial. The pilot experiment was terminated on day 8.

Table 4-2: Duration of EEG recordings obtained from each mouse during the pilot trial.

Mouse #	Genotype (Strain)	Diet	Treated/Untreated	Day of start of EEG recording	Duration of continuous EEG recording (hours)
1	KO (B6)	SD1	Untreated	2	16.9*
2	KO (B6;129)	SD1	Untreated	1	46.7
3	KO (B6)	SD2	Treated	3	22.5
4	KO (B6;129)	SD2	Treated	4	31.7
5	WT (B6)	SD1	Untreated	2	46.1
6	WT (B6;129)	SD1	Untreated	1	46.9

* Recording session was terminated due to animal's death.

4.2.2.2 Follow-up dietary induction experiments

In follow-up trials, mice were also divided to two dietary groups. The first group received SD1 without other treatment and included 4 KO and 10 WT mice. The second group received SD2 and were given i.p. injections of 200 µg/g PN-HCl q.o.d starting from day 2. This group included 6 KO mice. Mice were checked on a daily basis and their body weights and diet consumption were recorded. Assessment of seizures in KO mice under SD1 was based on visual inspection and type; severity and duration of seizure events were documented in monitoring sheets and by video recording. All mice used in follow-up trials were non-implanted, from the B6 strain and aged 11 – 14.5 months. All mice were followed until day 10 of the experiment or until euthanized because of seizure activity.

Mice that reached a humane endpoint of seizure severity and frequency were euthanized according to a protocol approved by the University of British Columbia Animal Care and Use Program (Animal Protocol # A15-0200). Seizure severity was graded from 0 – 6 as follows: 0 = no visible signs of seizure, 1 = high-pitched vocalizations, 2 = continuous running in the cage, 3 = tongue biting, 4 = twisting of trunk, ataxic gait, 5 = loss of consciousness in supine position, tonic-clonic extensions, tremors of the limbs, 6 = status epilepticus: any of the above signs sustained for more than three minutes. Based on seizure severity (SS) and frequency, humane endpoints were defined as: SS = 1, 2, 3, or 4 at frequency > 3/hour or > 5/day, SS= 5 at frequency > 2/hour or > 4/day, SS=6 at frequency > 1/hour or > 2/day. The endpoint was also reached in an animal in which a seizure caused self-inflicted trauma or the animal became cyanotic or apneic during an attack.

4.2.3 Statistical analysis

Survival under modified diets was analyzed using the Kaplan-Meier method and statistical difference between curves was tested using Log-rank (Mantel-Cox) test. All statistical analyses

and graphical plotting of data were carried out using GraphPad Prism software. *p* values below 0.05 were considered significant.

4.3 Results

Prior to conduct of the special diet trials, all mice maintained on the regular diet showed complete survival. No seizures were observed on EEG recordings of either WT or KO mice (described in Chapter 3).

4.3.1 Pilot dietary induction trial

Both untreated KO mice fed SD1 died 1.5 – 2 days from the start of the diet due to uncontrolled seizures. EEG recordings from both animals showed extensive seizure activity (Fig. 4-2). Clinical seizures were observed in the B6-KO mouse as early as 23.5 hours post-diet (PD), at which point the mouse had consumed 2.63 g of the diet. Analysis of continuous 17-hours EEG recording from this mouse revealed the presence of recurrent epileptiform discharges. The discharges, which were synchronous in all EEG channels, correlated with abrupt and intense movement changes along the three accelerometer axes, indicative of a convulsive seizure. Typical EEGs during the ictal discharges are shown in Fig. 4-2. The seizure initiated with a burst of fast 13.7 Hz spikes of amplitude 766 µV (Fig. 4-2A iii). The spikes' amplitude escalated with time until reaching about 998 µV at the peak of the episode (Fig. 4-2A iv). Generalized convulsions, lasting 12 – 35 s, were occasionally preceded by a series of single-spike discharges that coincided with brief jumps on the accelerometer axes (Fig. 4-2A i). This pattern of pre-ictal single spikes evolved with time to a distinct electrographic pattern that consisted of bursts of high-voltage polyspikes with intervening periods of attenuated background activity (burst-suppression pattern) (Fig. 4-3). The burst episodes correlated with simultaneous sharp jumps on the accelerometer readout (Fig. 4-3). These burst-suppression seizures, 40 – 186 s in duration, terminated in either a major

generalized convulsion (Fig. 4-8A) or subsided gradually to single spikes before the background de-suppressed to normal baseline amplitude (Fig. 4-8B). Sharp spikes that causes sudden arrest in mouse movement (freezing behaviour) were also repeatedly observed (Fig. 4-4).

In the B6;129 KO mouse, total of 46.9 hours of continuous EEG recording were collected. Analysis showed frequent electroclinical seizure events with the first seizure occurring 31.9 hours PD. Multiple electrographic patterns were noted including focal (Fig. 4-7), generalized (Fig. 4-5) and burst-suppression (Fig. 4-6). Fig. 4-5 shows an example of ictal EEG during generalized seizures in this mouse. Epileptiform discharges seemed to become progressively worse with time; initially emerging as isolated single spikes followed by poly-spikes without a clinical correlate, then focal discharges followed by severe generalized seizures and culminating in burst-suppression status epilepticus.

Burst-suppression was also the dominating terminal seizure pattern in the B6 mouse. Post- and inter-ictal spikes were also frequently observed in both mice (Fig. 4-2 and 4-5) and seizures were occasionally followed by long periods of post-ictal behavioural arrest. Both mice had a prolonged status epilepticus (lasting for up to 29 minutes) in the form of burst-suppression prior to death. The amount of diet each mouse had consumed until death was 2.77 g for the B6 mouse and 2.95 g for the B6;129 mouse. Normal EEGs taken from both of these mice under regular diet are shown in Fig. 3-23 of Chapter 3.

All other mice (WTs and PN-treated KOs) survived to the end of study. Analysis of EEG data collected from two PN-treated KOs fed SD2 (54.25 hours) and two WT fed SD1 (93 hours) showed no epileptic seizures. Reducing PN dose to 100 µg/g q.d. and skipping one dose for 12 hours did not cause any seizures. It was therefore empirically determined that a dose of 200 µg/g given every other day (q.o.d) should be sufficient to prevent seizures. This new PN regimen was

implemented in the follow-up trials described below. Every other day dosage was useful to reduce the frequency of injections and avoid side effects like peritonitis associated with repeated i.p. injections.

4.3.1 Follow-up dietary induction trials

All four KO mice that received SD1 exhibited seizures. Based on visual monitoring, seizure onset in the first 3 mice ranged from 24.25 – 26.5 hours PD while in the 4th mouse the first noted seizure was at 47.2 hours PD. Following the first seizure, KO mice had multiple episodes of status epilepticus lasting for 3 – 13 minutes, reached humane endpoints and were euthanized at 27.4 - 51.3 hours PD.

Several types of seizures were observed, including vocalizations, head jerks, head bobbing and gasping, limb tremors, generalized myoclonic jerks, and continuous running and jumping that terminated in whole body myoclonic jerks. The most severe type was prolonged episodes of continuous running with repetitive jumping and head banging against the cage top or side walls. By looking at the EEG data obtained from similar mice in the pilot experiment, this convulsive behaviour of alternating running and jumping resembled the distinct accelerometer pattern observed during burst-suppression seizures (Fig. 4-3, 4-6 and 4-8). Freezing behaviour was also frequently noted in KO mice in the follow-up study. By the time these mice were euthanized, they had consumed 1.82 – 3.41 g of diet. Table 4-3 compares time and diet consumption at seizure onset and death in all 6 KO mice fed SD1.

No seizures were noted in WT or PN-treated KO mice. One PN-treated KO mouse that received SD2 was excluded from the study because it did not eat the diet. All other mice survived to the end of the study. Their total diet consumption by the end of the study ranged from 8.01 – 16.39 g in PN-treated KO mice and from 15.73 – 21.0 g in WT mice. Follow-up dietary trials were

terminated on day 10. Fig. 4-9 shows a comparison of survival curves between mice under different tested diets and PN treatment ($p<0.0001$).

Table 4-3: Summary of time and amount of diet consumed until first seizure and death or humane endpoint in untreated *Aldh7a1*-KO mice exposed to SD1.

Mouse #	**Strain**	**Latency to first seizure (hours PD)***	**Time to death/HE (hours PD)***	**Diet consumed until first seizure (g)**	**Diet consumed until death/HE (g)**
Pilot trials					
1	B6	23.5	36.5	2.63	2.77
2	B6;129	31.9	45.66	1.67 - 2.69**	2.95
Follow-up trials					
3	B6	47.2	51.3	NM	2.08
4	B6	24.25	47.6	3.0	3.41
5	B6	26.5	36.9	1.61	1.82
6	B6	26.1	27.4	1.95	1.95

*Based on EEG data and spontaneous death in pilot trials and on visual monitoring and humane endpoints in follow-up trials.
**The exact amount at seizure onset is not available. The range here is based on the closest measurements taken before and after the first seizure.
Abbreviations, PD: post-diet; HE: humane endpoint; NM: not measured.

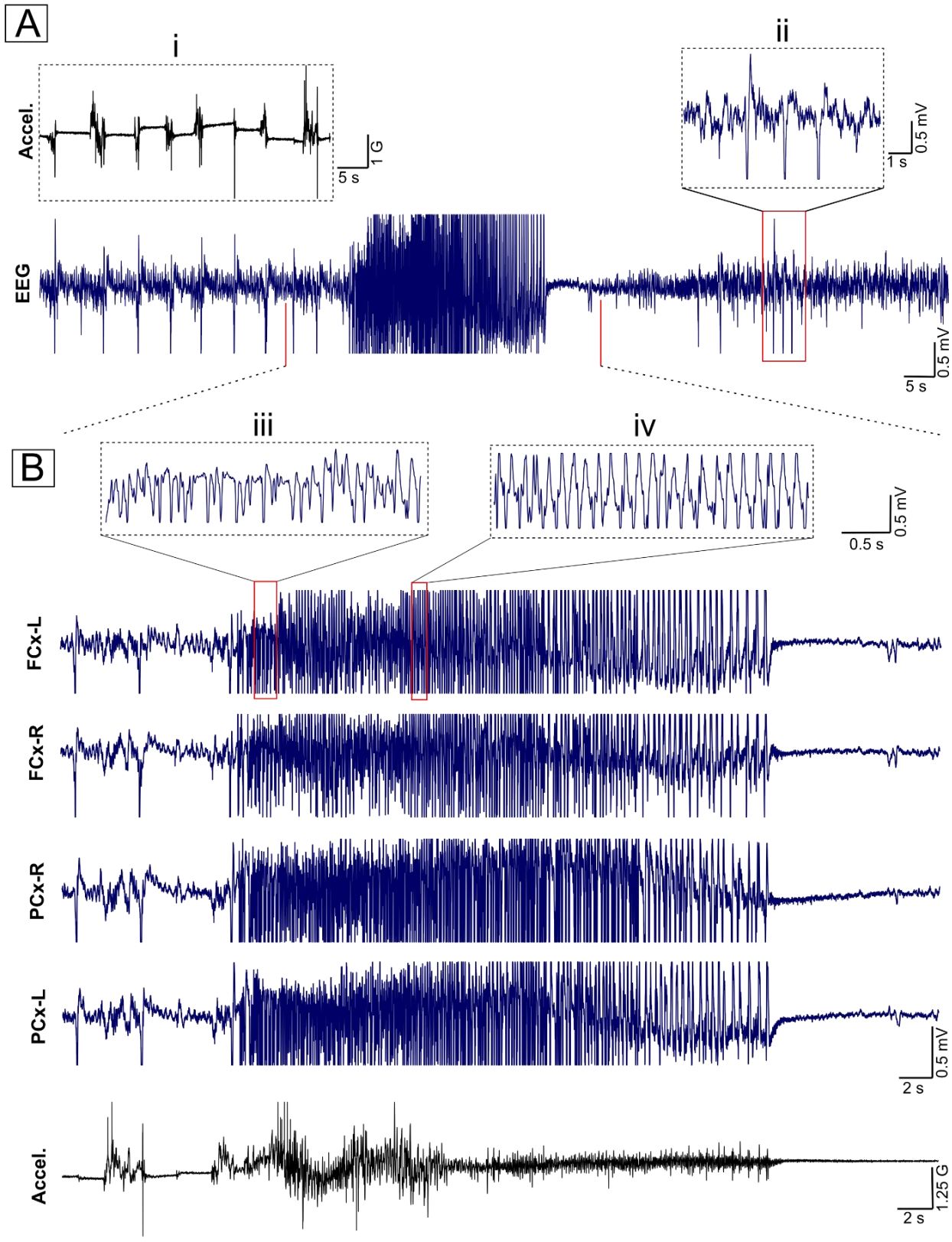
A
i
ii
Accel.
1 G
5 s
0.5 mV
1 s
EEG
0.5 mV
5 s
iii
iv
B
0.5 mV
0.5 s
FCx-L
FCx-R
PCx-R
PCx-L
0.5 mV
2 s
Accel.
1.25 G
2 s

Fig. 4-2: Representative EEG from untreated KO mouse (B6 strain) fed SD1 showing epileptiform discharges. A) condensed view of 150-seconds epoch showing a burst of high-amplitude discharges. B) expanded views of the burst showing synchronous ictal discharges from the 4 EEG channels along with concurrent trace from accelerometer x-axis. The discharges begin and coincide with changes in the accelerometer and become more intense with time and then taper down and flatten towards the end of the episode. C) further expanded views showing waveform morphology of post-ictal spikes (ii) and from the beginning (iii) and middle (iv) of the ictal phase. (i): a snapshot of the accelerometer readout in the pre-ictal phase showing brief alterations that concur with pre-ictal spikes. Abbreviations, FCx-L: left frontal cortex, FCx-R: right frontal cortex, PCx-L: left parietal cortex, PCx-R: right parietal cortex, Accel.: accelerometer, sec: seconds, mV: millivolts, G: acceleration of Earth's gravity (~9.8 m/s^2).

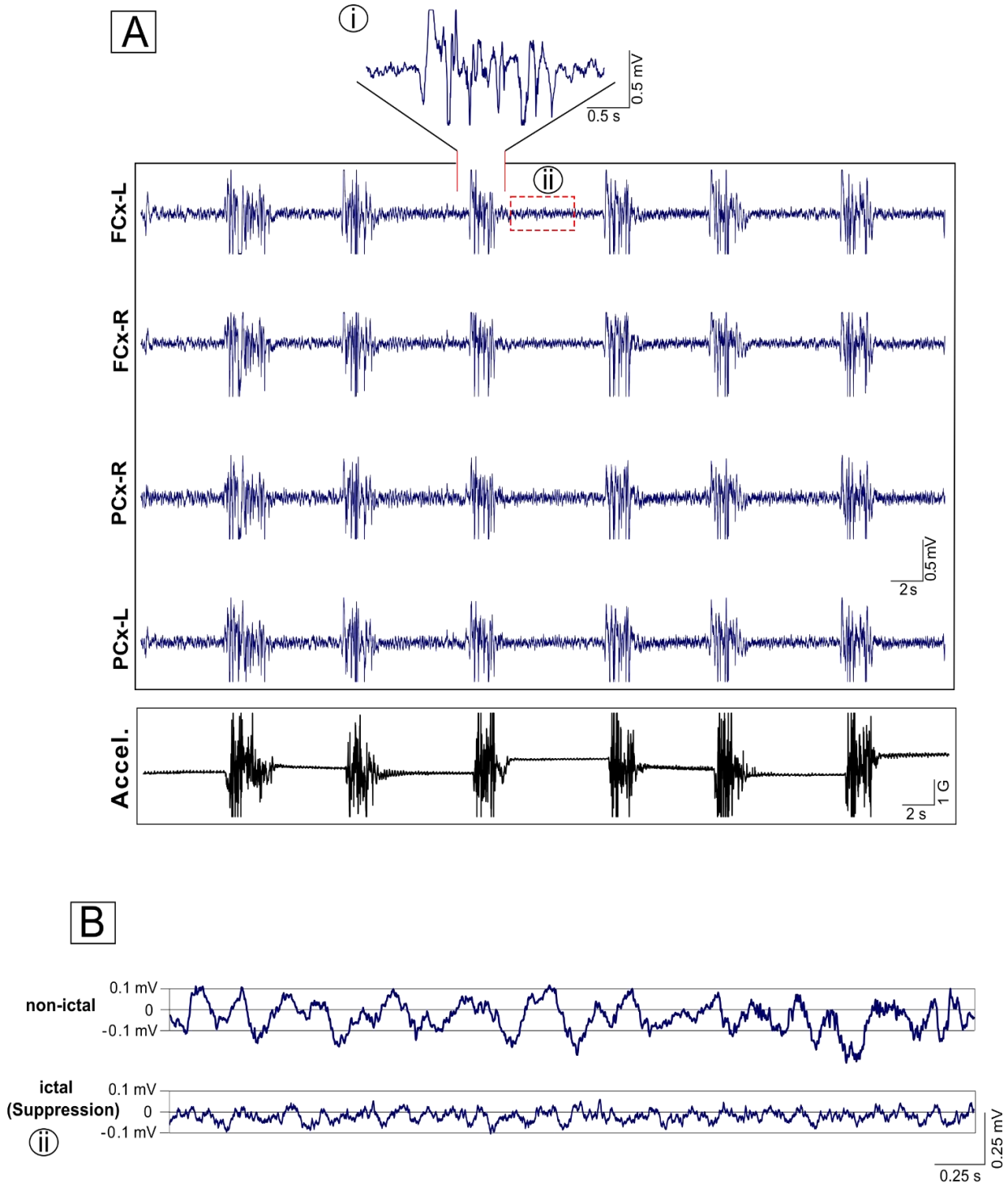
A
i
0.5 mV
0.5 s
ii
FCx-L
FCx-R
PCx-R
PCx-L
0.5mV
2 s
Accel.
1 G
2 s
B
non-ictal
0.1 mV
0
-0.1 mV
ictal
(Suppression)
ii
0.1 mV
0
-0.1 mV
0.25 mV
0.25 s

Fig. 4-3: Burst-suppression seizure in untreated KO mouse (B6 strain) fed SD1. A) 4-channel EEG traces showing bursts of polyspikes [expanded in (i)] alternating with periods of suppressed background. Bursting spikes of mixed frequency (7 – 14 Hz) were up to 998 μV in amplitude and 1.0 – 7.1 sec in duration per episode, while the suppression phase lasted 0.9 – 4.44 sec. Concurrent accelerometer trace shows high-amplitude changes simultaneous with burst episodes on EEG. B) View of the inter-burst segment delineated by a red box at expanded time scale (ii) showing suppressed background compared to normal baseline trace taken form a non-ictal EEG.

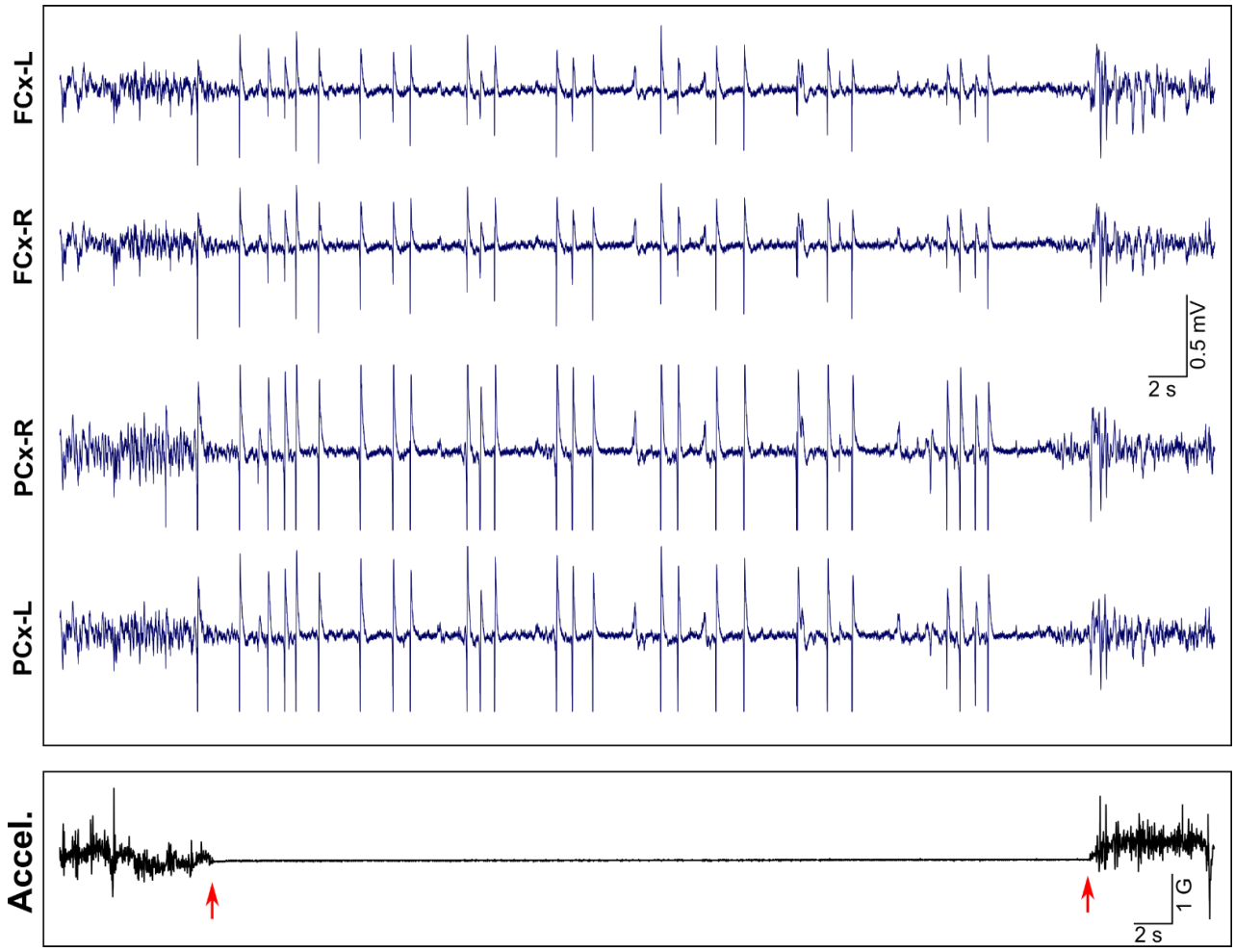

Fig. 4-4: Sharp spike discharges caused freezing behaviour in untreated KO mouse (B6 strain) fed SD1. The advent of these spikes correlates with a sudden immobility in mouse as indicated by the flat line in accelerometer output (red arrows). Notably, isoelectric background activity intervenes between the spikes.

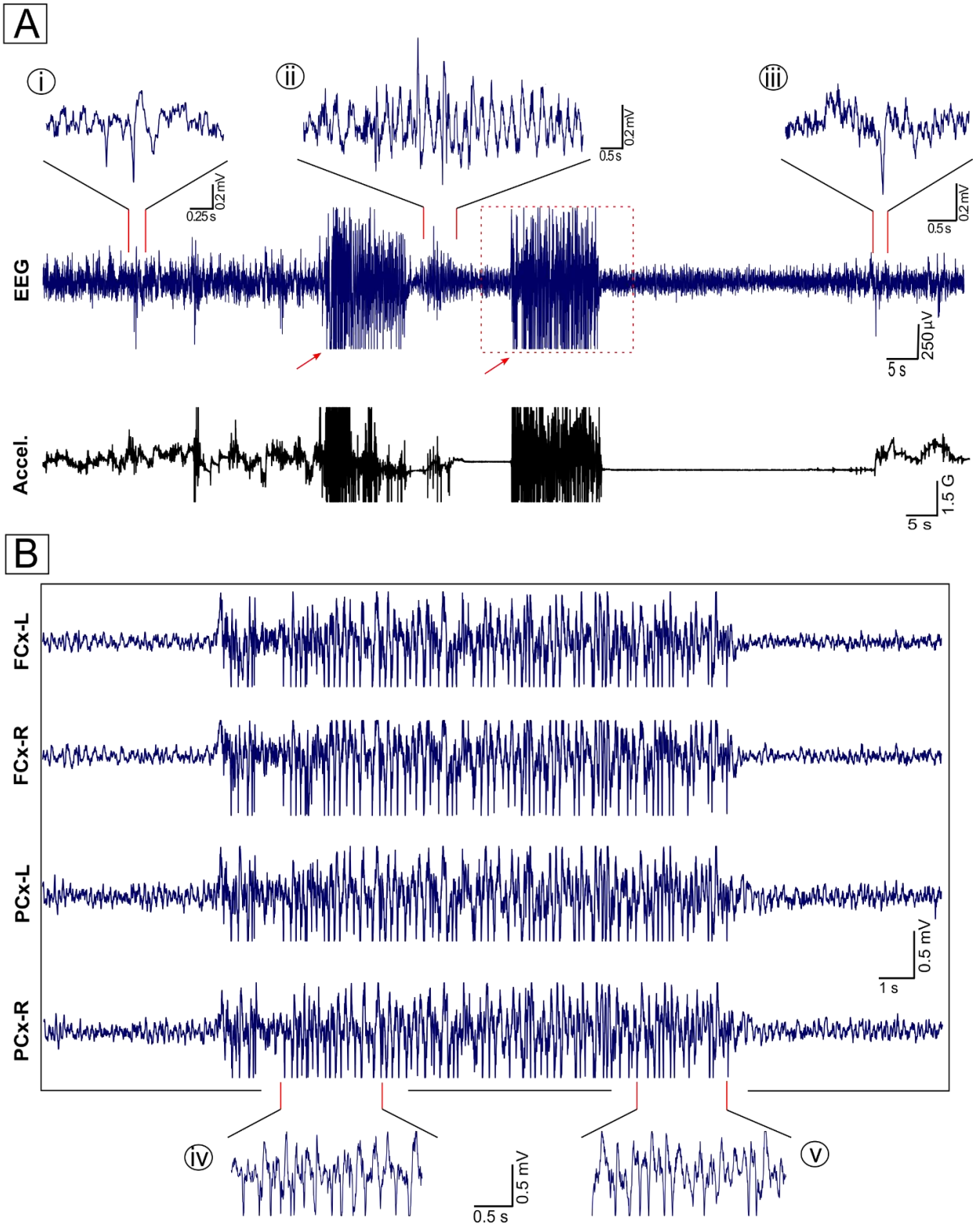
A
i
ii
iii
0.2 mV
0.25 s
0.5 s
0.2 mV
0.5 s
0.2 mV
EEG
250 µV
5 s
Accel.
1.5 G
5 s
B
FCx-L
FCx-R
PCx-L
PCx-R
0.5 mV
1 s
iv
v
0.5 mV
0.5 s

Fig. 4-5: Generalized seizure in the untreated KO mouse (B6;129 strain) fed SD1. A) condensed view of 150-seconds epoch showing two consecutive seizures (indicated by red arrows) with expanded views of the pre-ictal (i), inter-ictal (ii) and post-ictal (iii) spike discharges. B) higher time-resolution view of the burst delineated by dashed red box showing synchronous ictal discharges from the 4 EEG channels along with concurrent trace from accelerometer x-axis. The ictal phase lasts for 14.4. sec and is composed of fast 9 Hz run of spikes of amplitude 714 – 996 μV. (iv) and (v): further expanded views showing waveform morphology at the beginning (iv) and end (v) of the ictal phase.

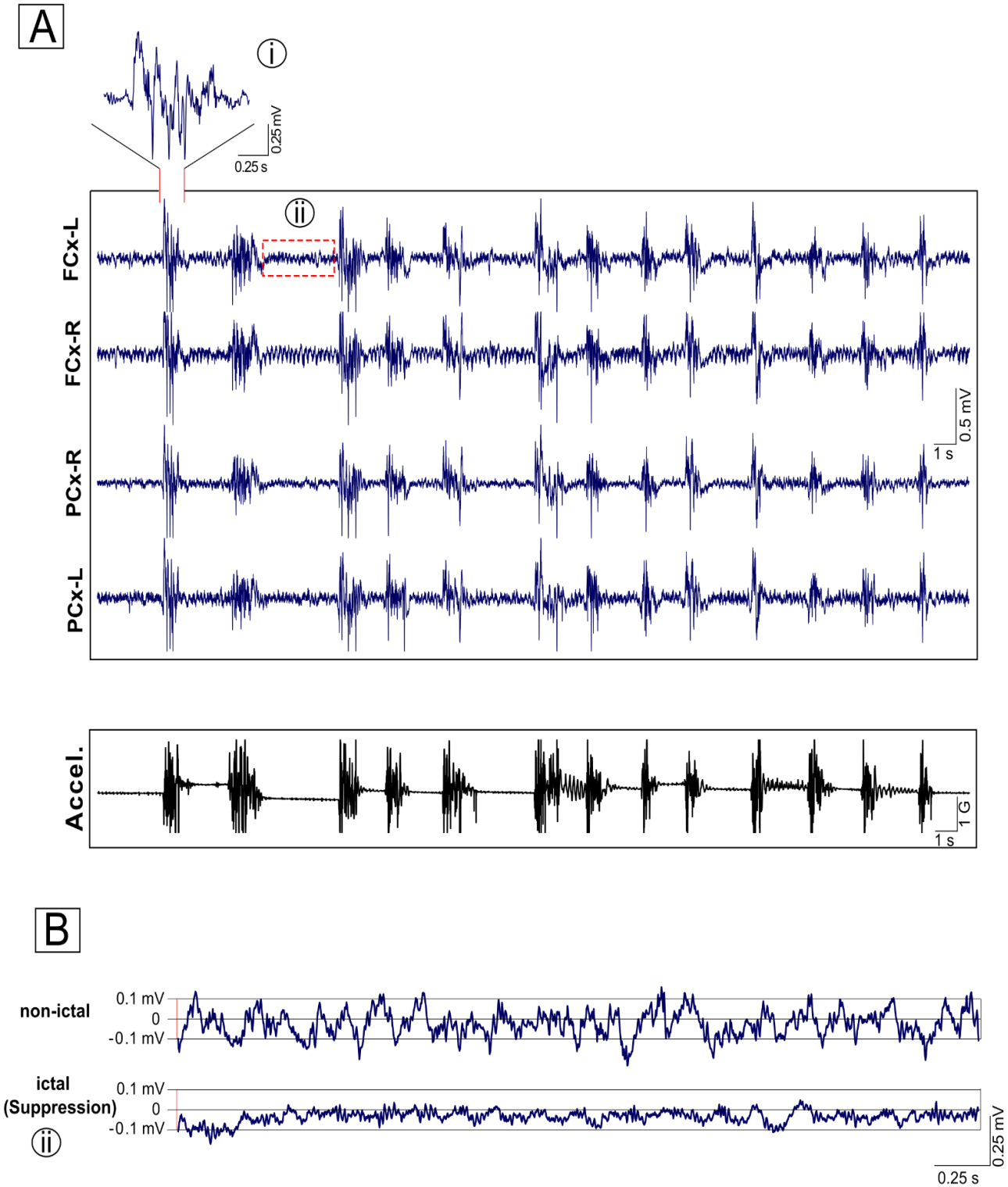
A
i
0.25 mV
0.25 s
ii
FCx-L
FCx-R
PCx-R
PCx-L
0.5 mV
1 s
Accel.
1 G
1 s
B
non-ictal
0.1 mV
0
-0.1 mV
ictal
(Suppression)
ii
0.1 mV
0
-0.1 mV
0.25 mV
0.25 s

Fig. 4-6: Burst-suppression seizure in untreated KO mouse (B6;129 strain) fed SD1. A) 4-channel EEG traces showing bursts of approximately 9 Hz polyspikes [expanded in (i)] alternating with periods of suppressed background. Burst episodes ranged from 609 – 922 μV in amplitude and 0.6 – 2.68 sec in duration while the suppression periods lasted 0.9 – 4.44 sec. Concurrent accelerometer trace shows sharp jumps that correlate with the burst episodes on EEG. B) close-up view of the inter-burst segment delineated by a red box (ii) showing suppressed background compared to normal baseline trace taken form a non-ictal EEG.

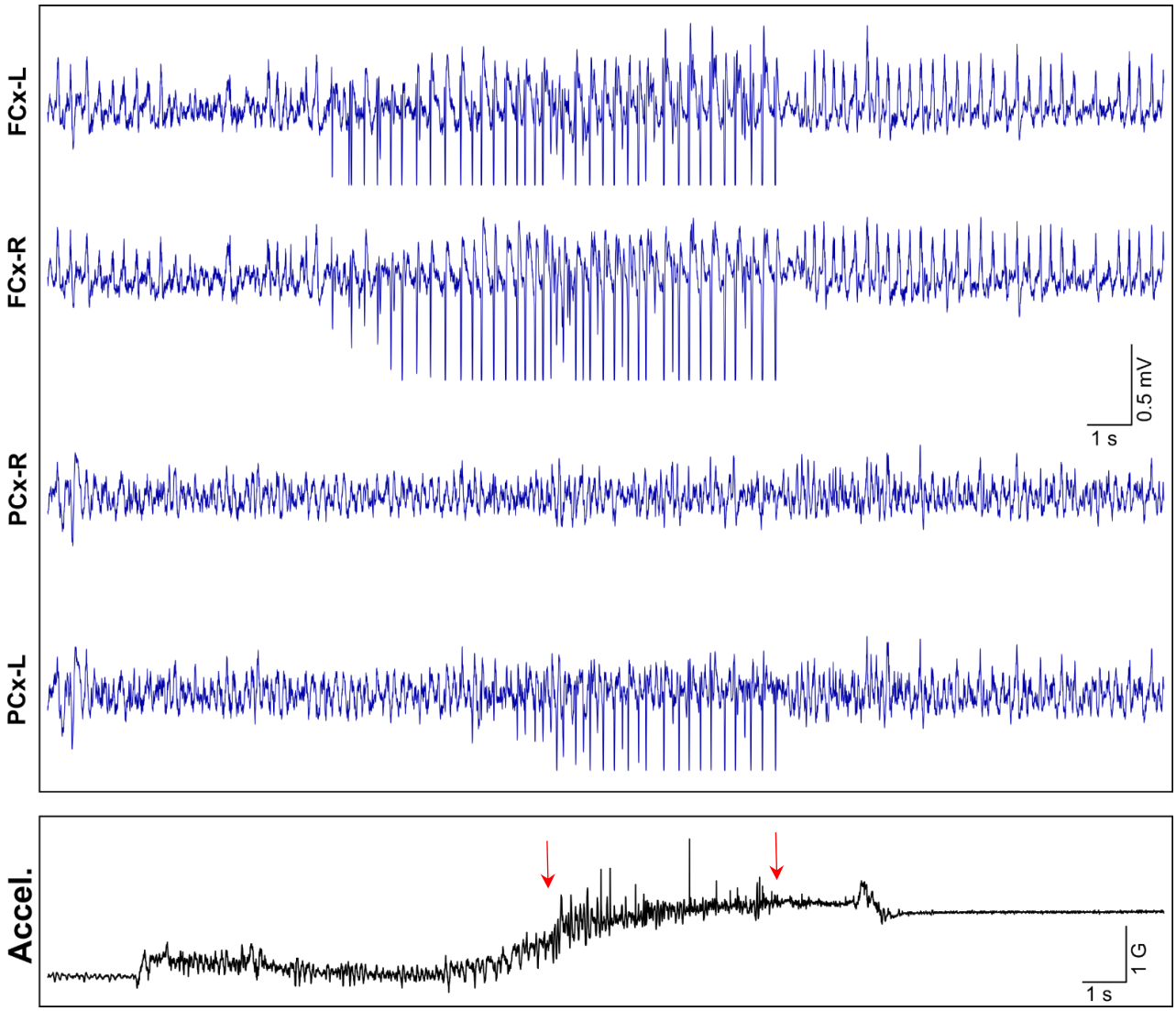

Fig. 4-7: Focal discharges in untreated KO mouse (B6;129 strain) fed SD1. High-amplitude spike discharges affecting mainly frontocortical channels (FCx-L & R). The discharges are absent in the right parietocortical channel (PCx-R) and show delayed onset in the left parietocortical channel (PCx-L). The advent of these dyssynchronous discharges in the PCx-L channel seems to be concomitant with more intense changes in the accelerometer as marked by the red arrows.

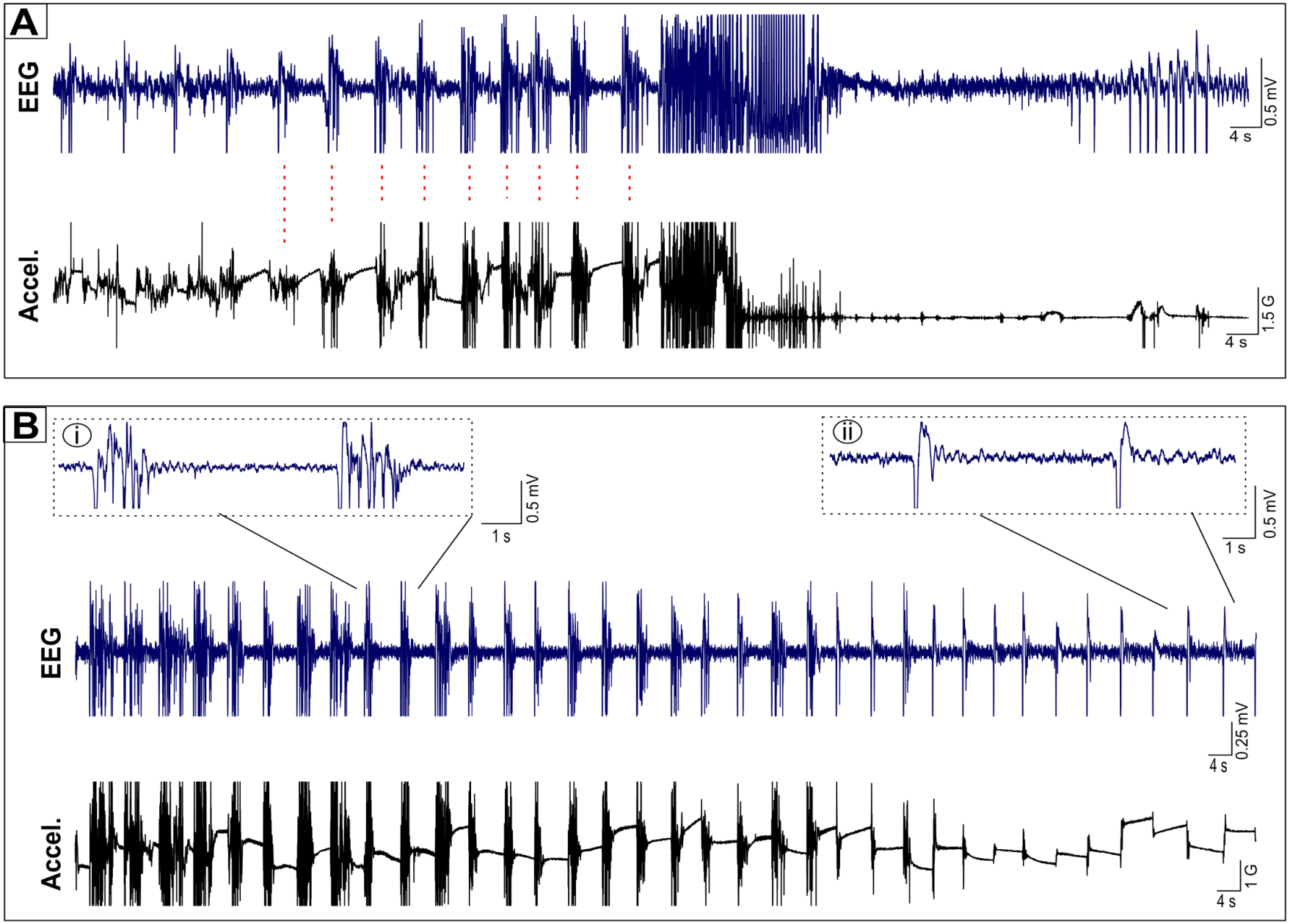
A
EEG
0.5 mV
4 s
Accel.
1.5 G
4 s
B
i
0.5 mV
1 s
ii
0.5 mV
1 s
EEG
0.25 mV
4 s
Accel.
1 G
4 s

Fig. 4-8: Two types of burst-suppression seizure patterns in untreated KO mouse (B6 strain) fed SD1. A) Burst-suppression seizure terminates in a generalized convulsion. B) Burst-suppression seizure gradually tapers down in intensity from polyspikes (i) to single spikes (ii) before it diminishes.

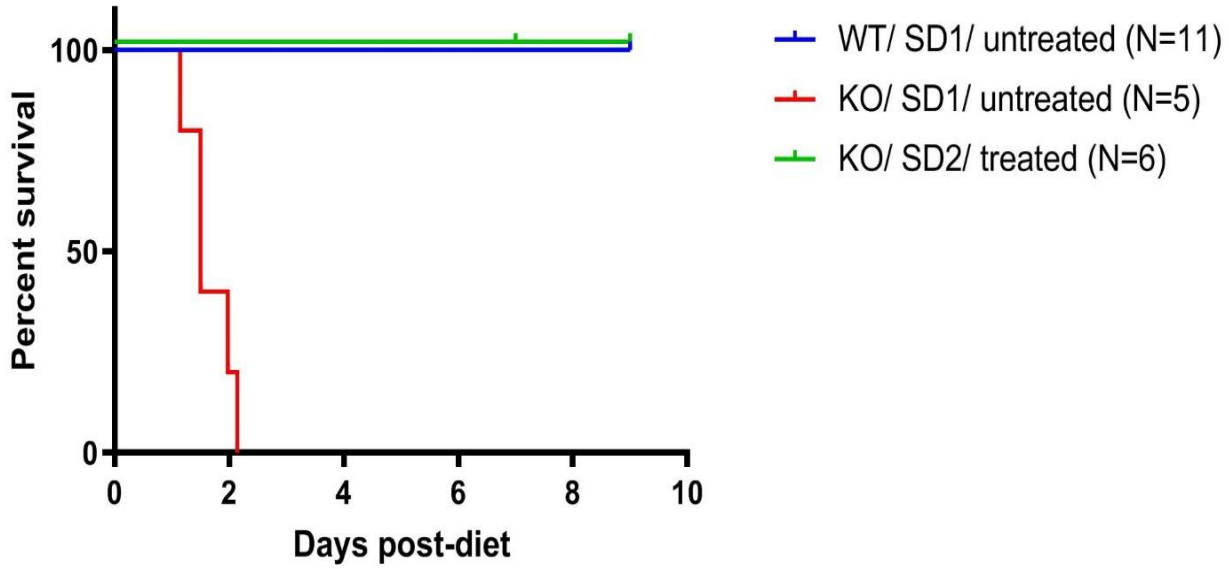

Fig. 4-9: Survival curves comparing mice fed modified diets with or without PN treatment (B6 strain only). High-lysine SD1 induced seizures and acute death in untreated KO mice and PN treatment rescued both phenotypes. Curves are significantly different ($p<0.0001$). Abbreviations: KO: *Aldh7a1*-knockout mice; WT: wildtype mice; SD1: Special Diet 1; SD2: Special Diet 2.

4.3 Discussion

The basic pathophysiology in PDE-ALDH7A1 is a blockade in the lysine degradative pathway that results in the buildup of secondary metabolites (Mills et al., 2006). These metabolites, mainly P6C and α-AASA, are thought to underlie most of the clinicopathological features of PDE-ALDH7A1 (Jansen et al., 2014). While the contribution of these compounds to the non-epileptic phenotype in PDE-ALDH7A1 (i.e. neurodevelopmental disabilities and brain lesions) has remained hypothetical, there is experimental evidence that accumulation of P6C traps pyridoxal 5'-phosphate (PLP) and causes its depletion *in vitro* (Mills et al., 2006), providing a mechanistic link to the possible cause of seizures. There is ample evidence from the literature that conditions that lead to PLP depletion in mice cause seizures, consistent with the human phenotype, based on several genetic (Gachon et al., 2004; Narisawa et al., 1997, 2001; Waymire et al., 1995), nutritional (Coleman & Schlesinger, 1965; Narisawa et al., 2001) and pharmacological (Bonner et al., 1999; Mizuno et al., 1989; Sasaki et al., 1997; Yamashita, 1976) models of PLP deficiency. In Chapter 3, we demonstrated that Aldh7a1-deficient mice fed a regular diet accumulate PDE-associated lysine metabolites including P6C. However, their brain PLP profile was not different from WT mice, and they were clinically asymptomatic.

Because ALDH7A1 is involved in the lysine catabolism pathway, the phenotypic effect of ALDH7A1 deficiency in both mice and humans is expected to vary with changes to lysine and other nutrients, particularly PN, in the diet. Lysine is the principal upstream substrate that, through its catabolic pathways, generates the pathognomonic metabolites in PDE-ALDH7A1. The use of a low-lysine diet in affected children has led to improved seizure control and better developmental outcomes (Coughlin et al., 2015; van Karnebeek et al., 2012, 2015), validating the importance of this gene-environment interaction. Examination of the standard mouse chow used in our animal

facility revealed that it contains 0.9% lysine and 18 ppm PN. We recognized that these levels represent a diet that is low in lysine (~50% lower compared to other standard chows (Sauer et al., 2011, 2015)) and relatively high in PN, which therefore had the potential to mitigate the effects of ALDH7A1 deficiency in our mice.

To validate this hypothesis, we assessed the effects of modulating lysine and PN content through specialized diets. The first diet, SD1, contained higher lysine (4.7%) and lower PN (1.6 ppm). The 4.7% lysine level was based on the previously high lysine diet-induced mouse model of GA-1 (Zinnanti et al., 2006). Testing this diet on untreated KO mice unveiled a vigorous seizure phenotype and led to their quick death due to sustained status epilepticus. Similar sequelae occur in untreated patients in whom ALDH7A1 deficiency causes prolonged status epilepticus that may lead to death of affected infants (Naasan et al., 2009; Nabbout et al., 1999; Stockler et al., 2011). Lysine supplementation in a*ldh7a1*-KO zebrafish exacerbated the seizure phenotype and led to earlier death of KO larvae (Pena et al., 2017). As shown in Table 4-3, the timeframe and amount of consumed diet until first seizure is consistent among KO mice. This might point to the presence of a threshold of toxic P6C accumulation at which sufficient PLP inactivation occurs to trigger seizures and subsequent neurological sequelae.

Analysis of ictal EEG tracings showed a spectrum of electrographic patterns including focal, generalized, absence-like (freezing behaviour) and burst-suppression, all of which have also been described in ALDH7A1 deficiency patients (Al Teneiji et al., 2017; Mills et al., 2010; Naasan et al., 2009; Pérez et al., 2013). Interestingly, the terminal seizure pattern in our KO mice was predominantly burst-suppression, a pattern that is also commonly seen in PDE-ALDH7A1 patients (Gallagher et al., 2009; Millet et al., 2011; Stockler et al., 2011; Yeghiazaryan et al., 2011).

An important and distinguishing clinical feature of PDE-ALDH7A1 is the effective control of seizures with high-dose pyridoxine therapy. To validate this in the current mouse model, another cohort of *Aldh7a1*-KO mice were fed a similar high-lysine diet and treated with prophylactic PN injections. It was noted from the pilot trial that there was only a short interval between seizure onset and death in untreated KO mice exposed to high-lysine diet (about 13 hours in both mice, Table 4-3). PN treatment was given pre-emptively in the treated cohort, which helped to avoid unexpected death before intervening with PN. High-dose PN treatment effectively prevented seizures in KO mice under high lysine intake, as was evident from EEG analysis in recorded mice.

In summary, our results indicate that high lysine diet can induce a PN-responsive seizure phenotype in Aldh7a1-deficient mice that recapitulates important clinical aspects of PDE-ALDH7A1. Taken together with the previously demonstrated biochemical phenotype of the mice while on the regular diet, this study provides further evidence that *Aldh7a1*-KO mice constitute a good biochemical and clinical model for PDE-ALDH7A1 that can be utilized to elucidate the disease pathophysiology and as a tool for drug screening and testing. These findings also underscore the importance of controlling lysine levels in PDE-ALDH7A1 patients' diet.

5 Discussion

5.1 Clinical and functional studies in PLPHP deficiency

PLPHP deficiency is a newly discovered form of vitamin B6-dependent epileptic encephalopathy (B6EE). The genetic cause of this disease, first described by Darin et al. (2016), is homozygous or compound heterozygous mutations in the *PLPBP* gene. The gene codes for a protein known as PLPHP, a pyridoxal 5'-phosphate (PLP)-binding protein of hitherto unknown function.

PLPHP deficiency appears to be one of the most severe forms of B6EE discovered so far. The disease caused neurodevelopmental disabilities and brain structural defects in most affected children reported to date. Out of the 24 cases described so far in whom neurodevelopment was assessed, 20 patients (83%) suffered some form of neurodevelopmental deficits (Darin et al., 2016; Jensen et al., 2019; Johannsen et al., 2019; Johnstone et al., 2019; Plecko et al., 2017; Shiraku et al., 2018). In comparison, 25 - 30% of patients with ALDH7A1 deficiency have normal neurodevelopmental outcome (Darin et al., 2016; van Karnebeek et al., 2016). Previous investigations in PLPHP deficiency patients (Darin et al., 2016) revealed an abnormal PLP profile in patient fibroblasts and cerebrospinal fluid, pointing to a role of this protein in PLP homeostatic regulation (Darin et al., 2016). However, the mechanism by which PLPHP dysfunction disrupts PLP homeostasis and leads to the observed encephalopathy in patients was still elusive. Recognizing these gaps in our understanding of disease pathophysiology, we characterized the clinical, genomic and biochemical abnormalities in a new series of 12 PLPHP deficiency patients. In addition, we generated and characterized knockout (KO) models in zebrafish, yeast and HEK293 cells to gain more insight into disease biology.

Our results identified previously undescribed clinical features of PLPHP deficiency, including non-epileptic movement disorder, fatal mitochondrial encephalopathy and folinic acid-responsive seizures. Given this extended phenotypic spectrum, PLPHP deficiency should be considered in early onset refractory epilepsy as well as in patients who present with nonepileptic paroxysmal events or a clinical picture of mitochondrial encephalopathy. In the latter case, a failure to recognize and treat the underlying PLPHP deficiency may lead to fatal complications as evident from two of our patients who died soon after presenting with a severe mitochondrial disease picture.

PLPHP deficiency has overlap in its clinical and biochemical presentation with other mitochondrial neurometabolic diseases like pyruvate dehydrogenase (PDH) deficiency, which also may cause epilepsy and lactic acidosis (Prasad et al., 2011). Jensen et al. (2019) described another diagnostic pitfall in which the presence of hyperglycinemia in a PLPHP deficiency patient led to a misdiagnosis of glycine encephalopathy (MIM# 605899). This highlights the importance of distinguishing metabolic biomarkers for early diagnosis of PLPHP deficiency. However, such disease-specific biomarkers are still lacking. Elevated levels of lactate and glycine in blood and/or CSF were the most consistently detected biochemical alterations in PLPHP deficiency patients from our cohort as well as in others (Darin et al., 2016; Jensen et al., 2019; Johnstone et al., 2019). A combination of both features, hyperglycinemia and hyperlactatemia, has been suggested to aid in differential diagnosis between PLPHP deficiency and mitochondrial diseases with similar clinical picture (Johnstone et al., 2019).

PLPHP deficiency patients showed a wide spectrum of clinical severity that extended from early neonatal lethality to mild cases with normal developmental outcome and well-controlled seizures with relatively low dose of vitB6. In the middle between these two extremes of the clinical

spectrum, there were severe cases that presented with neurodevelopmental deficits, brain structural defects and seizures that required larger doses of vitB6 along with adjuvant therapy for optimal control (Johnstone et al., 2019). Our analysis of patients' *PLPBP* variants revealed a genotype-phenotype correlation. We found that variants with proven or predicted damaging effect and those which lie in close proximity with the PLP-binding pocket correlated with a more severe clinical picture. PLPHP deficiency and other B6EEs cause depletion of PLP, the cofactor required by many enzymatic activities, most notably in neurotransmitter and amino acid metabolic pathways. Secondary deficiencies of PLP-dependent enzymes have been proposed to underlie many of the biochemical and clinical features in these diseases (Johnstone et al., 2019; Murty et al., 2013; Pena, Roussel, et al., 2017). In addition to variants within the primary locus (*PLPBP*), the clinical picture in PLPHP deficiency could also be influenced by functional polymorphic variants in genes involved in PLP-dependent metabolic pathways. The epistatic effect of these secondary loci could act as disease modifiers and thus provide further explanation for the clinical heterogeneity observed in PLPHP deficiency.

In the analysis of vitB6 vitamers in our patients, we noted markedly increased levels of pyridoxine 5'-phosphate (PNP) in patient fibroblasts and PLPHP-deficient HEK293 cells. Consistent with this finding, a recent study of *YggS*, the PLPHP orthologue in bacteria, showed that YggS-deficient *Escherichia coli* accumulated high levels of PNP (Ito et al., 2020). Using multiple lines of experimental evidence, this study demonstrated that accumulating PNP inhibits the glycine cleavage system by competing with the binding of its normal cofactor, PLP. The glycine cleavage system is a PLP-dependent multi-enzyme complex that is responsible for breakdown of glycine in human and other species (Ichinohe et al., 2004; Sakata et al., 2001; Wilson

et al., 2019). Given that hyperglycinemia is a common abnormality in PLPHP-deficient patients, this warrants further investigation of the functional impact of PNP accumulation in these patients.

Our *plpbp*-KO zebrafish model replicated the clinical phenotype of PLPHP-deficient patients by showing vitB6-dependent seizures and death in untreated KO larvae. Consistent with the biochemical picture in patients, Plphp-deficient fish displayed decreased systemic levels of PLP in addition to other metabolic aberrations involving various amino acids and neurotransmitters. In the future this model can be utilized as a tool for investigating the disease pathophysiology, drug screening and identifying diagnostic biomarkers.

5.2 *Aldh7a1*-KO mice as a tool for studying pyridoxine-dependent epilepsy

The aim of this study was to generate mice with constitutive deletion of *Aldh7a1* and validate its use as a model for pyridoxine-dependent epilepsy (PDE-ALDH7A1). An ideal disease model should accurately replicate the human condition, both at the molecular and phenotypic levels. This is a particularly important aspect to validate, if the model is to be used in preclinical therapeutic trials that will be translated to human patients (Justice & Dhillon, 2016). Another level of validation comes from the response of the model to a treatment that is known to be beneficial in the human disease (Justice & Dhillon, 2016).

Initial characterization of the *Aldh7a1*-KO mice was carried out using a regular diet that is low in lysine (0.9% or 9 g of lysine per kg of diet) and relatively high in pyridoxine (PN). At the molecular level, KO mice fed this diet showed accumulation of upstream lysine metabolites that are the biochemical hallmark of ALDH7A1 deficiency in patients. The level of these metabolites with 0.9% dietary lysine was, however, insufficient to cause PLP deficiency or drive an overt clinical phenotype in the KO mice. The composition of the regular diet resembles a therapeutic

low-lysine diet that is used in conjunction with high PN supplementation in PDE-ALDH7A1 patients to ameliorate the clinical phenotype.

Higher lysine intake was expected to increase the flux through its catabolic pathway and thus generate higher concentration of upstream metabolites. Therefore, we designed a modified diet that contained higher lysine (4.7%) and lower PN content. Untreated KO mice exposed to this high lysine diet suffered severe clinical seizures that rapidly led to their death. PN treatment prevented high lysine-elicited seizures and death. These experiments validated the model for three clinical features of PDE-ALDH7A1: recurrent seizures, death in untreated cases and response to PN treatment.

The amenability of our mouse model to dietary manipulations is an important feature that makes this model suitable for studying the effect of dietary interventions like lysine restriction or arginine supplementation. The results of high lysine exposure in Aldh7a1-deficient mice highlights dietary lysine as a potential environmental factor that influences the severity of the phenotype in ALDH7A1 deficiency and that could explain why genotype-phenotype correlation has proven challenging in PDE-ALDH7A1 (Pena et al., 2017). In line with this, data from previous studies show that amount of lysine in human breast milk varies widely between different populations due to the variation in the nutritional composition of commonly consumed diets. For example, Wurtman and Fernstrom (1979) found that the mean concentration of free lysine in breast milk from American women was significantly higher compared to milk samples taken from Guatemalan women (11.8 versus 3.4 µmol/L). The authors attributed this to the fact that diet consumed by Guatemalan women (mostly cereal grains and legumes) contained significantly lower protein than the American diet. Other reported levels of lysine in human breast milk were 39.0 µmol/L (Italy) (Agostoni et al., 2000) and 27.2 µmol/L (Ecuador) (Baldeón et al., 2014). The detrimental effects

of high lysine intake observed in our Aldh7a1-deficient mice strongly support the use of adjuvant therapies that aim to minimize lysine exposure in patients.

Our biochemical analysis uncovered a number of previously undescribed abnormalities in ALDH7A1 deficiency. These included accumulation of saccharopine and α-aminoadipic acid, two lysine derivative compounds of known cellular toxicity, and oxidative stress biomarker in brain of KO mice. In a recent work, 6-(2-oxopropyl)piperidine-2-carboxylic acid, a novel biomarker discovered in PDE-ALDH7A1 patients (Coene et al., 2019) was also demonstrated in tissue samples from Aldh7a1-KO mice (Dr. K. Coene, personal communication). These findings demonstrate that Aldh7a1-KO mice can be utilized as a platform to explore new pathophysiological mechanisms and biochemical markers in PDE-ALDH7A1.

Our data showed that lysine metabolites accumulated in the liver of KO mice at magnitudes similar to or higher than those in the brain. This finding raises an intriguing question of why extra-neuronal symptoms are rarely seen in ALDH7A1 deficiency patients despite the accumulation of these presumably pathogenic metabolites in peripheral tissues. One reason could be different levels of tolerance and response to these metabolites between different tissues. Except for saccharopine which has been shown to cause mitochondrial toxicity and liver damage in mice (Zhou et al., 2019), studies on the specific functional effects of other metabolites are lacking. Furthermore, PLP, the deficient enzymatic cofactor in PDE-ALDH7A1, is required for proper functioning of over 140 enzymes that are involved in a diverse array of cellular processes in different body tissues. PLP deficiency is expected to impair the activity of PLP-dependent enzymes including those that function in peripheral tissues. Genetic deficiencies of several of these enzymes are known to cause diseases with peripheral manifestations. Examples include glycogen storage disease types V and VI (MIM: 232600, 232700) caused by glycogen phosphorylase deficiency, nephrotic syndrome

with systemic manifestations (MIM: 617575) due to sphingosine-1-phosphate lyase deficiency, and sideroblastic anaemia (MIM: 300751) due to Δ-aminolevulinic acid synthase deficiency (Wilson et al., 2019).

5.3 Future directions

5.3.1 PLPHP deficiency

It is clear that much remains to be learned about this novel form of B6EE. The next step towards better understanding of disease biology would be creating a *PLPBP*-knockout mouse model and characterizing its phenotypic abnormalities. In addition to investigating disease pathophysiology, there is also a need for diagnostic biomarkers for early detection of PLPHP deficiency. One of the powerful tools for biomarker discovery is non-targeted metabolomics. This cutting-edge technique allows simultaneous profiling of thousands of metabolites to obtain a comprehensive metabolic snapshot of body fluids, tissue lysates, and cells using mass spectrometry (Patti et al., 2012; Wikoff et al., 2007). As evident from other studies (Ciborowski et al., 2012; Jansson et al., 2009; Sabatine et al., 2005; Wikoff et al., 2007), this assay can be used to identify a unique pattern of metabolites that can be exploited as useful diagnostic biomarkers for PLPHP deficiency.

5.3.2 *Aldh7a1*-KO mouse model

The relative contribution of specific tissues and cell types to the development of phenotypic abnormalities in *Aldh7a1*-KO mice remains undetermined. In the brain, *Aldh7a1* is primarily expressed in astrocytes and cells of glial origin but not in neurons (Jansen et al., 2014). Glial cell dysfunction has been suggested to cause some of the neuropathological abnormalities observed in PDE-ALDH7A1 (Jansen et al., 2014). Moreover, it is currently unknown whether lysine

metabolites that accumulate in the brain in PDE-ALDH7A1 are produced locally or sourced from the liver. Antiquitin is highly expressed in liver, suggesting that hepatocytes are the main tissue for lysine catabolism (Zhou et al., 2019)**.** In line with this, upon lysine injection to normal mice, the amount of lysine catabolites produced by the liver was found to be higher than the amount produced by the brain by several orders of magnitude (Pena et al., 2017).

To fill these knowledge gaps, conditional knockout mice could be used to produce strains in which gene knockout occurs only in a specific cell type. We generated a conditional *Aldh7a1*-targeted line in which exon 6 of the mouse *Aldh7a1* gene is flanked by loxP sites (floxed mice). These floxed mice can be crossed to Cre-recombinase-expressing mice in which the recombinase transgene is driven by a cell-type specific promoter. This will result in deletion of the critical exon occurring only in the targeted cells, thus producing a cell-specific gene knockout model. Astrocyte-specific knockout can be produced using mouse GFAP promoter to drive Cre recombinase expression, while mouse albumin promoter can be used to generate hepatocyte-specific knockout. Phenotypic characterization of these cell-type specific *Aldh7a1*-knockout strains will allow us to determine which cell types are critical for ALDH7A1-deficiency mediated biochemical and neuropathological abnormalities.

An important clinical feature of PDE-ALDH7A1 yet to be validated in Aldh7a1-deficient mice is the presence of neurobehavioural deficits. This is a useful outcome measure for testing future therapeutics in *Aldh7a1*-KO mice. Behavioural testing could not be performed in KO mice exposed to 4.7% lysine/1.6 ppm PN diet because of the vigorous seizures and short survival. This can be overcome by using alternative diets containing lower levels of lysine to produce an intermediate phenotype that can be used for behavioural testing. We suggest characterizing *Aldh7a1*-KO under a range of lysine diets containing 2.5 – 3.5% lysine to find the optimal lysine

content. The new lysine diet should also be tested in combination with PN treatment to evaluate if PN can rescue any of the biochemical, neuropathological and behavioural abnormalities. As an alternative method, lysine can be added to drinking water instead of chow to avoid non-compliance of mice with lysine modified diets as we noted in our previous special diet trials. Lysine-supplemented water was successfully implemented by Sauer et al. (2015) for testing varying concentrations of lysine in the *Gcdh*-KO mice. The authors noted a decline in diet consumption by the KO mice, probably with onset of neurological symptoms, while their drinking behaviour was not affected (Sauer et al., 2015).

The effect of loss of other, non-lysine related functions of ALDH7A1 should be assessed more comprehensively. ALDH7A1 has been shown to protect the cell from toxicity induced by reactive aldehydes and oxidative stress (Brocker et al., 2011). Oxidative stress occurs when there is an imbalance between oxidants produced during normal metabolic processes and antioxidant levels in favor of oxidants (Birben et al., 2012; Bloomer, 2008). These oxidants, like reactive oxygen species (ROS), attack cellular molecules like lipids, proteins and DNA, leading to compromised cellular function (Bloomer, 2008). One of the common methods for evaluating oxidative stress is by analyzing its biomarkers, which are products of reaction of ROS with cellular molecules. Examples include lipid hydroperoxides, protein carbonyls and oxidized amino acids (like methionine sulfoxide) and 8-hydroxydeoxyguanosine (8-oxodG) formed by reaction of ROS with DNA (Bloomer, 2008; Ock et al., 2012; Sova et al., 2010; Suzuki et al., 2016). In our study, we analyzed oxidative stress by quantifying methionine sulfoxide using mass spectrometry methods. To add further evidence to our preliminary finding using this biomarker, additional oxidative stress biomarkers should be analyzed in *Aldh7a1*-KO mice. Using *in situ* detection

methods like immunohistochemistry will allow identification of the extent of oxidative stress in different brain regions and cell types.

Our overarching goal in producing the mouse model for ALDH7A1 deficiency was to develop and test effective therapeutics for this debilitating disease. One of the therapeutic strategies used in treatment of metabolic diseases is upstream enzyme inhibition. This strategy is based on the inhibition of an enzyme that functions upstream of the defective step in the metabolic pathway to reduce the generation of toxic metabolites. In this category, α-aminoadipic semialdehyde synthase (AASS) has emerged as a potential therapeutic target in PDE-ALDH7A1. AASS catalyzes the first two steps of the saccharopine pathway of lysine catabolism and works upstream of ALDH7A1. A recent study (Pena et al., 2017) showed that AASS seems to be the main enzyme that drives the production of the metabolic intermediates in the lysine degradation pathway in all tested tissues (liver, kidney and brain). Moreover, a study in PDE-ALDH7A1 patient fibroblasts suggested that AASS activity could be upregulated in ALDH7A1-deficient fibroblasts compared to control cells (Crowther et al., 2019). Deficiency of AASS in humans due to mutations in its encoding gene, *AASS*, is most likely a benign phenotype causing no or mild symptoms only (Houten et al., 2013). In line with this, *in vitro* knockdown of *AASS* did not cause any abnormal phenotype in the tested human cell line (HEK293 cells) (Pena, 2015). Therefore, targeted inhibition of this enzyme appears to be a plausible therapeutic approach. Antisense oligonucleotides-based knockdown of *Aass* in *Aldh7a1*-KO mice could be used to provide a proof of principle for the efficacy of this approach in lowering the cerebral concentrations of neurotoxic metabolites.

Another therapeutic experiment that can be conducted in the *Aldh7a1*-KO mice is antenatal PN and dietary therapy. Adjunct dietary treatments like lysine-restricted diet and L-arginine supplementation (Coughlin et al., 2015; van Karnebeek et al., 2012, 2015) have been tested in PDE-ALDH7A1 patients and shown to decrease the levels of secondary metabolites and improve developmental outcomes. However, metabolites were still at supraphysiological levels and outcomes were not optimal. ALDH7A1 dysfunction and subsequent PLP depletion and accumulation of secondary metabolites might interfere with brain development during early embryonic life; therefore, antenatal treatment might be advantageous. We have shown that *Aldh7a1*-KO mice fed a 0.9% lysine diet still accumulate high levels of lysine metabolites and appear to have increased prenatal mortality. As a future experiment, modified diets with lower lysine content combined with higher arginine and PN could be tested in KO mice starting from the prenatal stage. The resulting pups will be examined for the effect of this antenatal triple therapy (Coughlin et al., 2015) in normalizing or reducing the lysine metabolites and also in improving the genotypic ratio of KO mice.

6.4 Conclusion

The main objectives of this thesis were 1) to improve our understanding of the clinical, biochemical and pathophysiological features of PLPHP deficiency using patients and model organisms, and 2) to generate and carry out phenotypic characterization of a mouse model of ALDH7A1 deficiency in order to evaluate its use as a model of PDE-ALDH7A1.

We expanded the clinical and biochemical spectrum of PLPHP deficiency by describing 12 new patients affected with this disease. We generated and characterized *PLPBP*-KO models in zebrafish, yeast and HEK293 cells. Our results provided insight about mitochondrial localization

of PLPHP and confirmed its important role of PLPHP in maintaining PLP homeostasis. We report the first animal model for PLPHP deficiency that can be used for further investigations of the disease pathophysiology and for drug screening.

We generated and characterized a novel mouse model for ALDH7A1 deficiency. Aldh7a1-KO mice, initially fed a low lysine diet, showed a biochemical signature of defective lysine catabolism and amino acid perturbations consistent with the biochemical picture seen in patients. Analysis also revealed a number of novel biochemical alterations that warrant further investigations. The mice, however, did not show seizures or behavioural deficits on the tests that were performed.

We next sought to validate the effect of dietary lysine enrichment in inducing a clinical phenotype by designing special high lysine diets. The high lysine diet in KO mice caused acute seizures and death that could be rescued by PN treatment.

In conclusion, our results indicate that *Aldh7a1*-KO mice are a good model for characterizing human PDE-ALDH7A1. This model may be used to further elucidate the underlying pathophysiology and biochemistry of this disease, paving the way for better therapies. The response of the model to dietary PN and lysine manipulations indicates that the model may be used for preclinical testing of dietary and pharmacological treatments that aim to modulate the cerebral lysine catabolism.

Bibliography

Agostoni, C., Carratù, B., Boniglia, C., Riva, E., & Sanzini, E. (2000). Free amino acid content in standard infant formulas: Comparison with human milk. *Journal of the American College of Nutrition*, *19*(4), 434–438. https://doi.org/10.1080/07315724.2000.10718943

Al Teneiji, A., Bruun, T. U. J., Cordeiro, D., Patel, J., Inbar-Feigenberg, M., Weiss, S., Struys, E., & Mercimek-Mahmutoglu, S. (2017). Phenotype, biochemical features, genotype and treatment outcome of pyridoxine-dependent epilepsy. *Metabolic Brain Disease*, *32*(2), 443–451. https://doi.org/10.1007/s11011-016-9933-8

Albersen, M., Bosma, M., Knoers, N. V. V. A. M., de Ruiter, B. H. B., Diekman, E. F., de Ruijter, J., Visser, W. F., de Koning, T. J., & Verhoeven-Duif, N. M. (2013). The Intestine Plays a Substantial Role in Human Vitamin B6 Metabolism: A Caco-2 Cell Model. *PLoS ONE*, *8*(1), e54113. https://doi.org/10.1371/journal.pone.0054113

Allgood, V. E., & Cidlowski, J. A. (1992). Vitamin B6 modulates transcriptional activation by multiple members of the steroid hormone receptor superfamily. *The Journal of Biological Chemistry*, *267*(6), 3819–3824.

Amadasi, A., Bertoldi, M., Contestabile, R., Bettati, S., Cellini, B., Luigi di Salvo, M., Borri-Voltattorni, C., Bossa, F., & Mozzarelli, A. (2007). *Pyridoxal 5'-Phosphate Enzymes as Targets for Therapeutic Agents* [Text]. Bentham Science Publishers. https://doi.org/info:doi/10.2174/092986707780597899

Baldeón, M. E., Mennella, J. A., Flores, N., Fornasini, M., & San Gabriel, A. (2014). Free amino acid content in breast milk of adolescent and adult mothers in Ecuador. *SpringerPlus*, *3*(1), 104. https://doi.org/10.1186/2193-1801-3-104

Baraban, S. C., Dinday, M. T., & Hortopan, G. A. (2013). Drug screening in Scn1a zebrafish mutant identifies clemizole as a potential Dravet syndrome treatment. *Nat Commun*, *4*, 2410.

Baraban, S. C., Taylor, M. R., Castro, P. A., & Baier, H. (2005). Pentylenetetrazole induced changes in zebrafish behavior, neural activity and c-fos expression. *Neuroscience*, *131*(3), 759–68.

Barić, I., Zschocke, J., Christensen, E., Duran, M., Goodman, S. I., Leonard, J. V., Müller, E., Morton, D. H., Superti-Furga, A., & Hoffmann, G. F. (1998). Diagnosis and management of glutaric aciduria type I. *Journal of Inherited Metabolic Disease*, *21*(4), 326–340. https://doi.org/10.1023/A:1005390105171

Barrientos, A. (2003). Yeast models of human mitochondrial diseases. *IUBMB Life*, *55*(2), 83–95.

Basura, G. J., Hagland, S. P., Wiltse, A. M., & Gospe, S. M. (2009). Clinical features and the management of pyridoxine-dependent and pyridoxine-responsive seizures: Review of 63 North American cases submitted to a patient registry. *European Journal of Pediatrics*, *168*(6), 697–704. https://doi.org/10.1007/s00431-008-0823-x

Baumgartner-Sigl, S., Haberlandt, E., Mumm, S., Scholl-Bürgi, S., Sergi, C., Ryan, L., Ericson, K. L., Whyte, M. P., & Högler, W. (2007). Pyridoxine-responsive seizures as the first symptom of infantile hypophosphatasia caused by two novel missense mutations (c.677T>C, p.M226T; c.1112C>T, p.T371I) of the tissue-nonspecific alkaline phosphatase gene. *Bone*, *40*(6), 1655–1661. https://doi.org/10.1016/j.bone.2007.01.020

Baxter. (2001). Pyridoxine-dependent and pyridoxine-responsive seizures. *Developmental Medicine and Child Neurology*, *43*(6), 416–420. https://doi.org/10.1017/S0012162201000779

Baxter, P. (1999). Epidemiology of pyridoxine dependent and pyridoxine responsive seizures in the UK. *Archives of Disease in Childhood*, *81*(5), 431–433. https://doi.org/10.1136/adc.81.5.431

Baxter, P. (2003). Pyridoxine-dependent seizures: A clinical and biochemical conundrum. *Biochimica et Biophysica Acta (BBA) - Proteins and Proteomics*, *1647*(1), 36–41. https://doi.org/10.1016/S1570-9639(03)00045-1

Bejsovec, M., Kulenda, Z., & Ponca, E. (1967). Familial intrauterine convulsions in pyridoxine dependency. *Archives of Disease in Childhood*, *42*(222), 201–207.

Bender, D. A. (2012). *Amino Acid Metabolism*. John Wiley & Sons. https://books.google.ca/books?id=CLok9jcTFVsC&printsec=copyright#v=onepage&q&f=false

Biagosch, C., Ediga, R. D., Hensler, S.-V., Faerberboeck, M., Kuehn, R., Wurst, W., Meitinger, T., Kölker, S., Sauer, S., & Prokisch, H. (2017). Elevated glutaric acid levels in Dhtkd1-/Gcdh- double knockout mice challenge our current understanding of lysine metabolism. *Biochimica et Biophysica Acta (BBA) - Molecular Basis of Disease*, *1863*(9), 2220–2228. https://doi.org/10.1016/j.bbadis.2017.05.018

Bilski, P., Li, M. Y., Ehrenshaft, M., Daub, M. E., & Chignell, C. F. (2000). Vitamin B6 (pyridoxine) and its derivatives are efficient singlet oxygen quenchers and potential fungal antioxidants. *Photochemistry and Photobiology*, *71*(2), 129–134. https://doi.org/10.1562/0031-8655(2000)071<0129:sipvbp>2.0.co;2

Birben, E., Sahiner, U. M., Sackesen, C., Erzurum, S., & Kalayci, O. (2012). Oxidative Stress and Antioxidant Defense. *World Allergy Organization Journal*, *5*(1), 9–19. https://doi.org/10.1097/WOX.0b013e3182439613

Bloomer, R. J. (2008). Chapter 1 Effect Of Exercise On Oxidative Stress Biomarkers. In *Advances in Clinical Chemistry* (Vol. 46, pp. 1–50). Elsevier. https://doi.org/10.1016/S0065-2423(08)00401-0

Bohney, J. P., Fonda, M. L., & Feldhoff, R. C. (1992). Identification of Lys190 as the primary binding site for pyridoxal 5′-phosphate in human serum albumin. *FEBS Letters*, *298*(2), 266–268. https://doi.org/10.1016/0014-5793(92)80073-P

Bok, L. A., Been, J. V., Struys, E. A., Jakobs, C., Rijper, E. A. M., & Willemsen, M. A. (2010). Antenatal treatment in two Dutch families with pyridoxine-dependent seizures. *European Journal of Pediatrics*, *169*(3), 297–303. https://doi.org/10.1007/s00431-009-1020-2

Bok, L. A., Halbertsma, F. J., Houterman, S., Wevers, R. A., Vreeswijk, C., Jakobs, C., Struys, E., Van Der Hoeven, J. H., Sival, D. A., & Willemsen, M. A. (2012). Long-term outcome in pyridoxine-dependent epilepsy. *Developmental Medicine and Child Neurology*, *54*(9), 849–854. https://doi.org/10.1111/j.1469-8749.2012.04347.x

Bonner, A. B., Peterson, S. L., & Weir, M. R. (1999). Seizures induced by theophylline and isoniazid in mice. *Veterinary and Human Toxicology*, *41*(3), 175–177.

Brocker, C., Cantore, M., Failli, P., & Vasiliou, V. (2011). Aldehyde dehydrogenase 7A1 (ALDH7A1) attenuates reactive aldehyde and oxidative stress induced cytotoxicity. *Chemico-Biological Interactions*, *191*(1–3), 269–277. https://doi.org/10.1016/j.cbi.2011.02.016

Brocker, C., Lassen, N., Estey, T., Pappa, A., Cantore, M., Orlova, V. V., Chavakis, T., Kavanagh, K. L., Oppermann, U., & Vasiliou, V. (2010). Aldehyde dehydrogenase 7A1 (ALDH7A1) is a novel enzyme involved in cellular defense against hyperosmotic stress. *The Journal of Biological Chemistry*, *285*(24), 18452–18463. https://doi.org/10.1074/jbc.M109.077925

Brown, D. R., & Kretzschma, H. A. (1998). The glio-toxic mechanism of α-aminoadipic acid on cultured astrocytes. *Journal of neurocytology*, *27*(2), 109–118.

Brun, L., Ngu, L. H., Keng, W. T., Ch'ng, G. S., Choy, Y. S., & Hwu, W. L. (2010). Clinical and biochemical features of aromatic L-amino acid decarboxylase deficiency. *Neurology*, *75*(1), 64–71.

Calvo, S. E., Clauser, K. R., & Mootha, V. K. (2016). MitoCarta2.0: An updated inventory of mammalian mitochondrial proteins. *Nucleic Acids Res*, *44*(D1), 1251–7.

Chan, C.-L., Wong, J. W. Y., Wong, C.-P., Chan, M. K. L., & Fong, W.-P. (2011). Human antiquitin: Structural and functional studies. *Chemico-Biological Interactions*, *191*(1–3), 165–170. https://doi.org/10.1016/j.cbi.2010.12.019

ChemIDplus Lite—Chemical information with searchable synonyms, structures, and formulas. (n.d.). Retrieved October 17, 2019, from https://chem.nlm.nih.gov/chemidplus/chemidlite.jsp

Chen, W. W., Freinkman, E., & Sabatini, D. M. (2017). Rapid immunopurification of mitochondria for metabolite profiling and absolute quantification of matrix metabolites. *Nat Protoc*, *12*(10), 2215–31.

Christmann-Franck, S., Fermandjian, S., Mirambeau, G., & Der Garabedian, P. A. (2007). Molecular modelling studies on the interactions of human DNA topoisomerase IB with pyridoxal-compounds. *Biochimie*, *89*(4), 468–473. https://doi.org/10.1016/j.biochi.2006.10.007

Ciborowski, M., Teul, J., Martin-Ventura, J. L., Egido, J., & Barbas, C. (2012). Metabolomics with LC-QTOF-MS Permits the Prediction of Disease Stage in Aortic Abdominal

Aneurysm Based on Plasma Metabolic Fingerprint. *PLoS ONE*, *7*(2), e31982. https://doi.org/10.1371/journal.pone.0031982

Cingolani, P., Platts, A., L, W., Coon, M., Nguyen, T., & Wang, L. (2012). *A program for annotating and predicting the effects of single nucleotide polymorphisms, SnpEff: SNPs in the genome of Drosophila melanogaster strain w1118* (Vol. 6, Issue 2). Fly.

Clarke, A. R. (1994). Murine genetic models of human disease. *Current Opinion in Genetics & Development*, *4*(3), 453–460. https://doi.org/10.1016/0959-437X(94)90035-3

Clayton, P. T. (2006). B6-responsive disorders: A model of vitamin dependency. *Journal of Inherited Metabolic Disease*, *29*(2–3), 317–326. https://doi.org/10.1007/s10545-005-0243-2

Coburn, S. P., & Mahuren, J. D. (1976). In vivo metabolism of 4'-deoxypyridoxine in rat and man. *Journal of Biological Chemistry*, *251*(6), 1646–1652.

Coburn, S. P., & Mahuren, J. D. (1987). Identification of pyridoxine 3-sulfate, pyridoxal 3-sulfate, and N-methylpyridoxine as major urinary metabolites of vitamin B6 in domestic cats. *Journal of Biological Chemistry*, *262*(6), 2642–2644.

Coburn, Stephen P., Mahuren, J. D., Wostmann, B. S., Snyder, D. L., & Townsend, D. W. (1989). Role of Intestinal Microflora in the Metabolism of Vitamin B-6 and 4′-Deoxypyridoxine Examined Using Germfree Guinea Pigs and Rats. *The Journal of Nutrition*, *119*(2), 181–188. https://doi.org/10.1093/jn/119.2.181

Coene, K., Martens, J., Van Outersterp, R., Engelke, U., Berden, G., Houthuijs, K., Kluijtmans, L., Huigen, M., De Boer, S., Van der Heeft, E., Van Karnebeek, C., Wevers, R., & Oomens, J. (2019). *Discovery of novel antiquitin deficiency biomarkers through the combination of untargeted metabolomics and infrared ion spectroscopy*. *42*, 6.

Coker, S. B. (1992). Postneonatal vitamin B6-dependent epilepsy. *Pediatrics*, *90*(2 Pt 1), 221–223.

Coleman, D. L., & Schlesinger, K. (1965). Effects of Pyridoxine Deficiency on Audiogenic Seizure Susceptibility in Inbred Mice. *Proceedings of the Society for Experimental Biology and Medicine*, *119*(1), 264–266. https://doi.org/10.3181/00379727-119-30154

Cormier-Daire, V., Dagoneau, N., Nabbout, R., Burglen, L., Penet, C., Soufflet, C., Desguerre, I., Munnich, A., & Dulac, O. (2000). A Gene for Pyridoxine-Dependent Epilepsy Maps to Chromosome 5q31. *American Journal of Human Genetics*, *67*(4), 991–993.

Coughlin, C. R., Swanson, M. A., Spector, E., Meeks, N. J. L., Kronquist, K. E., Aslamy, M., Wempe, M. F., van Karnebeek, C. D. M., Gospe, S. M., Aziz, V. G., Tsai, B. P., Gao, H., Nagy, P. L., Hyland, K., van Dooren, S. J. M., Salomons, G. S., & Van Hove, J. L. K. (2018). The genotypic spectrum of ALDH7A1 mutations resulting in pyridoxine dependent epilepsy: A common epileptic encephalopathy. *Journal of Inherited Metabolic Disease*. https://doi.org/10.1007/s10545-018-0219-7

Coughlin, C. R., van Karnebeek, C. D. M., Al-Hertani, W., Shuen, A. Y., Jaggumantri, S., Jack, R. M., Gaughan, S., Burns, C., Mirsky, D. M., Gallagher, R. C., & Van Hove, J. L. K. (2015). Triple therapy with pyridoxine, arginine supplementation and dietary lysine restriction in pyridoxine-dependent epilepsy: Neurodevelopmental outcome. *Molecular Genetics and Metabolism*, *116*(1–2), 35–43. https://doi.org/10.1016/j.ymgme.2015.05.011

Crowther, L. M., Mathis, D., Poms, M., & Plecko, B. (2019). New insights into human lysine degradation pathways with relevance to pyridoxine-dependent epilepsy due to antiquitin deficiency. *Journal of Inherited Metabolic Disease*, *42*(4), 620–628. https://doi.org/10.1002/jimd.12076

da Silva, V. R., Ralat, M. A., Quinlivan, E. P., DeRatt, B. N., Garrett, T. J., Chi, Y.-Y., Frederik Nijhout, H., Reed, M. C., & Gregory, J. F. (2014). Targeted metabolomics and mathematical modeling demonstrate that vitamin B-6 restriction alters one-carbon metabolism in cultured HepG2 cells. *American Journal of Physiology-Endocrinology and Metabolism*, *307*(1), E93–E101. https://doi.org/10.1152/ajpendo.00697.2013

Dakshinamurti, S., & Dakshinamurti, K. (2007). Vitamin B6. In *Handbook of Vitamins* (4th ed.). CRC Press. https://books.google.ca/books?id=6fYso23Mi5IC&lpg=PA322&vq=vitamin%20b6&pg=PP1#v=onepage&q&f=false

Darin, N., Reid, E., Prunetti, L., Samuelsson, L., Husain, R. A., Wilson, M., El Yacoubi, B., Footitt, E., Chong, W. K., Wilson, L. C., Prunty, H., Pope, S., Heales, S., Lascelles, K., Champion, M., Wassmer, E., Veggiotti, P., de Crécy-Lagard, V., Mills, P. B., & Clayton, P. T. (2016). Mutations in PROSC Disrupt Cellular Pyridoxal Phosphate Homeostasis and Cause Vitamin-B6-Dependent Epilepsy. *American Journal of Human Genetics*, *99*(6), 1325–1337. https://doi.org/10.1016/j.ajhg.2016.10.011

de Ligt, J., MH, W., BW, B., T, K., HG, Y., & T, K. (2012). Diagnostic exome sequencing in persons with severe intellectual disability. *N Engl J Med*, *367*(20), 1921–9.

Delorme, A., & Makeig, S. (2004). EEGLAB: An open source toolbox for analysis of single-trial EEG dynamics including independent component analysis. *Journal of Neuroscience Methods*, *134*(1), 9–21. https://doi.org/10.1016/j.jneumeth.2003.10.009

di Salvo, M. L., Contestabile, R., & Safo, M. K. (2011). Vitamin B(6) salvage enzymes: Mechanism, structure and regulation. *Biochimica Et Biophysica Acta*, *1814*(11), 1597–1608. https://doi.org/10.1016/j.bbapap.2010.12.006

Dias-Lopes, C., Neshich, I. A., Neshich, G., Ortega, J. M., Granier, C., & Chavez-Olortegui, C. (2013). Identification of new sphingomyelinases D in pathogenic fungi and other pathogenic organisms. *PLoS One*, *8*(11), 79240.

Doğan, Ö. A., Demir, G. Ü., Kosukcu, C., Taskiran, E. Z., Simsek-Kiper, P. Ö., Utine, G. E., Alikaşifoğlu, M., & Boduroğlu, K. (2019). Hyperphosphatasia with mental retardation syndrome type 4 In two siblings-expanding the phenotypic and mutational spectrum. *European Journal of Medical Genetics*, *62*(6), 103535. https://doi.org/10.1016/j.ejmg.2018.09.002

Ducker, G. S., & Rabinowitz, J. D. (2017). One-Carbon Metabolism in Health and Disease. *Cell Metabolism*, *25*(1), 27–42. https://doi.org/10.1016/j.cmet.2016.08.009

Dyment, D. A., Smith, A. C., Alcantara, D., Schwartzentruber, J. A., Basel-Vanagaite, L., & Curry, C. J. (2013). Mutations in PIK3R1 cause SHORT syndrome. *Am J Hum Genet*, *93*(1), 158–66.

Edwards, P., Liu, P. K. S., & Rose, G. A. (1990). Liquid chromatographic studies of vitamin B6 metabolism in man. *Clinica Chimica Acta*, *190*(1), 67–80. https://doi.org/10.1016/0009-8981(90)90281-V

Eifel, P. J., Brown, D. M., Lee, W. W., & Brown, J. M. (1983). Misonidazole neurotoxicity in mice decreased by administration with pyridoxine. *International Journal of Radiation Oncology*Biology*Physics*, *9*(10), 1513–1519. https://doi.org/10.1016/0360-3016(83)90326-7

Emsley, P., Lohkamp, B., Scott, W. G., & Cowtan, K. (2010). Features and development of Coot. *Acta Crystallogr D Biol Crystallogr*, *66*(Pt 4), 486–501.

Engstrom, F. L., & Woodbury, D. M. (1988). Seizure Susceptibility in DBA and C57 Mice: The Effects of Various Convulsants. *Epilepsia*, *29*(4), 389–395. https://doi.org/10.1111/j.1528-1157.1988.tb03736.x

Eswaramoorthy, S., Gerchman, S., Graziano, V., Kycia, H., Studier, F. W., & Swaminathan, S. (2003). Structure of a yeast hypothetical protein selected by a structural genomics approach. *Acta Crystallographica. Section D, Biological Crystallography*, *59*(Pt 1), 127–135. https://doi.org/10.1107/s0907444902018012

Farrant, R. D., Walker, V., Mills, G. A., Mellor, J. M., & Langley, G. J. (2001). Pyridoxal Phosphate De-activation by Pyrroline-5-carboxylic Acid INCREASED RISK OF VITAMIN B6 DEFICIENCY AND SEIZURES IN HYPERPROLINEMIA TYPE II. *Journal of Biological Chemistry*, *276*(18), 15107–15116. https://doi.org/10.1074/jbc.M010860200

Ferraro, T. N., Golden, G. T., Smith, G. G., & Berrettini, W. H. (1995). Differential Susceptibility to Seizures Induced by Systemic Kainic Acid Treatment in Mature DBA/2J and C57BLl6J Mice. *Epilepsia*, *36*(3), 301–307. https://doi.org/10.1111/j.1528-1157.1995.tb00999.x

Ferraro, T. N., Golden, G. T., Smith, G. G., DeMuth, D., Buono, R. J., & Berrettini, W. H. (2002). Mouse strain variation in maximal electroshock seizure threshold. *Brain Research*, *936*(1), 82–86. https://doi.org/10.1016/S0006-8993(02)02565-9

Footitt, E. J., Clayton, P. T., Mills, K., Heales, S. J., Neergheen, V., Oppenheim, M., & Mills, P. B. (2013). Measurement of plasma B6 vitamer profiles in children with inborn errors of vitamin B6 metabolism using an LC-MS/MS method. *Journal of Inherited Metabolic Disease*, *36*(1), 139–145. https://doi.org/10.1007/s10545-012-9493-y

Footitt, E. J., Heales, S. J., Mills, P. B., Allen, G. F., Oppenheim, M., & Clayton, P. T. (2011). Pyridoxal 5'-phosphate in cerebrospinal fluid; factors affecting concentration. *Journal of Inherited Metabolic Disease*, *34*(2), 529–538.

Frankel, W. N., Taylor, L., Beyer, B., Tempel, B. L., & White, H. S. (2001). Electroconvulsive Thresholds of Inbred Mouse Strains. *Genomics*, *74*(3), 306–312. https://doi.org/10.1006/geno.2001.6564

Friedman, S. D., Ishak, G. E., Poliachik, S. L., Poliakov, A. V., Otto, R. K., Shaw, D. W. W., Willemsen, M. A., Bok, L. A., & Gospe, S. M. (2014). Callosal alterations in pyridoxine-dependent epilepsy. *Developmental Medicine and Child Neurology*, *56*(11), 1106–1110. https://doi.org/10.1111/dmcn.12511

Gachon, F., Fonjallaz, P., Damiola, F., Gos, P., Kodama, T., Zakany, J., Duboule, D., Petit, B., Tafti, M., & Schibler, U. (2004). The loss of circadian PAR bZip transcription factors results in epilepsy. *Genes & Development*, *18*(12), 1397–1412. https://doi.org/10.1101/gad.301404

Gallagher, R. C., Van Hove, J. L. K., Scharer, G., Hyland, K., Plecko, B., Waters, P. J., Mercimek-Mahmutoglu, S., Stockler-Ipsiroglu, S., Salomons, G. S., Rosenberg, E. H., Struys, E. A., & Jakobs, C. (2009). Folinic acid-responsive seizures are identical to pyridoxine-dependent epilepsy. *Annals of Neurology*, *65*(5), 550–556. https://doi.org/10.1002/ana.21568

Garweg, G., Rehren, D. V., & Hintze, U. (1980). l-Pipecolate Formation in the Mammalian Brain. Regional Distribution of Δ1Pyrroline-2-carboxylate Reductase Activity. *Journal of Neurochemistry*, *35*(3), 616–621. https://doi.org/10.1111/j.1471-4159.1980.tb03700.x

Geraghty, M. T., Vaughn, D., Nicholson, A. J., Lin, W.-W., Jimenez-Sanchez, G., Obie, C., Flynn, P., Valle, D., & Hu, C. A. (1998). Mutations in the Δ1-Pyrroline 5-Carboxylate Dehydrogenase Gene Cause Type II Hyperprolinemia. *Human Molecular Genetics*, *7*(9), 1411–1415. https://doi.org/10.1093/hmg/7.9.1411

Ghatge, M. S., Di Salvo, M. L., Contestabile, R., Eseonu, D. N., Karve, S., Schirch, V., & Safo, M. K. (2012). Molecular Defects of Vitamin B6 Metabolism Associated with Neonatal Epileptic Encephalopathy. In R. Tanasescu (Ed.), *Miscellanea on Encephalopathies—A Second Look*. InTech. https://doi.org/10.5772/29149

Giardina, G., Brunotti, P., Fiascarelli, A., Cicalini, A., Costa, M. G., & Buckle, A. M. (2015). How pyridoxal 5'-phosphate differentially regulates human cytosolic and mitochondrial serine hydroxymethyltransferase oligomeric state. *FEBS J*, *282*(7), 1225–41.

Gospe, S. M. (2010). Pyridoxine-dependent epilepsy and pyridoxine phosphate oxidase deficiency: Unique clinical symptoms and non-specific EEG characteristics. *Developmental Medicine and Child Neurology*, *52*(7), 602–603. https://doi.org/10.1111/j.1469-8749.2010.03668.x

Goto, T., Matsuo, N., & Takahashi, T. (2001). CSF glutamate/GABA concentrations in pyridoxine-dependent seizures: Etiology of pyridoxine-dependent seizures and the mechanisms of pyridoxine action in seizure control. *Brain & Development*, *23*(1), 24–29. https://doi.org/10.1016/s0387-7604(00)00193-5

Goutières, F., & Aicardi, J. (1985). Atypical presentations of pyridoxine-dependent seizures: A treatable cause of intractable epilepsy in infants. *Annals of Neurology*, *17*(2), 117–120. https://doi.org/10.1002/ana.410170203

Gregory, J. F., & Kirk, J. R. (1979). Determination of urinary 4-pyridoxic acid using high performance liquid chromatography. *The American Journal of Clinical Nutrition*, *32*(4), 879–883. https://doi.org/10.1093/ajcn/32.4.879

Gutierrez, M. D. C., & Giacobini, E. (1985). Identification and characterization of pipecolic acid binding sites in mouse brain. *Neurochemical Research*, *10*(5), 691–702. https://doi.org/10.1007/BF00964407

Hallen, A., Jamie, J. F., & Cooper, A. J. (2013). Lysine metabolism in mammalian brain: An update on the importance of recent discoveries. *Amino Acids*, *45*(6), 1249–1272.

Han, Q., Cai, T., Tagle, D. A., & Li, J. (2010). Structure, expression, and function of kynurenine aminotransferases in human and rodent brains. *Cellular and Molecular Life Sciences : CMLS*, *67*(3), 353–368. https://doi.org/10.1007/s00018-009-0166-4

Hassel, B., Rogne, A. G., & Hope, S. (2019). Intellectual Disability Associated With Pyridoxine-Responsive Epilepsies: The Need to Protect Cognitive Development. *Frontiers in Psychiatry*, *10*. https://doi.org/10.3389/fpsyt.2019.00116

Hellmann, H., & Mooney, S. (2010). Vitamin B6: A molecule for human health? *Molecules (Basel, Switzerland)*, *15*(1), 442–459. https://doi.org/10.3390/molecules15010442

Higashino, K., Fujioka, M., & Yamamura, Y. (1971). The conversion of l-lysine to saccharopine and α-aminoadipate in mouse. *Archives of Biochemistry and Biophysics*, *142*(2), 606–614. https://doi.org/10.1016/0003-9861(71)90525-X

Hoffmann, G. F., & Kölker, S. (2012). Cerebral Organic Acid Disorders and Other Disorders of Lysine Catabolism. In J. M. Saudubray, G. Van den Berghe, & J. Walter (Eds.), *Inborn Metabolic Diseases: Diagnosis and Treatment* (5th ed, p. 656). Springer-Verlag. https://doi.org/10.1007/978-3-642-15720-2_23

Hoffmann, G. F., Schmitt, B., Windfuhr, M., Wagner, N., Strehl, H., Bagci, S., & Steinmann, B. (2007). Pyridoxal 5′-phosphate may be curative in early-onset epileptic encephalopathy. *Journal of Inherited Metabolic Disease: Official Journal of the Society for the Study of Inborn Errors of Metabolism*, *30*(1), 96–99.

Horn, D., Krawitz, P., Mannhardt, A., Korenke, G. C., & Meinecke, P. (2011). Hyperphosphatasia-mental retardation syndrome due to PIGV mutations: Expanded clinical spectrum. *American Journal of Medical Genetics Part A*, *155*(8), 1917–1922. https://doi.org/10.1002/ajmg.a.34102

Hortopan, G. A., Dinday, M. T., & Baraban, S. C. (2010). Zebrafish as a model for studying genetic aspects of epilepsy. *Dis Model Mech*, *3*(3–4), 144–8.

Houten, S. M., te Brinke, H., Denis, S., Ruiter, J. P., Knegt, A. C., de Klerk, J. B., Augoustides-Savvopoulou, P., Häberle, J., Baumgartner, M. R., Coşkun, T., Zschocke, J., Sass, J. O., Poll-The, B. T., Wanders, R. J., & Duran, M. (2013). Genetic basis of hyperlysinemia. *Orphanet Journal of Rare Diseases*, *8*(1), 57. https://doi.org/10.1186/1750-1172-8-57

Huck, S., Grass, F., & Hatten, M. E. (1984). Gliotoxic effects of α-aminoadipic acid on monolayer cultures of dissociated postnatal mouse cerebellum. *Neuroscience*, *12*(3), 783–791. https://doi.org/10.1016/0306-4522(84)90170-2

Hunt, A. D., Stokes, J., McCrory, W. W., & Stroud, H. H. (1954). Pyridoxine dependency: Report of a case of intractable convulsions in an infant controlled by pyridoxine. *Pediatrics*, *13*(2), 140–145.

Hwang, W. Y., Fu, Y., Reyon, D., Maeder, M. L., Tsai, S. Q., & Sander, J. D. (2013). Efficient genome editing in zebrafish using a CRISPR-Cas system. *Nat Biotechnol*, *31*(3), 227–9.

Hyland, K. (1999). Neurochemistry and defects of biogenic amine neurotransmitter metabolism. *Journal of Inherited Metabolic Disease*, *22*(4), 353–363. https://doi.org/10.1023/A:1005587719505

Ichinohe, A., Kure, S., Mikawa, S., Ueki, T., Kojima, K., Fujiwara, K., Iinuma, K., Matsubara, Y., & Sato, K. (2004). Glycine cleavage system in neurogenic regions. *European Journal of Neuroscience*, *19*(9), 2365–2370. https://doi.org/10.1111/j.0953-816X.2004.03345.x

Ikegawa, S., Isomura, M., Koshizuka, Y., & Nakamura, Y. (1999). Cloning and characterization of human and mouse PROSC (proline synthetase co-transcribed) genes. *J Hum Genet*, *44*(5), 337–42.

Ito, T., Hori, R., Hemmi, H., Downs, D. M., & Yoshimura, T. (2020). Inhibition of glycine cleavage system by pyridoxine 5′-phosphate causes synthetic lethality in glyA yggS and serA yggS in Escherichia coli. *Molecular Microbiology*, *113*(1), 270–284. https://doi.org/10.1111/mmi.14415

Ito, T., Iimori, J., Takayama, S., Moriyama, A., Yamauchi, A., Hemmi, H., & Yoshimura, T. (2013). Conserved pyridoxal protein that regulates Ile and Val metabolism. *Journal of Bacteriology*, *195*(24), 5439–5449. https://doi.org/10.1128/JB.00593-13

Jain-Ghai, S., Mishra, N., Hahn, C., Blaser, S., & Mercimek-Mahmutoglu, S. (2014). Fetal Onset Ventriculomegaly and Subependymal Cysts in a Pyridoxine Dependent Epilepsy Patient. *Pediatrics*, *133*(4), e1092–e1096. https://doi.org/10.1542/peds.2013-1230

Jansen, L. A., Hevner, R. F., Roden, W. H., Hahn, S. H., Jung, S., & Gospe, S. M. (2014). Glial localization of antiquitin: Implications for pyridoxine-dependent epilepsy. *Annals of Neurology*, *75*(1), 22–32. https://doi.org/10.1002/ana.24027

Jansson, J., Willing, B., Lucio, M., Fekete, A., Dicksved, J., Halfvarson, J., Tysk, C., & Schmitt-Kopplin, P. (2009). Metabolomics Reveals Metabolic Biomarkers of Crohn's Disease. *PLoS ONE*, *4*(7). https://doi.org/10.1371/journal.pone.0006386

Jeanclos, E., Albersen, M., Ramos, R. J. J., Raab, A., Wilhelm, C., Hommers, L., Lesch, K.-P., Verhoeven-Duif, N. M., & Gohla, A. (2019). Improved cognition, mild anxiety-like behavior and decreased motor performance in pyridoxal phosphatase-deficient mice. *Biochimica et Biophysica Acta (BBA) - Molecular Basis of Disease*, *1865*(1), 193–205. https://doi.org/10.1016/j.bbadis.2018.08.018

Jensen, K. V., Frid, M., Stödberg, T., Barbaro, M., Wedell, A., Christensen, M., Bak, M., Ek, J., Madsen, C. G., Darin, N., & Grønborg, S. (2019). Diagnostic pitfalls in vitamin B6-dependent epilepsy caused by mutations in the PLPBP gene. *JIMD Reports*, *50*(1), 1–8. https://doi.org/10.1002/jmd2.12063

Johannsen, J., Bierhals, T., Deindl, P., Hecher, L., Hermann, K., Hempel, M., Kloth, K., & Denecke, J. (2019). Excessive Seizure Clusters in an Otherwise Well-Controlled Epilepsy as a Possible Hallmark of Untreated Vitamin B6-Responsive Epilepsy due to a Homozygous PLPBP Missense Variant. *Journal of Pediatric Genetics*, *08*(4), 222–225. https://doi.org/10.1055/s-0039-1685501

Johnstone, D. L., Al-Shekaili, H. H., Tarailo-Graovac, M., Wolf, N. I., Ivy, A. S., Demarest, S., Roussel, Y., Ciapaite, J., van Roermund, C. W. T., Kernohan, K. D., Kosuta, C., Ban, K., Ito, Y., McBride, S., Al-Thihli, K., Abdelrahim, R. A., Koul, R., Al Futaisi, A., Haaxma, C. A., … van Karnebeek, C. D. M. (2019). PLPHP deficiency: Clinical, genetic, biochemical, and mechanistic insights. *Brain: A Journal of Neurology*, *142*(3), 542–559. https://doi.org/10.1093/brain/awy346

Jubb, H. C., Higueruelo, A. P., Ochoa-Montano, B., Pitt, W. R., Ascher, D. B., & Blundell, T. L. (2017). Arpeggio: A web server for calculating and visualising interatomic interactions in protein structures. *J Mol Biol*, *429*(3), 365–71.

Justice, M. J., & Dhillon, P. (2016). Using the mouse to model human disease: Increasing validity and reproducibility. *Disease Models & Mechanisms*, *9*(2), 101–103. https://doi.org/10.1242/dmm.024547

Kanehisa, M., & Goto, S. (2000). KEGG: Kyoto Encyclopedia of Genes and Genomes. *Nucleic Acids Research*, *28*(1), 27–30.

Kanellis, P., Gagliardi, M., Banath, J. P., Szilard, R. K., Nakada, S., Galicia, S., Sweeney, F. D., Cabelof, D. C., Olive, P. L., & Durocher, D. (2007). A Screen for Suppressors of Gross Chromosomal Rearrangements Identifies a Conserved Role for PLP in Preventing DNA Lesions. *PLOS Genetics*, *3*(8), e134. https://doi.org/10.1371/journal.pgen.0030134

Khurgel, M., Koo, A. C., & Ivy, G. O. (1996). Selective ablation of astrocytes by intracerebral injections of α-aminoadipate. *Glia*, *16*(4), 351–358.

Kikuchi, G., Motokawa, Y., Yoshida, T., & Hiraga, K. (2008). Glycine cleavage system: Reaction mechanism, physiological significance, and hyperglycinemia. *Proc Jpn Acad Ser B Phys Biol Sci*, *84*(7), 246–63.

Kilkenny, C., Browne, W. J., Cuthill, I. C., Emerson, M., & Altman, D. G. (2012). Improving bioscience research reporting: The ARRIVE guidelines for reporting animal research. *Osteoarthr Cartil*, *20*(4), 256–60.

Kim, J. S., & Giacobini, E. (1985). Pipecolic acid levels and transport in developing mouse brain. *Developmental Brain Research*, *22*(2), 181–186. https://doi.org/10.1016/0165-3806(85)90169-5

Kircher, M., Witten, D. M., Jain, P., O'Roak, B. J., Cooper, G. M., & Shendure, J. (2014). A general framework for estimating the relative pathogenicity of human genetic variants. *Nat Genet*, *46*(3), 310–5.

Kluger, G., Blank, R., Paul, K., Paschke, E., Jansen, E., Jakobs, C., Wörle, H., & Plecko, B. (2008). Pyridoxine-dependent epilepsy: Normal outcome in a patient with late diagnosis after prolonged status epilepticus causing cortical blindness. *Neuropediatrics*, *39*(5), 276–279. https://doi.org/10.1055/s-0029-1202833

Knaus, A., Awaya, T., Helbig, I., Afawi, Z., Pendziwiat, M., Abu-Rachma, J., Thompson, M. D., Cole, D. E., Skinner, S., Annese, F., Canham, N., Schweiger, M. R., Robinson, P. N., Mundlos, S., Kinoshita, T., Munnich, A., Murakami, Y., Horn, D., & Krawitz, P. M. (2016). Rare Noncoding Mutations Extend the Mutational Spectrum in the PGAP3 Subtype of Hyperphosphatasia with Mental Retardation Syndrome. *Human Mutation*, *37*(8), 737–744. https://doi.org/10.1002/humu.23006

Koeller, D. M., Woontner, M., Crnic, L. S., Kleinschmidt-DeMasters, B., Stephens, J., Hunt, E. L., & Goodman, S. I. (2002). Biochemical, pathologic and behavioral analysis of a mouse model of glutaric acidemia type I. *Human Molecular Genetics*, *11*(4), 347–357. https://doi.org/10.1093/hmg/11.4.347

Kölker, S., Christensen, E., Leonard, J. V., Greenberg, C. R., Boneh, A., Burlina, A. B., Burlina, A. P., Dixon, M., Duran, M., García Cazorla, A., Goodman, S. I., Koeller, D. M., Kyllerman, M., Mühlhausen, C., Müller, E., Okun, J. G., Wilcken, B., Hoffmann, G. F., & Burgard, P. (2011). Diagnosis and management of glutaric aciduria type I – revised recommendations. *Journal of Inherited Metabolic Disease*, *34*(3), 677. https://doi.org/10.1007/s10545-011-9289-5

Korevaar, T. I. M., & Grossman, A. B. (2011). Pheochromocytomas and paragangliomas: Assessment of malignant potential. *Endocrine*, *40*(3), 354–365. https://doi.org/10.1007/s12020-011-9545-3

Kosobud, A. E., & Crabbe, J. C. (1990). Genetic correlations among inbred strain sensitivities to convulsions induced by 9 convulsant drugs. *Brain Research*, *526*(1), 8–16. https://doi.org/10.1016/0006-8993(90)90243-5

Kosuta, C., Daniel, K., Johnstone, D. L., Mongeon, K., Ban, K., LeBlanc, S., MacLeod, S., Et-Tahiry, K., Ekker, M., MacKenzie, A., & Pena, I. (2018). High-throughput DNA Extraction and Genotyping of 3dpf Zebrafish Larvae by Fin Clipping. *Journal of Visualized Experiments: JoVE*, *136*. https://doi.org/10.3791/58024

Krawitz, P. M., Schweiger, M. R., Rödelsperger, C., Marcelis, C., Kölsch, U., Meisel, C., Stephani, F., Kinoshita, T., Murakami, Y., Bauer, S., Isau, M., Fischer, A., Dahl, A., Kerick, M., Hecht, J., Köhler, S., Jäger, M., Grünhagen, J., de Condor, B. J., … Robinson, P. N. (2010). Identity-by-descent filtering of exome sequence data identifies PIGV mutations in hyperphosphatasia mental retardation syndrome. *Nature Genetics*, *42*(10), 827–829. https://doi.org/10.1038/ng.653

Langmead, B., & Salzberg, S. L. (2012). Fast gapped-read alignment with Bowtie 2. *Nat Methods*, *9*(4), 357–9.

Lasserre, J. P., Dautant, A., Aiyar, R. S., Kucharczyk, R., Glatigny, A., & Tribouillard-Tanvier, D. (2015). Yeast as a system for modeling mitochondrial disease mechanisms and discovering therapies. *Dis Model Mech*, *8*(6), 509–26.

Leandro, J., & Houten, S. M. (2019). Saccharopine, a lysine degradation intermediate, is a mitochondrial toxin. *J Cell Biol*, *218*(2), 391–392.

Lee, Y.-P., Kim, D.-W., Lee, M.-J., Jeong, M.-S., Kim, S.-Y., Lee, S.-H., Jang, S.-H., Park, J.-S., Kang, T.-C., Won, M.-H., Cho, S.-W., Kwon, O.-S., Eum, W.-S., & Choi, S.-Y. (2008). Human brain pyridoxal-5'-phosphate phosphatase (PLPP): Protein transduction of PEP-1-PLPP into PC12 cells. *BMB Reports*, *41*(5), 408–413. https://doi.org/10.5483/BMBRep.2008.41.5.408

Lek, M., Karczewski, K. J., Minikel, E. V., Samocha, K. E., Banks, E., & Fennell, T. (2016). Analysis of protein-coding genetic variation in 60,706 humans. *Nature*, *536*(7616), 285–91.

Lelieveld, S. H., Reijnders, M. R., Pfundt, R., Yntema, H. G., Kamsteeg, E. J., & Vries, P. (2016). Meta-analysis of 2,104 trios provides support for 10 new genes for intellectual disability. *Nat Neurosci*, *19*(9), 1194–6.

Levine, S., & Saltzman, A. (2002). Pyridoxine (vitamin B6) toxicity: Enhancement by uremia in rats. *Food and Chemical Toxicology*, *40*(10), 1449–1451. https://doi.org/10.1016/S0278-6915(02)00072-8

Levtova, A., Camuzeaux, S., Laberge, A. M., Allard, P., Brunel-Guitton, C., Diadori, P., & Mitchell, G. A. (2015). Normal cerebrospinal fluid pyridoxal 5′-phosphate level in a PNPO-deficient patient with neonatal-onset epileptic encephalopathy. In *JIMD Reports* (Vol. 22, pp. 67–75). Springer.

Li, H., Handsaker, B., Wysoker, A., Fennell, T., Ruan, J., & Homer, N. (2009). The Sequence Alignment/Map format and SAMtools. *Bioinformatics*, *25*(16), 2078–9.

Liu, X., Jian, X., & Boerwinkle, E. (2011). DbNSFP: a lightweight database of human nonsynonymous SNPs and their functional predictions. *Hum Mutat*, *32*(8), 894–9.

Liu, X., Jian, X., & Boerwinkle, E. (2013). dbNSFP v2.0: A database of human non-synonymous SNVs and their functional predictions and annotations. *Hum Mutat*, *34*(9), 2393–402.

Locasale, J. W. (2013). Serine, glycine and the one-carbon cycle: Cancer metabolism in full circle. *Nature Reviews. Cancer*, *13*(8), 572–583. https://doi.org/10.1038/nrc3557

Lott, I. T., Coulombe, T., Di Paolo, R. V., Richardson, E. P., & Levy, H. L. (1978). Vitamin B6-dependent seizures: Pathology and chemical findings in brain. *Neurology*, *28*(1), 47–47.

Luboshitzky, R., Ophir, U., Nave, R., Epstein, R., Shen-Orr, Z., & Herer, P. (2002). The effect of pyridoxine administration on melatonin secretion in normal men. *Neuro Endocrinology Letters*, *23*(3), 213–217.

Maeda, Y., Ashida, H., & Kinoshita, T. (2006). CHO Glycosylation Mutants: GPI Anchor. In *Methods in Enzymology* (Vol. 416, pp. 182–205). Academic Press. https://doi.org/10.1016/S0076-6879(06)16012-7

Mahajnah, M., Corderio, D., Austin, V., Herd, S., Mutch, C., Carter, M., Struys, E., & Mercimek-Mahmutoglu, S. (2016). A Prospective Case Study of the Safety and Efficacy of Lysine-Restricted Diet and Arginine Supplementation Therapy in a Patient With Pyridoxine-Dependent Epilepsy Caused by Mutations in ALDH7A1. *Pediatric Neurology*, *60*, 60–65. https://doi.org/10.1016/j.pediatrneurol.2016.03.008

Mahuren, J. D., Pauly, T. A., & Coburn, S. P. (1991). Identification of 5-pyridoxic acid and 5-pyridoxic acid lactone as metabolites of vitamin B6 in humans. *The Journal of Nutritional Biochemistry*, *2*(8), 449–453. https://doi.org/10.1016/0955-2863(91)90115-L

Marguet, F., Barakizou, H., Tebani, A., Abily-Donval, L., Torre, S., Bayoudh, F., Jebnoun, S., Brasseur-Daudruy, M., Marret, S., Laquerriere, A., & Bekri, S. (2016). Pyridoxine-

dependent epilepsy: Report on three families with neuropathology. *Metabolic Brain Disease*, *31*(6), 1435–1443. https://doi.org/10.1007/s11011-016-9869-z

Mashima, R., Nakanishi-Ueda, T., & Yamamoto, Y. (2003). Simultaneous determination of methionine sulfoxide and methionine in blood plasma using gas chromatography-mass spectrometry. *Analytical Biochemistry*, *313*(1), 28–33.

Mathis, D., Abela, L., Albersen, M., Burer, C., Crowther, L., & Beese, K. (2016). The value of plasma vitamin B6 profiles in early onset epileptic encephalopathies. *J Inherit Metab Dis*, *39*(5), 733–41.

McCormick, D. B. (1994). Vitamin B6 transport and metabolism: Clues for delivery of bioactive compounds. In G. Marino, G. Sannia, & F. Bossa (Eds.), *Biochemistry of Vitamin B6 and PQQ* (pp. 311–317). Birkhäuser. https://doi.org/10.1007/978-3-0348-7393-2_50

McKenna, A., Hanna, M., Banks, E., Sivachenko, A., Cibulskis, K., & Kernytsky, A. (2010). The Genome Analysis Toolkit: A MapReduce framework for analyzing next-generation DNA sequencing data. *Genome Res*, *20*(9), 1297–303.

Mercimek-Mahmutoglu, S., Cordeiro, D., Cruz, V., Hyland, K., Struys, E. A., Kyriakopoulou, L., & Mamak, E. (2014). Novel therapy for pyridoxine dependent epilepsy due to ALDH7A1 genetic defect: L-arginine supplementation alternative to lysine-restricted diet. *European Journal of Paediatric Neurology*, *18*(6), 741–746. https://doi.org/10.1016/j.ejpn.2014.07.001

Mercimek-Mahmutoglu, S., Corderio, D., Nagy, L., Mutch, C., Carter, M., Struys, E., & Kyriakopoulou, L. (2014). Lysine-restricted diet and mild cerebral serotonin deficiency in a patient with pyridoxine-dependent epilepsy caused by ALDH7A1 genetic defect.

Molecular Genetics and Metabolism Reports, *1*, 124–128. https://doi.org/10.1016/j.ymgmr.2014.02.001

Mercimek-Mahmutoglu, S., Horvath, G. A., Coulter-Mackie, M., Nelson, T., Waters, P. J., Sargent, M., Struys, E., Jakobs, C., Stockler-Ipsiroglu, S., & Connolly, M. B. (2012). Profound neonatal hypoglycemia and lactic acidosis caused by pyridoxine-dependent epilepsy. *Pediatrics*, *129*(5), e1368-1372. https://doi.org/10.1542/peds.2011-0123

Metz, T. O., Alderson, N. L., Chachich, M. E., Thorpe, S. R., & Baynes, J. W. (2003). Pyridoxamine traps intermediates in lipid peroxidation reactions in vivo: Evidence on the role of lipids in chemical modification of protein and development of diabetic complications. *The Journal of Biological Chemistry*, *278*(43), 42012–42019. https://doi.org/10.1074/jbc.M304292200

Metz, T. O., Alderson, N. L., Thorpe, S. R., & Baynes, J. W. (2003). Pyridoxamine, an inhibitor of advanced glycation and lipoxidation reactions: A novel therapy for treatment of diabetic complications. *Archives of Biochemistry and Biophysics*, *419*(1), 41–49. https://doi.org/10.1016/j.abb.2003.08.021

Millán, J. L., & Whyte, M. P. (2016). Alkaline Phosphatase and Hypophosphatasia. *Calcified Tissue International*, *98*(4), 398–416. https://doi.org/10.1007/s00223-015-0079-1

Millet, A., Salomons, G. S., Cneude, F., Corne, C., Debillon, T., Jakobs, C., Struys, E., & Hamelin, S. (2011). Novel mutations in pyridoxine-dependent epilepsy. *European Journal of Paediatric Neurology*, *15*(1), 74–77. https://doi.org/10.1016/j.ejpn.2010.03.011

Mills, P. B., Footitt, E. J., Mills, K. A., Tuschl, K., Aylett, S., Varadkar, S., Hemingway, C., Marlow, N., Rennie, J., Baxter, P., Dulac, O., Nabbout, R., Craigen, W. J., Schmitt, B., Feillet, F., Christensen, E., De Lonlay, P., Pike, M. G., Hughes, M. I., … Clayton, P. T.

(2010). Genotypic and phenotypic spectrum of pyridoxine-dependent epilepsy (ALDH7A1 deficiency). *Brain: A Journal of Neurology*, *133*(Pt 7), 2148–2159. https://doi.org/10.1093/brain/awq143

Mills, P. B., Struys, E., Jakobs, C., Plecko, B., Baxter, P., Baumgartner, M., Willemsen, M. A. A. P., Omran, H., Tacke, U., Uhlenberg, B., Weschke, B., & Clayton, P. T. (2006). Mutations in antiquitin in individuals with pyridoxine-dependent seizures. *Nature Medicine*, *12*(3), 307–309. https://doi.org/10.1038/nm1366

Mills, P. B., Surtees, R. A. H., Champion, M. P., Beesley, C. E., Dalton, N., Scambler, P. J., Heales, S. J. R., Briddon, A., Scheimberg, I., Hoffmann, G. F., Zschocke, J., & Clayton, P. T. (2005). Neonatal epileptic encephalopathy caused by mutations in the PNPO gene encoding pyridox(am)ine 5'-phosphate oxidase. *Human Molecular Genetics*, *14*(8), 1077–1086. https://doi.org/10.1093/hmg/ddi120

Mizuno, A., Mizobuchi, T., Ishibashi, Y., & Matsuda, M. (1989). C-Fos mRNA induction under vitamin B6 antagonist-induced seizure. *Neuroscience Letters*, *98*(3), 272–275. https://doi.org/10.1016/0304-3940(89)90412-6

Mooney, S., Leuendorf, J.-E., Hendrickson, C., & Hellmann, H. (2009). Vitamin B6: A long known compound of surprising complexity. *Molecules (Basel, Switzerland)*, *14*(1), 329–351. https://doi.org/10.3390/molecules14010329

Mozzarelli, A., & Bettati, S. (2006). Exploring the pyridoxal 5'-phosphate-dependent enzymes. *Chemical Record (New York, N.Y.)*, *6*(5), 275–287. https://doi.org/10.1002/tcr.20094

Mukherjee, T., Hanes, J., Tews, I., Ealick, S. E., & Begley, T. P. (2011). Pyridoxal phosphate: Biosynthesis and catabolism. *Biochimica et Biophysica Acta (BBA) - Proteins and Proteomics*, *1814*(11), 1585–1596. https://doi.org/10.1016/j.bbapap.2011.06.018

Murthy, S. N., & Janardanasarma, M. K. (1999). Identification of L-amino acid/L-lysine α-amino oxidase in mouse brain. *Molecular and Cellular Biochemistry*, *197*(1), 13–23. https://doi.org/10.1023/A:1006906505745

Murty, V. S. S. Y., Kishore, M. S. S., & Patel, M. R. (2013). A Rare Case of Pyridoxine-dependent Seizures in Infancy. *Journal of Clinical Neonatology*, *2*(1), 39–41. https://doi.org/10.4103/2249-4847.109248

Naasan, G., Yabroudi, M., Rahi, A., & Mikati, M. A. (2009). Electroencephalographic changes in pyridoxine-dependant epilepsy: New observations. *Epileptic Disorders: International Epilepsy Journal with Videotape*, *11*(4), 293–300. https://doi.org/10.1684/epd.2009.0280

Nabbout, R., Soufflet, C., Plouin, P., & Dulac, O. (1999). Pyridoxine dependent epilepsy: A suggestive electroclinical pattern. *Archives of Disease in Childhood - Fetal and Neonatal Edition*, *81*(2), F125–F129. https://doi.org/10.1136/fn.81.2.F125

Nagano, N., Orengo, C. A., & Thornton, J. M. (2002). One fold with many functions: The evolutionary relationships between TIM barrel families based on their sequences, structures and functions. *J Mol Biol*, *321*(5), 741–65.

Narisawa, S., Fröhlander, N., & Millán, J. L. (1997). Inactivation of two mouse alkaline phosphatase genes and establishment of a model of infantile hypophosphatasia. *Developmental Dynamics*, *208*(3), 432–446. https://doi.org/10.1002/(SICI)1097-0177(199703)208:3<432::AID-AJA13>3.0.CO;2-1

Narisawa, S., Wennberg, C., & Millán, J. L. (2001). Abnormal vitamin B6 metabolism in alkaline phosphatase knock-out mice causes multiple abnormalities, but not the impaired bone mineralization. *The Journal of Pathology*, *193*(1), 125–133. https://doi.org/10.1002/1096-9896(2000)9999:9999<::AID-PATH722>3.0.CO;2-Y

Nichols, T. W., & Gaiteri, C. (2014). Morton's foot and pyridoxal 5′-phosphate deficiency: Genetically linked traits. *Medical Hypotheses*, *83*(6), 644–648. https://doi.org/10.1016/j.mehy.2014.09.003

Ock, C.-Y., Kim, E.-H., Choi, D. J., Lee, H. J., Hahm, K.-B., & Chung, M. H. (2012). 8-Hydroxydeoxyguanosine: Not mere biomarker for oxidative stress, but remedy for oxidative stress-implicated gastrointestinal diseases. *World Journal of Gastroenterology : WJG*, *18*(4), 302–308. https://doi.org/10.3748/wjg.v18.i4.302

Ormazabal, A., Oppenheim, M., Serrano, M., García-Cazorla, A., Campistol, J., Ribes, A., & Heales, S. (2008). Pyridoxal 5′-phosphate values in cerebrospinal fluid: Reference values and diagnosis of PNPO deficiency in paediatric patients. *Molecular genetics and metabolism*, *94*(2), 173–177.

Pagliarini, D. J., Calvo, S. E., Chang, B., Sheth, S. A., Vafai, S. B., & Ong, S. E. (2008). A mitochondrial protein compendium elucidates complex I disease biology. *Cell*, *134*(1), 112–23.

Palanza, K. M., Nesta, A. V., Tumu, R., Walton, C. M., Davis, M. A., & King, T. R. (2016). Auxotrophy-Based Detection of Hyperornithinemia in Mouse Blood and Urine. *Journal of Inborn Errors of Metabolism and Screening*, *4*, 2326409816649600. https://doi.org/10.1177/2326409816649600

Pandey, S., Garg, P., Lim, K. T., Kim, J., Choung, Y.-H., Choi, Y.-J., Choung, P.-H., Cho, C.-S., & Chung, J. H. (2013). The efficiency of membrane transport of vitamin B6 coupled to poly(ester amine) gene transporter and transfection in cancer cells. *Biomaterials*, *34*(14), 3716–3728. https://doi.org/10.1016/j.biomaterials.2013.01.098

Papes, F., Kemper, E. L., Cord-Neto, G., Langone, F., & Arruda, P. (1999). Lysine degradation through the saccharopine pathway in mammals: Involvement of both bifunctional and monofunctional lysine-degrading enzymes in mouse. *Biochemical Journal*, *344*(2), 555–563. https://doi.org/10.1042/bj3440555

Papes, F., Surpili, M. J., Langone, F., Trigo, J. R., & Arruda, P. (2001). The essential amino acid lysine acts as precursor of glutamate in the mammalian central nervous system. *FEBS Letters*, *488*(1–2), 34–38. https://doi.org/10.1016/S0014-5793(00)02401-7

Patti, G. J., Yanes, O., & Siuzdak, G. (2012). Metabolomics: The apogee of the omics trilogy. *Nature Reviews Molecular Cell Biology*, *13*(4), 263–269. https://doi.org/10.1038/nrm3314

Paulose, C. S., Dakshinamurti, K., Packer, S., & Stephens, N. L. (1988). Sympathetic stimulation and hypertension in the pyridoxine-deficient adult rat. *Hypertension*, *11*(4), 387–391.

Pena, I. A. (2015). *Aminoadipate-semialdehyde synthase (AASS) as a novel therapeutic target for pyridoxine-dependent epilepsy* [Doctoral dissertation, State Uinversity of Campinas]. http://repositorio.unicamp.br/handle/REPOSIP/317230

Pena, I. A., MacKenzie, A., & Van Karnebeek, C. D. M. (2017). Current knowledge for pyridoxine-dependent epilepsy: A 2016 update. *Expert Review of Endocrinology & Metabolism*, *12*(1), 5–20. https://doi.org/10.1080/17446651.2017.1273107

Pena, I. A., Marques, L. A., Laranjeira, Â. B. A., Yunes, J. A., Eberlin, M. N., MacKenzie, A., & Arruda, P. (2017). Mouse lysine catabolism to aminoadipate occurs primarily through the saccharopine pathway; implications for pyridoxine dependent epilepsy (PDE). *Biochimica et Biophysica Acta (BBA) - Molecular Basis of Disease*, *1863*(1), 121–128. https://doi.org/10.1016/j.bbadis.2016.09.006

Pena, I. A., Roussel, Y., Daniel, K., Mongeon, K., Johnstone, D., Weinschutz Mendes, H., Bosma, M., Saxena, V., Lepage, N., Chakraborty, P., Dyment, D. A., van Karnebeek, C. D. M., Verhoeven-Duif, N., Bui, T. V., Boycott, K. M., Ekker, M., & MacKenzie, A. (2017). Pyridoxine-Dependent Epilepsy in Zebrafish Caused by Aldh7a1 Deficiency. *Genetics*, *207*(4), 1501–1518. https://doi.org/10.1534/genetics.117.300137

Percudani, R., & Peracchi, A. (2003). A genomic overview of pyridoxal-phosphate-dependent enzymes. *EMBO Reports*, *4*(9), 850–854. https://doi.org/10.1038/sj.embor.embor914

Pérez, B., Gutiérrez-Solana, L. G., Verdú, A., Merinero, B., Yuste-Checa, P., Ruiz-Sala, P., & Ruiz, M. Á. (2013). Clinical, biochemical, and molecular studies in pyridoxine-dependent epilepsy. Antisense therapy as possible new therapeutic option. *Epilepsia*, *54*(2), 239–248.

Pires, D. E., Ascher, D. B., & Blundell, T. L. (2014). DUET: a server for predicting effects of mutations on protein stability using an integrated computational approach. *Nucleic Acids Res.*

Plecko, B., Hoeger, H., Jakobs, C. A. J. M., Struys, E., Stromberger, C., Leschnik, M., & Stoeckler-Ipsiroglu, S. (2005). Pipecolic acid concentrations in brain tissue of nutritionally pyridoxine-deficient rats. *Journal of Inherited Metabolic Disease*, *28*(5), 689–693.

Plecko, B., Paul, K., Paschke, E., Stoeckler-Ipsiroglu, S., Struys, E., Jakobs, C., Hartmann, H., Luecke, T., di Capua, M., Korenke, C., Hikel, C., Reutershahn, E., Freilinger, M., Baumeister, F., Bosch, F., & Erwa, W. (2007). Biochemical and molecular characterization of 18 patients with pyridoxine-dependent epilepsy and mutations of the antiquitin (ALDH7A1) gene. *Human Mutation*, *28*(1), 19–26. https://doi.org/10.1002/humu.20433

Plecko, B., Stöckler-Ipsiroglu, S., Paschke, E., Erwa, W., Struys, E. A., & Jakobs, C. (2000). Pipecolic acid elevation in plasma and cerebrospinal fluid of two patients with pyridoxine-

dependent epilepsy. *Annals of Neurology*, *48*(1), 121–125. https://doi.org/10.1002/1531-8249(200007)48:1<121::AID-ANA20>3.0.CO;2-V

Plecko, B., Struys, E. A., & Jakobs, C. (2014). Vitamin B6-Dependent and Responsive Disorders. In N. Blau, M. Duran, K. M. Gibson, & C. Dionisi Vici (Eds.), *Physician's Guide to the Diagnosis, Treatment, and Follow-Up of Inherited Metabolic Diseases* (pp. 179–190). Springer. https://doi.org/10.1007/978-3-642-40337-8_11

Plecko, B., Zweier, M., Begemann, A., Mathis, D., Schmitt, B., & Striano, P. (2017). Confirmation of mutations in PROSC as a novel cause of vitamin B 6 -dependent epilepsy. *J Med Genet*, *54*(12), 809–14.

Posset, R., Opp, S., Struys, E. A., Völkl, A., Mohr, H., Hoffmann, G. F., Kölker, S., Sauer, S. W., & Okun, J. G. (2015). Understanding cerebral L-lysine metabolism: The role of L-pipecolate metabolism in Gcdh-deficient mice as a model for glutaric aciduria type I. *Journal of Inherited Metabolic Disease*, *38*(2), 265–272. https://doi.org/10.1007/s10545-014-9762-z

Prasad, C., Rupar, T., & Prasad, A. N. (2011). Pyruvate dehydrogenase deficiency and epilepsy. *Brain Dev*, *33*(10), 856–65.

Prinsen, H. C. M. T., Schiebergen-Bronkhorst, B. G. M., Roeleveld, M. W., Jans, J. J. M., de Sain-van der Velden, M. G. M., Visser, G., van Hasselt, P. M., & Verhoeven-Duif, N. M. (2016). Rapid quantification of underivatized amino acids in plasma by hydrophilic interaction liquid chromatography (HILIC) coupled with tandem mass-spectrometry. *Journal of Inherited Metabolic Disease*, *39*(5), 651–660. https://doi.org/10.1007/s10545-016-9935-z

Prunetti, L., El Yacoubi, B., Schiavon, C. R., Kirkpatrick, E., Huang, L., & Bailly, M. (2016). Evidence That COG0325 Proteins are involved in PLP Homeostasis. *Microbiology*, *162*(4), 694–706.

PubChem. (n.d.). *PubChem*. Retrieved January 22, 2020, from https://pubchem.ncbi.nlm.nih.gov/

Ramos, R. J., Pras-Raves, M. L., Gerrits, J., van der Ham, M., Willemsen, M., Prinsen, H., Burgering, B., Jans, J. J., & Verhoeven-Duif, N. M. (2017). Vitamin B6 is essential for serine de novo biosynthesis. *Journal of Inherited Metabolic Disease*, *40*(6), 883–891. https://doi.org/10.1007/s10545-017-0061-3

Rankin, P. M., Harrison, S., Chong, W. K., Boyd, S., & Aylett, S. E. (2007). Pyridoxine-dependent seizures: A family phenotype that leads to severe cognitive deficits, regardless of treatment regime. *Developmental Medicine and Child Neurology*, *49*(4), 300–305. https://doi.org/10.1111/j.1469-8749.2007.00300.x

Rao, V. V., Pan, X., & Chang, Y. F. (1992). Developmental changes of L-lysine-ketoglutarate reductase in rat brain and liver. *Comparative Biochemistry and Physiology. B, Comparative Biochemistry*, *103*(1), 221–224.

Rao, V. V., Tsai, M. J., Pan, X., & Chang, Y. F. (1993). L-pipecolic acid oxidation in rat: Subcellular localization and developmental study. *Biochimica et Biophysica Acta (BBA)-Protein Structure and Molecular Enzymology*, *1164*(1), 29–35.

Rios-Avila, L., Nijhout, H. F., Reed, M. C., Sitren, H. S., & Gregory, J. F. (2013). A mathematical model of tryptophan metabolism via the kynurenine pathway provides insights into the effects of vitamin B-6 deficiency, tryptophan loading, and induction of tryptophan 2,3-dioxygenase on tryptophan metabolites. *The Journal of Nutrition*, *143*(9), 1509–1519. https://doi.org/10.3945/jn.113.174599

Robinson, J. T., Thorvaldsdottir, H., Winckler, W., Guttman, M., Lander, E. S., & Getz, G. (2011). Integrative genomics viewer. *Nat Biotechnol*, *29*(1), 24–6.

Rockman-Greenberg, C. (2013). Hypophosphatasia. *Pediatric Endocrinology Reviews : PER*, *10 Suppl 2*, 380–388.

Ruiz, A., García-Villoria, J., Ormazabal, A., Zschocke, J., Fiol, M., Navarro-Sastre, A., Artuch, R., Vilaseca, M. A., & Ribes, A. (2008). A new fatal case of pyridox(am)ine 5′-phosphate oxidase (PNPO) deficiency. *Molecular Genetics and Metabolism*, *93*(2), 216–218. https://doi.org/10.1016/j.ymgme.2007.10.003

Sabatine, M. S., Liu Emerson, Morrow David A., Heller Eric, McCarroll Robert, Wiegand Roger, Berriz Gabriel F., Roth Frederick P., & Gerszten Robert E. (2005). Metabolomic Identification of Novel Biomarkers of Myocardial Ischemia. *Circulation*, *112*(25), 3868–3875. https://doi.org/10.1161/CIRCULATIONAHA.105.569137

Sadilkova, K., Gospe, S. M., & Hahn, S. H. (2009). Simultaneous determination of alpha-aminoadipic semialdehyde, piperideine-6-carboxylate and pipecolic acid by LC-MS/MS for pyridoxine-dependent seizures and folinic acid-responsive seizures. *Journal of Neuroscience Methods*, *184*(1), 136–141. https://doi.org/10.1016/j.jneumeth.2009.07.019

Said, H. M. (2011). Intestinal absorption of water-soluble vitamins in health and disease. *Biochemical Journal*, *437*(3), 357–372. https://doi.org/10.1042/BJ20110326

Said, H. M., Ortiz, A., & Ma, T. Y. (2003). A carrier-mediated mechanism for pyridoxine uptake by human intestinal epithelial Caco-2 cells: Regulation by a PKA-mediated pathway. *American Journal of Physiology-Cell Physiology*, *285*(5), C1219–C1225. https://doi.org/10.1152/ajpcell.00204.2003

Said, H. M., Ortiz, A., & Vaziri, N. D. (2002). Mechanism and regulation of vitamin B6 uptake by renal tubular epithelia: Studies with cultured OK cells. *American Journal of Physiology-Renal Physiology*, *282*(3), F465–F471. https://doi.org/10.1152/ajprenal.00267.2001

Said, Z. M., Subramanian, V. S., Vaziri, N. D., & Said, H. M. (2008). Pyridoxine uptake by colonocytes: A specific and regulated carrier-mediated process. *American Journal of Physiology-Cell Physiology*, *294*(5), C1192–C1197. https://doi.org/10.1152/ajpcell.00015.2008

Sakata, Y., Owada, Y., Sato, K., Kojima, K., Hisanaga, K., Shinka, T., Suzuki, Y., Aoki, Y., Satoh, J., Kondo, H., Matsubara, Y., & Kure, S. (2001). Structure and expression of the glycine cleavage system in rat central nervous system. *Molecular Brain Research*, *94*(1), 119–130. https://doi.org/10.1016/S0169-328X(01)00225-X

Sander, J. D., Maeder, M. L., Reyon, D., Voytas, D. F., Joung, J. K., & Dobbs, D. (2010). ZiFiT (Zinc Finger Targeter): An updated zinc finger engineering tool. *Nucleic Acids Res*.

Sasaki, K., Wada, K., Hatta, S., Ohshika, H., & Haga, M. (1997). Bilobalide, a constituent of Ginkgo biloba L., potentiates drug-metabolizing enzyme activities in mice: Possible mechanism for anticonvulsant activity against 4-O-methylpyridoxine-induced convulsions. *Research Communications in Molecular Pathology and Pharmacology*, *96*(1), 45–56.

Sauer, S. W., Opp, S., Hoffmann, G. F., Koeller, D. M., Okun, J. G., & Kölker, S. (2011). Therapeutic modulation of cerebral l-lysine metabolism in a mouse model for glutaric aciduria type I. *Brain*, *134*(1), 157–170. https://doi.org/10.1093/brain/awq269

Sauer, S. W., Opp, S., Komatsuzaki, S., Blank, A.-E., Mittelbronn, M., Burgard, P., Koeller, D. M., Okun, J. G., & Kölker, S. (2015). Multifactorial modulation of susceptibility to l-lysine

in an animal model of glutaric aciduria type I. *Biochimica Et Biophysica Acta*, *1852*(5), 768–777. https://doi.org/10.1016/j.bbadis.2014.12.022

Scharer, G., Brocker, C., Vasiliou, V., Creadon-Swindell, G., Gallagher, R. C., Spector, E., & Van Hove, J. L. (2010). The genotypic and phenotypic spectrum of pyridoxine-dependent epilepsy due to mutations in ALDH7A1. *Journal of Inherited Metabolic Disease*, *33*(5), 571–581.

Schmitt, B., Baumgartner, M., Mills, P. B., Clayton, P. T., Jakobs, C., Keller, E., & Wohlrab, G. (2010). Seizures and paroxysmal events: Symptoms pointing to the diagnosis of pyridoxine-dependent epilepsy and pyridoxine phosphate oxidase deficiency. *Developmental Medicine and Child Neurology*, *52*(7), e133-142. https://doi.org/10.1111/j.1469-8749.2010.03660.x

Schrodinger, L. L. C. (2015). *The PyMOL Molecular Graphics System, Version 1.8*.

Schwarz, J. M., Cooper, D. N., Schuelke, M., & Seelow, D. (2014). MutationTaster2: Mutation prediction for the deep-sequencing age. *Nat Methods*, *11*(4), 361–2.

Sherry, S. T., Ward, M. H., Kholodov, M., Baker, J., Phan, L., & Smigielski, E. M. (2001). DbSNP: the NCBI database of genetic variation. *Nucleic Acids Res*, *29*(1), 308–11.

Shi, H., Enriquez, A., Rapadas, M., Martin, E., Wang, R., & Moreau, J. (2017). NAD Deficiency, Congenital Malformations, and Niacin Supplementation. *N Engl J Med*, *377*(6), 544–52.

Shiraku, H., Nakashima, M., Takeshita, S., Khoo, C.-S., Haniffa, M., Ch'ng, G.-S., Takada, K., Nakajima, K., Ohta, M., Okanishi, T., Kanai, S., Fujimoto, A., Saitsu, H., Matsumoto, N., & Kato, M. (2018). PLPBP mutations cause variable phenotypes of developmental and epileptic encephalopathy. *Epilepsia Open*, *3*(4), 495–502. https://doi.org/10.1002/epi4.12272

Smith, A. C., & Robinson, A. J. (2016). MitoMiner v3.1, an update on the mitochondrial proteomics database. *Nucleic Acids Res*, *44*(D1), 1258–61.

Soiferma, D., & Saada, A. (2015). The Use of Fibroblasts from Patients with Inherited Mitochondrial Disorders for Pathomechanistic Studies and Evaluation of Therapies. In V.K (Ed.), *The Functions, Disease-Related Dysfunctions, and Therapeutic Targeting of Neuronal Mitochondria* (pp. 378–398). E.A Jonas and J.M. Hardwick.

Sorolla, M. A., Rodríguez-Colman, M. J., Tamarit, J., Ortega, Z., Lucas, J. J., Ferrer, I., Ros, J., & Cabiscol, E. (2010). Protein oxidation in Huntington disease affects energy production and vitamin B6 metabolism. *Free Radical Biology and Medicine*, *49*(4), 612–621. https://doi.org/10.1016/j.freeradbiomed.2010.05.016

Sova, H., Jukkola-Vuorinen, A., Puistola, U., Kauppila, S., & Karihtala, P. (2010). 8-Hydroxydeoxyguanosine: A new potential independent prognostic factor in breast cancer. *British Journal of Cancer*, *102*(6), 1018–1023. https://doi.org/10.1038/sj.bjc.6605565

Srikanth, V., Maczurek, A., Phan, T., Steele, M., Westcott, B., Juskiw, D., & Münch, G. (2011). Advanced glycation endproducts and their receptor RAGE in Alzheimer's disease. *Neurobiology of Aging*, *32*(5), 763–777. https://doi.org/10.1016/j.neurobiolaging.2009.04.016

Srinivasaraghavan, R., Parameswaran, N., Mathis, D., Bürer, C., & Plecko, B. (2018). Antiquitin Deficiency with Adolescent Onset Epilepsy: Molecular Diagnosis in a Mother of Affected Offsprings. *Neuropediatrics*, *49*(2), 154–157. https://doi.org/10.1055/s-0037-1621721

Stockler, S., Plecko, B., Gospe, S. M., Coulter-Mackie, M., Connolly, M., van Karnebeek, C., Mercimek-Mahmutoglu, S., Hartmann, H., Scharer, G., Struijs, E., Tein, I., Jakobs, C., Clayton, P., & Van Hove, J. L. K. (2011). Pyridoxine dependent epilepsy and antiquitin

deficiency: Clinical and molecular characteristics and recommendations for diagnosis, treatment and follow-up. *Molecular Genetics and Metabolism*, *104*(1–2), 48–60. https://doi.org/10.1016/j.ymgme.2011.05.014

Stolz, J., & Vielreicher, M. (2003). Tpn1p, the Plasma Membrane Vitamin B6 Transporter of Saccharomyces cerevisiae. *Journal of Biological Chemistry*, *278*(21), 18990–18996. https://doi.org/10.1074/jbc.M300949200

Stolz, J., Wöhrmann, H. J. P., & Vogl, C. (2005). Amiloride Uptake and Toxicity in Fission Yeast Are Caused by the Pyridoxine Transporter Encoded by bsu1+ (car1+). *Eukaryotic Cell*, *4*(2), 319–326. https://doi.org/10.1128/EC.4.2.319-326.2005

Strachan, T., & Read, A. (1999). *Human Molecular Genetics* (2nd ed.). Wiley-Liss. http://www.ncbi.nlm.nih.gov/books/NBK7563/

Striano, P., Battaglia, S., Giordano, L., Capovilla, G., Beccaria, F., Struys, E. A., Salomons, G. S., & Jakobs, C. (2009). Two novel ALDH7A1 (antiquitin) splicing mutations associated with pyridoxine-dependent seizures. *Epilepsia*, *50*(4), 933–936. https://doi.org/10.1111/j.1528-1167.2008.01741.x

Struys, E. A., Bok, L. A., Emal, D., Houterman, S., Willemsen, M. A., & Jakobs, C. (2012). The measurement of urinary Δ1-piperideine-6-carboxylate, the alter ego of α-aminoadipic semialdehyde, in Antiquitin deficiency. *Journal of Inherited Metabolic Disease*, *35*(5), 909–916. https://doi.org/10.1007/s10545-011-9443-0

Struys, E. A., & Jakobs, C. (2010). Metabolism of lysine in alpha-aminoadipic semialdehyde dehydrogenase-deficient fibroblasts: Evidence for an alternative pathway of pipecolic acid formation. *FEBS Letters*, *584*(1), 181–186. https://doi.org/10.1016/j.febslet.2009.11.055

Struys, E. A., Jansen, E. E., & Salomons, G. S. (2014). Human pyrroline-5-carboxylate reductase (PYCR1) acts on Δ 1-piperideine-6-carboxylate generating L-pipecolic acid. *Journal of Inherited Metabolic Disease*, *37*(3), 327–332.

Surtees, R., Mills, P., & Clayton, P. (2006). Inborn errors affecting vitamin B6 metabolism. *Future Neurology*, *1*(5), 615–620. https://doi.org/10.2217/14796708.1.5.615

Suzuki, S., Kodera, Y., Saito, T., Fujimoto, K., Momozono, A., Hayashi, A., & Shichiri, M. (2016). Methionine sulfoxides in serum proteins as potential clinical biomarkers of oxidative stress. *Scientific Reports*, *6*, 38299.

Szydlowski, N., Bürkle, L., Pourcel, L., Moulin, M., Stolz, J., & Fitzpatrick, T. B. (2013). Recycling of pyridoxine (vitamin B6) by PUP1 in Arabidopsis. *The Plant Journal*, *75*(1), 40–52. https://doi.org/10.1111/tpj.12195

Tanaka, A. J., Cho, M. T., Millan, F., Juusola, J., Retterer, K., & Joshi, C. (2015). Mutations in SPATA5 Are Associated with Microcephaly, Intellectual Disability, Seizures, and Hearing Loss. *Am J Hum Genet*, *97*(3), 457–64.

Tarailo-Graovac, M., Shyr, C., Ross, C. J., Horvath, G. A., Salvarinova, R., & Ye, X. C. (2016). Exome Sequencing and the Management of Neurometabolic Disorders. *N Engl J Med*, *374*(23), 2246–55.

Teng, Y., Xie, X., Walker, S., Rempala, G., Kozlowski, D. J., & Mumm, J. S. (2010). Knockdown of zebrafish Lgi1a results in abnormal development, brain defects and a seizure-like behavioral phenotype. *Hum Mol Genet*, *19*(22), 4409–20.

Tews, J. K. (1969). Pyridoxine Deficiency and Brain Amino Acids*. *Annals of the New York Academy of Sciences*, *166*(1), 74–82. https://doi.org/10.1111/j.1749-6632.1969.tb54258.x

Tremino, L., Forcada-Nadal, A., Contreras, A., & Rubio, V. (2017). Studies on cyanobacterial protein PipY shed light on structure, potential functions, and vitamin B6 -dependent epilepsy. *FEBS Lett*, *591*(20), 3431–42.

Tremino, L., Forcada-Nadal, A., & Rubio, V. (2018). Insight into vitamin B6 -dependent epilepsy due to PLPBP (previously PROSC) missense mutations. *Hum Mutat*, *39*(7), 1002–1013.

Uhlen, M., Fagerberg, L., Hallstrom, B. M., Lindskog, C., Oksvold, P., & Mardinoglu, A. (2015). *Proteomics. Tissue-based map of the human proteome* (Vol. 347, Issue 6220). Science.

Ulvik, A., Midttun, Ø., Pedersen, E. R., Eussen, S. J., Nygård, O., & Ueland, P. M. (2014). Evidence for increased catabolism of vitamin B-6 during systemic inflammation. *The American Journal of Clinical Nutrition*, *100*(1), 250–255. https://doi.org/10.3945/ajcn.114.083196

van der Ham, M., Albersen, M., de Koning, T. J., Visser, G., Middendorp, A., Bosma, M., Verhoeven-Duif, N. M., & de Sain-van der Velden, M. G. M. (2012). Quantification of vitamin B6 vitamers in human cerebrospinal fluid by ultra performance liquid chromatography-tandem mass spectrometry. *Analytica Chimica Acta*, *712*, 108–114. https://doi.org/10.1016/j.aca.2011.11.018

van Karnebeek, C. D. M., Hartmann, H., Jaggumantri, S., Bok, L. A., Cheng, B., Connolly, M., Coughlin, C. R., Das, A. M., Gospe, S. M., Jakobs, C., van der Lee, J. H., Mercimek-Mahmutoglu, S., Meyer, U., Struys, E., Sinclair, G., Van Hove, J., Collet, J.-P., Plecko, B. R., & Stockler, S. (2012). Lysine restricted diet for pyridoxine-dependent epilepsy: First evidence and future trials. *Molecular Genetics and Metabolism*, *107*(3), 335–344. https://doi.org/10.1016/j.ymgme.2012.09.006

van Karnebeek, C. D. M., Stockler-Ipsiroglu, S., Jaggumantri, S., Assmann, B., Baxter, P., Buhas, D., Bok, L. A., Cheng, B., Coughlin, C. R., Das, A. M., Giezen, A., Al-Hertani, W., Ho, G., Meyer, U., Mills, P., Plecko, B., Struys, E., Ueda, K., Albersen, M., … Hartmann, H. (2015). Lysine-Restricted Diet as Adjunct Therapy for Pyridoxine-Dependent Epilepsy: The PDE Consortium Consensus Recommendations. In J. Zschocke, K. M. Gibson, G. Brown, E. Morava, & V. Peters (Eds.), *JIMD Reports, Volume 15* (pp. 47–57). Springer. https://doi.org/10.1007/8904_2014_296

van Karnebeek, C. D. M., Tiebout, S. A., Niermeijer, J., Poll-The, B. T., Ghani, A., Coughlin, C. R., Van Hove, J. L. K., Richter, J. W., Christen, H. J., Gallagher, R., Hartmann, H., & Stockler-Ipsiroglu, S. (2016). Pyridoxine-Dependent Epilepsy: An Expanding Clinical Spectrum. *Pediatric Neurology*, *59*, 6–12. https://doi.org/10.1016/j.pediatrneurol.2015.12.013

Vermeersch, J. J., Christmann-Franck, S., Karabashyan, L. V., Fermandjian, S., Mirambeau, G., & Der Garabedian, P. A. (2004). Pyridoxal 5'-phosphate inactivates DNA topoisomerase IB by modifying the lysine general acid. *Nucleic Acids Research*, *32*(18), 5649–5657. https://doi.org/10.1093/nar/gkh897

Vliet, D., VM, B., PN, M., MH, F., P, B., & IP, K. (2015). Large Neutral Amino Acid Supplementation Exerts Its Effect through Three Synergistic Mechanisms: Proof of Principle in Phenylketonuria Mice. *PLoS One*, *10*(12), 0143833.

Walker, V., Mills, G. A., Peters, S. A., & Merton, W. L. (2000). Fits, pyridoxine, and hyperprolinaemia type II. *Archives of Disease in Childhood*, *82*(3), 236–237. https://doi.org/10.1136/adc.82.3.236

Wassenberg, T., Willemsen, M. A., Geurtz, P. B., Lammens, M., Verrijp, K., & Wilmer, M. (2010). Urinary dopamine in aromatic L-amino acid decarboxylase deficiency: The unsolved paradox. *Mol Genet Metab*, *101*(4), 349–56.

Waterhouse, A. M., Procter, J. B., Martin, D. M., Clamp, M., & Barton, G. J. (2009). Jalview Version 2–a multiple sequence alignment editor and analysis workbench. *Bioinformatics*, *25*(9), 1189–91.

Waymire, K. G., Mahuren, J. D., Jaje, J. M., Guilarte, T. R., Coburn, S. P., & MacGregor, G. R. (1995). Mice lacking tissue non–specific alkaline phosphatase die from seizures due to defective metabolism of vitamin B–6. *Nature Genetics*, *11*(1), 45–51. https://doi.org/10.1038/ng0995-45

Wempe, M. F., Kumar, A., Kumar, V., Choi, Y. J., Swanson, M. A., Friederich, M. W., Hyland, K., Yue, W. W., Van Hove, J. L. K., & Coughlin, C. R. (2019). Identification of a novel biomarker for pyridoxine-dependent epilepsy: Implications for newborn screening. *Journal of Inherited Metabolic Disease*, *42*(3), 565–574. https://doi.org/10.1002/jimd.12059

Westerfield, M. (1993). *The zebrafish book: A guide for the laboratory use of zebrafish (Brachydanio rerio*. M. Westerfield.

Wiederstein, M., & Sippl, M. J. (2007). ProSA-web: Interactive web service for the recognition of errors in three-dimensional structures of proteins. *Nucleic Acids Res*.

Wierenga, R. K. (2001). The TIM-barrel fold: A versatile framework for efficient enzymes. *FEBS Lett*, *492*(3), 193–8.

Wikoff, W. R., Gangoiti, J. A., Barshop, B. A., & Siuzdak, G. (2007). Metabolomics Identifies Perturbations in Human Disorders of Propionate Metabolism. *Clinical Chemistry*, *53*(12), 2169–2176. https://doi.org/10.1373/clinchem.2007.089011

Wilson, M. P., Plecko, B., Mills, P. B., & Clayton, P. T. (2019). Disorders affecting vitamin B6 metabolism. *Journal of Inherited Metabolic Disease*, *42*(4), 629–646. https://doi.org/10.1002/jimd.12060

Wong, J. W., Chan, C. L., Tang, W. K., Cheng, C. H., & Fong, W. P. (2010). Is antiquitin a mitochondrial Enzyme? *Journal of Cellular Biochemistry*, *109*(1), 74–81.

Wurtman, J. J., & Fernstrom, J. D. (1979). Free amino acid, protein, and fat contents of breast milk from Guatemalan mothers consuming a corn-based diet. *Early Human Development*, *3*(1), 67–77. https://doi.org/10.1016/0378-3782(79)90021-5

Yamashita, J. (1976). Convulsive seizure induced by intracerebral injection of semicarbazide (an anti-vitamin B6) in the mouse. *Journal of Nutritional Science and Vitaminology*, *22*(1), 1–6. https://doi.org/10.3177/jnsv.22.1

Yeghiazaryan, N. S., Striano, P., Spaccini, L., Pezzella, M., Cassandrini, D., Zara, F., & Mastrangelo, M. (2011). Long-term follow-up in two siblings with pyridoxine-dependent seizures associated with a novel ALDH7A1 mutation. *European Journal of Paediatric Neurology*, *15*(6), 547–550. https://doi.org/10.1016/j.ejpn.2011.05.011

Yusuf, I. H., Sandford, V., & Hildebrand, G. D. (2013). Congenital cataract in a child with pyridoxine-dependent epilepsy. *Journal of AAPOS: The Official Publication of the American Association for Pediatric Ophthalmology and Strabismus*, *17*(3), 315–317. https://doi.org/10.1016/j.jaapos.2013.01.006

Yuzyuk, T., Thomas, A., Viau, K., Liu, A., De Biase, I., Botto, L. D., Pasquali, M., & Longo, N. (2016). Effect of dietary lysine restriction and arginine supplementation in two patients with pyridoxine-dependent epilepsy. *Molecular Genetics and Metabolism*, *118*(3), 167–172. https://doi.org/10.1016/j.ymgme.2016.04.015

Zhang, Z. M., & McCormick, D. B. (1991). Uptake of N-(4'-pyridoxyl)amines and release of amines by renal cells: A model for transporter-enhanced delivery of bioactive compounds. *Proceedings of the National Academy of Sciences*, *88*(23), 10407–10410. https://doi.org/10.1073/pnas.88.23.10407

Zhou, J., Wang, X., Wang, M., Chang, Y., Zhang, F., Ban, Z., & Zhang, Q. (2019). The lysine catabolite saccharopine impairs development by disrupting mitochondrial homeostasis. *J Cell Biol*, *218*(2), 580–597.

Zhu, X., Xu, Y., Yu, S., Lu, L., Ding, M., & Cheng, J. (2014). An efficient genotyping method for genome-modified animals and human cells generated with CRISPR/Cas9 system. *Sci Rep*, *4*, 6420.

Zinnanti, W. J., Lazovic, J., Wolpert, E. B., Antonetti, D. A., Smith, M. B., Connor, J. R., Woontner, M., Goodman, S. I., & Cheng, K. C. (2006). A diet-induced mouse model for glutaric aciduria type I. *Brain*, *129*(4), 899–910. https://doi.org/10.1093/brain/awl009